Novel Aspects of Layered Double Hydroxide Chemistry

Charles Ivor Markland

A thesis submitted in part fulfilment of the requirements for the degree of Doctor of Philosophy at the University of Oxford

Balliol College
Oxford
August 2011

The work described in this thesis was carried out in the Chemistry Research Laboratory, Mansfield Road, Oxford from October 2007 to August 2011 under the supervision of Professor Dermot O'Hare. All the work described is my own unless stated to the contrary, and has not been submitted for any degree at this or any other university.

Charles Ivor Markland

August 2011

Abstract

Novel Aspects of Layered Double Hydroxide Chemistry

Charles Markland Balliol College

D.Phil Thesis Trinity 2011

Chapter 1 serves as an introduction to the concept of intercalation chemistry, and the layered hosts which are capable of intercalating guest species. The structures, syntheses and applications of layered metal hydroxides (including layered double hydroxides, hydroxy double salts, and lanthanide hydroxy salts) are covered in detail.

In **Chapter 2**, the synthesis of a number of novel hybrids of LDHs with artificial sweeteners is reported, in addition to intercalation compounds of ferulate and theobromine. The solids produced are characterised, and the release of the guests from each hybrid studied in faux-biological conditions. The mechanisms contributing to release in each system are determined using a number of kinetic models.

In **Chapter 3**, intercalation compounds of agrochemicals and drugs in LDH and HS hosts are synthesised and characterised. The release from the new compounds is studied using a soil column (for the agrochemicals), and by immobilisation in enterically-coated alginate beads (for the drugs). Analysis of the kinetics suggests two distinct phases in the release processes of these unusual systems.

In **Chapter 4**, the LDH hybrids of thiosulfate and tartrazine are studied. The tartrazine intercalates are investigated as reagents for testing the hardness of water, and the thiosulfate compounds for use in colour fixation. *In situ* X-ray experiments are used to directly observe the progress of the release reactions of the compounds.

Chapter 5 covers a systematic application of the salt-oxide method of layered metal hydroxide synthesis to all practical combinations of oxides and salts. Novel syntheses of many LDH and HDS hosts are reported, along with the synthesis and characterisation of an unreported LDH containing cadmium and gallium.

Chapter 6 contains details of the experimental procedures for each reaction, in addition to the instrumentation used for characterising each of the products.

Appendix A contains the lattice parameters determined for all new LDH phases, and details of the calculations for determining the orientations of guest molecules.

Appendix B contains the results of elemental microanalysis for each LDH intercalation compound reported in the experimental chapters.

Acknowledgments

First of all, I would like to thank Professor Dermot O'Hare for allowing me to conduct both my Part II and D.Phil research projects in his research group, along with his help and guidance on my various projects throughout.

Secondly, I would like to thank the group's postdocs over the years, and in particular Dr. Gareth Williams for proofreading the whole of this thesis, in addition to collecting SEM data and performing almost all of my metals analyses. I definitely owe you several pints next time you're in Oxford! It would of course, be hard to ignore Dr. Andrew Ashley for making the lab so much more noisily interesting than it would otherwise have been, and for his fascinating stories about anyone and anything. I should also thank Drs. Kang Min Ok and Jong Hyeon Lee for teaching me how to use the TGA machine, and for driving to Daresbury at the most absurd hours of the morning.

Thirdly I shall thank the various D.Phil students of the group, especially Drs. Gang Hu and Yi Du for their supervision of my Part II project and teaching me to use most of the instruments. To the former D.Phils, now doctors, Moss, Fletcher, Gowrie, Aguirre and Ransom, my warmest thanks. For the current batch: Coops, keep the nicotine levels up, and you'll be there in no time; Joyce, if you ever find any pictures of cats doing something funny, be sure to keep me informed; Hasna, remember there's always time for Sporcle and a Kinder Egg; Chadwick, stop being so grumpy; Saul, make sure to keep up your regular periodic table races; Anchalee, keep the SCG money rolling in; and Henry - Henry? Where are you? Mustard?

Many thanks to the past Part IIs, particularly amongst them Mark O'Brien, Richard Bull and Aran Samra, whose work I supervised in their time here (even if the last of the three fell prey to the lure of the organometallic dark side). To the rest, in a long list: Jon, Dave, Louis, Ryan, Nikki, Jonny, Luke, Rosey, Simon, Herrington, Tom, Hannah, Sam and Emily – thank you all for the entertainment you've provided in your all-too-brief times in the group.

Thanks too to the support staff, both in Daresbury and Oxford. At the SRS, Drs. Dave Taylor and Chris Martin made sure I could collect as many results as I did. Thanks to Dr. Nick Rees for running my solid state NMR samples; Dr. Phil Wiseman, for always knowing how to fix the XRD machine; Ann in the ICL, for running my elemental analyses in the now-defunct facility, and Stephen Boyer at London Met for taking over that role; Trish, Pam and Rita for making sure the orders kept flowing smoothly; the guys in stores for making sure I could get anything I needed 36 hours hence; and the staff of the atrium café for their varied menus and hearty portions, and keeping me supplied with coffee. *Mais où sont les Peanut KitKat Chunkies d'antan?*

Appreciative thanks also to the Christ Church bunch: Charlie, Jennie, Simon and Irene from chemistry (now all moved on to better things), and Statto, Chloë, Rebekah, Clym, Ivo, Tom, Paw, Iain, Kerrith and Rosalind for more fun times than I can recall.

Finally, thanks most of all to my family for their encouragement and support through my time at Oxford, at school, and before. I would not be where I am now without them.

Contents

Abbreviations

[X]	The concentration of species X, in mol dm^{-3}
2,4,5T	2,4,5-trichlorophenoxyacetic acid
2,4DB	4-(2,4-dichlorophenoxy)butyric acid
2D	Two-dimensional
α	The degree of progression of a reaction
β	The number of steps involved in the formation of a reaction nucleus
δ_{AB}	The bending vibration of the bond between atoms A and B
λ	The dimensionality of the growth of a nucleus
λ_{CROSS}	The wavelength at which the UV spectrum of a solution crosses the spectrometer-defined arbitrary intensity of '1'
λ_{MAX}	The wavelength of the maximum UV absorption intensity of a molecule.
ν_{AB}	The stretching vibration of the bond between atoms A and B
C_0	The concentration of a species present in the solid host at the beginning of the reaction ($t = 0$)
C_t	The concentration of a species present in solution after time 't'
Ca/Al-NO_3	$[Ca_2Al(OH)_6]NO_3 \cdot yH_2O$
Ca/Al-X	$[Ca_2Al(OH)_6]X \cdot yH_2O$
CHN	Carbon, Nitrogen and Hydrogen (Elemental Analysis)
CP/MAS	Cross-Polarisation Magic Angle Spinning (Nuclear Magnetic Resonance Spectroscopy)
Dichlorprop	2-(2,4-dichlorophenoxy)propanoic acid
DNA	Deoxyribonucleic Acid

EDX	Energy-Dispersive X-ray (Spectroscopy)
EDXRD	Energy-Dispersive X-ray Diffraction
Et	Ethyl (C_2H_5-)
FTIR	Fourier-Transform Infra-Red (Spectroscopy)
GIC	Graphite Intercalation Compound
HDS	Hydroxy Double Salt
HMT	Hexamethylenetetramine
HS	Hydroxy salt
IB	Interdigitated Bilayer
ICP	Inductively-Coupled Plasma (Elemental Analysis)
ICSD	Inorganic Crystal Structural Database
IR	Infra-Red
k_r	Rate constant
LDH	Layered Double Hydroxide
LDH-X	Layered Double Hydroxide intercalated with anion X
LDO	Layered Double Oxide
LHS	Lanthanide Hydroxy Salt
Li/Al-Cl	$[LiAl_2(OH)_6]Cl{\cdot}yH_2O$
Li/Al-X	$[LiAl_2(OH)_6]X{\cdot}yH_2O$
Ln	A nonspecific rare-earth element
m	Arbitrary reaction coefficient
M	In formulae such as MX_2, a nonspecific metal
MCPA	2-methyl-4-chlorophenoxyacetic acid

$M^{II}O$	The oxide of a metal with a formal oxidation state of 2
$M^{III}X_3$	The halide or nitrate salt of a metal with a formal oxidation state of 3
M^{IV}	A metal ion with a formal oxidation state of 4.
M^{II}/M^{II}-HDS	A Hydroxy Double Salt containing two different M^{II} cations
M^{II}/M^{III}-LDH	A Layered Double Hydroxide containing M^{II} as the dispositive layer cation, and M^{III} as the tripositive layer cation
M^{II}/M^{III}-X	$[M^{II}_2M^{III}(OH)_6]X\cdot yH_2O$
Mg/Al-NO_3	$[Mg_2Al(OH)_6]NO_3\cdot yH_2O$
Mg/Al-X	$[Mg_2Al(OH)_6]X\cdot yH_2O$
Mg/Fe-Cl	$[Mg_2Fe(OH)_6]Cl\cdot yH_2O$
Mg/Fe-X	$[Mg_2Fe(OH)_6]X\cdot yH_2O$
n	Reaction exponent
n-butyl	'Normal' butyl; $CH_3CH_2CH_2CH_2$-
NaDDS	Sodium dodecylsulfate
NIR	Near Infra-Red
NMR	Nuclear Magnetic Resonance (Spectroscopy)
NSAID	Non-Steroidal Anti-Inflammatory Drug
R^2	The coefficient of determination of a linear regression line
SEM	Scanning Electron Microscopy
t_0	Induction time
t_{50}	The time (in minutes) required for the release of 50% of the concentration of the anion present in solution at the point of the final release aliquot
t_{90}	The time (in minutes) required for the release of 90% of the anions present in the layered host solid into solution

TGA	Thermogravimetric Analysis
TPPS	Tetraphenylporphinesulfonate
UV	Ultraviolet (Spectroscopy)
UV/Vis	Ultraviolet/Visible (Spectroscopy)
X	In formulae such as MX_2, a nonspecific non-metal or molecular anion
XRD	(Powder) X-ray Diffraction
y	An indeterminate number of cointercalated water molecules
Y-Cl LHS	$[Y_2(OH)_5]Cl \cdot yH_2O$
Zn_5-NO_3	$[Zn_5(OH)_8](NO_3)_2 \cdot yH_2O$
Zn_5-X	$[Zn_5(OH)_8]X \cdot yH_2O$

Chapter 1

Introduction

1.1 Intercalation

The process of intercalation may be defined as "a reaction that involves the penetration of a host material by guest species without causing a major structural modification of the host"; the intercalated guest species are not distributed randomly throughout the host solid, but occupy positions that are defined by the structure of the host.[1] The host material itself must possess a long-range ordered structure, and may possess any sort of dimensional interconnectivity: intercalation has been most frequently reported into rigid, three-dimensional framework hosts (in materials such as tungsten trioxide and zeolites),[2-5] and two-dimensional layered materials bound together by van der Waals forces (in graphite, molybdenum disulfide and many other materials, *vide infra*). A number of lower-dimensional solids are also considered to undergo intercalation reactions: examples of one-dimensional chain-like materials which may intercalate guest species include $NbSe_3$ and $RuBr_3$,[6-8] and some instances of guest adoption in the molecular structures of C_{60} and DNA have been considered to represent examples of intercalation into a zero-dimensional (molecular) host, even in the absence of a rigidly interconnected framework.[9-12]

The products formed after the intercalation of a guest often display altered chemical, electrical, magnetic and optical properties compared to their precursors. These intercalates have found applications in many fields of chemistry: the bronze-coloured potassium-intercalated graphite C_8K is commonly used in organic synthesis

as a reducing agent, in the debromination of aryl bromide derivatives, and as a reagent in the alkylations of nitriles, imines, and phenylacetic acid esters.[13-15]

1.2 Layered Intercalation Hosts

1.2.1 Graphite

Graphite is the simplest layered compound, consisting of staggered layers of infinite trigonal arrays of carbon atoms. The distance between consecutive layers is 3.35Å, corresponding to approximately twice the van der Waals radius of a carbon atom.[16] The structure of graphite is depicted in Figure 1.1.

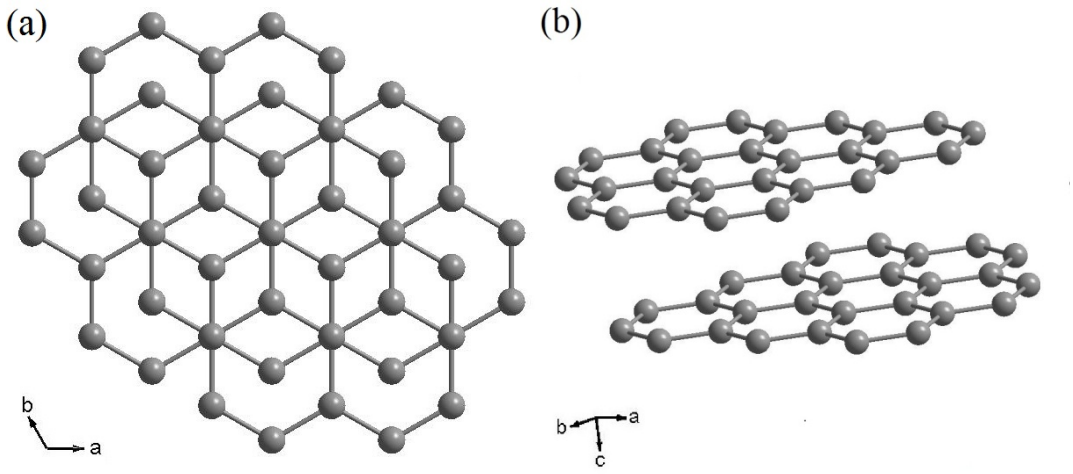

Figure 1.1: The structure of graphite, viewed perpendicular to (a) the (001) plane, and (b) the (34-6) plane.[17] Structure from the Inorganic Crystal Structure Database (ICSD).

Unusually for an intercalation host, graphite may intercalate positively- and negatively-charged guest species, as well as neutral molecules. The first successful exfoliation of graphite was performed by Schafhaeutl, after attempting to dissolve the host in concentrated sulfuric acid:[18] however,[19] its first genuine intercalation compound was reported by Brodie in 1859, who formed graphite bisulfate by reaction with a mixture of concentrated sulfuric and nitric acids.[20] This deep blue compound, with an approximate formula $C_{24}HSO_4 \cdot 2H_2SO_4$, shows an interlayer separation of

7.98Å,[21] and a near-tenfold increase in in-plane conductivity compared to pristine graphite.[22]

Other graphite intercalation compounds (GICs) of note include calcium graphite (C_6Ca) which shows superconductive properties below 11.5K (the highest critical temperature of any GIC),[23] and the intercalation compounds of the alkali metals C_8M (M = Li – Cs), which are able to additionally intercalate neutral ammonia upon extrusion of some of the metal ions, as summarised in Equation 1.1.

$$3C_8K + 4NH_3 \rightarrow 2C_{12}K(NH_3)_2 + K \qquad \textbf{Equation 1.1}$$

Although somewhat more difficult to achieve, it is also possible to intercalate potassium and other guest species into the hexagonal form of boron nitride, an isoelectronic analogue of graphite.[24]

1.2.2 Chalcogenides

Many chalcogenides of the transition metals in groups 4, 5 and 6 of the periodic table possess similar layered structures, and these compounds may intercalate a range of positively-charged and neutral species. The contrasting structures of two of these compounds, molybdenum disulfide and titanium disulfide, are illustrated below in Figure 1.2.

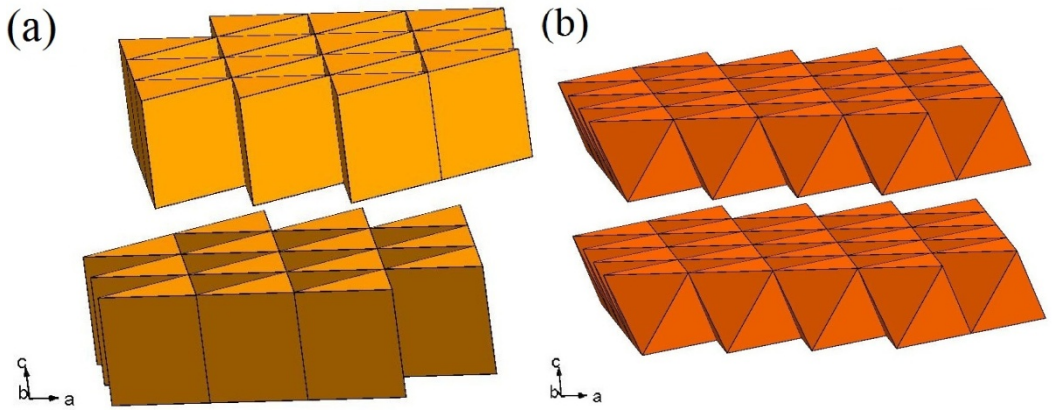

Figure 1.2: The structures of (a) molybdenum disulfide,[25] and (b) titanium disulfide.[26]

These dichalcogenides, with the general formula MX_2 (M = Ti, Zr, Hf, V, Nb, Ta, Mo or W; X = S, Se or Te), each possess one of the two structures given above, forming layers of edge-sharing trigonal prisms (as found in MoS_2) or edge-sharing octahedra (in TiS_2). Guest species that may be intercalated into these hosts include alkali metals, ammonia, and even larger organometallic species such as metallocenes.[27-29] Positively-charged species may be intercalated by exploiting the redox activity of the layer metal cations, allowing charge neutrality to be preserved without any change in the stoichiometry of the layers. As with GICs, fundamental changes in the physical properties of the solids are observed upon intercalation: for instance, the wide band-gap semiconductor HfS_2 acquires metallic conductive properties upon the intercalation of potassium.[30] Similarly, $SnSe_2$ intercalated with cobaltocene demonstrates superconductive properties below 8.3K, whereas the pristine host shows no such transition.[31, 32]

1.2.3 Oxides

Layered metal oxyhalides (such as FeOCl) and oxides (such as MoO_3 and V_2O_5) also demonstrate varied intercalation chemistry. The structure of FeOCl is depicted in Figure 1.3.

The structure consists of corrugated layers of double-stacked edge-sharing $FeCl_2O_4$ octahedra.[33] Intercalation of lithium into FeOCl (by reaction of the solid with *n*-butyllithium) results in an intercalated solid, $Li_{0.5}FeOCl$, which shows an order-of-magnitude increase in magnetic susceptibility and a three-hundred-fold increase in its electrical conductivity compared to the unaltered host.[34] This intercalation process is made possible, as for the transition metal chalcogenides, by the redox activity of the host, which is partially reduced upon reaction with the alkyllithium reagent. The

analogous oxychloride hosts TiOCl, VOCl and CrOCl show similar reactivity,[35, 36] as do a number of lanthanide oxychlorides of the general formula LnOCl.[37]

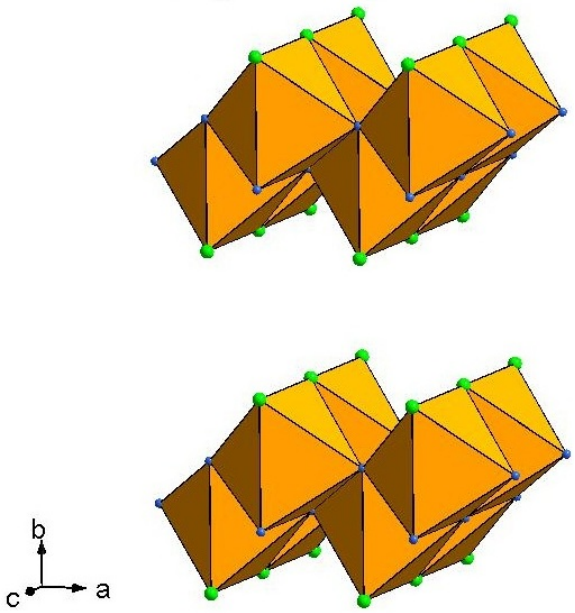

Figure 1.3: The structure of iron hydroxychloride, FeOCl.[38] Chlorine and oxygen atoms are shown as green and blue spheres, respectively.

The layered oxide MoO_3 forms a series of bronzes by the intercalation of small cations, similarly to the three-dimensional WO_3. Unusually, this not only includes small alkali metals such as lithium, but also protons from acidic reducing solutions to form a continuum of compounds with the general formula H_xMoO_3.[39] Once again, the redox activity of the transition metal cation is the key to this behaviour.

1.2.4 Layered Clays

Most naturally-occurring layered clay materials are formed from negatively-charged aluminosilicate layers intercalated with exchangeable interlayer cations. The montmorillonite family of materials are amongst the most commonly-found anionic clays, and the structure of a typical material from this family is shown in Figure 1.4.

The ions present in the interlayer space of the montmorillonite structure (Ca^{2+} in Figure 1.4) may readily be exchanged for other cations including those of alkali

metals, alkylammonium cations, transition metal complexes, and much larger organic species including drug molecules such as ibuprofen.[40-43]

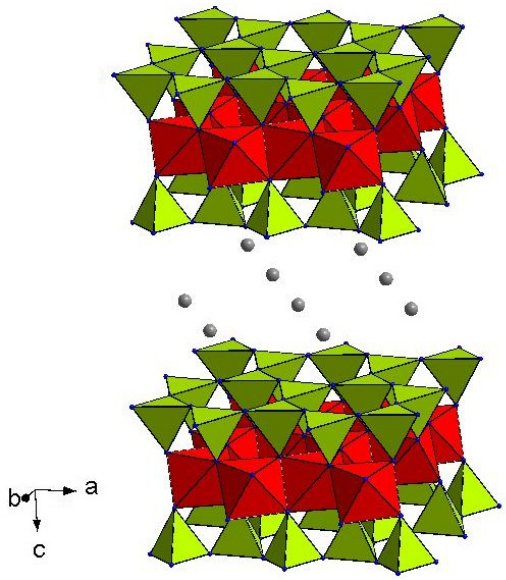

Figure 1.4: The structure of a montmorillonite clay, $Ca[Al_4Si_8O_{22}(OH)_2]$.[44] SiO_4 tetrahedra are shown in green, $AlO_2(OH)_4$ octahedra in red.

While significant changes in the structure of anionic clays are observed upon the intercalation of guest species (for instance, an increase in the interlayer spacing), the physical properties are not found to change greatly. This may be due to the lack of any redox behaviour by the metal atoms in the layers, as well as the increased separation between consecutive layers which often arises due to the presence of cointercalated water in the interlayer space. The very high affinity of montmorillonite clays for water is well-known: primary hydration of the compound results in absorption of water into the interlayer space, forming up to four distinct layers of H_2O molecules and a doubling of the interlayer separation, with a total uptake of up to 0.5g H_2O per gram of clay.[45] Further 'secondary' hydration of the solid leads to uptakes in excess of 10g H_2O per gram of clay, which cannot be described by absorption into the interlayer space (the apparent 'interlayer separation' of the compound at this degree of hydration is in excess of 300Å),[46] and even further hydration leads to the formation of a

thixotropic gel, with laminar separations calculated by Langmuir to be in excess of 1300Å.[47, 48]

1.3 Layered Metal Hydroxides

1.3.1 Aluminium Hydroxide

Aluminium hydroxide exists as a number of different polymorphs, the most commonly found of which is gibbsite (γ-$Al(OH)_3$). The other forms (bayerite, nordstrandite and doyleite) are all based upon the same intralayer structure of edge-sharing AlO_6 octahedra, but with different stacking sequences: these are illustrated in Figure 1.5.

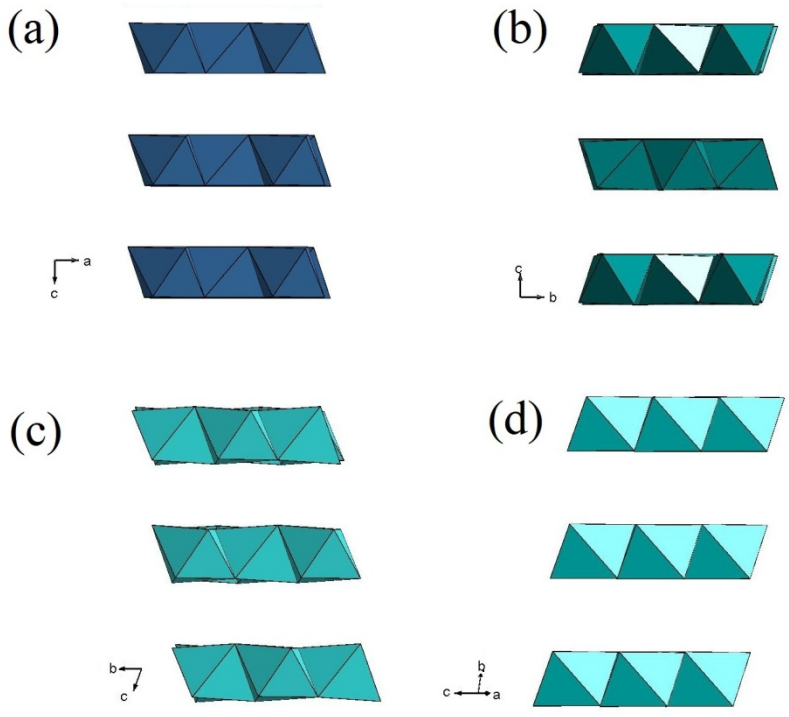

Figure 1.5: The layer stacking sequences of (a) bayerite,[49] (b) gibbsite,[50] (c) nordstrandite,[51] and (d) doyleite.[52] The structures of nordstrandite and doyleite differ only in their horizontal shifting parallel to the layers.[53]

The principal intercalation chemistry of these aluminium hydroxides is by the 'imbibition' of metal salts from solution. This was first observed in the formation of

lithium aluminates ($LiX.2Al(OH)_3$) from the reaction of aluminium hydroxides with solutions of lithium salts (LiX). These compounds were initially believed to consist of aluminium hydroxide layers with free Li^+ and X^- anions present in the interlayer space;[54] further investigation suggested that a more representative chemical formula would be $[LiAl_2(OH)_6]^+X^-$, as the lithium cation is incorporated into the octahedral holes in aluminium hydroxide layers, while the salt anion is found with cointercalated water in the interlayer space.[55] The octahedral holes of gibbsite, and the lithium ions within them, are depicted below.

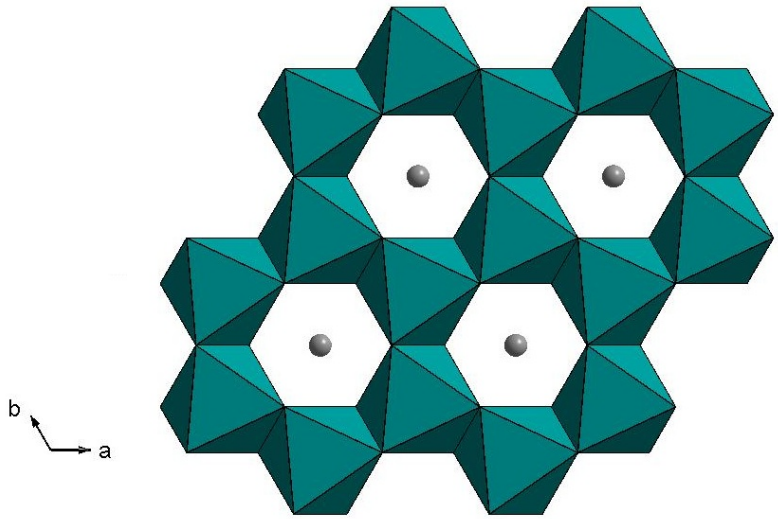

Figure 1.6: A single layer of lithium-intercalated gibbsite. The grey lithium ions sit in the vacant octahedral holes of the layers formed by the teal $Al(OH)_6$ octahedra.[56]

The lithium-gibbsite intercalation compound shows an 'aba' stacking sequence in the interlayer direction ('*c*'), which is normally indexed to a hexagonal unit cell; the lithium-bayerite and lithium-nordstrandite compounds show 'abca' stacking sequences, and are commonly indexed to a rhombohedral unit cell.[57]

Later research established that it was also possible to intercalate small transition metals into the octahedral holes in the layers. This is only possible through the combination of activating an aluminium hydroxide host by grinding in a ball-mill, along with performing the reaction in highly concentrated nitrate solutions under

hydrothermal conditions.[58] These compounds possess the unusual chemical formula $[MAl_4(OH)_{12}](NO_3)_2 \cdot yH_2O$ (where M = Co, Ni, Cu or Zn), and contain M^{2+} cations in only half of the octahedral holes in the layers. Similar structures containing mixtures of M^{2+} ions within the layers have also been prepared,[59] and recent work has demonstrated the existence of a magnesium-containing chloride analogue formed by the direct reaction of gibbsite with solid $MgCl_2$ under hydrothermal conditions, yielding a solid with the formula $[MgAl_4(OH)_{12}]Cl_2 \cdot 2.4H_2O$.[60]

1.3.2 Layered Double Hydroxides

The most widely investigated layered metal hydroxide compounds known are the layered double hydroxides (LDHs). These may be thought of as being based on the structure of magnesium hydroxide (which occurs in nature as the mineral brucite) with partial substitution of the dipositive cations for tripositive ones. The archetypal example of this class of compound is hydrotalcite, an LDH mineral containing magnesium and aluminium as layer cations. The structures of brucite and hydrotalcite are given in Figure 1.7.

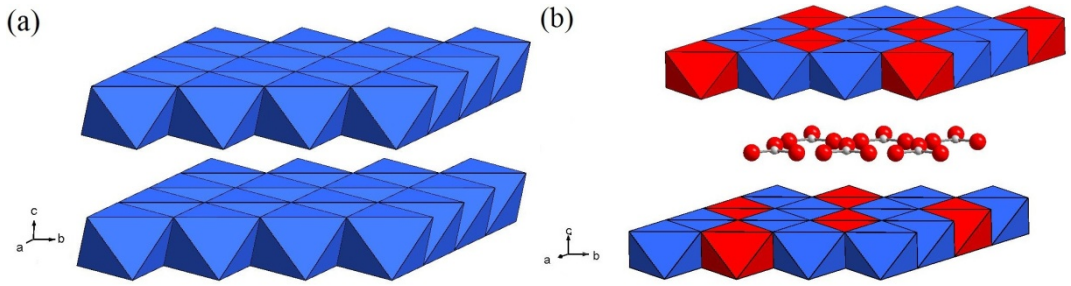

Figure 1.7: The structures of (a) brucite ($Mg(OH)_2$),[61] and (b) hydrotalcite ($[Mg_2Al(OH)_6](CO_3)_{0.5} \cdot 1.5H_2O$.[62] MgO_6 octahedra are shown in blue, and AlO_6 octahedra are depicted in red. A number of the red and white interlayer carbonate molecules are not shown for clarity.

The first characterisation of the structure of hydrotalcite suggested alternate layers of magnesium hydroxide and aluminium hydroxide,[63] but successive refinement of similar structures through X-ray crystallography determined that both cations were

present in every layer.[64, 65] Hydrotalcite stacks rhombohedrally, with a repeat distance of three layers. The less common mineral manasseite is chemically identical but has been found to adopt a hexagonal stacking sequence, with a repeat distance of two layers.[66] Although the primitive unit cell of a hydrotalcite-like LDH is rhombohedral, the structures are typically indexed using a slightly larger hexagonal unit cell, in which the *c*-axis is oriented perpendicular to the layers and the *a*- and *b*-axes follow the hexagonal arrangement of the interlayer cations. This axis system is indicated by the unit cell coordinates shown in Figure 1.7. Structure factor calculations for a rhombohedrally-stacked hydrotalcite-like LDH provide a selection rule for the observed powder X-ray Bragg reflections from the solid: reflections are absent unless they satisfy the condition $-h + k + l = 3n$, where n is an integer and h, k and l represent the Miller indices of the reflection.[67] A simulated powder pattern of the hydrotalcite structure from Figure 1.7 is depicted in Figure 1.8, with the principal diagnostic reflections indexed according to the above-described cell.

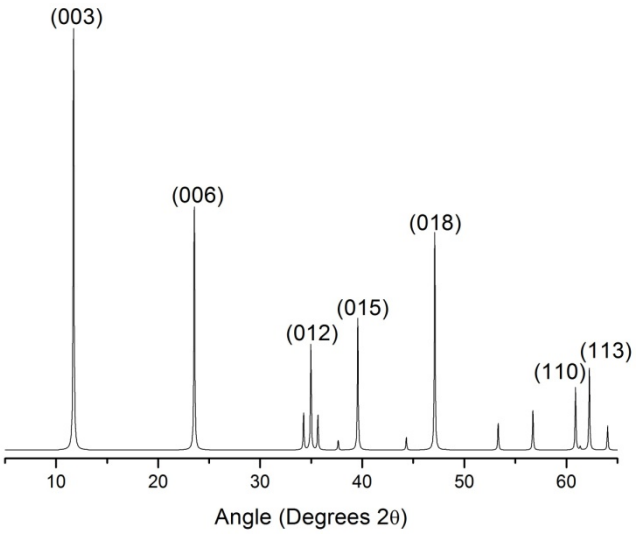

Figure 1.8: The indexed powder pattern of hydrotalcite ($[Mg_2Al(OH)_6](CO_3)_{0.5}\cdot 1.5H_2O$.[62]

Indexing the pattern using a hexagonal unit cell allows for rapid determination of structural information based on the positions of the reflections. The d-spacing of the first (00*l*) 'basal' reflection, (003), is equal to the thickness of one LDH layer

(approximately 4.8Å)[68] plus the height of the interlayer gallery space; alternatively, this can be thought of as directly providing the separation between the centres of two consecutive layers, or the value of the *c* lattice parameter divided by three. Knowledge of the interlayer separation, along with the dimensions of an intercalated molecule allows for predictions of the orientations of the interlayer anions to be made. The (110) and similar non-basal reflections allow the *a* and *b* parameters to be calculated.

The general formula of hydrotalcite-like LDH compounds may be represented as $[M^{2+}_{1-x}M^{3+}_{x}(OH)_2]^{x+}(X^{n-})_{x/n}\cdot yH_2O$. Pure-phase LDH compounds have been synthesised with $0.2 \leq x \leq 0.33$,[69, 70] although there are reports of synthetic LDHs over a greater range with $0.1 \leq x \leq 0.5$.[70-72] This range is logically limited by the proximity of consecutive $M^{3+}O_6$ octahedra within the layers: when x = 0.33, as in the hydrotalcite structure above, no such octahedra are adjacent, and this is also true for values of x below 0.33. However, when the value of x is much less than this, the separation of the $M^{3+}O_6$ octahedra is so great that segregation of the compound to form a monometallic $M^{2+}(OH)_2$ phase is thermodynamically probable – correspondingly, at great values of x, the high contiguity of adjacent $M^{3+}O_6$ octahedra will lead to the preferential formation of a $M^{3+}(OH)_3$ phase, rather than a mixed double hydroxide.[73] Solid-state NMR data further suggest that, even when x = 0.33, regions of localised Mg and Al clustering still exist in the layers of hydrotalcite.[74]

In practice, few LDHs are found to have the complete cation ordering illustrated in Figure 1.7, due to the similarity in cation sizes and bonding modes between the cations, which does not enforce one single arrangement on the octahedra. Complete ordering has been observed in $[Ca_2Al(OH)_6]_2SO_4\cdot 6H_2O$, and in related calcium-containing LDHs with Sc^{3+}, Fe^{3+} and Ga^{3+} cations;[75] this phenomenon arises from the large difference in the ionic radii of the cations, which leads to a slight distortion of

the structure in which the calcium ions protrude slightly from the layers, and adopt a formally seven-coordinate environment to minimise the strain that would otherwise be enforced on the structure.[76]

Dipositive metal ions that form pure LDH compounds include Mg^{2+}, Ca^{2+}, Mn^{2+}, Fe^{2+}, Co^{2+}, Ni^{2+}, Cu^{2+}, Zn^{2+} and Cd^{2+}, while tripositive metals involved in the compounds include Sc^{3+}, V^{3+}, Cr^{3+}, Mn^{3+}, Fe^{3+}, Co^{3+}, Al^{3+}, Ga^{3+} and In^{3+}. Partial substitution of the layer cations has been observed for noble metal cations, such as Pd^{2+}, Pt^{2+}, Rh^{3+}, Ir^{3+}, Ru^{3+}, and rare-earth cations including Y^{3+}, Ce^{3+}, and Eu^{3+}.[77-81] Some ternary LDH compounds have been reported to contain M^{4+} cations replacing a fraction of the M^{3+} cations within the layers, including Ti^{4+}, Zr^{4+} and Sn^{4+}; [82-84] however, it is possible to show that the tetrapositive cations are not present in the layers, but are segregated into amorphous M^{IV} oxide particles.[85, 86] An unusual oxyhydroxide compound with an LDH-like structure containing only Ti^{4+} as the layer cation has been recently reported – however, this compound shows no anion-exchange intercalation chemistry.[87]

In addition to the anions intercalated into the interlayer space, water is cointercalated within the host. The water molecules are only bound to the layers by hydrogen bonding,[88] and NMR investigations suggest that the water molecules possess a degree of free motion within the interlayer space, and as a result are continually breaking and reforming their hydrogen bonds.[89, 90]

1.3.3 Hydroxynitrate Salts

A number of families of layered metal hydroxides are known which contain only dipositive cations within the layers. They are functionally similar to LDHs, but each show subtly different structures from the brucite-type layers of hydrotalcite. In addition, many of them share a significant structural dependence upon the presence of

nitrate or acetate anions for their formation, although these ions may be exchanged after the compounds have formed. The general formula of these phases is $M(OH)_{2-x}(NO_3)_x \cdot yH_2O$ (M = Co, Ni, Cu or Zn).[91] Common values of x include 0.5 (observed in the common copper hydroxynitrate salt $[Cu_2(OH)_3]NO_3 \cdot yH_2O$),[92] 0.67 (in the nickel nitrate phase $[Ni_3(OH)_4](NO_3)_2 \cdot yH_2O$),[93] and 1 (in the cobalt salt $[Co(OH)]NO_3 \cdot yH_2O$).[94] These structures may be described as brucite-type layers with fractional substitution of layer hydroxide groups by coordinated nitrates: when x = 0.5, one quarter of the layer hydroxide groups have been replaced; when x =1, as in the cobalt salt above, half of the hydroxide groups are replaced, and as a result the structure deteriorates from layers into a network of nitrate-bridged CoO_6 octahedra.[95] The other commonly found structure is that of the basic zinc nitrate salt $[Zn_5(OH)_8](NO_3)_2 \cdot yH_2O$, which adopts a structure in which no nitrate anions are coordinated to the layers; rather, the excess layer charge arises from the replacement of one quarter of the ZnO_6 octahedra with a pair of ZnO_4 tetrahedra that protrude into the interlayer space. The structures of $[Cu_2(OH)_3]NO_3 \cdot yH_2O$ and $[Zn_5(OH)_8](NO_3)_2 \cdot yH_2O$ are illustrated in Figure 1.9. The CuO_6 octahedra in Figure 1.9(a) are noticeably distorted, through a combination of the Jahn-Teller preference of the Cu^{2+} ions and the out-of-plane positioning of the coordinated nitrate: this also results in a visible corrugation of the layers.

In addition to the monometallic hydroxynitrate salts, it is possible to synthesise hydroxy double salts (HDSs) containing pairs of different metal cations within the layers. Great differences in ionic radii between the metallic cations are not tolerated; they are formed only by the same four transition metals as above, which possess a range of ionic radii of only 0.05Å.[96] The synthetic chemistry of these compounds was reported in detail before that of the layered double hydroxides at the turn of the 20th

century by Recoura and Sabatier,[97, 98] and later examined in further detail by Feitknecht.[99-102]

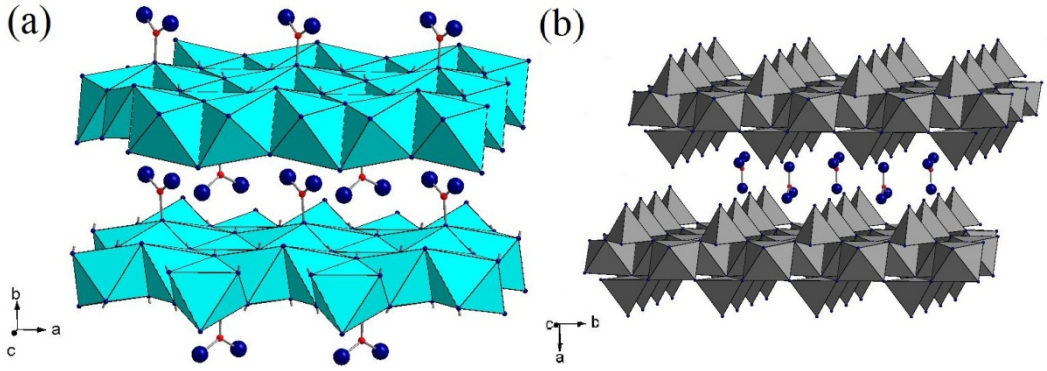

Figure 1.9: The structures of (a) the copper hydroxynitrate salt $[Cu_2(OH)_3]NO_3$,[103] and (b) the zinc hydroxynitrate salt $[Zn_5(OH)_8](NO_3)_2 \cdot 2H_2O$.[104] CuO_6 quasi-octahedra are shown in cyan, and ZnO_6 octahedra and ZnO_4 tetrahedra are depicted in grey.

The structural chemistry of the mixed products is similarly interesting: while the compounds adopt structures much like their monometallic equivalents, it is possible to synthesise, for example, a Zn/Cu-HDS and Cu/Zn-HDS with almost identical Zn:Cu ratios, but with different structures (one resembling the copper salt in Figure 1.9(a), and the other similar to the zinc salt in Figure 1.9(b)).[96]

1.3.4 Lanthanide Hydroxy Salts

In addition to the monometallic layered hydroxides containing only dipositive cations, several series of compounds exist containing only tripositive ions, specifically those of rare earths and lanthanides, known as the lanthanide hydroxy salts (LHSs). Some of these phases, as with HDSs, are dependent upon the presence of nitrate for their formation, and possess the generalised formula $[Ln_2(OH)_{6-x}](NO_3)_x \cdot yH_2O$. For the smaller rare earths, typically x = 1 (Ln = Y, or Gd-Lu), giving rise to compounds such as $[Y_2(OH)_5]NO_3 \cdot 1.5H_2O$, which shows considerable ion-exchange activity.[105-107] Larger rare earths (Ln = La, Pr, Nd, or Sm-Dy) have been found to form structures with x = 2, possessing formulae such as $[Ln(OH)_2]NO_3 \cdot yH_2O$, which demonstrate

similar behaviour.[108, 109] Due to the higher coordination requirements of the layer metal cations, the structures form corrugated layers based around seven-, eight-, or nine-coordinate rare-earth polyhedra, with some coordination of nitrate ions to the layers, as seen in the hydroxynitrate salts.

Similar chloride compounds are also known, which necessarily do not require coordination of the interlayer halide to the layers. These hydroxychlorides, with the general formula $[Ln_2(OH)_5]Cl{\cdot}yH_2O$, have been described for yttrium and a number of lanthanides (La, Nd, Sm, Gd, Dy, Er, and Yb).[110-112] Example structures of $[Gd(OH)_2]NO_3{\cdot}yH_2O$, and the orthorhombic form of $[Yb_2(OH)_5]Cl{\cdot}yH_2O$ are depicted in Figure 1.10.

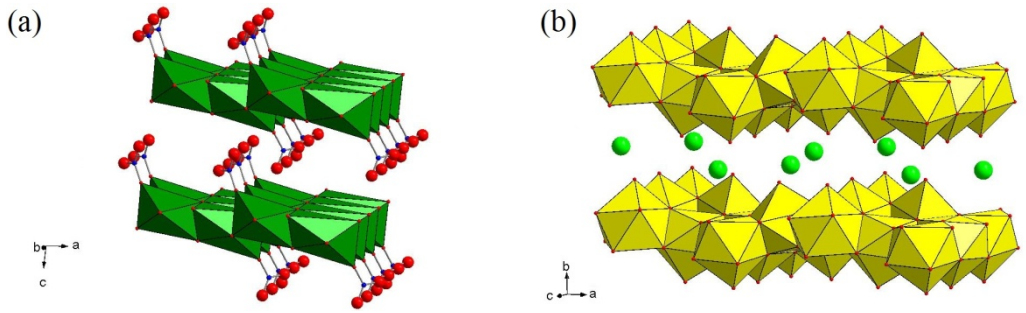

Figure 1.10: The structures of (a) the gadolinium hydroxynitrate salt $[Gd(OH)_2]NO_3{\cdot}yH_2O$,[113] and (b) the ytterbium hydroxychloride salt $[Yb_2(OH)_5]Cl{\cdot}yH_2O$.[106] GdO_x polyhedra are shown in green, and YbO_x polyhedra are depicted in yellow.

The anion-exchange abilities of the hydroxychloride compounds have been extensively explored by Fogg *et al.*,[106] and show reactivity that resembles that of the hydroxy double salt and layered double hydroxide compounds. Recent work has shown that related lanthanide oxyhydroxide compounds show similar intercalation and ion-exchange behaviour.[114]

1.4 Methods of Synthesis of Layered Metal Hydroxides

1.4.1 Coprecipitation from Solution

The synthesis of layered double hydroxides may be conducted by a number of different methods. The most abundantly applied of these is coprecipitation of the solid from the reaction of a basic solution with a solution of mixed metal salts. Two variants of this method are commonly used:[115] the reaction may be performed at low supersaturation (by the separate but simultaneous addition of the metal salt and basic solutions to a third solution containing a high concentration of the intended interlayer anion, maintained at constant pH),[71, 116, 117] or at high supersaturation (by adding the metal salt solution directly to the base solution at a slow, constant rate).[118-120] An alternative approach to the low supersaturation method is to maintain the pH not by external means (such as an automatic pH titrator), but by the gradual hydrolysis of a reagent such as urea or hexamethylenetetramine (HMT) which decomposes to cause a slow increase in the basicity of the solution by the formation of ammoniacal bases.[69, 121, 122] A drawback of the latter method is the presence of carbonate as a by-product which, due to its small size and high charge-density, will intercalate irreversibly into the LDH product; however, recent work has shown it to be possible to produce ion-exchangeable nitrate LDHs by using urea as the hydrolysis compound.[123]

The coprecipitation process can be altered to allow the production of LDH nanoparticles: one such modification uses a high-speed rotor in a colloid mill as the vessel for the reaction process to allow separation of the nucleation and aging steps in the formation of the solid.[124, 125] An alternative approach uses the micelles formed in a water-in-oil reverse microemulsion as ‘microreactors’ to yield uniform nanoscale particles.[126, 127] The typical morphology of these nanoparticles is that of nanoplatelets;

however, modification of this method by the addition of a non-ionic triblock copolymer at the nucleation stage causes the formation of belt-like nanostructures. SEM images of these two distinct morphologies are shown in Figure 1.11.

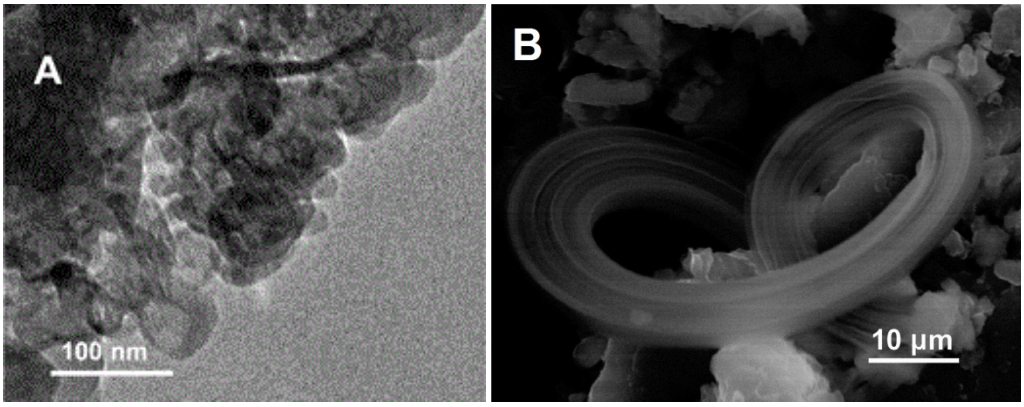

Figure 1.11: (a) The LDH nanoplatelets formed from coprecipitation in a reverse-micelle system. (b) The nano-belt structures formed by the same synthesis method in the presence of a block copolymer. Images taken from Hu and O'Hare.[126]

1.4.2 Synthesis from Oxide and Hydroxide Precursors

It is also possible to use metal oxides and hydroxides as starting materials for the synthesis of hydrotalcite-like phases. Calcium hydroxide, aluminium hydroxide and calcium carbonate can be directly reacted to form a Ca/Al-LDH compound, although only by performing the reaction under hydrothermal conditions at 100ºC for one month.[128] More rapid solvent-free syntheses of LDHs have only recently been developed, and still require hydrothermal conditions to proceed to completion.[60, 129] Heterogeneous reactions of metal (II) oxides with metal (III) salt solutions are known: these proceed much more rapidly, and this 'salt-oxide' method provides a route to a number of LDHs difficult to access by coprecipitation methods, such as those containing Cu^{2+} and Cr^{3+}.[130-132]

The salt-oxide method represents the most common route to the synthesis of hydroxynitrate and hydroxy double salts. While the monometallic compounds may be formed by controlled addition of alkali to a solution of the nitrate salt, or by urea

hydrolysis over solid nitrate salts at various temperatures,[91, 109] the reaction of one metal's oxide with a nitrate solution of the other allows HDS materials containing almost every possible permutation of viable metallic combinations to be synthesised.[96] It is by this method that one may access the two Cu/Zn-HDS products referred to in Section 1.3.3: one is the product of the reaction of zinc oxide with a solution of copper nitrate, while the other may be formed from the reaction of copper oxide with a zinc nitrate solution. Some monometallic salts are also accessible by this method, such as $[Zn_5(OH)_8](NO_3)_2 \cdot yH_2O$ (from ZnO and $Zn(NO_3)_2$),[99] and $[Cu_2(OH)_3]NO_3 \cdot yH_2O$ (from CuO and $Cu(NO_3)_2$).[133]

The first reported syntheses of lanthanide hydroxynitrate compounds were by hydrothermal means; specifically, by the reaction of the lanthanide sesquioxide with a solution of the lanthanide nitrate.[108, 134] However, most syntheses of these compounds are performed by simple precipitation from a solution of the lanthanide nitrate (or halide) with a mixed solution of sodium hydroxide and sodium nitrate/halide, followed by hydrothermal treatment to increase the crystallinity of the product.[106, 107]

1.5 Methods of Intercalation into Layered Metal Hydroxides

1.5.1 Ion Exchange

For the LDHs, HDSs and the lanthanide hydroxy salts, the principal and most simple means of intercalating a new anion into the interlayer space is by ion exchange, performed by adding the host to an aqueous solution containing an excess of the new guest anion, stirring the mixture at a predetermined temperature and for a fixed time, then recovering the solid by filtration and drying.[71, 96] For a successful reaction to take place, the guest anion initially contained in the host interlayers must be easily exchangeable (typically a small monoanion, such as nitrate or a halide).

Polyanions are typically strongly bound into the interlayer spaces of layered metal hydroxides, particularly those with small anionic radii (and thus high charge density). The prototypical example of this is the carbonate anion, which is almost impossible to remove from an LDH once intercalated; its removal may only be accomplished by destroying the guest anion with a solution of dilute acid, whilst taking care not to simultaneously destroy the host lattice.[69, 135, 136] Previous work has suggested a hierarchy of preference for guest anions in LDHs, as below.[115, 137-139]

$$CO_3^{2-} > HPO_4^{2-} > SO_4^{2-} > OH^- > F^- > Cl^- > Br^- > NO_3^- > I^-$$

This scale was established by Miyata using LDH hosts containing magnesium and aluminium, and has been found to be generally accurate. However, as a generalisation this series may not hold: recent work by Tezuka *et al.* on LDH hosts with a M^{II}:M^{III} ratio of 4:1 has found a strong host dependence on the preference of oxoanions as guests. New series were established for different hosts, shown below (the starred Ni/Fe-LDH was treated hydrothermally to improve crystallinity after synthesis by coprecipitation).[140]

HPO_4^{2-}, SO_4^{2-}, CO_3^{2-} >> NO_3^- (for a Mg/Al-LDH)

CO_3^{2-} > HPO_4^{2-} >> NO_3^- > SO_4^{2-} (for a Co/Fe-LDH)

HPO_4^{2-}, CO_3^{2-} >> NO_3^- > SO_4^{2-} (for a Mg/Fe-LDH)

CO_3^{2-} >> NO_3^- > HPO_4^{2-} > SO_4^{2-} (for a Ni/Fe-LDH)

CO_3^{2-}, NO_3^- >> HPO_4^{2-} > SO_4^{2-} (for a Ni/Fe-LDH*)

The preference for the nitrate ion varies greatly with the host, and in the hydrothermally-treated Ni/Fe-LDH is almost exactly as strong as for carbonate. This has been explained by the optimal size-matching between the nitrate anions and the ion-sieve effect dependent on the spacing between the brucite layers; this selectivity arises in much the same way as for a zeolite. Some limited research has established a

preference series for HDS compounds, which is somewhat similar to the preference pattern of an LDH:[141, 142]

$$PO_4^{3-} >> SO_4^{2-} > NO_3^- \qquad \text{(for a Ni/Zn-HDS)}$$

$$PO_4^{3-} > SeO_3^{2-} > AsO_3^{2-} > SeO_4^{2-} > AsO_4^{3-} > SO_4^{2-} \qquad \text{(for a Ni/Cu-HDS)}$$

1.5.2 Coprecipitation

A simple alternative to ion exchange is to exploit the coprecipitation method used in the synthesis of the host: if the coprecipitation reaction is performed under low supersaturation (as described above) but with no counterion sodium salt present, only a large excess concentration of the target guest in the common solution into which the base and metal salts are added, then an LDH containing the new guest may precipitate immediately. This method is commonly applied for large or unusually shaped guest anions,[143] such as substituted porphyrins,[144] polyoxometallates[145] and metal complexes.[146]

1.5.3 Reconstruction

Another method for intercalating particularly intractable guest anions utilises an unusual property of layered double hydroxides: the so-called 'memory effect' observed after calcining the materials.[147, 148] When an LDH is heated to approximately 450ºC, it sequentially loses its cointercalated water, its interlayer cation (to decomposition) and further water from the hydroxide groups in the layers (the order in which the latter two steps occur is dependent upon the identity of the intercalated anion). The final result is a mixed metal layered double oxide (LDO). When this LDO is added to water, it will reform an LDH structure, and concomitantly uptake anions from solution to balance the newly-reacquired layer charge. By adding an LDO to a highly-concentrated solution of the target guest, the anion will be adopted into the

structure as the LDH reforms. In addition to large guests such as organometallic complexes and extended dye molecules,[149-151] this method may even be used to uptake limited amounts of neutral guests into the interlayer space, such as pentose and hexose sugars.[152, 153]

1.5.4 Other Methods

Several other less commonly applied methods of LDH synthesis include sol-gel methods from organometallic precursors,[154] and the topochemical synthesis of "monometallic" LDHs from the oxidation of a metal (II) hydroxide, such as the conversion of β-$Co(OH)_2$ to $[Co^{II}_2Co^{III}(OH)_6]Br\cdot 1.2H_2O$ by Sasaki *et al.*, using bromine in acetonitrile.[155]

1.6 Applications of Layered Metal Hydroxides

A vast number of applications for layered metal hydroxides are known based on many of their functional physical properties, such as their high ion-exchange capacities, ability to undergo topotactic reversible intercalation, and the activated functional oxides that they form after being calcined at high temperatures.

1.6.1 Antacid Properties

One of the most simplistic, and highly commercialised, applications of LDH materials is the use of hydrotalcite suspended in water as an antacid; two commercially available compounds, Altacite© and Talcid©, are based on this composition. The basicity of the hydroxide, along with that of the intercalated carbonate, acts to reduce stomach acidity – parallels may be drawn with Milk of Magnesia, which consists of a suspension of the near-isostructural magnesium hydroxide (brucite) in water.

1.6.2 Selective Uptake of Anions

The high anion-exchange capacities of LDH materials are principally exploited in their use for the uptake of anions from solution. As discussed in Section 1.5.1, this process is selective for small anions – however, LDHs also demonstrate significant selectivity between near-identical structural isomers of larger molecules: the Li/Al-Cl LDH shows up to 95% selectivity for the *para*-benzenedicarboxylate dianion over its *ortho*- and *meta*- isomers from an equimolar solution at 90ºC,[156] and similar selectivity is show for the 1,5-naphthalenedicarboxylate over the 2,6- isomer at 100ºC (although inverse selectivity is shown at room temperature).[157] Some examples of selectivity have also been observed in the intercalation reactions of HDSs, which will uptake 2-naphthoic acid in preference to 1-naphthoic acid or, unusually, 2,7-dinaphthoic acid, suggesting that the shape of the ion may be a more important consideration than charge density in HDS intercalation.[158] The uptake abilities of layered hydroxide materials have also been applied to the removal of unwanted and toxic oxoanions,[159-161] dye molecules,[162-164] and even biological organisms and materials from liquid waste streams.[165-167] Further uptake experiments have also been performed with the LDOs that result from calcining an LDH.[168-170]

1.6.3 Anionic Hosts for Storage and Release

The identities of anions that may be intercalated into the interlayer space of an LDH are almost unlimited. Apart from the simple inorganic anions mentioned in Section 1.5.1, LDH materials have been successfully intercalated with dye molecules, polymers, polyoxometallate anions, porphyrins, surfactants, and a number of common agrochemicals. [115, 171-184] A rapidly expanding field of interest in LDH chemistry is the intercalation, storage, and release of biological molecules, due to the known

biocompatibility of the hosts[185, 186] – examples of such intercalated anions include amino acids, polypeptides, sugars, vitamins, drug molecules, and even macromolecules including DNA.[152, 187-191] The varied structures of a number of molecules that have been successfully intercalated into LDH hosts are shown in Figure 1.12.

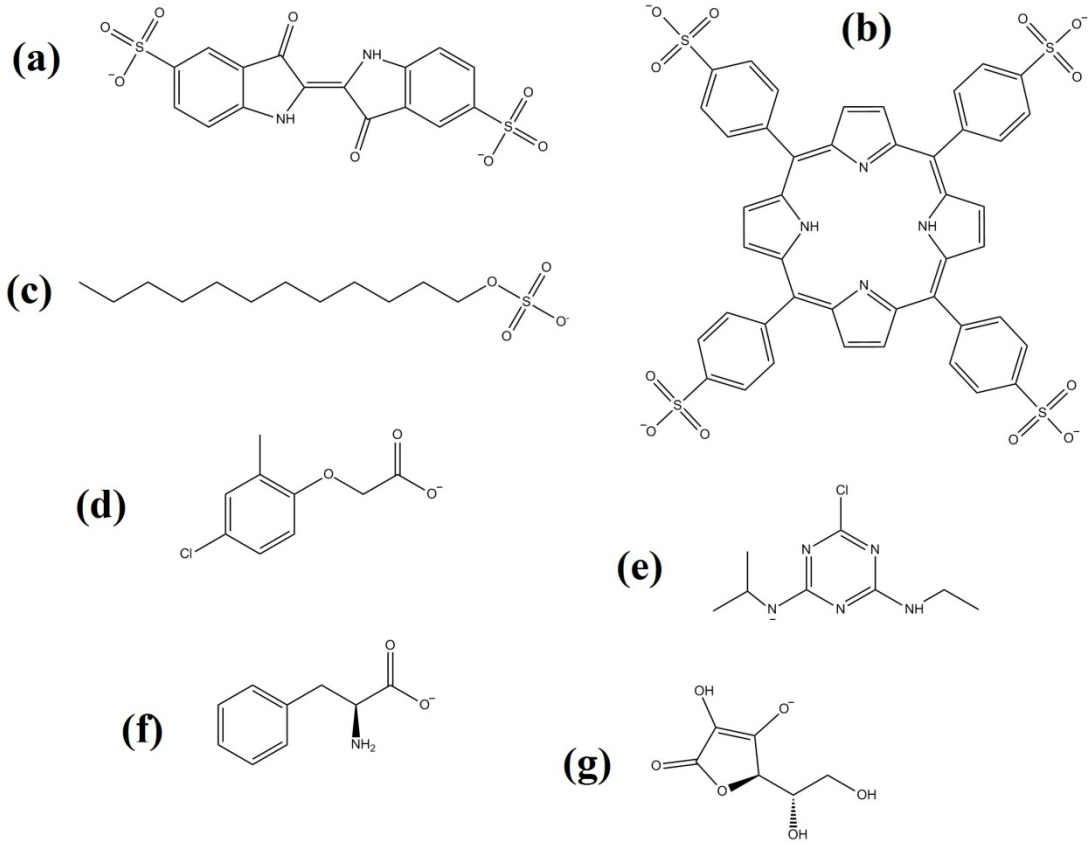

Figure 1.12: The structures of selected anions that have been successfully intercalated into LDH hosts: (a) the anionic dye 'indigo carmine',[171] (b) the sulfonated porphyrin known as 'TPPS',[179] (c) the surfactant dodecylsulfate,[180] (d) the selective herbicide 'MCPA',[181] (e) the herbicide 'atrazine',[184] (f) phenylalanine (an amino acid),[188] and (g) ascorbic acid (also known as Vitamin C).[192]

Studies of the release of these molecules from LDH hosts suggest that they would be highly effective as gradual delivery systems, with the additional benefits of, for example, overcoming drug resistance to cellular uptake.[193-195] The concentration, and

subsequent phosphorylation, of simple aldehydes in sulfite-rich hydrotalcite-like minerals has recently been implicated in the origins of life on earth.[196]

1.6.4 Catalytic Properties

Many recent studies of LDHs, and also hydroxynitrate and hydroxy double salts, have focussed on the catalytic properties of the materials, the anions intercalated within them, and the activated oxides formed from their calcination, as well as their use as inert catalyst supports. A polyoxometallate such as $[WZn_3(ZnW_9O_{34})_2]^{12-}$ is found to catalyse the epoxidation of prenol (3-methyl-2-buten-1-ol) as both a sodium salt in solution, or when intercalated into an LDH: however, the degree of subsequent hydrolysis of the epoxide product is 73% when catalysed by the salt in solution, compared to less than 2% for the LDH-intercalated catalyst – furthermore, it is easier to recover the catalyst intact from the LDH host.[197] The activated layered double oxides have been used to catalyse Knoevenagel condensations, Michael additions, Henry reactions and aldol condensations,[198-200] in addition to the steam reforming reaction of methane and carbon monoxide.[201, 202]

Some catalytic activity has been observed in the mixed oxides derived from HDSs. Fujita *et al.* compared the catalytic activity in the formation of methanol from carbon dioxide and hydrogen of the oxides derived from zinc hydroxynitrate and copper hydroxynitrate. While a mixture of the oxides derived from the calcination of each was found to successfully catalyse the reaction, a ten-fold increase in yield was observed when the oxides were derived from a calcined Zn/Cu-HDS.[203, 204]

1.7 Kinetics of Anion Release

Analysis of the kinetics of anionic deintercalation is key to determining mechanistic information on the processes occurring, and thus understanding the chemical and

physical factors that affect guest release rates and the stability of the intercalated host. A number of kinetic models have been used to determine rate constants and mechanistic data from the release of guests from LDHs; classically, the most effective and informative of these is the Avrami-Erofe'ev model, which describes solid state reactions as a sequence of nucleation and growth steps, introduced by Melvin Avrami[205-207] and later modified by Boris Vasilyevich Erofe'ev.[208] Other models recently examined for this system include the Elovich model, simple first-order models, a modified version of the Freundlich equation, and parabolic diffusion models.[209, 210] The mathematics of these models will be outlined in the sections below.

1.7.1 The Avrami-Erofe'ev Model

The basic form of the rate equation for this model is given as Equation 1.2.[211]

$$[-\ln(1-\alpha)]^{\frac{1}{n}} = k_r(t - t_0) \qquad \textbf{Equation 1.2}$$

In this equation, α represents the degree of progression of the reaction (from zero at initiation to one at completion), t represents the amount of time elapsed since the beginning of the reaction, and t_0 represents the induction time after the initiation of the reaction (which equals zero if the reaction begins immediately). The two kinetic factors that may be derived from this model are n, the reaction exponent, from which information about the reaction mechanism may be recovered, and k_r, which is the rate constant. This model is most effectively applied during the middle of the reaction process, when $0.15 \leq \alpha \leq 0.85$.

In order to interpret the determined value of n (which typically lies between 0 and 4), the two principal factors affecting the formation and growth of reaction nuclei must be considered: specifically, the number of steps involved in formation of a nucleus (represented by β), and the dimensionality with which the growth process

occurs (λ).[115] The value of λ may be 1, 2 or 3, depending on the directions available for particle growth; the value of β lies between 0 and 1, with the former representing instantaneous growth and nucleation, and the latter representing constant, stepwise growth (intermediate values correspond to cases which initially proceed stepwise, but gradually decelerate as the space for the growth of nuclei becomes limited). The value of n may be considered to be equal to a sum of the two rate components, β and λ. Hulbert suggests that when diffusion is also present as a significant factor affecting the growth rate of the nuclei (rather than being purely dependent on the expansion of the boundary of the reacting phase) that the component of the reaction exponent dependent on the dimensionality will be decreased: in this case, the value of n may be expressed as $\beta + 0.5\lambda$. The possible values that n may take, through every permutation of dimensionality and number of nuclei formation steps, are summarised in Table 1.1.

Table 1.1: The values of n from the Avrami-Erofe'ev model likely to arise for each combination of dimensionality (λ) and number of nuclei growth steps (β).[212]

Dimensionality of growth (λ)	**Number of nuclei growth steps (β)**	**Value of Reaction Exponent**	
		Phase-Boundary Control	**Diffusion Control**
1	0 (Instantaneous)	1	0.5
	$0 < \beta < 1$ (Decelerating)	1 - 2	0.5 – 1.5
	1 (Constant)	2	1.5
2	0 (Instantaneous)	2	1
	$0 < \beta < 1$ (Decelerating)	2 - 3	1 – 2
	1 (Constant)	3	2
3	0 (Instantaneous)	3	1.5
	$0 < \beta < 1$ (Decelerating)	3 - 4	1.5 – 2.5
	1 (Constant)	4	2.5

Considering the layered structures of LDHs and HDSs, in which reactivity almost exclusively occurs at defect sites at the layers' edges, it would seem likely that a nucleation-and-growth reaction in the interlayer space would involve two-dimensional growth, and thus $\lambda = 2$. It is also likely that such a reaction would proceed rapidly at first, but then become increasingly limited upon encountering other expanding nuclei, and sites where reaction has already occurred – this suggests deceleratory nucleation. As LDH anion release experiments are typically performed in an aqueous solution, there is likely to be a significant diffusion-controlled element present in the reaction. Combining these facts, it would be suggested that the most likely value of the reaction exponent to be observed in an LDH anion release reaction would be 1-2. Alternatively, Williams and O'Hare suggest that in the case of exceptionally rapid reactions, the rate of anionic diffusion into the interlayer space may be so great compared to the rate of nucleation at the layers' edges that release may appear to proceed instantaneously from a kinetic point of view. This will lead to an apparent dominant one-dimensional component as the layers 'diffuse' apart, in a direction perpendicular to the layers themselves: in this case, assuming deceleratory conditions once more, the value of the reaction exponent should lie between 0.5 and 1.5.[115, 212]

To determine the values of n and k_r from experimental data, taking the natural logarithm of Equation 1.2 and rearranging yields the following expression:

$$\ln(-\ln(1-\alpha) = n \ln k_r + n \ln(t - t_0) \qquad \textbf{Equation 1.3}$$

When the left side of this equation is evaluated for all values of α, and plotted against $\ln (t - t_0)$, the resulting plot has a gradient equal to n, and a y-intercept at $n \ln k_r$, allowing the values of the two constants to be determined. This method of graphical determination is known as a Sharp-Hancock plot.[213]

1.7.2 The Elovich Model

This model, initially applied to gas sorption reactions by Zeldovich and Roginskii,[214] and later modified by Elovich *et al.*,[215] has also been applied to desorption processes, and the release of guests from host materials. The initial form of the model, for sorption processes, is of the form:

$$\frac{\mathrm{d}\alpha}{\mathrm{d}t} = me^{-n\alpha} \qquad \textbf{Equation 1.4}$$

Where α again represents the progression of the reaction towards completion, and *m* and *n* are constants. Chien and Clayton derived a simplified and modified version of this equation to describe phosphate release from soils, the form of which is:[216]

$$1 - \alpha = n \ln t + m \qquad \textbf{Equation 1.5}$$

The reaction constants *m* and *n* have not been shown to consistently provide any physical or mechanistic meaning, and their chemical significance is unknown.[217]

1.7.3 The First-Order Model

This simple model assumes a logarithmic relationship between the reaction progression and time, using the following equation (for a desorption or ion-release process):

$$1 - \alpha = e^{-k_r t} \qquad \textbf{Equation 1.6}$$

A more useful version of this equation, for producing a linear plot with a gradient of -k_r is:

$$\ln(1 - \alpha) = -k_r t \qquad \textbf{Equation 1.7}$$

Despite its simplicity, this equation provides an excellent fit to a number of ion exchange and desorption processes.[218, 219]

1.7.4 The Modified Freundlich Model

This model is based ultimately upon the Freundlich adsorption isotherm, proposed by Herbert Freundlich to empirically describe adsorption processes in solution.[220] This has the general form:[217]

$$\alpha = k_r C^{\frac{1}{n}} \qquad \textbf{Equation 1.8}$$

C represents the equilibrium concentration of the adsorbent, and *n* is a fitted constant. The modified form of this isotherm created for the description of the rates of desorption reactions of clays by Kuo and Lotse, takes the following time-dependent form:[221]

$$\alpha = k_r t^n \qquad \textbf{Equation 1.8}$$

This may be rearranged for linear plotting as:[222]

$$\ln \alpha = \ln k_r + n \ln t \qquad \textbf{Equation 1.9}$$

1.7.5 The Parabolic Diffusion Model

This model is derived from the rate of radial diffusion in a cylinder, in which diffusion in perpendicular directions is negligible.[217] The formula for the extent of a diffusion process may be expressed as:[223]

$$\alpha = \frac{4}{\sqrt{\pi}} \sqrt{\frac{Dt}{r^2}} - \frac{Dt}{r^2} \qquad \textbf{Equation 1.10}$$

In this case, *r* corresponds to the radius of the cylinder, and *D* represents the apparent diffusion constant. Division throughout by *t* yields:

$$\frac{\alpha}{t} = \frac{4}{\sqrt{\pi}} \left(\sqrt{\frac{D}{r^2}} \right) \frac{1}{\sqrt{t}} - \frac{D}{r^2} \qquad \textbf{Equation 1.10}$$

Replacing constants for clarity gives:

$$\frac{\alpha}{t} = \frac{m}{\sqrt{t}} + n \text{ , where } m = \frac{4}{\sqrt{\pi}} \left(\sqrt{\frac{D}{r^2}} \right) \text{ and } n = -\frac{D}{r^2}. \qquad \textbf{Equation 1.11}$$

This allows for linear plotting of (α/t) against ($1/t^{1/2}$) to determine the values of the constants.

1.8 Aims of this Thesis

The aim of this thesis, firstly, is to attempt to synthesise new intercalation hybrids of layered metal hydroxides with novel functional guests, and study the release of the anions from the solid under conditions that reflect their practical use in real-world applications. Through kinetic analysis of the progress of the release reactions with time, it will be possible to determine information about the mechanisms and kinetic processes involved in the deintercalation of a guest anion from a layered metal hydroxide host.

The second principal aim of this thesis is to explore whether a systematic application of previously known synthesis methods to unexplored metallic combinations may produce novel intercalation host phases.

1.9 References

1. J. Alemán, A. V. Chadwick, J. He, M. Hess, K. Horie, R. G. Jones, P. Kratochvíl, I. Meisel, I. Mita, G. Moad, S. Penczek and R. F. T. Stepto, *Pure and Applied Chemistry*, 2007, **79**, 1801-1829.
2. E. O. Brimm, J. C. Brantley, J. H. Lorenz and M. H. Jellinek, *Journal of the American Chemical Society*, 1951, **73**, 5427-5432.
3. Q. Zhong, J. R. Dahn and K. Colbow, *Physical Review B*, 1992, **46**, 2554.
4. A. Corma, *Chemical Reviews*, 1997, **97**, 2373-2420.
5. R. T. Pabalan and F. P. Bertetti, *Reviews in Mineralogy and Geochemistry*, 2001, **45**, 453-518.
6. S. F. Meyer, R. E. Howard, G. R. Stewart, J. V. Acrivos and T. H. Geballe, *Journal of Chemical Physics*, 1975, **62**, 4411-4419.
7. K. Motizuki, Y. Nishio, M. Shirai and N. Suzuki, *Journal of Physics and Chemistry of Solids*, 1996, **57**, 1091-1096.
8. R. Schöllhorn, R. Steffen and K. Wagner, *Angewandte Chemie International Edition in English*, 1983, **22**, 555-556.
9. M. J. Rosseinsky, *Journal of Materials Chemistry*, 1995, **5**, 1497-1513.
10. N. Sidorov, A. Palnichenko, O. Rybchenko and S. Khasanov, *Inorganic Materials*, 2010, **46**, 476-479.

11. E. C. Long and J. K. Barton, *Accounts of Chemical Research*, 1990, **23**, 271-273.
12. H.-K. Liu and P. J. Sadler, *Accounts of Chemical Research*, 2011, **44**, 349-359.
13. M. Rabinovitz and D. Tamarkin, *Synthetic Communications*, 1984, **14**, 377-379.
14. D. Savoia, C. Trombini and A. Umani-Ronchi, *Pure and Applied Chemistry*, 1985, **57**, 1887-1896.
15. S. Chakraborty, J. Chattopadhyay, W. Guo and W. E. Billups, *Angewandte Chemie International Edition*, 2007, **46**, 4486-4488.
16. D. O'Hare and D. W. Bruce, *Inorganic Materials*, Wiley, 1996.
17. A. W. Hull, *Physical Review*, 1917, **10**, 661-696.
18. C. Schafhaeutl, *Journal für Praktische Chemie*, 1840, **21**, 129.
19. H.-P. Boehm and E. Stumpp, *Carbon*, 2007, **45**, 1381-1383.
20. B. C. Brodie, *Philosophical Transactions of the Royal Society of London*, 1859, **149**, 249-259.
21. S. Aronson, S. Lemont and J. Weiner, *Inorganic Chemistry*, 1971, **10**, 1296-1298.
22. M. S. Dresselhaus and G. Dresselhaus, *Advances in Physics*, 1981, **30**, 139-326.
23. T. E. Weller, M. Ellerby, S. S. Saxena, R. P. Smith and N. T. Skipper, *Nature Physics*, 2005, **1**, 39-41.
24. G. L. Doll, J. S. Speck, G. Dresselhaus, M. S. Dresselhaus, K. Nakamura and S. I. Tanuma, *Journal of Applied Physics*, 1989, **66**, 2554-2558.
25. R. G. Dickinson and L. Pauling, *Journal of the American Chemical Society*, 1923, **45**, 1466-1471.
26. I. Oftedal, *Zeitschrift für Physikalische Chemie*, 1928, **134**, 301-310.
27. W. Rüdorff, *Angewandte Chemie*, 1959, **71**, 487-491.
28. R. Schöllhorn and H.-D. Zagefka, *Angewandte Chemie International Edition in English*, 1977, **16**, 199-200.
29. M. B. Dines, *Science*, 1975, **188**, 1210-1211.
30. R. H. Friend and A. D. Yoffe, *Advances in Physics*, 1987, **36**, 1-94.
31. C. A. Formstone, E. T. FitzGerald, D. O'Hare, P. A. Cox, M. Kurmoo, J. W. Hodby, D. Lillicrap and M. Goss-Custard, *Journal of the Chemical Society, Chemical Communications*, 1990, 501-503.
32. D. O'Hare, H.-V. Wong, S. Hazell and J. W. Hodby, *Advanced Materials*, 1992, **4**, 658-660.
33. R. H. Herber and Y. Maeda, *Inorganic Chemistry*, 1981, **20**, 1409-1415.
34. A. Sagua, E. Morán, M. A. Alario-Franco, A. Rivera, C. León, J. Santamaría and J. Sanz, *International Journal of Inorganic Materials*, 2001, **3**, 293-301.
35. T. R. Halbert, D. C. Johnston, L. E. McCandlish, A. H. Thompson, J. C. Scanlon and J. A. Dumesic, *Physica B+C*, 1980, **99**, 128-132.
36. L. Coïc, M. Spiesser, P. Palvadeau and J. Rouxel, *Materials Research Bulletin*, 1981, **16**, 229-236.
37. K. Song and S. M. Kauzlarich, *Chemistry of Materials*, 1994, **6**, 386-394.
38. M. S. Goldsztaub, *Comptes Rendus Hebdomadaires des Seances de l'Academie des Sciences*, 1934, **198**, 667-669.
39. O. Glemser, G. Lutz and G. Meyer, *Zeitschrift für anorganische und allgemeine Chemie*, 1956, **285**, 173-180.

40. R. M. Barrer and D. M. MacLeod, *Transactions of the Faraday Society*, 1955, **51**, 1290-1300.
41. N. K. Labhsetwar and O. P. Shrivastava, *Canadian Journal of Chemistry*, 1992, **70**, 1927-1931.
42. F. H. Lin, Y. H. Lee, C. H. Jian, J.-M. Wong, M.-J. Shieh and C.-Y. Wang, *Biomaterials*, 2002, **23**, 1981-1987.
43. J. P. Zheng, L. Luan, H. Y. Wang, L. F. Xi and K. D. Yao, *Applied Clay Science*, 2007, **36**, 297-301.
44. A. Viani, A. F. Gualtieri and G. Artioli, *American Mineralogist*, 2002, **87**, 966-975.
45. J. Mering, *Transactions of the Faraday Society*, 1946, **42**, B205-B219.
46. J. G. Falconer and S. Mattson, *Soil Science*, 1933, **36**, 317.
47. I. Langmuir, *Journal of Chemical Physics*, 1938, **6**, 873-896.
48. K. Norrish, *Discussions of the Faraday Society*, 1954, **18**, 120-134.
49. R. Rothbauer, F. Zigan and H. O'Daniel, *Zeitschrift für Kristallographie, Kristallgeometrie, Kristallphysik, Kristallchemie*, 1967, **125**, 317-331.
50. H. D. Megaw, *Zeitschrift für Kristallographie, Kristallgeometrie, Kristallphysik, Kristallchemie*, 1934, **87**, 185-204.
51. H. J. Bosmans, *Acta Crystallographica B*, 1970, **26**, 649-652.
52. G. R. Clark, K. A. Rodgers and G. S. Henderson, *Zeitschrift für Kristallographie*, 1998, **213**, 96-100.
53. G. Y. Chao, J. Baker, A. P. Sabina and A. C. Roberts, *Canadian Mineralogist*, 1985, **23**, 21-28.
54. J. L. Burba, *Crystalline Lithium Aluminates*, U.S. Patent 4,348,295, September 7, 1982.
55. K. R. Poeppelmeier and S. J. Hwu, *Inorganic Chemistry*, 1987, **26**, 3297-3302.
56. A. V. Besserguenev, A. M. Fogg, R. J. Francis, S. J. Price, D. O'Hare, V. P. Isupov and B. P. Tolochko, *Chemistry of Materials*, 1997, **9**, 241-247.
57. A. M. Fogg, A. J. Freij and G. M. Parkinson, *Chemistry of Materials*, 2002, **14**, 232-234.
58. A. M. Fogg, G. R. Williams, R. Chester and D. O'Hare, *Journal of Materials Chemistry*, 2004, **14**, 2369-2371.
59. G. R. Williams, S. J. Moorhouse, T. J. Prior, A. M. Fogg, N. H. Rees and D. O'Hare, *Dalton Transactions*, 2011, **40**, 6012-6022.
60. R. Chitrakar, Y. Makita, A. Sonoda and T. Hirotsu, *Journal of Hazardous Materials*, 2011, **185**, 1435-1439.
61. G. Aminoff, *Zeitschrift für Kristallographie, Kristallgeometrie, Kristallphysik, Kristallchemie*, 1921, **56**, 505-509.
62. A. V. Radha, P. V. Kamath and C. Shivakumara, *Acta Crystallographica B*, 2007, **63**, 243-250.
63. W. Feitknecht and M. Gerber, *Helvetica Chimica Acta*, 1942, **25**, 131-137.
64. R. Allmann, *Acta Crystallographica Section B*, 1968, **24**, 972-977.
65. H. F. W. Taylor, *Mineralogical Magazine*, 1969, **37**, 338.
66. M. Bellotto, B. Rebours, O. Clause, J. Lynch, D. Bazin and E. Elkaïm, *The Journal of Physical Chemistry*, 1996, **100**, 8527-8534.
67. M. Vucelic, G. D. Moggridge and W. Jones, *The Journal of Physical Chemistry*, 1995, **99**, 8328-8337.
68. R. Allmann, *Chimia*, 1970, **24**, 99-108.
69. U. Costantino, F. Marmottini, M. Nocchetti and R. Vivani, *European Journal of Inorganic Chemistry*, 1998, **1998**, 1439-1446.

70. F. Cavani, F. Trifiro and A. Vaccari, *Catalysis Today*, 1991, **11**, 173-301.
71. M. Meyn, K. Beneke and G. Lagaly, *Inorganic Chemistry*, 1990, **29**, 5201-5207.
72. M. R. Weir, J. Moore and R. A. Kydd, *Chemistry of Materials*, 1997, **9**, 1686-1690.
73. G. W. Brindley and S. Kikkawa, *American Mineralogist*, 1979, **64**, 836-843.
74. S. Cadars, G. Layrac, C. Gérardin, M. Deschamps, J. R. Yates, D. Tichit and D. Massiot, *Chemistry of Materials*, 2011, **23**, 2821-2831.
75. I. Rousselot, C. Taviot-Gueho, F. Leroux, P. Leone, P. Palvadeau and J. P. Besse, *Journal of Solid State Chemistry*, 2002, **167**, 137-144.
76. R. Allmann, *Neues Jahrbuch für Mineralogie, Monatshefte*, 1977, 136.
77. F. Basile, G. Fornasari, M. Gazzano and A. Vaccari, *Applied Clay Science*, 2000, **16**, 185-200.
78. J. M. Fernández, C. Barriga, M. A. Ulibarri, F. M. Labajos and V. Rives, *Chemistry of Materials*, 1997, **9**, 312-318.
79. J. M. García-García, M. E. Pérez-Bernal, R. J. Ruano-Casero and V. Rives, *Solid State Sciences*, 2007, **9**, 1115-1125.
80. Z. Chang, D. Evans, X. Duan, P. Boutinaud, M. de Roy and C. Forano, *Journal of Physics and Chemistry of Solids*, 2006, **67**, 1054-1057.
81. X. Gao, M. Hu, L. Lei, D. O'Hare, C. Markland, Y. Sun and S. Faulkner, *Chemical Communications*, 2011, **47**, 2104-2106.
82. S. Velu, V. Ramaswamy and S. Sivasanker, *Chemical Communications*, 1997, 2107-2108.
83. S. Velu, K. Suzuki, M. Okazaki, T. Osaki, S. Tomura and F. Ohashi, *Chemistry of Materials*, 1999, **11**, 2163-2172.
84. N. Das and A. Samal, *Microporous and Mesoporous Materials*, 2004, **72**, 219-225.
85. M. Intissar, J.-C. Jumas, J.-P. Besse and F. Leroux, *Chemistry of Materials*, 2003, **15**, 4625-4632.
86. M. Intissar, S. Holler, F. Malherbe, J.-P. Besse and F. Leroux, *Journal of Physics and Chemistry of Solids*, 2004, **65**, 453-457.
87. N. V. Tarakina, R. B. Neder, T. A. Denisova, L. G. Maksimova, Y. V. Baklanova, A. P. Tyutyunnik and V. G. Zubkov, *Dalton Transactions*, 2010, **39**, 8168-8176.
88. F. Zigan and R. Rothbauer, *Neues Jahrbuch für Mineralogie, Monatshefte*, 1967, **137**.
89. G. Marcelin, N. J. Stockhausen, J. F. M. Post and A. Schutz, *Journal of Physical Chemistry*, 1989, **93**, 4646-4650.
90. A. van der Pol, B. L. Mojet, E. van de Ven and E. de Boer, *The Journal of Physical Chemistry*, 1994, **98**, 4050-4054.
91. M. Rajamathi and P. V. Kamath, *International Journal of Inorganic Materials*, 2001, **3**, 901-906.
92. T. Biswick, W. Jones, A. Pacula and E. Serwicka, *Journal of Solid State Chemistry*, 2006, **179**, 49-55.
93. P. Gallezot and M. Prettre, *Bulletin de la Société Chimique de France*, 1969, 407.
94. K. Petrov, N. Zotov, O. Garcia-Martinez and R. Rojas, *Journal of Solid State Chemistry*, 1992, **101**, 145-153.
95. L. Eriksson, D. Louër and P. E. Werner, *Journal of Solid State Chemistry*, 1989, **81**, 9-20.

96. M. Meyn, K. Beneke and G. Lagaly, *Inorganic Chemistry*, 1993, **32**, 1209-1215.
97. A. C. R. Recoura, *Comptes Rendus de l'Académie des Sciences*, 1901, **132**, 1414.
98. O. Sabatier, *Comptes Rendus de l'Académie des Sciences*, 1901, **132**, 1538.
99. W. Feitknecht, *Helvetica Chimica Acta*, 1933, **16**, 427-454.
100. W. Feitknecht and K. Maget, *Helvetica Chimica Acta*, 1949, **32**, 1639-1653.
101. W. Feitknecht and K. Maget, *Helvetica Chimica Acta*, 1949, **32**, 1653-1667.
102. W. Feitknecht and K. Maget, *Helvetica Chimica Acta*, 1949, **32**, 1667-1674.
103. B. Bovio and S. Locchi, *Journal of Crystallographic and Spectroscopic Research*, 1982, **12**, 507-517.
104. W. Stählin and H. R. Oswald, *Acta Crystallographica*, 1970, **B26**, 860-863.
105. L. J. McIntyre, L. K. Jackson and A. M. Fogg, *Chemistry of Materials*, 2007, **20**, 335-340.
106. L. Poudret, T. J. Prior, L. J. McIntyre and A. M. Fogg, *Chemistry of Materials*, 2008, **20**, 7447-7453.
107. S. A. Hindocha, L. J. McIntyre and A. M. Fogg, *Journal of Solid State Chemistry*, 2009, **182**, 1070-1074.
108. M. Lundberg and A. J. Skarnulis, *Acta Crystallographica Section B*, 1976, **32**, 2944-2947.
109. S. P. Newman and W. Jones, *Journal of Solid State Chemistry*, 1999, **148**, 26-40.
110. F. L. Carter and S. Levinson, *Inorganic Chemistry*, 1969, **8**, 2788-2791.
111. K. Dornberger-Schiff and R. F. Klevtsova, *Acta Crystallographica*, 1967, **22**, 435-436.
112. C. Jouve, J. Marrot and D. Riou, *Acta Crystallographica Section C*, 2002, **58**, i14-i15.
113. D. F. Mullica, E. L. Sappenfield and D. A. Grossie, *Journal of Solid State Chemistry*, 1986, **63**, 231-236.
114. H. V. Goulding, S. E. Hulse, W. Clegg, R. W. Harrington, H. Y. Playford, R. I. Walton and A. M. Fogg, *Journal of the American Chemical Society*, 2010, **132**, 13618-13620.
115. X. Duan and D. G. Evans, eds., *Layered Double Hydroxides*, Springer, 2006.
116. S. K. Yun and T. J. Pinnavaia, *Chemistry of Materials*, 1995, **7**, 348-354.
117. K. Klemkaite, I. Prosycevas, R. Taraskevicius, A. Khinsky and A. Kareiva, *Central European Journal of Chemistry*, 2011, **9**, 275-282.
118. V. R. L. Constantino and T. J. Pinnavaia, *Inorganic Chemistry*, 1995, **34**, 883-892.
119. E. Gardner, K. M. Huntoon and T. J. Pinnavaia, *Advanced Materials*, 2001, **13**, 1263-1266.
120. W. Meng, F. Li, D. G. Evans and X. Duan, *Materials Research Bulletin*, 2004, **39**, 1185-1193.
121. N. Iyi, T. Matsumoto, Y. Kaneko and K. Kitamura, *Chemistry Letters*, 2004, **33**, 1122-1123.
122. N. Iyi, K. Tamura and H. Yamada, *Journal of Colloid and Interface Science*, 2009, **340**, 67-73.
123. A. Inayat, M. Klumpp and W. Schwieger, *Applied Clay Science*, 2011, **51**, 452-459.
124. Y. Zhao, F. Li, R. Zhang, D. G. Evans and X. Duan, *Chemistry of Materials*, 2002, **14**, 4286-4291.

125. Y. Wang, F. Zhang, S. Xu, X. Wang, D. G. Evans and X. Duan, *Industrial & Engineering Chemistry Research*, 2008, **47**, 5746-5750.
126. G. Hu and D. O'Hare, *Journal of the American Chemical Society*, 2005, **127**, 17808-17813.
127. C. J. Wang, Y. A. Wu, R. M. J. Jacobs, J. H. Warner, G. R. Williams and D. O'Hare, *Chemistry of Materials*, 2011, **23**, 171-180.
128. G. Renaudin and M. Francois, *Acta Crystallographica Section C*, 1999, **C55**, 835.
129. R. Chitrakar, S. Tezuka, A. Sonoda, K. Sakane, K. Ooi and T. Hirotsu, *Chemistry Letters*, 2007, **36**, 446-447.
130. H.-P. Boehm, J. Steinle and C. Vieweger, *Angewandte Chemie International Edition in English*, 1977, **16**, 265-266.
131. K. El Malki, A. De Roy and J. P. Besse, *European Journal of Solid State Inorganic Chemistry*, 1989, **26**, 339.
132. E. Zhouri and A. El Hajbi, *Annales de Chimie Science des Matériaux*, 1999, **24**, 57-62.
133. H. Hayashi and M. J. Hudson, *Journal of Materials Chemistry*, 1995, **5**, 781-783.
134. J. M. Haschke, *Inorganic Chemistry*, 1974, **13**, 1812-1818.
135. N. Iyi, T. Matsumoto, Y. Kaneko and K. Kitamura, *Chemistry of Materials*, 2004, **16**, 2926-2932.
136. N. Iyi and T. Sasaki, *Applied Clay Science*, 2008, **42**, 246-251.
137. S. Miyata and T. Kumura, *Chemistry Letters*, 1975, 843.
138. S. Miyata and A. Okada, *Clays and Clay Minerals*, 1977, **25**, 14.
139. S. Miyata, *Clays and Clay Minerals*, 1980, **28**, 50.
140. S. Tezuka, R. Chitrakar, A. Sonoda, K. Ooi and T. Tomida, *Green Chemistry*, 2004, **6**, 104-109.
141. S. Komarneni, Q. H. Li and R. Roy, *Journal of Materials Research*, 1996, **11**, 1866-1869.
142. N. Kozai, H. Mitamura, H. Fukuyama, F. Esaka and S. Komarneni, *Microporous and Mesoporous Materials*, 2006, **89**, 123-131.
143. W. T. Reichle, *Journal of Catalysis*, 1985, **94**, 547-557.
144. S. Bonnet, C. Forano, A. de Roy, J. P. Besse, P. Maillard and M. Momenteau, *Chemistry of Materials*, 1996, **8**, 1962-1968.
145. W. Kagunya, Z. Hassan and W. Jones, *Inorganic Chemistry*, 1996, **35**, 5970-5974.
146. A. I. Tsyganok, K. Suzuki, S. Hamakawa, K. Takehira and T. Hayakawa, *Chemistry Letters*, 2001, **30**, 24.
147. K. Chibwe and W. Jones, *Journal of the Chemical Society, Chemical Communications*, 1989, 926-927.
148. F. Kooli, C. Depege, A. Ennaqadi, A. deRoy and J. P. Besse, *Clays and Clay Minerals*, 1997, **45**, 92-98.
149. A. Corma, V. Fornes, F. Rey, A. Cervilla, E. Llopis and A. Ribera, *Journal of Catalysis*, 1995, **152**, 237-242.
150. S.-I. Katahira and K. Yasue, *Journal of Materials Research*, 1999, **14**, 1178-1180.
151. H. Tagaya, A. Ogata, T. Kuwahara, S. Ogata, M. Karasu, J.-i. Kadokawa and K. Chiba, *Microporous Materials*, 1996, **7**, 151-158.
152. S. Aisawa, H. Hirahara, K. Ishiyama, W. Ogasawara, Y. Umetsu and E. Narita, *Journal of Solid State Chemistry*, 2003, **174**, 342-348.

153. S. Aisawa, H. Hirahara, S. Takahashi, Y. Umetsu and E. Narita, *Chemistry Letters*, 2004, **33**, 306-307.
154. T. Lopez, E. Ramos, P. Bosch, M. Asomoza and R. Gomez, *Materials Letters*, 1997, **30**, 279-282.
155. R. Ma, K. Takada, K. Fukuda, N. Iyi, Y. Bando and T. Sasaki, *Angewandte Chemie International Edition*, 2008, **47**, 86-89.
156. A. M. Fogg, J. S. Dunn, S.-G. Shyu, D. R. Cary and D. O'Hare, *Chemistry of Materials*, 1998, **10**, 351-355.
157. A. M. Fogg, V. M. Green, H. G. Harvey and D. O'Hare, *Advanced Materials*, 1999, **11**, 1466-1469.
158. H. Tagaya, N. Sasaki, H. Morioka and J. Kadokawa, *Molecular Crystals and Liquid Crystals Science and Technology. Section A. Molecular Crystals and Liquid Crystals*, 2000, **341**, 413-418.
159. Y. Seida and Y. Nakano, *Water Research*, 2002, **36**, 1306-1312.
160. Y. Xu, Y. Dai, J. Zhou, Z. P. Xu, G. Qian and G. Q. M. Lu, *Journal of Materials Chemistry*, 2010, **20**, 4684-4691.
161. K. H. Goh, T. T. Lim and Z. L. Dong, *Water Science and Technology*, 2010, **61**, 1411-1417.
162. M. Z. b. Hussein, Z. Zainal, I. Yaziz and T. C. Beng, *Journal of Environmental Science and Health, Part A*, 2001, **36**, 565-573.
163. F. B. D. Saiah, B.-L. Su and N. Bettahar, *Macromolecular Symposia*, 2008, **273**, 125-134.
164. F. B. D. Saiah, B.-L. Su and N. Bettahar, *Journal of Hazardous Materials*, 2009, **165**, 206-217.
165. S. Jin, P. H. Fallgren, J. M. Morris and Q. Chen, *Science and Technology of Advanced Materials*, 2007, **8**, 67-70.
166. J. M. Morris, S. Jin and K. Cui, *Chemical Engineering Journal*, 2008, **145**, 160-163.
167. J.-A. Park, C.-G. Lee, S.-J. Park, J.-H. Kim and S.-B. Kim, *Environmental Engineering Research*, 2010, **15**, 149-156.
168. R. Chitrakar, S. Tezuka, A. Sonoda, K. Sakane, K. Ooi and T. Hirotsu, *Journal of Colloid and Interface Science*, 2005, **290**, 45-51.
169. L. Lv, *Journal of Water Supply: Research and Technology*, 2006, **55**, 413-418.
170. L. P. Cardoso and J. B. Valim, *Journal of Physics and Chemistry of Solids*, 2006, **67**, 987-993.
171. I. Y. Park, K. Kuroda and C. Kato, *Journal of the Chemical Society, Dalton Transactions*, 1990, 3071-3074.
172. T. Kuwahara, H. Tagaya and K. Chiba, *Microporous Materials*, 1995, **4**, 247-250.
173. S. Mandal, D. Tichit, D. A. Lerner and N. Marcotte, *Langmuir*, 2009, **25**, 10980-10986.
174. Z. Sun, L. Jin, W. Shi, M. Wei, D. G. Evans and X. Duan, *Langmuir*, 2011, **27**, 7113-7120.
175. O. C. Wilson, T. Olorunyolemi, A. Jaworski, L. Borum, D. Young, A. Siriwat, E. Dickens, C. Oriakhi and M. Lerner, *Applied Clay Science*, 1999, **15**, 265-279.
176. T. Kwon, G. A. Tsigdinos and T. J. Pinnavaia, *Journal of the American Chemical Society*, 1988, **110**, 3653-3654.
177. C. Misra and A. J. Perrotta, *Clays and Clay Minerals*, 1992, **40**, 145-150.

178. E. L. Salinas and Y. Ono, *Bulletin of the Chemical Society of Japan*, 1992, **65**, 2465-2470.
179. E. Káfuňková, C. Taviot-Guého, P. Bezdička, M. Klementová, P. Kovář, P. Kubát, J. Mosinger, M. Pospíšil and K. Lang, *Chemistry of Materials*, 2010, **22**, 2481-2490.
180. A. Clearfield, M. Kieke, J. Kwan, J. L. Colon and R. C. Wang, *Journal of Inclusion Phenomena and Macrocyclic Chemistry*, 1991, **11**, 361-378.
181. J. Inacio, C. Taviot-Guého, C. Forano and J. P. Besse, *Applied Clay Science*, 2001, **18**, 255-264.
182. L. P. Cardoso, R. Celis, J. Cornejo and J. o. B. Valim, *Journal of Agricultural and Food Chemistry*, 2006, **54**, 5968-5975.
183. J. Cornejo, R. Celis, I. Pavlovic and M. A. Ulibarri, *Clay Minerals*, 2008, **43**, 155-175.
184. E. Touloupakis, A. Margelou and D. F. Ghanotakis, *Pest Management Science*, 2011, **67**, 837-841.
185. C. Del Hoyo, *Applied Clay Science*, 2007, **36**, 103-121.
186. M. Baek, I.-S. Kim, J. Yu, H.-E. Chung, J.-H. Choy and S.-J. Choi, *Journal of Nanoscience and Nanotechnology*, 2011, **11**, 1803-1806.
187. S. Aisawa, S. Takahashi, W. Ogasawara, Y. Umetsu and E. Narita, *Journal of Solid State Chemistry*, 2001, **162**, 52-62.
188. S. Aisawa, S. Sasaki, S. Takahashi, H. Hirahara, H. Nakayama and E. Narita, *Journal of Physics and Chemistry of Solids*, 2006, **67**, 920-925.
189. M. S. Gasser, *Colloids and Surfaces B: Biointerfaces*, 2009, **73**, 103-109.
190. V. Ambrogi, G. Fardella, G. Grandolini and L. Perioli, *International Journal of Pharmaceutics*, 2001, **220**, 23-32.
191. J.-H. Choy, S.-Y. Kwak, J.-S. Park, Y.-J. Jeong and J. Portier, *Journal of the American Chemical Society*, 1999, **121**, 1399-1400.
192. S. Aisawa, N. Higashiyama, S. Takahashi, H. Hirahara, D. Ikematsu, H. Kondo, H. Nakayama and E. Narita, *Applied Clay Science*, 2007, **35**, 146-154.
193. S.-J. Choi, G. E. Choi, J.-M. Oh, Y.-J. Oh, M.-C. Park and J.-H. Choy, *Journal of Materials Chemistry*, 2010, **20**, 9463-9469.
194. A. C. S. Alcantara, P. Aranda, M. Darder and E. Ruiz-Hitzky, *Journal of Materials Chemistry*, 2010, **20**, 9495-9504.
195. L. Perioli, V. Ambrogi, L. di Nauta, M. Nocchetti and C. Rossi, *Applied Clay Science*, 2011, **51**, 407-413.
196. S. Pitsch, R. Krishnamurthy and G. Arrhenius, *Helvetica Chimica Acta*, 2000, **83**, 2398-2411.
197. P. Liu, C. Wang and C. Li, *Journal of Catalysis*, 2009, **262**, 159-168.
198. B. M. Choudary, B. Bharathi, C. V. Reddy, M. L. Kantam and K. V. Raghavan, *Chemical Communications*, 2001, 1736-1737.
199. M. L. Kantam, A. Ravindra, C. V. Reddy, B. Sreedhar and B. M. Choudary, *Advanced Synthesis & Catalysis*, 2006, **348**, 569-578.
200. S. Abelló, S. Dhir, G. Colet and J. Pérez-Ramírez, *Applied Catalysis A: General*, 2007, **325**, 121-129.
201. J. Ashok, M. Subrahmanyam and A. Venugopal, *International Journal of Hydrogen Energy*, 2008, **33**, 2704-2713.
202. Z. P. Xu, J. Zhang, M. O. Adebajo, H. Zhang and C. Zhou, *Applied Clay Science*, 2011, **53**, 139-150.
203. S.-i. Fujita, Y. Kanamori, A. M. Satriyo and N. Takezawa, *Catalysis Today*, 1998, **45**, 241-244.

204. G. G. C. Arizaga, K. G. Satyanarayana and F. Wypych, *Solid State Ionics*, 2007, **178**, 1143-1162.
205. M. Avrami, *The Journal of Chemical Physics*, 1939, **7**, 1103-1112.
206. M. Avrami, *The Journal of Chemical Physics*, 1940, **8**, 212-224.
207. M. Avrami, *The Journal of Chemical Physics*, 1941, **9**, 177-184.
208. B. V. Erofe'ev, *Comptes Rendus de l'Académie des Sciences de l'URSS*, 1946, **52**, 511.
209. R. M. R. Bull, C. Markland, G. R. Williams and D. O'Hare, *Journal of Materials Chemistry*, 2011, **21**, 1822-1828.
210. W. Huang, H. Zhang and D. Pan, *AIChE Journal*, 2011, **57**, 1936-1946.
211. D. W. Henderson, *Journal of Thermal Analysis and Calorimetry*, 1979, **15**, 325-331.
212. G. R. Williams, D.Phil Thesis, University of Oxford, 2005.
213. J. D. Hancock and J. H. Sharp, *Journal of the American Ceramic Society*, 1972, **55**, 74-77.
214. J. Zeldovich and S. Z. Roginsky, *Acta Physicochimia (U.R.S.S.)*, 1934, **1**, 449.
215. S. Y. Elovich and G. M. Zhabrova, *Zhurnal Fizicheskoi Khimii*, 1939, **13**, 1761-1775.
216. S. H. Chien and W. R. Clayton, *Soil Science Society of America Journal*, 1980, **44**, 265-268.
217. D. L. Sparks, *Environmental Soil Chemistry*, Elsevier Science (USA), 2003.
218. D. L. Sparks and P. M. Jardine, *Soil Science Society of America Journal*, 1981, **45**, 1094-1099.
219. T. Kodama, Y. Harada, M. Ueda, K.-i. Shimizu, K. Shuto and S. Komarneni, *Langmuir*, 2001, **17**, 4881-4886.
220. H. Freundlich, *Zeitschrift für Physikalische Chemie*, 1907, **57**, 385-471.
221. S. Kuo and E. G. Lotse, *Soil Science*, 1973, **116**, 400-406.
222. D. L. Sparks, L. W. Zelazny and D. C. Martens, *Soil Science Society of America Journal*, 1980, **44**, 37-40.
223. J. Crank, *The Mathematics of Diffusion*, Oxford University Press (Clarendon), 1976.

Chapter 2

Intercalation and Release of Taste-Modifying Agents

2.1 Introduction

One application of special interest in the use of layered double hydroxide materials is the preparation of bio-inorganic hybrids by the intercalation of bioanions into the LDH interlayer space.[1] The guest species, which can include amino acids,[2, 3] drugs[4-7] and vitamins,[8, 9] are stabilised with respect to heat and light upon intercalation.[10, 11] Furthermore, the resultant nanocomposites can act as reservoirs for the biomolecules, releasing them in a controlled manner under appropriate conditions. For most metallic combinations, the host materials are biocompatible both *in vitro* and *in vivo*,[12] and due to the excellent anion exchange capacities of the host, the amount of metal cations leached is typically low.

A seldom-examined application of LDH-biomolecule nanohybrids is the intercalation of fragrances or flavouring compounds for addition to foodstuffs to provide enhanced retention of flavour.[13, 14] This could be particularly useful in materials that are intended to persist in the mouth, such as chewing gum. It is even possible that the masticated compound may discharge its flavour over a lengthy period while simultaneously absorbing less pleasant-tasting anions. While there has been some work undertaken on the intercalation of sugars and sugar derivatives into LDH hosts,[15-17] the intercalation of artificial sweeteners and the applications of the hybrid materials produced have been neglected.[3]

Acesulfame K, cyclamate and saccharin are found commercially in a variety of food products including diet soft drinks, beverage concentrates, and low-calorie

confectionery. These sweeteners are often found individually to possess a somewhat unpleasant 'metallic' aftertaste,[18-20] which can be eliminated in practice through the use of combinations of the sweeteners,[21] or by addition of a bitterness-inhibiting agent (such as caffeic or ferulic acid).[22] It is possible to further potentiate the sweetness of the compounds through the addition in low concentrations of bitter methylxanthines such as caffeine or theobromine.[23, 24]

In this Chapter, the intercalation of three commercial sugar substitutes (acesulfame K, cyclamate, and saccharin) into $[Ca_2Al(OH)_6]NO_3 \cdot yH_2O$ ("Ca/Al-NO_3 LDH"), $[LiAl_2(OH)_6]Cl \cdot yH_2O$ ("Li/Al-Cl LDH") and $[Mg_2Al(OH)_6]NO_3 \cdot yH_2O$ ("Mg/Al-NO_3 LDH") is reported, in addition to the incorporation of ferulate and theobromine (a bitterness inhibitor and a flavour potentiator, respectively). The structures of the five guests are shown in Figure 2.1.

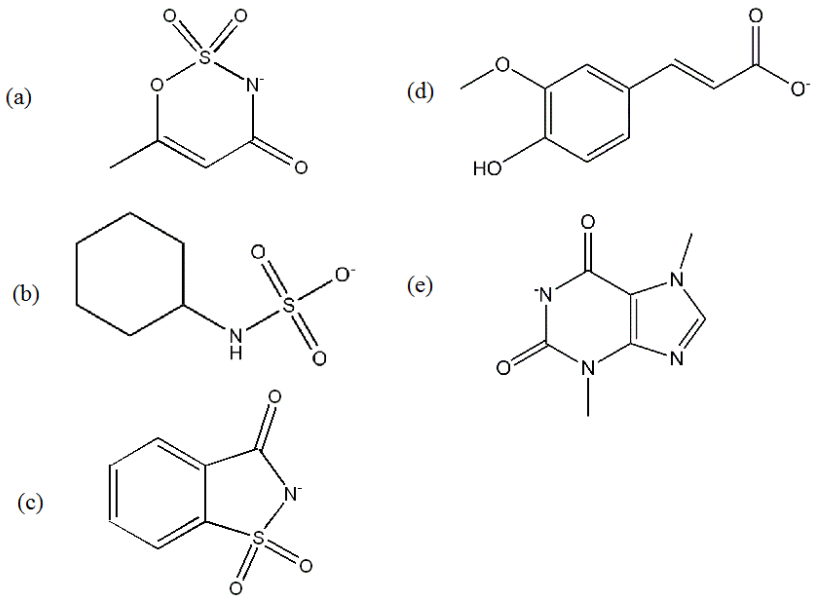

Figure 2.1: The structures of the anions of (a) acesulfame K, (b) cyclamate, (c) saccharin, (d) ferulic acid, and (e) theobromine.

Successful intercalation is confirmed by X-ray diffraction (XRD), Fourier transform infra-red (FTIR) and nuclear magnetic resonance spectroscopy (NMR), elemental microanalysis and thermogravimetric analysis (TGA). The release of the

guests from the solid is studied using UV/Vis spectroscopy in both deionised water, and an artificial saliva solution. The release processes are analysed using a variety of kinetic models.

Three of the guests intercalated (acesulfame K, saccharin, and theobromine) are formed initially by deprotonation of a N-atom in a heterocyclic ring system; this has only rarely been observed in guests intercalated into LDH systems.[25-27] The effect of these unusual guest structures on the apparent stacking of the guests in the interlayer space will also be investigated.

2.2 Powder X-ray Diffraction Data

2.2.1 Artificial Sweeteners

The XRD patterns of the intercalation compounds of the artificial sweeteners into Ca/Al-, Li/Al- and Mg/Al-LDH hosts are shown in Figures 2.2, 2.3 and 2.4 respectively, along with the patterns of the precursor LDHs from which they were synthesised.

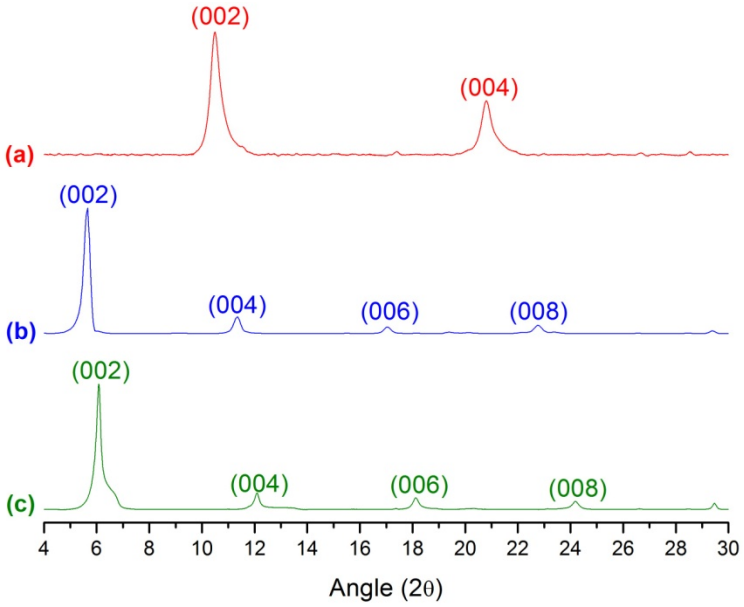

Figure 2.2: Powder XRD patterns of (a) the Ca/Al-NO_3 LDH, (b) the Ca/Al-Cyclamate LDH, and (c) the Ca/Al-Saccharin LDH. The d-spacings of the (002) reflections of the above patterns are 8.6, 15.5 and 14.7Å respectively.

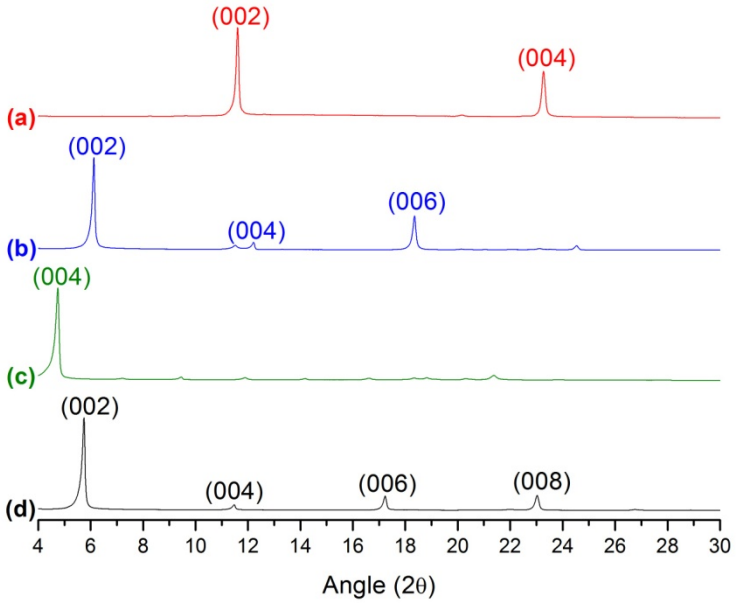

Figure 2.3: Powder XRD patterns of (a) the Li/Al-Cl LDH, (b) the Li/Al-Acesulfame LDH, (c) the Li/Al-Cyclamate LDH, and (d) the Li/Al-Saccharin LDH. The d-spacings of the (002) reflections of the above patterns are 7.2, 14.4, 37.2 and 15.4Å respectively.

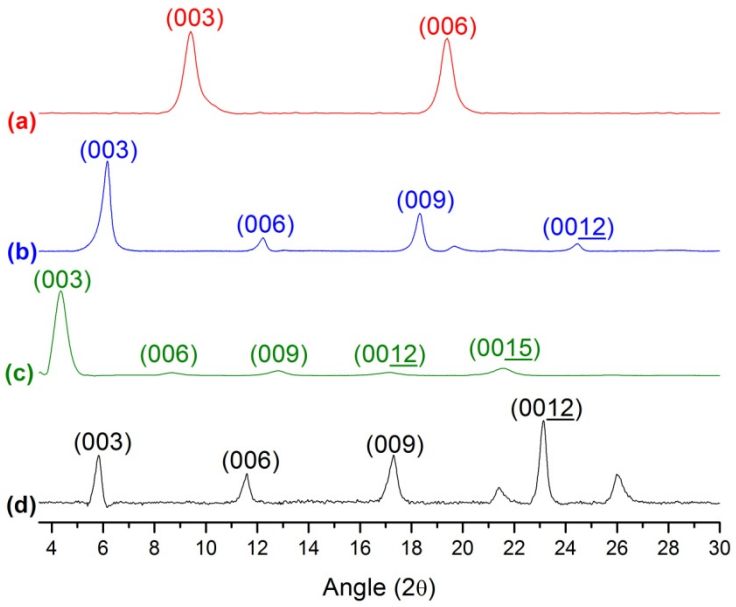

Figure 2.4: Powder XRD patterns of (a) the Mg/Al-NO_3 LDH, (b) the Mg/Al-Acesulfame LDH, (c) the Mg/Al-Cyclamate LDH, and (d) the Mg/Al-Saccharin LDH. The d-spacings of the (003) reflections of the above patterns are 8.5, 14.3, 21.8 and 15.2Å respectively.

The characteristic shift of the basal (00*l*) reflections to lower angle indicates expansion of the interlayer separation upon intercalation of the molecules. Comparison of the gallery heights with the dimensions of the intercalated molecules yields insights into the arrangement of the guest anions within the interlayer space. These calculations are summarised in Table 2.1. The length of the guest anion was determined in each case by measuring the through-space separation of the charge-bearing atom, and the most distant atom in the molecule, with the van der Waals radii of each atom added; further details of the molecular size calculations may be found in Appendix A, Section A.6. The thickness of an LDH metal hydroxide layer, as determined by single-crystal diffraction, is 4.8Å.[28]

Table 2.1: Comparison of the artificial sweetener guest molecule lengths to the observed gallery heights (IB = interdigitated bilayer). The d-spacing represents the distance between the centres of two consecutive layers, while the gallery height corresponds to the 'empty' space between two consecutive layers, and equals the d-spacing minus 4.8Å.

Guest	Guest Length (Å)	Metals	d-spacing (Å)	Gallery Height (Å)	(Gallery Height)/ (Guest Length)	Probable Arrangement
Acesulfame	7.5	Li/Al	14.4	9.6	1.3	IB
		Mg/Al	14.3	9.5	1.3	IB
Cyclamate	10.2	Ca/Al	15.5	10.7	1.0	Monolayer
		Li/Al	37.2 / 20.3	32.4 / 15.5	3.2 / 1.5	Hydrated Structure / IB
		Mg/Al	21.8	17.0	1.7	IB
Saccharin	8.6	Ca/Al	14.7	9.9	1.2	IB
		Li/Al	15.4	10.6	1.2	IB
		Mg/Al	15.2	10.4	1.2	IB

The gallery height is typically 20-70% greater than the length of the guest, suggesting the formation of an interdigitated bilayer in the interlayer space. For the Ca/Al-Cyclamate LDH, the gallery height is almost precisely equal to the guest length, suggesting the formation of a monolayer of anions. The gallery height of the Li/Al-Cyclamate LDH is somewhat unusual: the post-intercalation compound produces an X-ray pattern that suggests a gallery height of 32.4Å, which corresponds to approximately three times the length of the cyclamate molecule. It is thought that this occurs as a result of large amounts of water being present between the layers: when the Li/Al-Cyclamate LDH product is heated at 80ºC for one hour, the pattern changes significantly with a resultant gallery height of only 15.5Å in the product, corresponding to an interdigitated bilayer (analogous to the Mg/Al-Cyclamate LDH). The XRD patterns of the Li/Al-Cyclamate LDH before and after heating are shown in Figure 2.5.

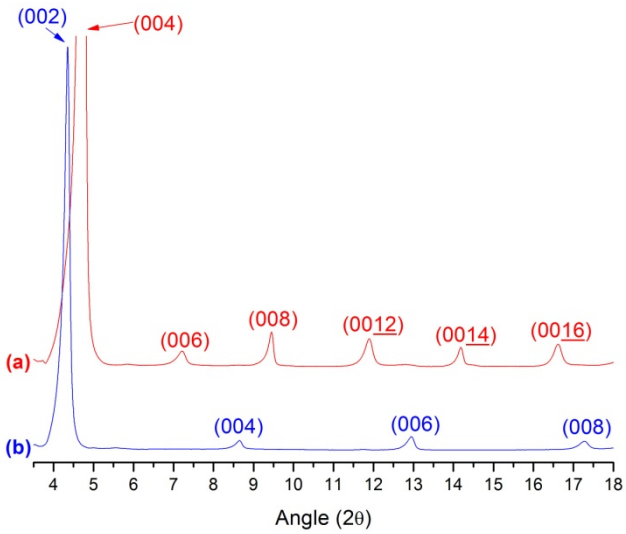

Figure 2.5: Powder XRD pattern of the Li/Al-Cyclamate LDH (a) in its hydrated form, and (b) after heating at 80ºC for one hour. The d-spacings of the (002) reflections of the above patterns are 37.2 and 20.3Å respectively.

The reflections of the first product are relatively broad and asymmetric, resulting from a high degree of disorder within the structure (most likely due to the turbostratification in the stacking of the solid, and the interstratification of varying numbers of cointercalated water molecules between consecutive layers). The heating of this greatly expanded, heavily hydrated structure leads to the loss of most of the interlayer water molecules, allowing the layers to realign into a more ordered structure. Subsequent attempts to reverse the effects of heating by the addition of water did not yield any changes to the X-ray pattern of the product, which is consistent with this hypothesis: once the more stable, ordered, structure has formed, it is not possible to re-form the original structure.

The '*a*' lattice parameter for these compounds is not observed to change substantially upon intercalation, as it is independent of their gallery heights. A typical interdigitated bilayer stacking arrangement, for the Mg/Al-Saccharin LDH hybrid, is illustrated in Figure 2.6.

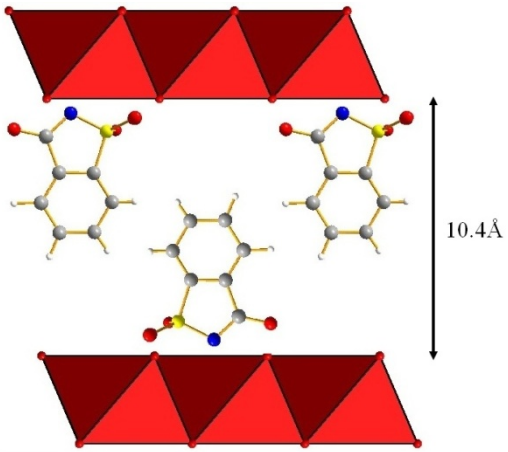

Figure 2.6: Schematic diagram illustrating the proposed orientation of Saccharin intercalated into a Mg/Al-LDH.

All three sweeteners could be intercalated into the Li/Al- and Mg/Al-LDHs. However, the attempted intercalation of acesulfame into the Ca/Al-NO_3 LDH consistently produced solid product that could not be indexed to an LDH unit cell. The product formed instead appeared to be a mixture of Ca and Al oxides and hydroxides.

The full structural parameters of the LDH products can be found in Appendix A, Section A.2.

2.2.2 Taste Modifiers

The XRD patterns of the Ca/Al-, Li/Al- and Mg/Al-LDH intercalation compounds of ferulate and theobromine are given in Figures 2.7, 2.8 and 2.9, as well as the pattern of the chloride precursor LDH. The relative sizes of the calculated gallery heights and the lengths of the intercalated molecules are shown in Table 2.2.

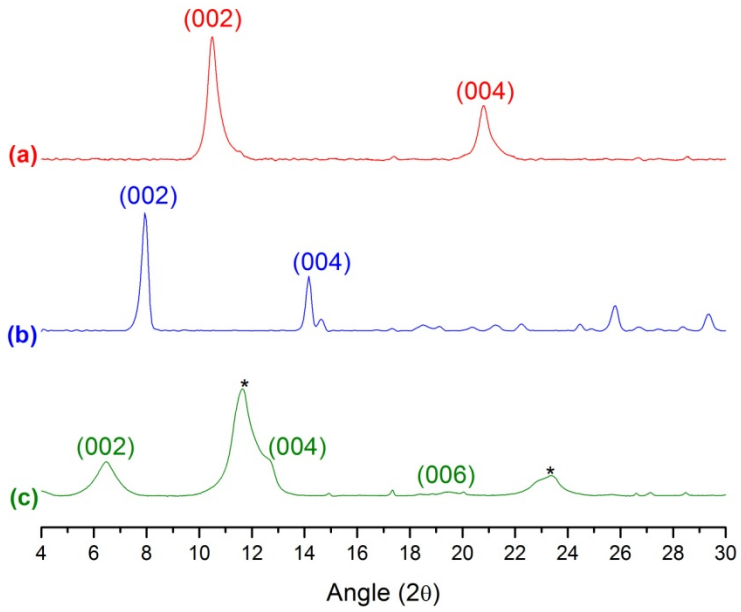

Figure 2.7: Powder XRD patterns of (a) the Ca/Al-NO_3 LDH, (b) the Ca/Al-Ferulate LDH, and (c) the Ca/Al-Theobromine LDH. The d-spacings of the (002) reflections of the above patterns are 8.6, 11.1 and 13.6Å respectively. Non-product phases are marked with asterisks.

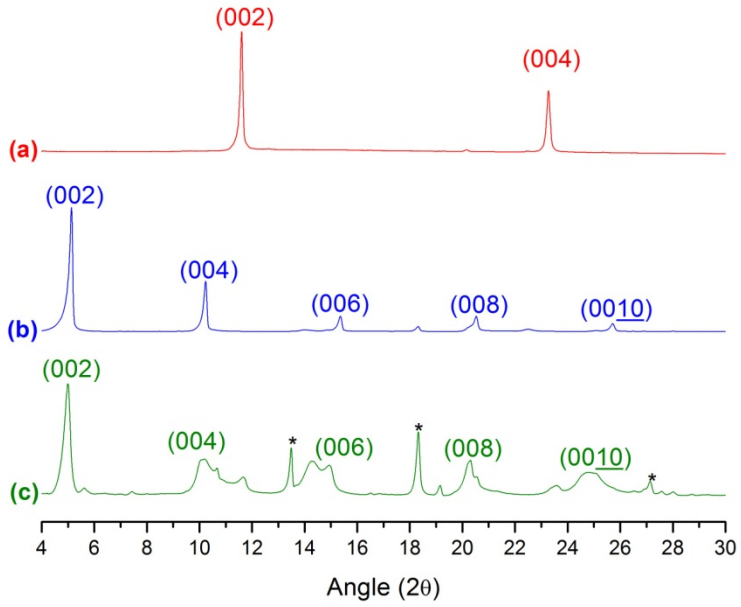

Figure 2.8: Powder XRD patterns of (a) the Li/Al-Cl LDH, (b) the Li/Al-Ferulate LDH, and (c) the Li/Al-Theobromine LDH. The d-spacings of the (002) reflections of the above patterns are 7.2, 17.2 and 17.7Å respectively. Non-product phases are marked with asterisks.

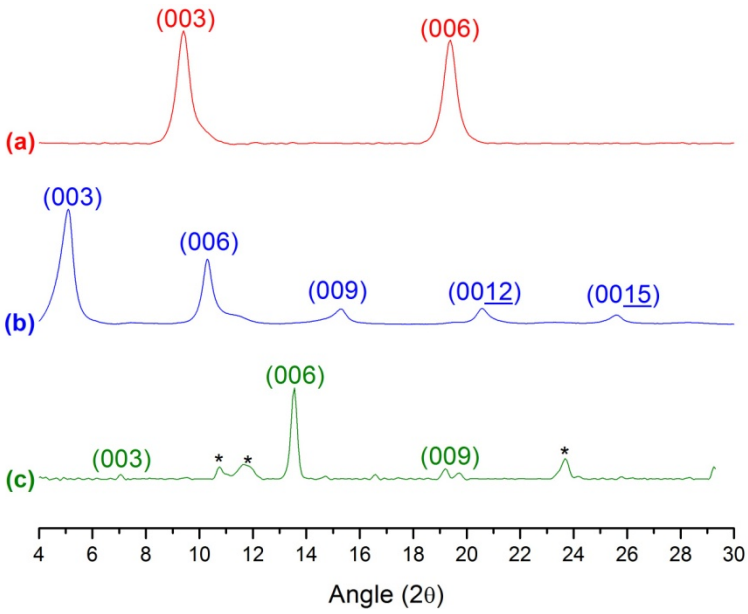

Figure 2.9: Powder XRD patterns of (a) the Mg/Al-NO_3 LDH, (b) the Mg/Al-Ferulate LDH, and (c) the Mg/Al-Theobromine LDH. The d-spacings of the (003) reflections of the above patterns are 8.5, 17.3 and 13.0Å respectively. Non-product phases are marked with asterisks.

Table 2.2: Comparison of the taste modifier molecule lengths to the observed gallery heights (IB = interdigitated bilayer).

Guest	Guest Length (Å)	Metals	d-spacing (Å)	Gallery Height (Å)	(Gallery Height)/ (Guest Length)	Probable Arrangement
Ferulate	11.9	Ca/Al	11.1	6.3	0.5	Tilted Monolayer
		Li/Al	17.2	12.4	1.0	Monolayer
		Mg/Al	17.3	12.5	1.1	Monolayer
Theobromine	10.0	Ca/Al	13.6	8.8	0.9	Tilted Monolayer
		Li/Al	17.7	12.9	1.3	IB
		Mg/Al	13.0	8.2	0.8	Tilted Monolayer

The ferulate and theobromine intercalation compounds demonstrate similarly increased interlayer spacings to the artificial sweeteners. The Li/Al- and Mg/Al-Ferulate LDH intercalates have gallery heights which match the end-to-end lengths of the guests to within 10%, indicating that an antiparallel monolayer of

anions nearly perpendicular to the metal hydroxide layers is adopted, while a tilted monolayer is more probable in the Ca/Al-Ferulate LDH compound. A similar arrangement is observed in the Mg/Al-Theobromine LDH, which shows a gallery height which is only equal to 80% of the maximum length of the molecule.

Both guests could be intercalated into all three LDH hosts. Upon intercalation of theobromine into the Li/Al-Cl LDH, partial leaching of lithium was observed from the structure, producing traces of gibbsite and other hydrated aluminium oxide species, marked as starred peaks in Figure 2.8.

2.3 FTIR Data

2.3.1 Artificial Sweeteners

It is possible to qualitatively determine the presence of anions in the interlayer space of a layered double hydroxide through examination of the FTIR spectrum of the solid before and after intercalation. Typically, after intercalation, IR absorptions associated with the exchangeable anions of the precursor LDH will be absent, while those of the newly-intercalated guest will be present. A comparison of the spectra of the precursor LDH, guest, and the intercalation product are plotted in Figure 2.10 for the case of the Li/Al-Acesulfame LDH.

The precursor LDH shows expectedly few IR absorptions: only the ν_{OH} absorptions of cointercalated water (centred at *ca.* 3400cm^{-1}), those of the δ_{OH} mode of the hydroxide layers and interlayer water molecules (*ca.* 1640cm^{-1}) and the various metal-oxygen stretching and bending modes found below 1000cm^{-1} are present. While the characteristically strong ν_{NO} absorption of to the nitrate anion can be seen at 1350cm^{-1} in the Ca/Al-NO_3 LDH and Mg/Al-NO_3 LDH precursors, there are predictably no absorptions attributable to Cl^- present in the Li/Al-Cl LDH.

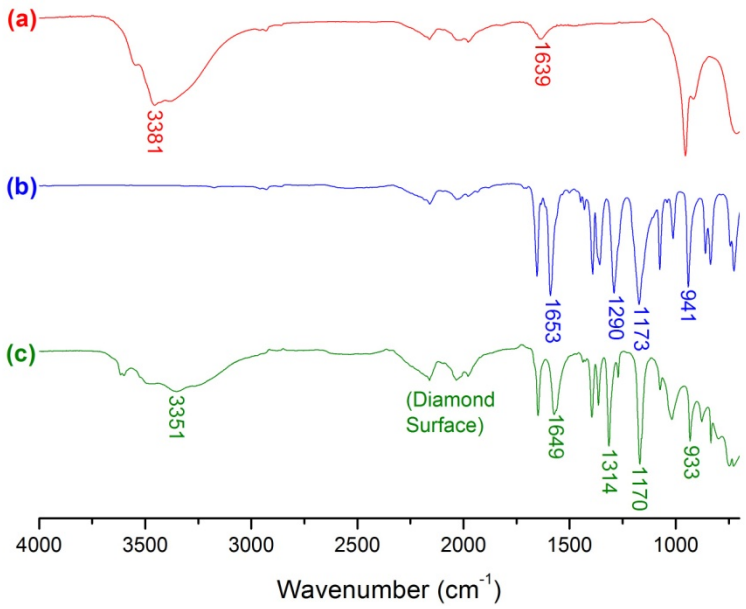

Figure 2.10: FTIR Transmittance Spectra of (a) the Li/Al-Cl LDH, (b) Acesulfame K and (c) the Li/Al-Acesulfame LDH. The irregular absorptions found between 1900 and 2200cm^{-1} are due to the diamond surface of the reflectance surface.

The spectrum of acesulfame K shows a number of absorptions that are also present in the intercalated product. These include, most prominently, the $\nu_{C=O}$ absorption (1655cm^{-1}), symmetric ν_{SO2} (1173cm^{-1}) and asymmetric ν_{CNS} vibrations (941cm^{-1}).[29] The asymmetric ν_{SO2} absorption, found in acesulfame K as a sharp absorption at 1290cm^{-1}, is found in the in the intercalated product at 1314cm^{-1}. This significant shift suggests that the S=O bonds may interact strongly with the metal hydroxide layers, indicating a possible orientation of the intercalated molecules.

2.3.2 Taste Modifiers

Similarly, the spectrum of the Mg/Al-Ferulate LDH is illustrated in Figure 2.11, along with that of sodium ferulate and the precursor nitrate LDH. The nitrate absorption in the precursor is very apparent at 1346cm^{-1}, and its absence in the intercalated product is a strong indicator of complete exchange. The symmetric ν_{COC} absorption of sodium ferulate is found at 1123cm^{-1}, and almost the same energy in the

the Mg/Al-Ferulate LDH product; however, the ν_{COH}, and symmetric and asymmetric ν_{OCO}- absorption bands are found to be noticeably shifted from the solid salt (1265, 1383 and 1499cm^{-1}) to the intercalation product (1279, 1393 and 1516cm^{-1}).[30] Given the structure of the molecule, and its perpendicular monolayer arrangement as determined by XRD, it seems possible that the charged carboxylate group and the polarised phenol are interacting with the charged metal layers to a certain extent.

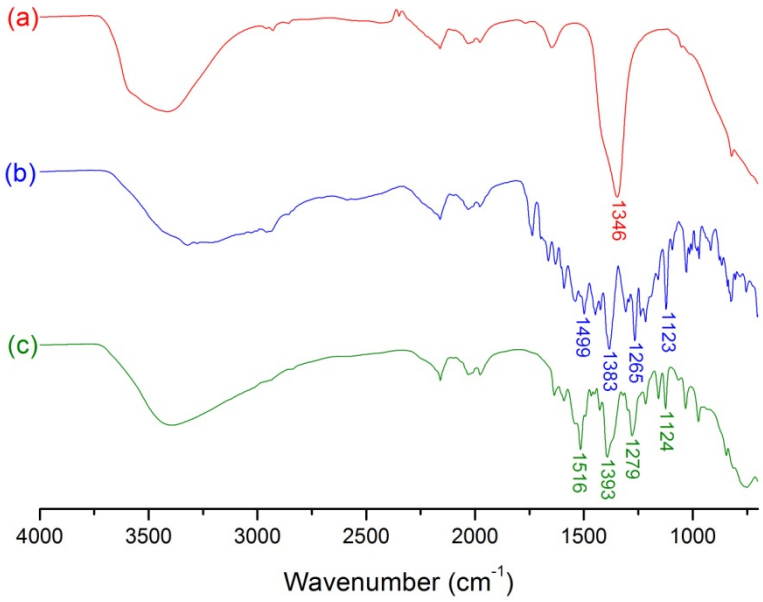

Figure 2.11: FTIR Transmittance Spectra of (a) the Mg/Al-NO_3 LDH, (b) Sodium Ferulate, and (c) the Mg/Al-Ferulate LDH.

2.4 TGA Data

2.4.1 Artificial Sweeteners

Thermogravimetric analysis (TGA) provides data on the behaviour of the LDH material when heated under an inert atmosphere. This allows for accurate determination of the cointercalated water content of the solid, in addition to establishing any stabilising effect that the LDH lattice may have on the intercalated guest. The TGA plot for the Li/Al-Cyclamate LDH (in its initial, hydrated form) is depicted in Figure 2.12.

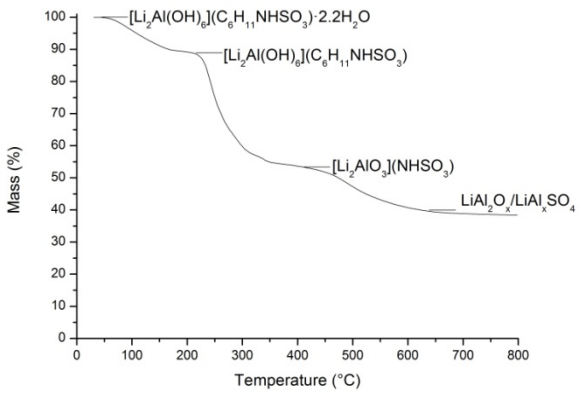

Figure 2.12: TGA plot of the Li/Al-Cyclamate LDH.

There are three principal mass losses observed. The first, beginning at *ca.* 60ºC and concluding at around 190ºC, corresponds to the evaporation of the cointercalated water, leaving a dehydrated LDH with the interlayer guest still intercalated (calculated mass loss 10.4%, observed loss 10.6%). The second loss of mass between 200 and 350ºC corresponds to two simultaneous processes: the partial dehydration of the LDH layers to a layered oxide, and the partial decomposition of the intercalated cyclamate, which loses its cyclohexyl moiety (calculated 41.2%, observed 36.2%). The final decomposition step is due to the final decomposition of the remaining sulfamate, leaving a final product that consists of a mixture of amorphous lithiated alumina and aluminium sulfates (calculated 14.9%, observed 12.5%).[31] Unusually for an LDH intercalated with a hydrocarbon-based guest, the final decomposition product after heating to 800ºC contains no carbon 'soot', as the cyclohexyl group is rapidly lost in the second step.

2.4.2 Taste Modifiers

TGA data was also collected for the Ca/Al-Ferulate LDH. The plot of this data is given in Figure 2.13.

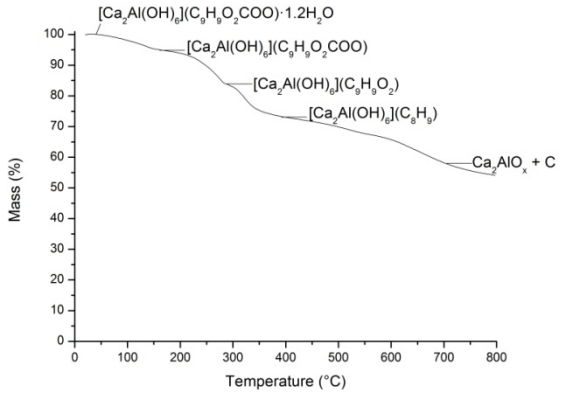

Figure 2.13: TGA plot of the Ca/Al-Ferulate LDH.

Four clear steps are observed in the process. In the first step, cointercalated water is lost at temperatures up to 150ºC, leaving a dehydrated LDH (calculated. 5.1%, observed 5.0%). This is then followed by the loss of water from the hydroxide layers (calculated. 12.8%, observed 11.5%), and the decarboxylation of the ferulate anion in two consecutive steps between 200 and 400ºC (calculated 10.4%, observed 10.3%).[30] The final step, from around 450ºC onwards, is a combination of the further decomposition of the guest and the dehydration of the hydroxide layers, resulting in a product that is a mixture of calcium and aluminium oxides, and an indeterminate amount of carbon soot (accompanied by an observed mass loss of 19.9%). The same decomposition processes are also observed in the Li/Al- and Mg/Al-Ferulate LDHs.

2.5 ^{13}C CP/MAS NMR Data

The artificial sweetener intercalates were studied by cross-polarisation magic angle spinning (CP/MAS) ^{13}C NMR to demonstrate the intact intercalation of the guests into the LDH lattice. The intercalates' spectra were found to match those of the corresponding guest salt, although a significant amount of line-broadening was observed in most cases, due to the increased disorder of the guests in the interlayer space (*cf.* their salts). Figure 2.14 shows the spectrum of solid Acesulfame K, compared to the spectrum of the same anion intercalated into a Mg/Al-LDH.

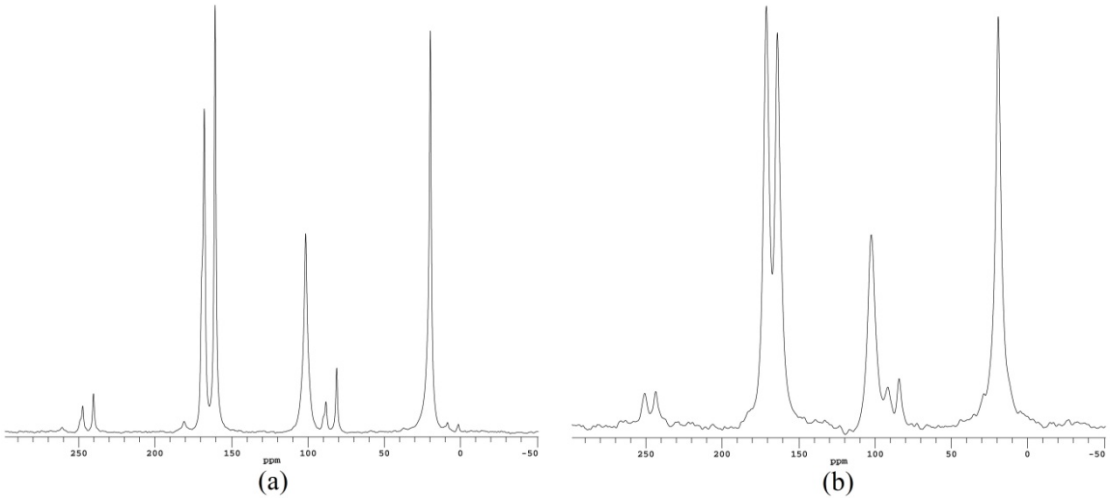

Figure 2.14: ^{13}C CP/MAS NMR spectra of (a) Acesulfame K, and (b) Mg/Al-Acesulfame LDH.

2.6 Elemental Analysis Data

2.6.1 Artificial Sweeteners

The approximate chemical formulae of the artificial sweetener LDH intercalates were determined through a combination of the TGA data (for the cointercalated water content), and CHN/ICP elemental microanalysis. The results are summarised in Table 2.3, and the precise elemental values determined can be found in Appendix B, Section B.2.

The artificial sweeteners are highly compatible with the LDHs, and in each case more than 70% of the layer charge is balanced by the sweetener guest anions. These high loadings suggest that these hosts would act as excellent reservoirs for these guests. The remaining charge is balanced by unexchanged chloride and nitrate anions, and some carbonate (from dissolution of atmospheric carbon dioxide in the basic reaction solutions). The numbers of cointercalated water molecules per mole are typical for LDH systems.

Table 2.3: Approximate chemical formulae of the sweetener-intercalated LDHs.

Metallic Combination	Intercalated Molecule	Chemical Formula
Ca/Al	Cyclamate	$[Ca_2Al(OH)_6](C_6H_{12}NO_3S)_{0.76}(CO_3)_{0.12}\cdot 2.4H_2O$
	Saccharin	$[Ca_2Al(OH)_6](C_7H_4NO_3S)_{0.76}(NO_3)_{0.24}\cdot 2H_2O$
Li/Al	Acesulfame	$[LiAl_2(OH)_6](C_4H_4NO_4S)_{0.73}Cl_{0.27}\cdot 1.5H_2O$
	Cyclamate	$[LiAl_2(OH)_6](C_6H_{12}NO_3S)\cdot 2.2H_2O$
	Saccharin	$[LiAl_2(OH)_6](C_7H_4NO_3S)\cdot 1.2H_2O$
Mg/Al	Acesulfame	$[Mg_2Al(OH)_6](C_4H_4NO_4S)_{0.99}(NO_3)_{0.01}\cdot H_2O$
	Cyclamate	$[Mg_2Al(OH)_6](C_6H_{12}NO_3S)_{0.7}(NO_3)_{0.3}\cdot 1.3H_2O$
	Saccharin	$[Mg_2Al(OH)_6](C_7H_4NO_3S)_{0.78}(CO_3)_{0.11}\cdot 0.9H_2O$

2.6.2 Taste Modifiers

The chemical formulae of the ferulate and theobromine materials were also determined by the same means. These are given in Table 2.4.

Table 2.4: Approximate chemical formulae of the taste modifier LDHs.

Metallic Combination	Intercalated Molecule	Chemical Formula
Ca/Al	Ferulate	$[Ca_2Al(OH)_6](C_{10}H_9O_4)\cdot 1.2H_2O$
	Theobromine	$[Ca_2Al(OH)_6](C_7H_7N_4O_2)_{0.21}(OH)_{0.79}\cdot H_2O$
Li/Al	Ferulate	$[LiAl_2(OH)_6](C_{10}H_9O_4)_{0.65}Cl_{0.35}\cdot 0.6H_2O$
	Theobromine	$[LiAl_2(OH)_6](C_7H_7N_4O_2)_{0.61}(OH)_{0.39}\cdot H_2O$
Mg/Al	Ferulate	$[Mg_2Al(OH)_6](C_{10}H_9O_4)_{0.85}(OH)_{0.15}\cdot H_2O$
	Theobromine	$[Mg_2Al(OH)_6](C_7H_7N_4O_2)_{0.69}(OH)_{0.31}\cdot H_2O$

While the loadings of these guests into these LDH products are somewhat less than those found for the artificial sweeteners, they are still sufficient for these compounds to be used for storage of the anions. A number of the theobromine products show hydroxide as the charge-balancing anion in addition to the target guest. This is due to

the relatively high pKa of theobromine, and the moderate instability of its anion in water, causing a degree of deprotonation of water to regenerate the neutral molecule and concurrently creating a slight excess of hydroxide anions in the solution.

2.7 Release Experiment Procedures

2.7.1 Preparation of Artificial Saliva

The artificial saliva solution used in the release experiments was prepared using the method described by Qiu:[32] to 500mL of deionised water were added 22mg of NaF, 1200mg of NaCl, 700mg of KCl, 55mg of $MgCl_2$, 520mg of KH_2PO_4 and 520mg of K_2HPO_4. 150mg of $CaCl_2$ was dissolved in a further 200mL of deionised water, and this solution was slowly added to the initial 500mL solution. This mixture was then made up to 1000mL by the addition of further deionised water.

2.7.2 Determination of Anion Concentrations

The degree of release of the anions from their hosts was determined by UV/Vis spectroscopy. Typically, 0.5g of the LDH-Guest composite was added to 50mL of either deionised water, or the artificial saliva solution, and stirred at a moderate rate at 37ºC. After the appropriate amount of time had elapsed, the reaction was filtered, and the concentration of release guest in the filtrate was determined.

The standard quantitative procedure for the determination of solution concentrations is the Beer-Lambert law, which logarithmically correlates the intensity of the most intense absorption peak to the concentration of the absorbing anion in solution. The UV spectra of four increasing concentrations of sodium saccharin that were used in preparing the calibration curve are shown in Figure 2.15.

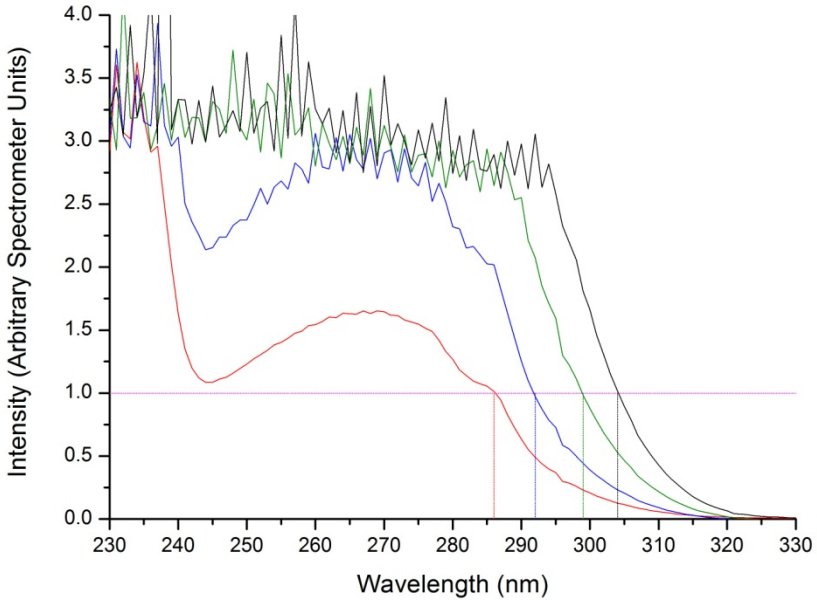

Figure 2.15: UV spectra of deionised water solutions containing sodium saccharin at concentrations of (a) 0.001M, (b) 0.002M, (c) 0.004M, and (d) 0.008M.

As can be seen above, attempting to use the conventional Beer-Lambert method for this anion results in a number of problems. The value of λ_{MAX} for sodium saccharin is 273nm,[33] and in the low-concentration calibration curve samples this absorption peak is clear and distinct, and its intensity accurately measurable (this can be seen for the 0.001M curve in Figure 2.15). However, as the concentration becomes higher, a degree of fine structure begins to appear in the absorption curves; as a result, precise measurement of the intensity maximum becomes highly challenging (noticeable in the 0.002M curve). Continuing slightly beyond this concentration leads to no discrete visible absorption, but a broad band nearly 100nm wide (seen in the 0.004 and 0.008M curves). In practice, many of the release samples lie in this region, making measurement of the intensities at λ_{MAX} essentially impossible, without repeated and carefully consistent dilution of every reaction filtrate.

Instead, a different surrogate approach was used to relate the spectra to the concentrations of the guest anions. It is apparent that one consistent feature for the UV spectra at successive increasing concentrations is the alignment of the spectra on their

initial rise in intensity. If an arbitrary, spectrometer-defined intensity of '1' is chosen, and the wavelength at which each spectrum crosses that intensity is calculated, it is possible to plot the value of this wavelength (λ_{CROSS}) against the known concentrations used. There is found to be a highly accurate logarithmic relationship between the two (as, in some ways, the value of λ_{CROSS} is a surrogate measure of the integral of the absorption peak). A plot of these λ_{CROSS} against the natural logarithm of the sodium saccharin concentration is shown in Figure 2.16.

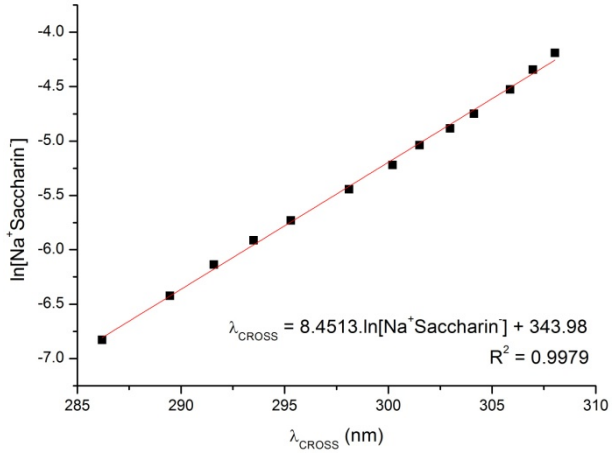

Figure 2.16: Plot of λ_{CROSS} against ln[$Na^+Saccharin^-$].

This consistent correlation was used throughout this Chapter to determine the solution concentrations of the deintercalated anions. The release of the anions was studied over time intervals of up to 180 minutes (considered to be a likely upper bound for the retention in the mouth of a confectionery product).

2.8 Kinetic Models for Release

The kinetic models used for analysing the data from the release profiles provided by the concentrations as determined by UV/Vis spectroscopy are briefly summarised in the sections below. Greater detail of the interpretation of these models is provided in Section 1.7 of Chapter 1.

For the equations of each model, a number of parameters are defined. t represents the amount of time (in minutes) that has elapsed since the beginning of the reaction – when there is an apparent induction time ('t_0'), this may be replaced by t - t_0. The concentration of the anion that has been released into solution after time t is given as C_t; the concentration of the anion present in the solid host before the reaction begins is given by C_0, so that the extent of the reaction (from zero to one) is defined as the ratio C_t/C_0, which may be abbreviated to the single extent of reaction parameter 'α'. The rate constant, where it may be determined, is represented as 'k_r', while 'm' and 'n' are reaction coefficients.

2.8.1 The Avrami-Erofe'ev Model

The general form of the Avrami-Erofe'ev equation is given as Equation 2.1 below.

$$[-\ln(1-\alpha)]^{\frac{1}{n}} = k_r t \qquad \textbf{Equation 2.1}$$

This may be rearranged to form Equation 2.2 below.

$$\ln[-\ln(1-\alpha)] = n \ln t + n \ln k_r \qquad \textbf{Equation 2.2}$$

Plotting the left side of the equation against ln t yields a straight line, with a gradient equal to n, and a y-axis intercept at n ln k_r. A plot of the data in this form is known as a Sharp-Hancock plot.[34]

2.8.2 The Elovich Model

The exponential Elovich model possesses the general form shown in Equation 2.3.[35]

$$1 - \frac{C_t}{C_0} = n \ln t + m \qquad \textbf{Equation 2.3}$$

This yields a linear plot when the left side is plotted against ln *t*, allowing reaction coefficients *n* and *m* to be determined from the gradient and intercept, respectively. These coefficients have not been determined to possess any chemical significance.[36]

2.8.3 The First-Order Model

The first-order model may be expressed in the form of Equation 2.4.

$$\ln\frac{C_t}{C_0} = -k_r t \qquad \textbf{Equation 2.4}$$

A simple plot of the left side against *t* yields a straight plot with a gradient of $-k_r$.

2.8.4 The Modified Freudlich Model

The modified Freundlich equation, proposed by Kuo and Lotse,[37, 38] is given in Equation 2.5.

$$C_0 - C_t = k_r C_0 t^n \qquad \textbf{Equation 2.5}$$

This may be arranged to give the form below (Equation 2.6), which may be plotted linearly.

$$\ln(C_0 - C_t) = (\ln k_r - \ln C_0) + n \ln t \qquad \textbf{Equation 2.6}$$

The left side may be plotted against ln *t* to give a straight line.

2.8.5 The Parabolic Diffusion Model

The form of the parabolic diffusion model used to give a linear plot is given below, in Equation 2.7.

$$\left(1 - \frac{C_t}{C_0}\right)\frac{1}{t} = k_r \frac{1}{\sqrt{t}} + n \qquad \textbf{Equation 2.7}$$

2.9 Release of Artificial Sweeteners

2.9.1 Release Profiles

Figure 2.17 shows the release of all three sweeteners from the Li/Al-LDH host in deionised water and saliva to indicate the relative release rates of the guests. Similarly, Figure 2.18 shows the release of saccharin from all three different hosts, to show the relative rate of release from each hybrid, with fitted lines provided to guide the eye. A summary of the t_{50} values and total release values is given in Table 2.5.

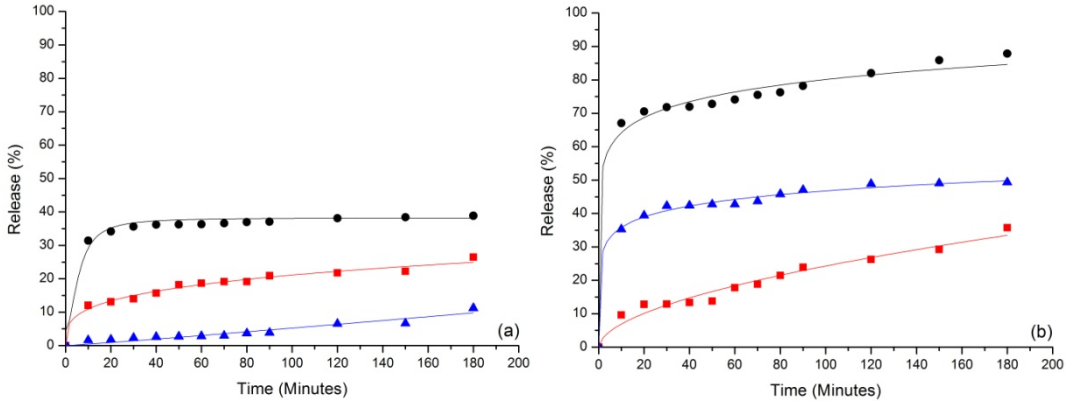

Figure 2.17: Release profiles of Acesulfame (■), Cyclamate (●), and Saccharin (▲) from Li/Al-LDH hosts in (a) deionised water, and (b) artificial saliva.

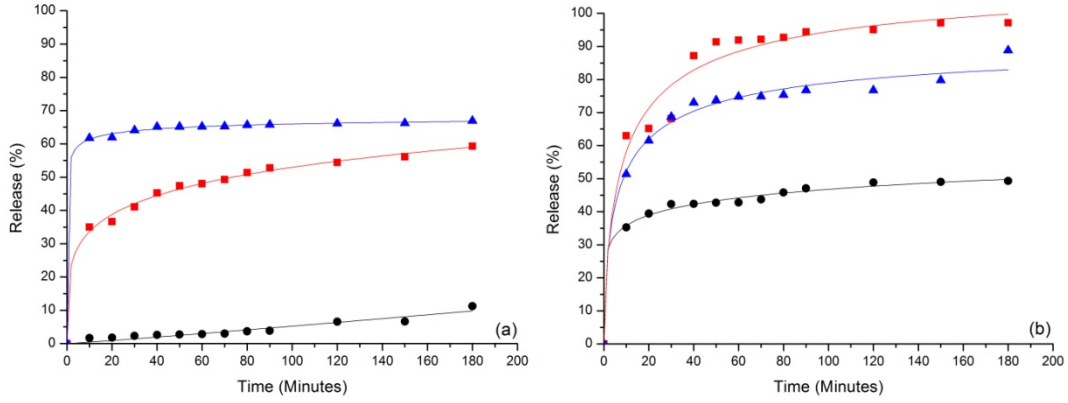

Figure 2.18: Release profiles of Saccharin from Ca/Al-Saccharin LDH (■), Li/Al-Saccharin LDH (●), and Mg/Al-Saccharin LDH (▲), in (a) deionised water, and (b) artificial saliva.

Table 2.5: The t_{50} values and total release values for the artificial sweetener intercalates. The t_{50} value is defined as the time in minutes required for the release of 50% of the amount of anion present in the solution after 180 minutes.

Metals	Guest	Release Medium	t_{50} (Minutes)	Release after 180 Minutes (%)
Ca/Al	Cyclamate	H_2O	17	35.2
		Saliva	< 10	91.9
	Saccharin	H_2O	< 10	59.3
		Saliva	< 10	97.2
Li/Al	Acesulfame	H_2O	21	26.5
		Saliva	61	35.8
	Cyclamate	H_2O	< 10	38.8
		Saliva	< 10	87.9
	Saccharin	H_2O	115	11.2
		Saliva	< 10	49.3
Mg/Al	Acesulfame	H_2O	25	21.9
		Saliva	< 10	90.8
	Cyclamate	H_2O	< 10	50.1
		Saliva	< 10	80.9
	Saccharin	H_2O	< 10	66.9
		Saliva	< 10	88.8

The values of both overall release after 180 minutes, and the time for 50% release vary greatly depending upon both the metallic combination found in the LDH layers and the guest being released. The t_{50} values vary from under 10 minutes, for most of the Ca/Al-LDH compounds, up to 115 minutes for the Li/Al-Saccharin LDH hybrid in water, suggesting the possibility of tuning the release through variation of the host/guest combination.

Many of the LDHs release in excess of 85% of their intercalated guest within 180 minutes, particularly the saccharin and cyclamate intercalates in saliva solutions. The release processes in artificial saliva are uniformly found to lead to greater release after three hours than the corresponding reactions in deionised water. The release from the Li/Al-LDH systems is typically found to be slow compared to the Ca/Al- and Mg/Al-LDH analogues; this is somewhat atypical, as the Li/Al-LDH systems often release their guest species rapidly, given their propensity to concomitantly deintercalate Li^+ from the layers.

2.9.2 Kinetics

The kinetic models described in Section 2.8 have been applied to the release of the guests from each LDH. Least-squares fits of these models to the release data from the Li/Al-Acesulfame LDH in deionised water are included in Figure 2.19.

According to the R^2 values of the linear plots, and for many of the other combinations of guests, it would appear that the parabolic diffusion model is the most accurate for describing the release of the sweeteners. However, visual inspection of the 'linear' plots of the parabolic model show a marked deviation from linearity, with high R^2 values arising from the 'bunching' of the data at low values on the x-axis. This is often found to be the case in modelling deintercalation reactions of layered metal hydroxides by this model.[39, 40] Where the parabolic model does not produce a linear plot, the most successful model for the release of sweeteners in deionised water is typically the Avrami-Erofe'ev model. The first-order model seems to most accurately describe their release in artificial saliva (although the Avrami-Erofe'ev model also provides a reasonable fit in the saliva solution). This would seem to indicate that a number of possible processes leading to sweetener release are operational in a deionised water solution, requiring the complexity of Avrami-Erofe'ev kinetics: such processes could include ion exchange with residual carbonate ions in the water, or simultaneous leaching of the guest anions and cations from the LDH matrix. In contrast, the process in artificial saliva seems to be dominated by a direct ion-exchange route that can be described by a simple first-order model.

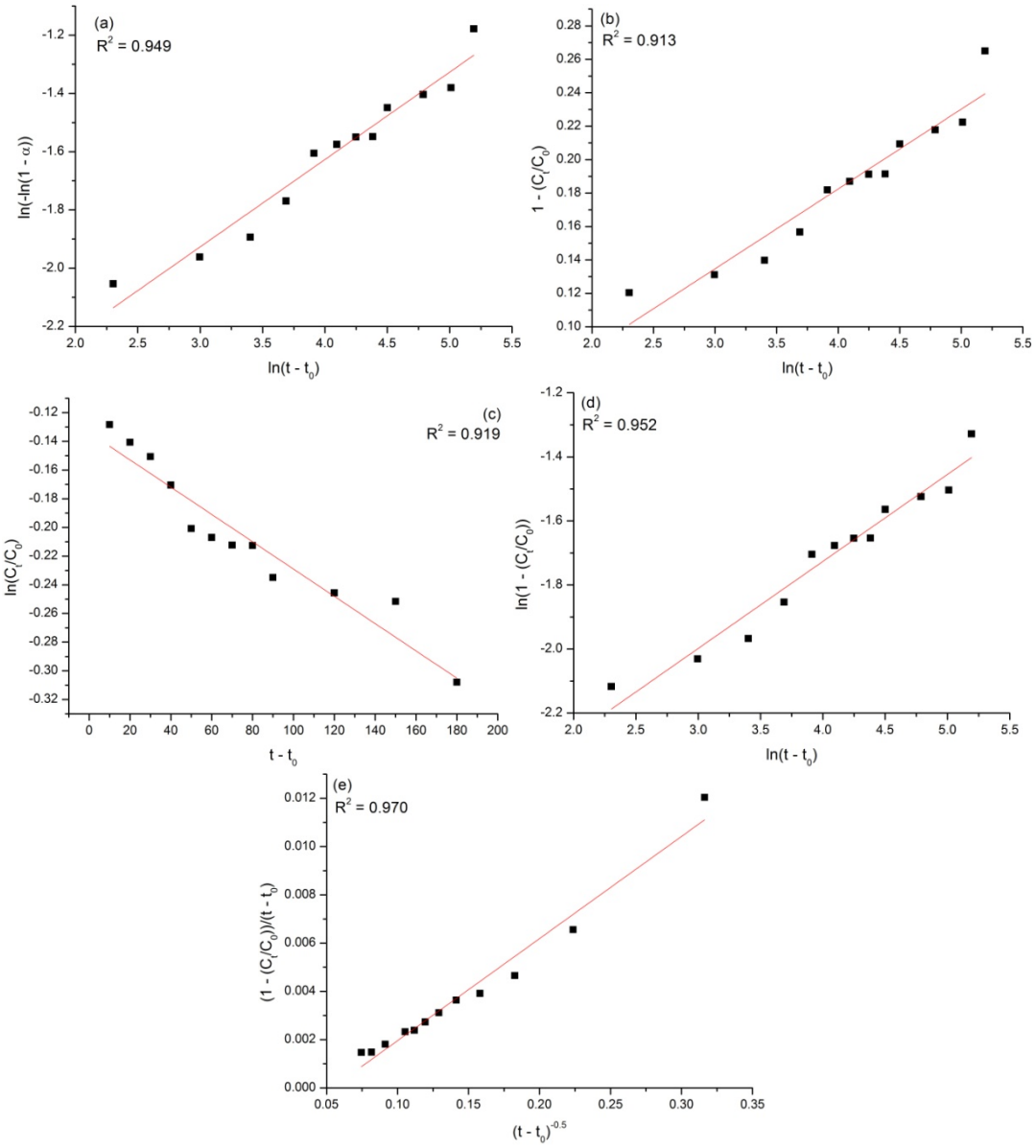

Figure 2.19: Least-squares fits of the various models to the release of Acesulfame from the Li/Al-Acesulfame LDH in deionised water. Fits for (a) the Avrami-Erofe'ev model, (b) the Elovich model, (c) the First-Order model, (d) the Freundlich model, and (e) the parabolic diffusion model, are shown.

Having identified the optimal models for simulating release in each solution, it is possible to extract kinetic parameters from the plotting of the data. The rate constants and reaction exponents for the release for each host and guest are given in Table 2.6, using the most effective models for each solution.

Table 2.6: Values of the rate constants (k_r) and reaction exponents (n) for the release of the sweeteners in deionised water (determined using the Avrami-Erofe'ev model), and in artificial saliva (determined using the first-order model).

Metals	Guest	Deionised H_2O		Artificial Saliva
		Rate Constant (k_r) (x 10^{-3})	Reaction Exponent (n)	Rate Constant (k_r) (x 10^{-3})
Ca/Al	Cyclamate	560.1	0.17	3.1
	Saccharin	3.50	0.27	26.6
Li/Al	Acesulfame	0.081	0.30	2.7
	Cyclamate	0.0011	0.08	15.3
	Saccharin	0.087	0.63	5.8
Mg/Al	Acesulfame	0.025	0.28	16.3
	Cyclamate	0.110	0.11	12.3
	Saccharin	43.7	0.30	9.9

2.10 Release of Taste Modifiers

2.10.1 Release Profiles

The release profiles of ferulate and theobromine from Li/Al-LDH hosts are depicted below in Figure 2.20, in both deionised water and artificial saliva. The release of the ferulate anion from each of the three different hosts in the two different solutions is illustrated in Figure 2.21, and the t_{50} values and total release values derived from these data are summarised in Table 2.7.

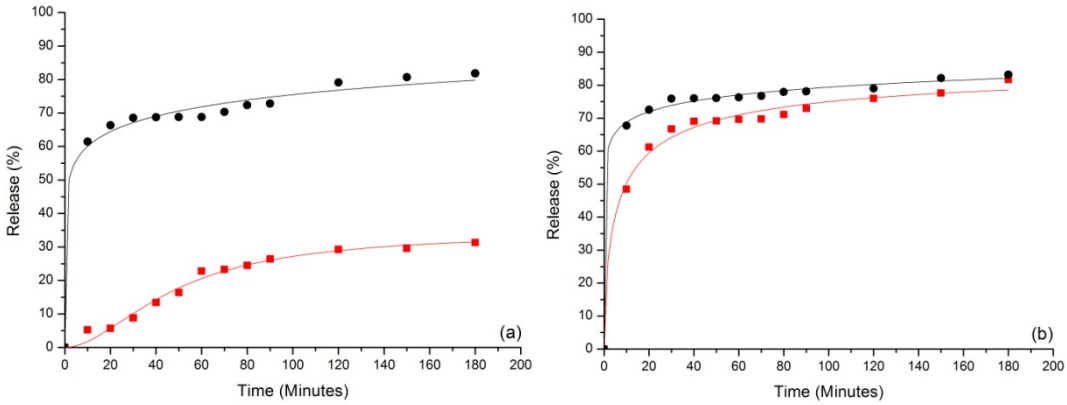

Figure 2.20: Release profiles of Ferulate (■), and Theobromine (●) from Li/Al-LDH hosts in (a) deionised water, and (b) artificial saliva.

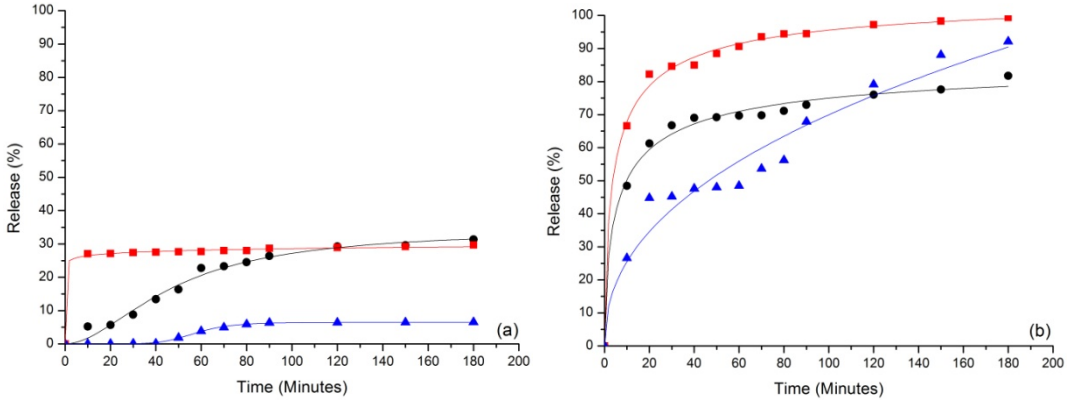

Figure 2.21: Release profiles of Ferulate from the Ca/Al-Ferulate LDH (■), the Li/Al-Ferulate LDH (●), and the Mg/Al-Ferulate LDH (▲), in (a) deionised water, and (b) artificial saliva.

Table 2.7: The t_{50} values and total release values for the ferulate and theobromine intercalates.

Metals	Guest	Release	t_{50} (Minutes)	Release after 180 Minutes (%)
Ca/Al	Ferulate	H_2O	< 10	29.7
		Saliva	< 10	99.4
	Theobromine	H_2O	< 10	63.7
		Saliva	30	90.5
Li/Al	Ferulate	H_2O	47	31.3
		Saliva	< 10	81.7
	Theobromine	H_2O	< 10	81.8
		Saliva	< 10	83.2
Mg/Al	Ferulate	H_2O	58	6.5
		Saliva	31	92.1
	Theobromine	H_2O	< 10	93.1
		Saliva	< 10	99.3

There is again a great deal of variation in the release rates for these guests. One especially noticeable phenomenon is the rapid release of theobromine from the host, with typically in excess of 50% being released within the first twenty minutes of addition to the release solution. This suggests that deintercalation of the anion may be kinetically favoured; given the slowing of the release rate that follows this initial burst, this would seem to be the case. Conversely, the release of ferulate seems to be more gradual than many of the other intercalates, particularly when released from

solids stirred in deionised water. The tightly-packed monolayer structure of the anions in the interlayer space, along with the relatively low amounts of cointercalated water may contribute to this effect. A number of general trends mentioned for the artificial sweeteners above also hold true here: release in saliva is uniformly more rapid than in deionised water, and the relative release rates of the different LDHs are much the same.

2.10.2 Kinetics

The same kinetic models as in section 2.9.2 have been used to model the release of ferulate and theobromine. Fits of these models to the release data from the Ca/Al-Ferulate LDH in artificial saliva are included in Figure 2.22.

The goodness-of-fit for the kinetic models is found to be similar to that observed for the artificial sweeteners. The data in Figure 2.22 demonstrate the same trends: the parabolic model provides a curved line, but yields the greatest nominal 'fit' according to a least-squares fitting line; the first-order model provides the best linear fit; and the Avrami-Erofe'ev plot gives very good agreement as well. The extracted values of k_r and n are shown in Table 2.8 below.

Table 2.8: Values of the rate constants (k_r) and reaction exponents (n) for the release of the flavour modifiers in deionised water (determined using the Avrami-Erofe'ev model), and in artificial saliva (determined using the first-order model).

Metals	**Guest**	**Deionised H_2O**		**Artificial Saliva**
		Rate Constant (k_r) (x 10^{-3})	**Reaction Exponent (n)**	**Rate Constant (k_r) (x 10^{-3})**
Ca/Al	Ferulate	0.00079	0.04	31.4
	Theobromine	6.78	0.11	14.8
Li/Al	Ferulate	2.16	0.80	12.7
	Theobromine	293.9	0.14	13.2
Mg/Al	Ferulate	14.2	0.66	13.5
	Theobromine	557.6	0.21	26.3

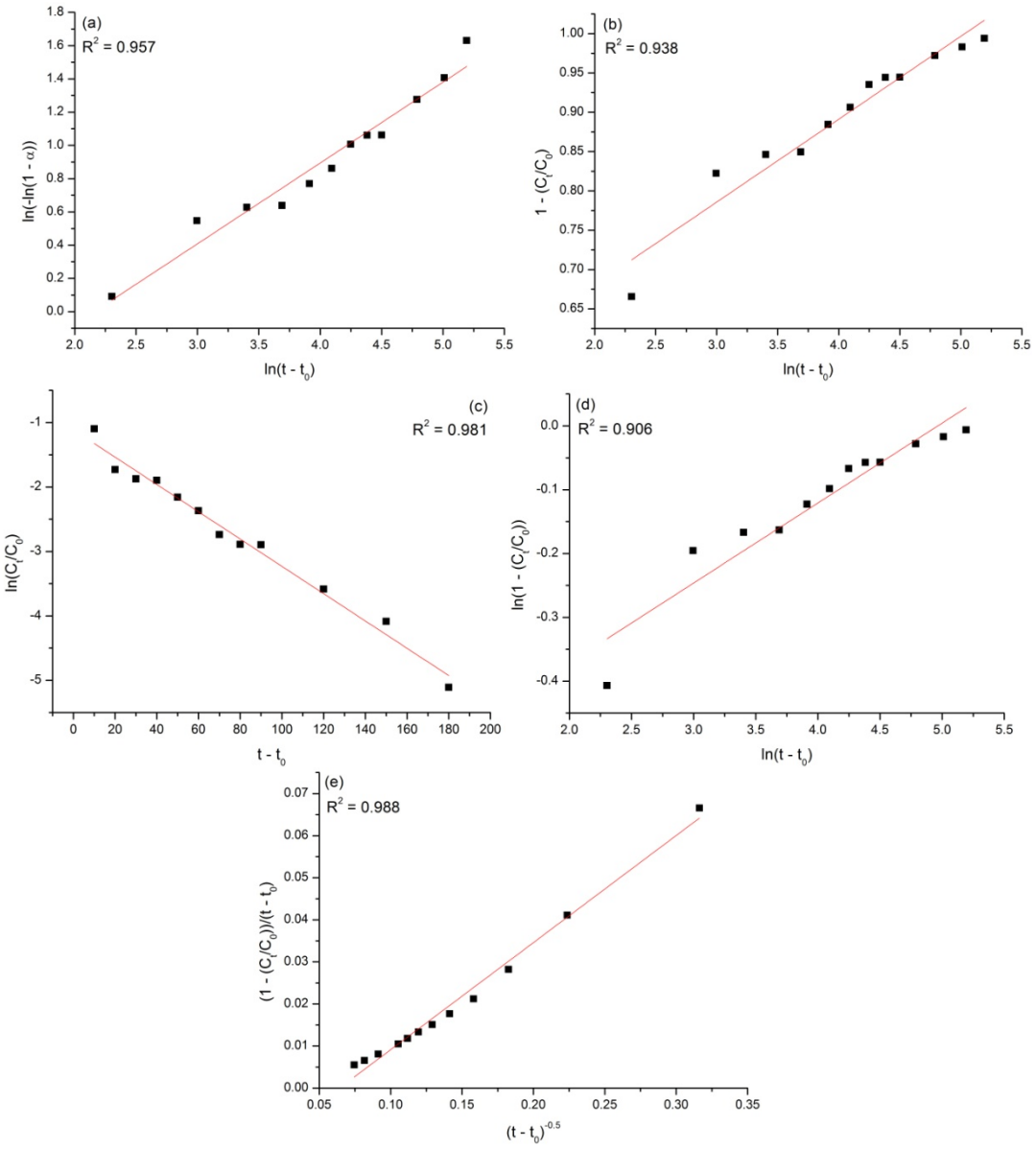

Figure 2.22: Least-squares fits of the various models to the release of Ferulate from the Ca/Al-Ferulate LDH in artificial saliva. Fits for (a) the Avrami-Erofe'ev model, (b) the Elovich model, (c) the First-Order model, (d) the Freundlich model, and (e) the parabolic diffusion model, are shown.

2.11 Discussion of Results

By determination of the reaction exponent, *n*, from the Avrami-Erofe'ev data, it is possible to gain some insight into the mechanism involved in the release of the guest anions. The values of *n* in deionised water are typically around 0.5, corresponding to pure diffusion control. However, the values observed in artificial saliva tend to be

closer to 1, a value indicating two-dimensional diffusion control following instantaneous nucleation. Some release reactions, particularly those in which a very low amount of the guest is released from the solid, are calculated to have *n* values that are close to zero; it is not possible to directly interpret mechanistic information from such systems. Indeed, in certain cases such as the release from the Li/Al-Cyclamate and Ca/Al-Ferulate LDHs in deionised water, the exceptionally low values of the reaction exponents arise from the apparent completion of the release process in less than ten minutes; as the release has completed before collection of the first data point, no information may be determined from application of the Avrami-Erofe'ev model to this system.

It is likely that the presence of significant amounts of replacement anions in the artificial saliva solution leads to ion exchange becoming the dominant release mechanism. For the functional guests to be released by this mechanism requires the replacement anions to move to the edges of the layers, and then force the guests out (leading to apparent nucleation control). This release route is barely available in deionised water, where release will occur by slow leaching of anions and cations from the LDH lattice. The rate of this leaching will be determined by the speed at which the ions diffuse out of the LDH matrix, giving rise to diffusion control. Elemental analysis and X-ray diffraction studies of the solids recovered after long release reactions in artificial saliva indicate that phosphate and carbonate ions are present in the solids, suggesting a noticeable degree of ion exchange driving the release. Reflections attributable to gibbsite are also observed in many of the solids recovered from release reactions of the Li/Al-LDHs, corroborating the theory that lithium leaching accompanies deintercalation of the guest in most instances.

2.12 Conclusions

Fourteen new functional LDH nanohybrids have been synthesised and characterised by X-ray diffraction, FTIR spectroscopy, elemental analysis, thermogravimetric analysis and ^{13}C solid-state NMR. These hybrids release their intercalated guests gradually upon stirring in either deionised water or an artificial saliva solution at 37ºC, with the potential to deliver tunable release rates through systematic variation of the host materials and guest anions. A number of these compounds, such as the Li/Al-Acesulfame LDH hybrid, show gradual but consistent release in artificial saliva over a period of three hours. Analysis of the release rates of the guest anions from the compounds indicates a diffusion-controlled deintercalation mechanism in deionised water, which changes to a first-order ion-exchange process in artificial saliva. The simplicity of the synthesis of these solids, together with the historically-known biocompatibility of hydrotalcite-like compounds, suggests potential applications of these hybrids in edible materials.

2.13 References

1. J.-H. Choy, S.-J. Choi, J.-M. Oh and T. Park, *Applied Clay Science*, 2007, **36**, 122-132.
2. S. Aisawa, S. Sasaki, S. Takahashi, H. Hirahara, H. Nakayama and E. Narita, *Journal of Physics and Chemistry of Solids*, 2006, **67**, 920-925.
3. H. Nakayama, N. Wada and M. Tsuhako, *International Journal of Pharmaceutics*, 2004, **269**, 469-478.
4. S.-J. Xia, Z.-M. Ni, Q. Xu, B.-X. Hu and J. Hu, *Journal of Solid State Chemistry*, 2008, **181**, 2610-2619.
5. F. Li, L. Jin, J. Han, M. Wei and C. Li, *Industrial & Engineering Chemistry Research*, 2009, **48**, 5590-5597.
6. A. Yasutake, S. Aisawa and E. Narita, *Journal of the Society of Inorganic Materials, Japan*, 2008, **15**, 392.
7. K. Ladewig, Z. P. Xu and G. Q. Lu, *Expert Opinion on Drug Delivery*, 2009, **6**, 907-922.
8. M. S. Gasser, *Colloids and Surfaces B: Biointerfaces*, 2009, **73**, 103-109.
9. S. H. Hwang, Y. S. Han and J. H. Choy, *Bulletin of the Korean Chemical Society*, 2001, **22**, 1019.

10. H. S. Panda, R. Srivastava and D. Bahadur, *The Journal of Physical Chemistry B*, 2009, **113**, 15090-15100.
11. S. Aisawa, N. Higashiyama, S. Takahashi, H. Hirahara, D. Ikematsu, H. Kondo, H. Nakayama and E. Narita, *Applied Clay Science*, 2007, **35**, 146-154.
12. C. Del Hoyo, *Applied Clay Science*, 2007, **36**, 103-121.
13. A. I. Khan, A. Ragavan, B. Fong, C. Markland, M. O'Brien, T. G. Dunbar, G. R. Williams and D. O'Hare, *Industrial & Engineering Chemistry Research*, 2009, **48**, 10196-10205.
14. M.-M. Hong, J.-M. Oh and J.-H. Choy, *Journal of Nanoscience and Nanotechnology*, 2008, **8**, 5018-5021.
15. S. Aisawa, H. Hirahara, K. Ishiyama, W. Ogasawara, Y. Umetsu and E. Narita, *Journal of Solid State Chemistry*, 2003, **174**, 342-348.
16. H. Zhao and G. F. Vance, *Dalton Transactions*, 1997, 1961.
17. S. Aisawa, H. Hirahara, S. Takahashi, Y. Umetsu and E. Narita, *Chemistry Letters*, 2004, **33**, 306-307.
18. S. S. Schiffman, V. A. Crofton and T. G. Beeker, *Physiology & Behavior*, 1985, **34**, 369-377.
19. C. E. Riera, H. Vogel, S. A. Simon, S. Damak and J. le Coutre, *Biochemical and Biophysical Research Communications*, 2008, **376**, 653-657.
20. C. E. Riera, H. Vogel, S. A. Simon and J. le Coutre, *American Journal of Physiology - Regulatory, Integrative and Comparative Physiology*, 2007, **293**, R626-R634.
21. G.-W. von Rymon Lipinski, *Food Chemistry*, 1985, **16**, 259-269.
22. J. A. Riemer, *Bitterness Inhibitors for Foods and Artificial Sweeteners*, U.S. Patent 5,336,513, August 9, 1994.
23. S. S. Schiffman, J. M. Gill and C. Diaz, *Pharmacology Biochemistry and Behavior*, 1985, **22**, 195-203.
24. G. M. Brosvic and M. M. Rowe, *Physiology & Behavior*, 1992, **52**, 559-563.
25. H. Hirahara, S. Aisawa, S. Takahashi, H. Sakuraba, Y. Akiba, E. Narita and K. Mori, *Nippon Gomu Kyokaishi*, 2006, **79**, 261-266.
26. C. Liu, W. Hou, L. Li, Y. Li and S. Liu, *Journal of Solid State Chemistry*, 2008, **181**, 1792-1797.
27. A. Yasutake, S. Aisawa, N. Kobashi, S. Takahashi, H. Hirahara and E. Narita, *Clay Science*, 2008, **14**, 49-54.
28. R. Allmann, *Chimia*, 1970, **24**, 99-108.
29. H. Icbudak, E. Adiyaman, N. Cetin, A. Bulut and O. Buyukgungor, *Transition Metal Chemistry*, 2006, **31**, 666-672.
30. A. Kula, L. Mazur and Z. Rzączyńska, *Journal of Coordination Chemistry*, 2007, **60**, 843 - 850.
31. L. de Carvalho, M. Segato, R. Nunes, C. Novak and É. Cavalheiro, *Journal of Thermal Analysis and Calorimetry*, 2009, **97**, 359-365.
32. S. Qiu, *Zhuanli Shenqing Gongkai Shuomingshu (People's Republic of China) CN*, 1996, 4.
33. E. Guney, V. T. Yilmaz and O. Buyukgungor, *Inorganica Chimica Acta*, 2010, **363**, 2416-2424.
34. J. D. Hancock and J. H. Sharp, *Journal of the American Ceramic Society*, 1972, **55**, 74-77.
35. Z. Li, *Langmuir*, 1999, **15**, 6438-6445.
36. T. Kodama, Y. Harada, M. Ueda, K.-i. Shimizu, K. Shuto and S. Komarneni, *Langmuir*, 2001, **17**, 4881-4886.

37. S. Kuo and E. G. Lotse, *Soil Science*, 1973, **116**, 400-406.
38. D. L. Sparks, L. W. Zelazny and D. C. Martens, *Soil Science Society of America Journal*, 1980, **44**, 37-40.
39. J.-H. Yang, Y.-S. Han, M. Park, T. Park, S.-J. Hwang and J.-H. Choy, *Chemistry of Materials*, 2007, **19**, 2679-2685.
40. R. M. R. Bull, C. Markland, G. R. Williams and D. O'Hare, *Journal of Materials Chemistry*, 2011, **21**, 1822-1828.

Chapter 3

Intercalation of Agrochemicals and Pharmaceuticals and Release in Representative Conditions

3.1 Introduction

While a good deal of research has been performed on the release properties of layered double hydroxides, in most cases kinetic information (and, thus, their predicted suitability for their potential applications) is inferred from simple methods such as stirring the powders in an aqueous solution in a flask.[1] There are few instances of release reactions of LDHs being performed under release conditions designed to genuinely approximate the conditions under which the compound would be used in practice.[2-4] In particular, two of the most heavily investigated applications of layered double hydroxides are for the delivery of agrochemicals (including pesticides and herbicides)[5-7] and of pharmaceuticals;[8-10] on the whole, little consideration is given to the delivery methods of these compounds in practical applications.

There are many reasons to attempt to improve upon current delivery methods of herbicides. Their persistence in the soil, and in the ground water, has been the source of great environmental concern. It has been found that as much as 90% of herbicides fail to reach their target destination once applied,[11] in part because of photochemical degradation and volatilisation of the compounds.[12, 13] While there has been much interest in the formation of agrochemical-clay composites with surface-modified cationic clays including bentonites,[14] montmorillonites,[15, 16] and sepiolites[17] (which are major components of soil), layered double hydroxides are also attractive materials, possessing much higher ion exchange capacities than these cationic clays.[18]

The biocompatibility of LDH materials is well-established,[19-21] and a number of medicinal treatments currently available contain hydrotalcite-like compounds either as an inert filler, or as an active ingredients (the antacids Altacite© and Talcid© contain a suspension of a Mg/Al-CO_3 LDH in water, to neutralise stomach acid in the same manner as 'Milk of Magnesia', which contains $Mg(OH)_2$). There are several benefits to intercalating a drug into an LDH before delivery: the intercalate is stabilised towards heat and light, and any unpleasant taste is masked. Ibuprofen, in particular, is known to cause a burning, irritating feeling in the mouth when consumed unmodified.[22] Most usefully, the gradual breakdown of the metal hydroxide structure allows the concentration of the drug in the bloodstream to remain at pharmaceutically active levels without successive redosing at short intervals, or the possibility of extended periods of over- or underdosing. These processes are demonstrated, in a simplified form, in Figure 3.1.

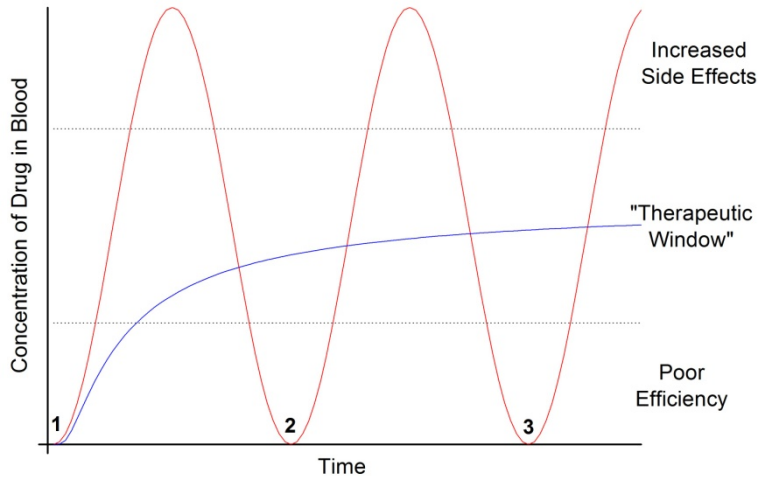

Figure 3.1: Comparing drug concentrations in the bloodstream for conventional dosage (red line, with successive doses taken at **1**, **2** and **3**) compared to idealised controlled release (blue line).

One problem is apparent when considering LDHs as an oral delivery system. The mildly alkaline pH of the mouth will result in very little release of the intercalated drug, but when the composite continues to the harshly acidic environment of the

stomach, the compound is likely to dissolve rapidly causing a sudden release of the drug on a short timescale (and the denaturing of any acid-sensitive drugs). What is required in this case is a coating or inert matrix in which the LDH powder may be imbedded that is stable at highly acidic pHs, but is able to dissolve in the mildly basic conditions of the upper small intestine, where optimal uptake of most drug molecules occurs. The use of these 'enteric coatings' is well-documented in the literature.[23-25]

In this study, three herbicides and three non-steroidal anti-inflammatory drugs (NSAIDs) are identified as candidates for intercalation into layered double hydroxides. The three herbicides chosen are 4-(2,4-dichlorophenoxy)butyric acid (known commercially as 2,4DB), 2,4,5-trichlorophenoxyacetic acid (known as 2,4,5T), and 2-(2,4-dichlorophenoxy)propanoic acid (also called Dichlorprop); their structures are depicted in Figure 3.2.

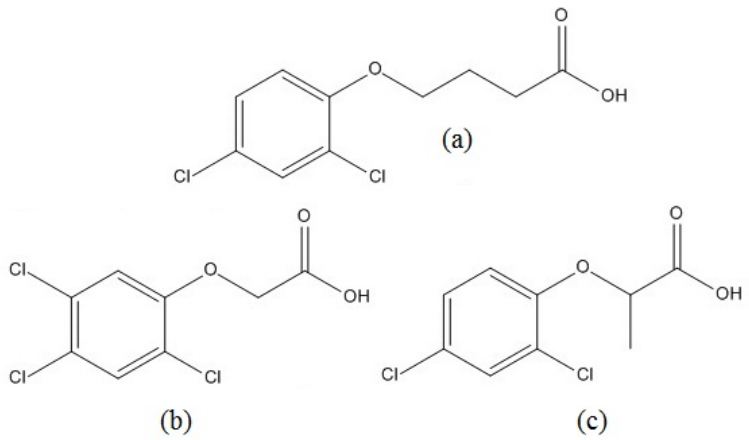

Figure 3.2: The chemical structures of (a) 2,4DB, (b) 2,4,5T, and (c) Dichlorprop.

The release of these herbicides is to be performed using a soil column; the LDH powder is dispersed on the upper surface, and tap water added periodically to simulate rain. Aliquots are collected from below the soil to determine the progression of the release, as quantified by UV/Vis spectroscopy.

The NSAIDs chosen for intercalation are diclofenac, ibuprofen and naproxen. The structures of these molecules are given in Figure 3.3.

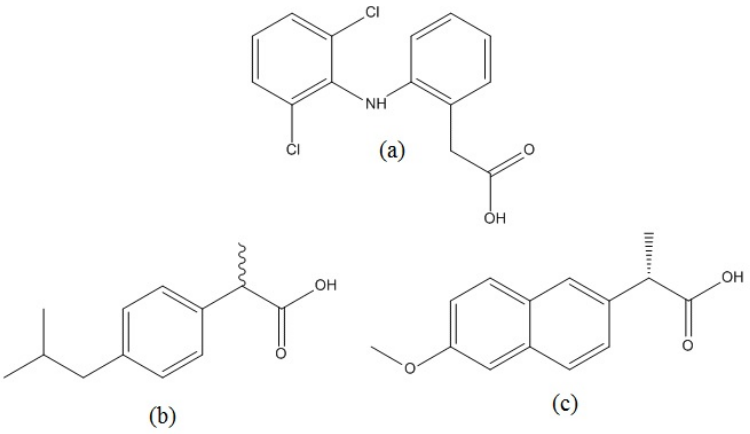

Figure 3.3: The chemical structures of (a) diclofenac, (b) ibuprofen, and (c) naproxen.

These compounds are released from LDHs that have been enterically coated with sodium alginate, an acid-resistant anionic polysaccharide that dissolves readily in basic conditions. The LDH beads are to be stirred at human body temperature in a pH 2.1 buffer solution (representing the acidity of the stomach), then transferred into a pH 7.3 buffer solution (corresponding to the mild alkalinity of the upper small intestine). Regular aliquots are removed, and the degree of release quantified by UV/Vis spectroscopy. For an effective enteric coating, no release should be observed in the pH 2.1 buffer solution, but gradual release should occur in the pH 7.3 solution.

The hosts investigated for use with these anions are three common LDHs (Ca/Al-, Li/Al- and Mg/Al-LDH), and also one hydroxynitrate salt (HS). Hydroxynitrate salts are stable and biocompatible,[26] and are structurally similar to LDHs. The HS used in this chapter is synthesised by the direct reaction of zinc oxide with a solution of zinc nitrate at room temperature,[27] and has the chemical formula $[Zn_5(OH)_8](NO_3)_2 \cdot yH_2O$ ('Zn_5-NO_3 HS'). The principal structural difference between this compound and an LDH is the projection of some of the metal cations above and below the layers themselves, leading to stronger interactions between the interlayer guest species and the layers. This may be predicted to lead to slower release of intercalated anions. The structure of the zinc HS is illustrated in Figure 3.4.

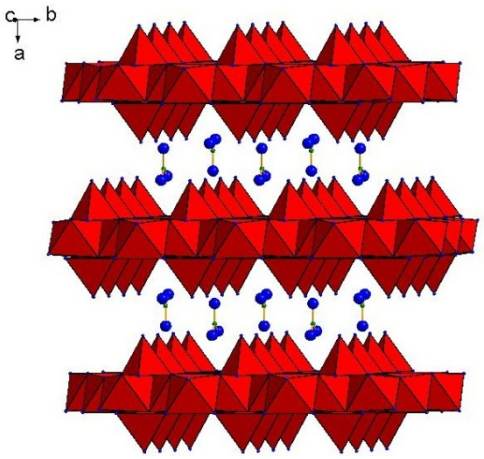

Figure 3.4: The structure of the zinc hydroxynitrate salt, $[Zn_5(OH)_8](NO_3)_2 \cdot yH_2O$,[28] showing the metal cations protruding into the interlayer space.

Although HSs undergo facile ion exchange,[29] there are only limited reports of their intercalation chemistry,[30-32] and a single report of their release properties.[33] The relative rates and mechanisms of release from the LDHs are compared to those of the HS, to determine the effect of the host structure on the release behaviour.

3.2 Powder X-ray Diffraction Data

3.2.1 Herbicides

The herbicides used in this chapter proved challenging to intercalate in deionised water, as their anions possessed relatively high pKa values. Solutions of the herbicide anions were typically prepared in a 1:1 volume/volume mixed solution of ethanol and water, using triethylamine as a base. The precursor chloride or nitrate LDHs were added to this solution (containing a threefold molar excess of the guest anion), and stirred at various temperatures, and over differing timescales; precise experimental details are outlined in Chapter 6, Section 6.3.2.

The powder X-ray diffraction patterns of the Ca/Al-, Li/Al-, and Mg/Al-Herbicide LDH intercalates are depicted in Figures 3.5, 3.6 and 3.7, respectively.

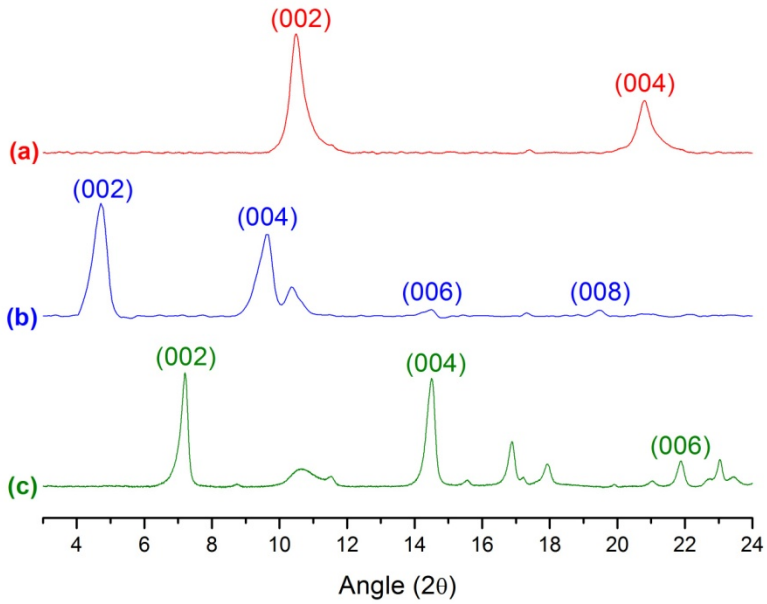

Figure 3.5: Powder XRD patterns of (a) the Ca/Al-NO_3 LDH, (b) the Ca/Al-2,4DB LDH, and (c) the Ca/Al-Dichlorprop LDH. The d-spacings of the (002) reflections of the above patterns are 8.6, 18.7 and 12.1Å respectively.

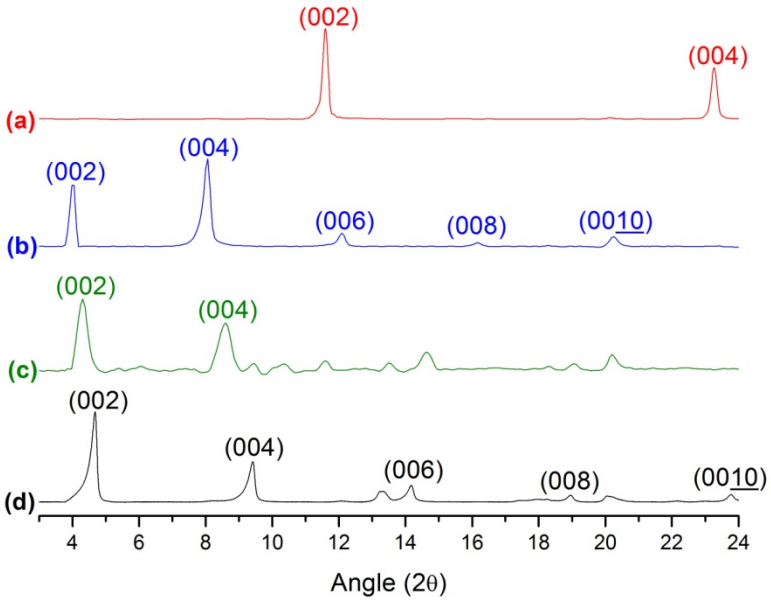

Figure 3.6: Powder XRD patterns of (a) the Li/Al-Cl LDH, (b) the Li/Al-2,4DB LDH, (c) the Li/Al-2,4,5T LDH, and (d) the Li/Al-Dichlorprop LDH. The d-spacings of the (002) reflections of the above patterns are 7.2, 22.0, 20.5 and 18.7Å respectively.

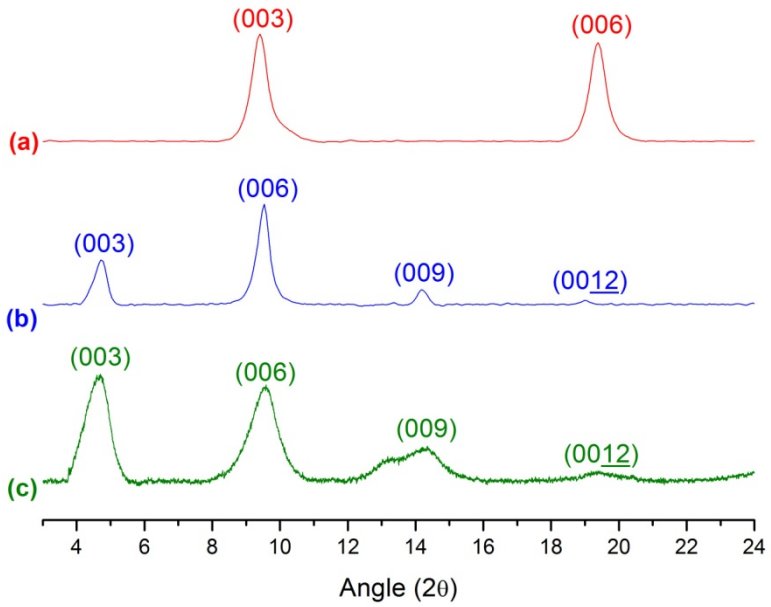

Figure 3.7: Powder XRD patterns of (a) the Mg/Al-NO_3 LDH, (b) the Mg/Al-2,4,5T LDH, and (c) the Mg/Al-Dichlorprop LDH. The d-spacings of the (003) reflections of the above patterns are 8.5, 18.4 and 17.9Å respectively.

In addition to the LDHs above, it was also found to be possible to intercalate 2,4,5T into the Zn_5-NO_3 HS. The product and its precursor are shown in Figure 3.8.

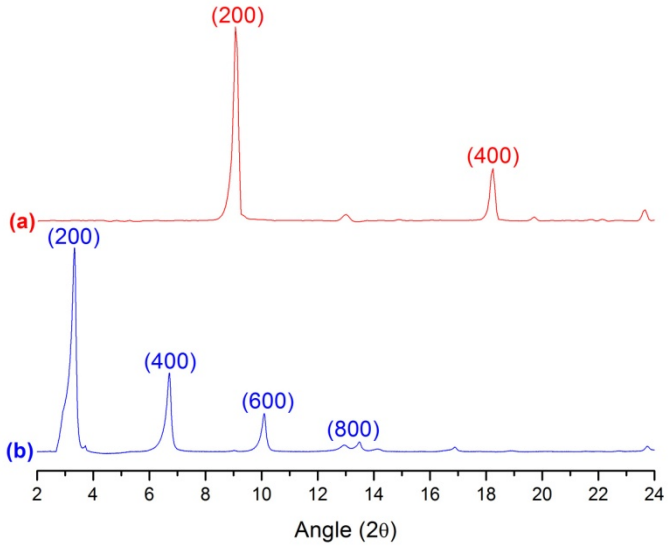

Figure 3.8: Powder XRD patterns of (a) the Zn_5-NO_3 HS, and (b) the Zn_5-2,4,5T HS. The d-spacings of the (200) reflections of the above patterns are 9.7 and 26.1Å respectively.

Despite extensive experimentation, it did not prove possible to achieve intercalation in every case. The attempted intercalation of 2,4,5T into the Ca/Al-LDH system was

not found to succeed under any reaction conditions; the reaction products recovered were a mixture of non-hydrotalcite-like metal oxides. Similarly, the intercalation of 2,4DB into the Mg/Al-LDH did not proceed significantly under any reaction conditions; only the nitrate starting material was observed in the powder pattern.

In each case an increase in the interlayer separation upon intercalation of the herbicide molecules into the solid is observed. Very similar expansions are seen for the 2,4,5T and Dichlorprop intercalates, as they have almost identical end-to-end molecular lengths (11.8Å and 12.3Å respectively). Comparison of the molecular lengths to the gallery heights suggests that an interdigitated antiparallel bilayer is the most probable arrangement of the molecules, as the separations typically exceed the molecular lengths by approximately 20%. This interlayer arrangement is illustrated in Figure 3.9(a). A similar orientation has been previously observed in LDH intercalates of 2,4,5T, with the carboxylate groups interacting with the metal hydroxide layers.[1]

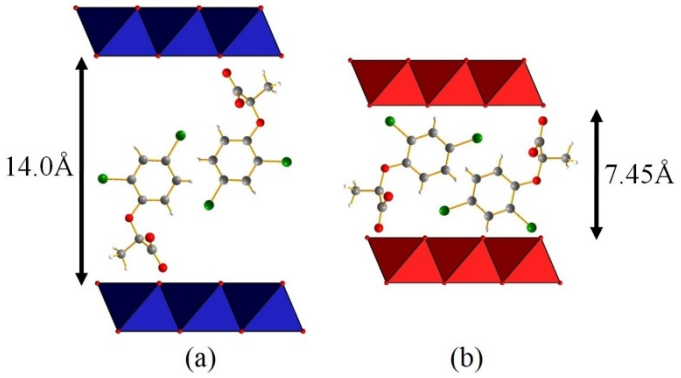

Figure 3.9: Possible molecular arrangements of Dichlorprop in the interlayer space of (a) the Mg/Al-Dichlorprop LDH, and (b) the Ca/Al-Dichlorprop LDH.

The principal exception to this general trend is the Ca/Al-LDH hybrids, where the gallery height of each is consistently less than the molecule's length, and thus a tilted monolayer is a more likely arrangement. In the case of the Zn_5-HS, the gallery height is 75% greater than the molecule's maximum length, so the likely arrangement of

2,4,5T is a less interdigitated bilayer. An example of the monolayer arrangement observed for the Ca/Al-LDHs is illustrated in Figure 3.9(b).

3.2.2 Anti-Inflammatory Drugs

Figures 3.10, 3.11 and 3.12 show the X-ray diffraction patterns of the Ca/Al-, Li/Al- and Mg/Al-Drug LDHs, along with the patterns of their precursors. The patterns of the two Zn_5-HS hybrids are shown in Figure 3.13.

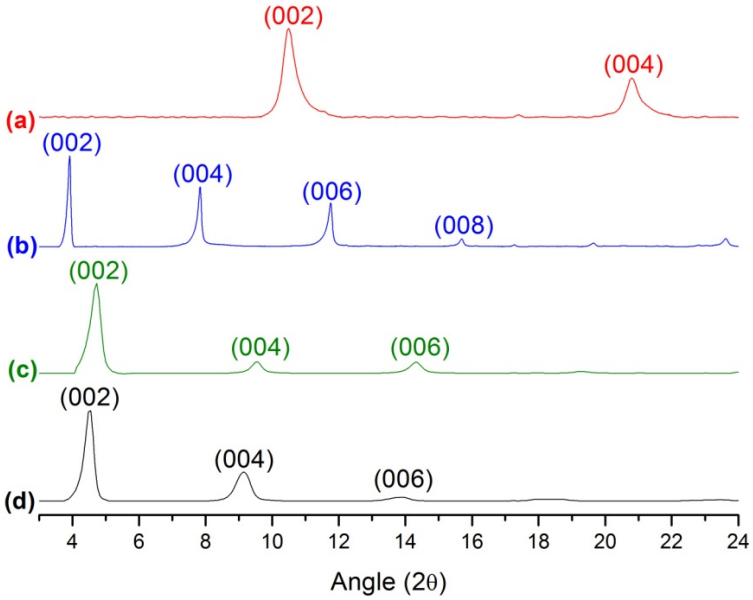

Figure 3.10: Powder XRD patterns of (a) the Ca/Al-NO_3 LDH, (b) the Ca/Al-Diclofenac LDH, (c) the Ca/Al-Ibuprofen LDH, and (d) the Ca/Al-Naproxen LDH. The d-spacings of the (002) reflections of the above patterns are 8.6, 22.5, 18.7 and 19.1Å respectively.

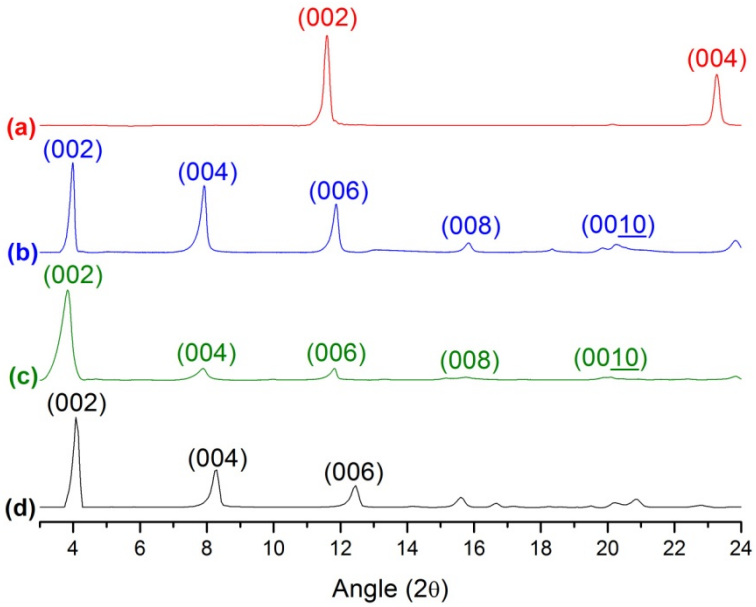

Figure 3.11: Powder XRD patterns of (a) the Li/Al-Cl LDH, (b) the Li/Al-Diclofenac LDH, (c) the Li/Al-Ibuprofen LDH, and (d) the Li/Al-Naproxen LDH. The d-spacings of the (002) reflections of the above patterns are 7.2, 22.2, 21.8 and 21.1Å respectively.

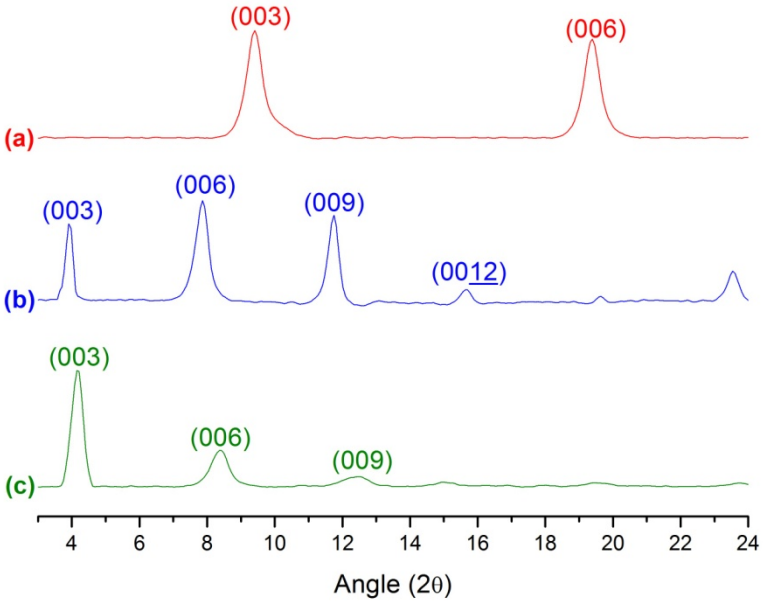

Figure 3.12: Powder XRD patterns of (a) the Mg/Al-NO_3 LDH, (b) the Mg/Al-Diclofenac LDH, and (c) the Mg/Al-Naproxen LDH. The d-spacings of the (003) reflections of the above patterns are 8.5, 22.3, and 20.9Å respectively.

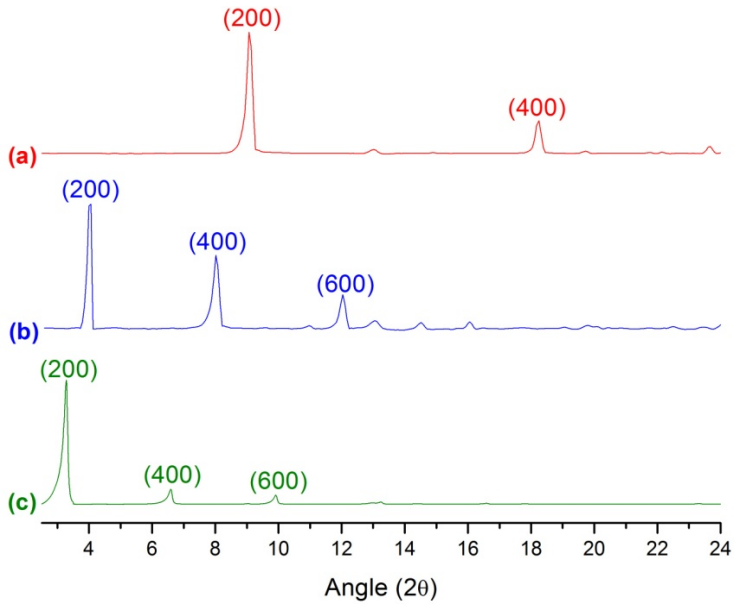

Figure 3.13: Powder XRD patterns of (a) the Zn_5-NO_3 HS, (b) the Zn_5-Diclofenac HS, and (c) the Zn_5-Ibuprofen HS. The d-spacings of the (200) reflections of the above patterns are 9.7, 22.1 and 26.6Å respectively.

The drug molecules were intercalated by the addition of the LDH hosts to solutions of the sodium salts of the drugs; the precise procedures involved in these reactions are also outlined in Chapter 6. The only host-guest combination where the reaction did not succeed was the attempted intercalation of ibuprofen into the Mg/Al-NO_3 LDH, which yielded a product which gave a powder pattern identical to the starting material, irrespective of reaction conditions.

Comparison of the observed interlayer spacings with the lengths of the intercalated molecules once again suggests the formation of interdigitated bilayers in the interlayer space, most likely with adjacent molecules antiparallel to each other, as the gallery heights are mostly 20-50% greater than their end-to-end lengths. Again, the Ca/Al-LDHs show smaller interlayer separations than the other LDH systems, but it is also notable that in the Zn_5-HS, the separation is much greater, suggesting almost a full bilayer in the cases of both diclofenac and ibuprofen (with the gallery heights exceeding the length of the molecules by over 75%). The bilayer arrangement of

ibuprofen between the charged layers of the HS is very similar to that previously reported in ibuprofen-intercalated LDHs.[1] Full details of the structural parameters of these new hybrids, and the interlayer orientations determined for them, are provided in Appendix A, Section A.3.

3.3 FTIR Data

3.3.1 Herbicides

IR spectroscopy was used to qualitatively analyse the presence of the three herbicides in the product LDHs and HSs. Figure 3.14 compares the IR spectra of the 2,4,5T intercalates of the Mg/Al-LDH and the Zn_5-HS, along with the absorption spectrum of solid 2,4,5T. The spectra below focus only on the 'fingerprint' region, below 2000cm^{-1}.

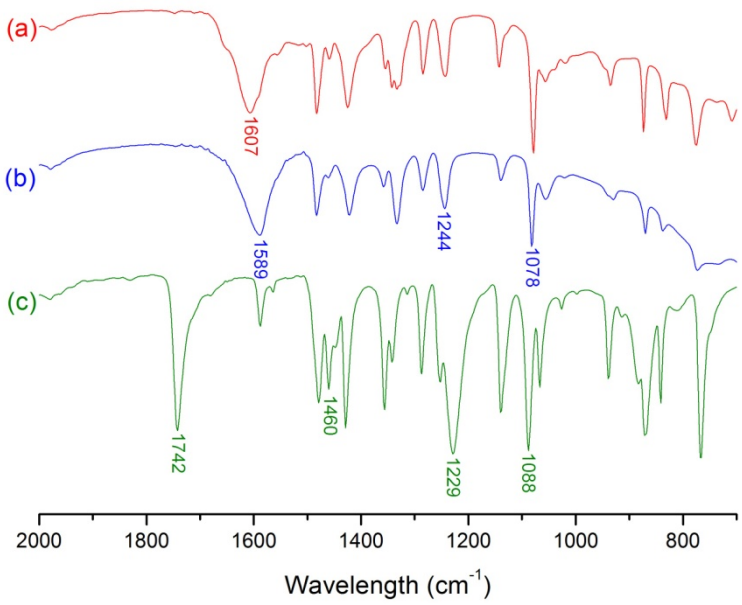

Figure 3.14: FTIR Transmittance Spectra of (a) the Zn_5-2,4,5T HS, (b) the Mg/Al-2,4,5T LDH and (c) 2,4,5T.

The spectra are predictably similar, with the principal difference being the shift of the carboxylic acid $\nu_{C=O}$ absorption from 1742cm^{-1} to approximately 1590cm^{-1} upon

deprotonation of the group. Other notable absorptions can be attributed to the aliphatic ether stretch (*ca.* 1085cm^{-1}), the various $\nu_{C=C}$ absorptions centred about 1460cm^{-1}, and the strong absorption at *ca.* 1230cm^{-1} which most likely arises from a superposition of the aromatic ether stretch and the δ_{O-C-O} of the carboxylic acid group. The FTIR spectra of the LDH and the HS are very similar to each other, with varying absorption intensities due to the differing loadings of 2,4,5T within each solid.

3.3.2 Anti-Inflammatory Drugs

Figure 3.15 compares the IR spectra of the ibuprofen intercalates of the Ca/Al- and Li/Al-LDHs and the Zn_5-HS with the sodium salt of ibuprofen. Once again, the 'fingerprint' region is shown enlarged for clarity.

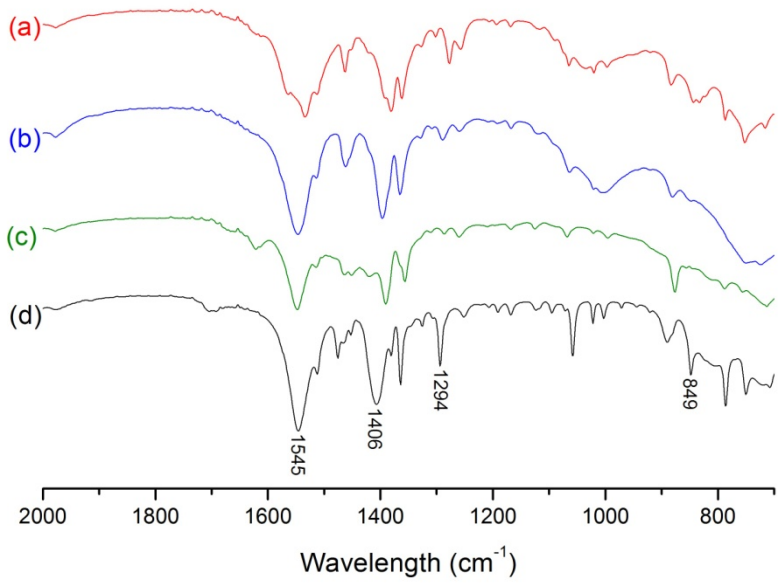

Figure 3.15: FTIR Transmittance Spectra of (a) the Zn_5-Ibuprofen HS, (b) the Li/Al-Ibuprofen LDH, (c) the Ca/Al-Ibuprofen LDH, and (d) Sodium ibuprofenate.

Once again, all four spectra are very similar, with transmittance intensities predominantly scaling in direct proportion to the ibuprofen loadings of the solids. The strongest absorption is that of $\nu_{C=O}$ found at 1545cm^{-1} in the solid ibuprofen salt, and at a similar position in the spectrum of each of the intercalation compounds. The other

major absorption, found at *ca.* 1405cm^{-1}, arises from a combination of the carbon-carbon stretches in the aromatic ring with the various δ_{C-H} absorptions from the aliphatic bonds throughout the structure. Also annotated in the diagram above are the aromatic C-H stretching absorptions at *ca.* 850cm^{-1}, and the sharp absorption at 1294cm^{-1} due to a combination of the various methyl C-H stretching absorptions with the δ_{O-C-O} from the carboxylate group.

3.4 TGA Data

3.4.1 Herbicides

Thermogravimetric analysis (TGA) was used to determine the amount of co-intercalated water in the various herbicide LDHs, and the progression of their decompositions at high temperatures. Decomposition processes typical of LDHs were seen in all cases; the TGA plot of Li/Al-2,4DB LDH is shown in Figure 3.16. This trace is typical of all the herbicide intercalates.

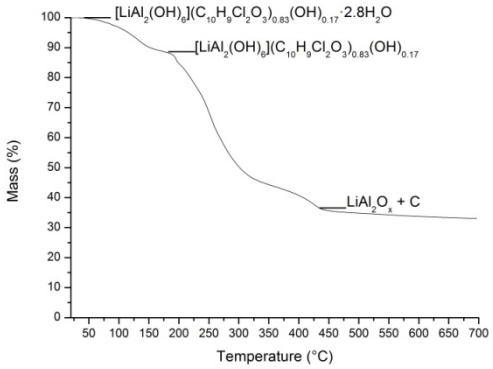

Figure 3.16: TGA plot of the Li/Al-2,4DB LDH.

The plot shows two major mass losses: the first begins at around 100°C and is completed at 180°C, and corresponds to the loss of 2.8 equivalents of co-intercalated water from the structure (calculated mass loss 12.0%, observed mass loss 12.0%); the second begins shortly after, at around 200°C, and is complete at 450°C. This arises from the decomposition of the interlayer anion to steam, gaseous carbon products and

volatile chlorine derivatives, along with partial decomposition of the LDH hydroxide layers. The remaining solid at 700°C is a mixture of carbon soot and an amorphous lithiated alumina of indeterminate composition (the observed mass loss for the final step is 51.3% of the initial mass).

3.4.2 Anti-Inflammatory Drugs

The results of the thermogravimetric analyses performed on the drug intercalates were similar to those for the herbicide nanocomposites; two example plots are depicted in Figure 3.17, of the Ca/Al-Ibuprofen LDH and the Zn_5-Ibuprofen HS.

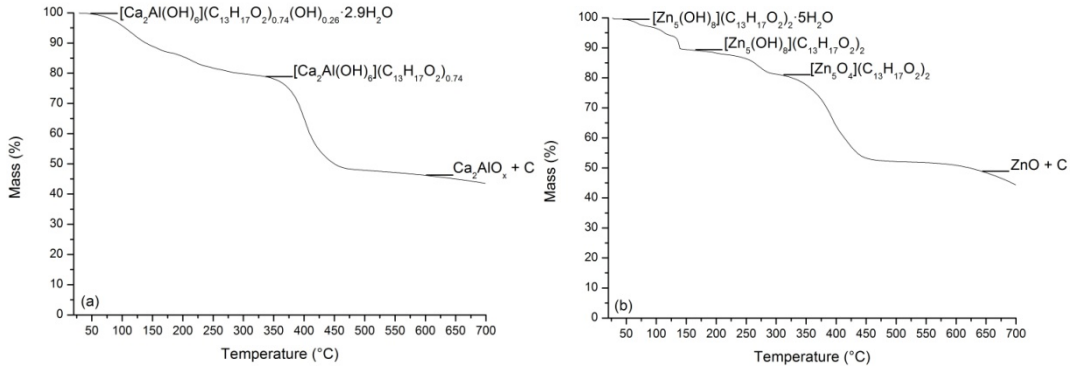

Figure 3.17: TGA plot of (a) the Ca/Al-Ibuprofen LDH, and (b) the Zn_5-Ibuprofen HS.

The plot for the Ca/Al LDH is very similar to the Li/Al LDH plot in Section 3.4.1, with two distinct losses associated firstly with cointercalated water (calculated 12.5%, observed 11.0%) and secondly with the simultaneous decomposition of the intercalated anion and the hydroxide layers, leaving a mixture of binary and unary oxides, along with carbon soot remaining from the organic anion as the final solid products, with an accompanying mass loss of 32.1%.

The decomposition of the Zn_5-HS is slightly different from the conventional LDH progression; three distinct losses are found, corresponding first to the loss of co-intercalated water (calculated 9.4%, observed 10.4%), and then secondly to the decomposition of the hydroxide layers alone (calculated 7.5%, observed 8.1%),

resulting in a zinc oxide phase. This is then followed by a final step in which the ibuprofen anion breaks down, resulting in the final product of zinc oxide and carbon soot, accompanied by a loss of 33.4% of the initial mass. This three-step process has been previously noted for zinc HSs intercalated by organic anions.[34]

3.5 SEM Data

3.5.1 Herbicides

Scanning Electron Microscopy (SEM) was used to investigate the particle sizes and morphologies of the synthesised LDHs, and to give corroborating elemental content data by energy-dispersive X-ray spectroscopy (EDX). Figures 3.18, 3.19 and 3.20 show particles of the Ca/Al-2,4DB LDH, the Mg/Al-Dichlorprop LDH, and the Li/Al-Dichlorprop LDH, along with the raw EDX data from the particles shown.

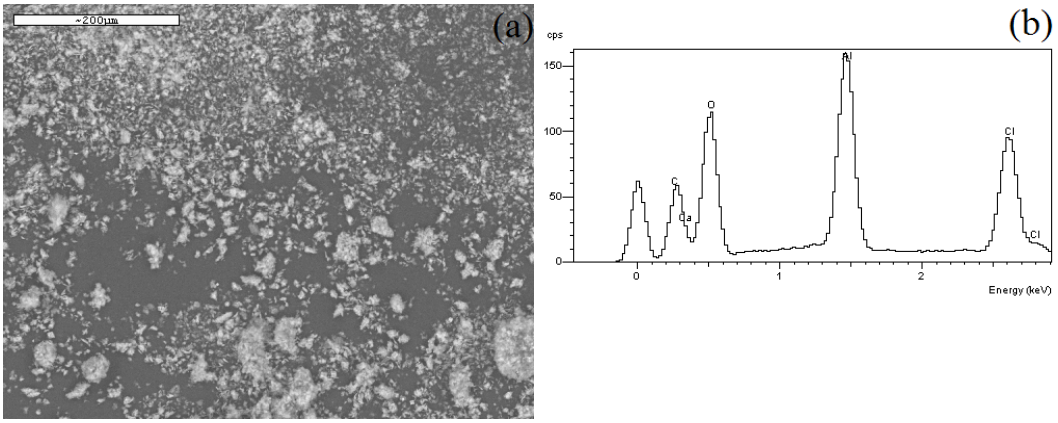

Figure 3.18: (a) Particles of the Ca/Al-2,4DB LDH, at approximately 600x magnification, and (b) a representative EDX spectrum.

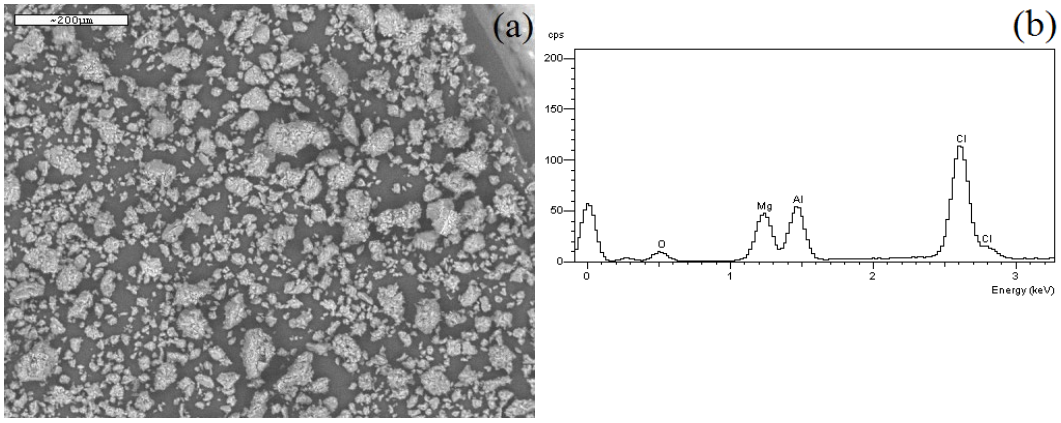

Figure 3.19: (a) Particles of the Mg/Al-Dichlorprop LDH, at approximately 600x magnification, and (b) a representative EDX spectrum.

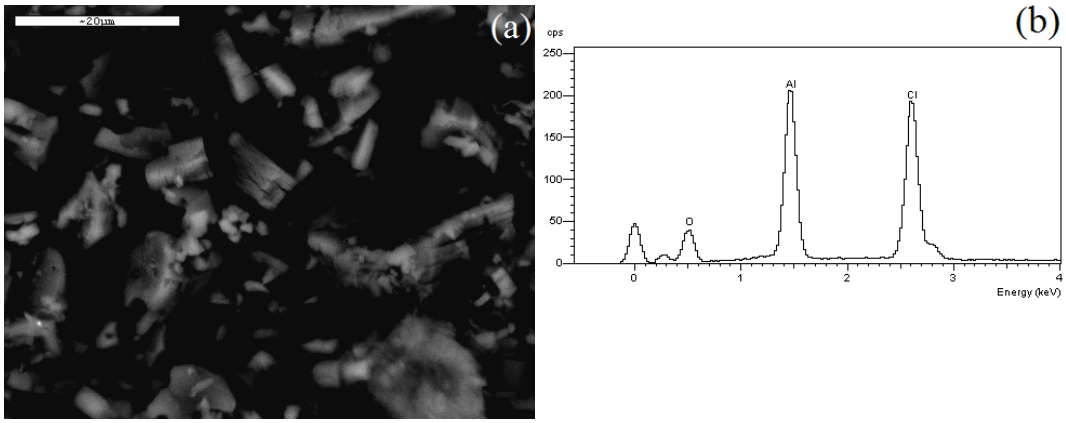

Figure 3.20: (a) Particles of the Li/Al-Dichlorprop LDH, at approximately 6000x magnification, and (b) a representative EDX spectrum.

The particles are predominantly of a platelet-like morphology, with median particle sizes of approximately 10-20µm for the Ca/Al-2,4DB LDH, 50µm for the Mg/Al-Dichlorprop LDH and 15µm for the Li/Al-Dichlorprop LDH. After making the appropriate intensity corrections for the various elements present, the elemental ratios were found to be in consistent agreement to those determined by ICP in Section 3.6.1 (within 5% in each case).

3.5.2 Anti-Inflammatory Drugs

SEM images were also collected for the drug-intercalated layered compounds, and the EDX elemental concentrations were once again found to be in good agreement

with those determined by other means. Representative images of two of the drug hybrids (Li/Al-Naproxen LDH, and Zn_5-Ibuprofen HS) are depicted in Figure 3.21 below.

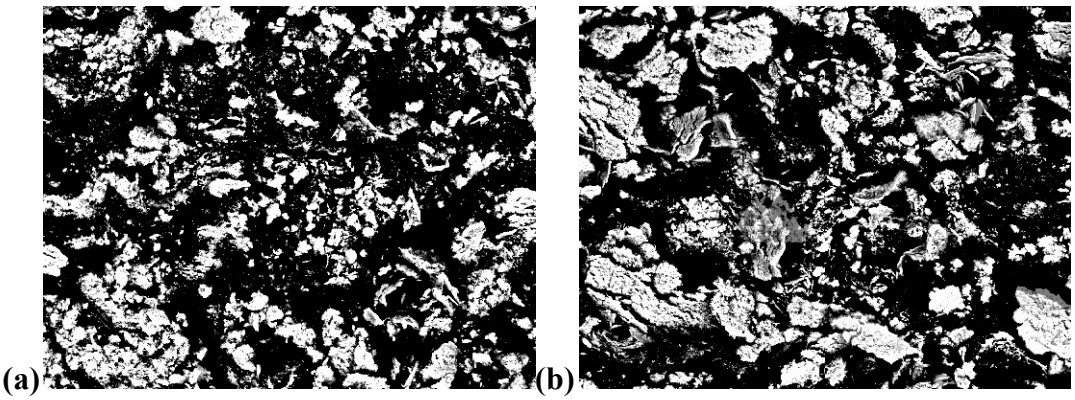

Figure 3.21: Particles of (a) the Li/Al-Naproxen LDH, and (b) the Zn_5-Ibuprofen HS, at approximately 75x magnification.

3.6 Elemental Analysis Data

3.6.1 Herbicides

The approximate formulae of the herbicide-containing LMHs were determined through a combination of the TGA data (for the cointercalated water content) and CHN/ICP analysis. The results are summarised in Table 3.1.

The data show loadings of well over 50% in almost all cases. The predominant non-herbicide charge-balancing species is the hydroxide anion, most likely present due to the additional basicity of the ion-exchange solution used (from the presence of NEt_3). The absence of nitrate from the precursors has been determined from the lack of observed nitrogen in the CHN analyses, and the absence of the strong, distinctive peak at *ca.* 1350cm^{-1} in the FTIR patterns such as those shown in Section 3.3.1.

The number of cointercalated water molecules per formula unit is typical for LDH systems. The Zn_5-HS intercalate shows the maximum possible uptake of 2,4,5T, with

no other charge-balancing anions in the interlayer space; this high loading would make it ideal as a reservoir of the herbicide.

Table 3.1: Approximate chemical formulae of the herbicide-intercalated LMHs.

Compound	Approximate Formula
Ca/Al-2,4DB LDH	$[Ca_2Al(OH)_6](C_{10}H_9Cl_2O_3)_{0.34}(OH)_{0.66}\cdot 2.4H_2O$
Li/Al-2,4DB LDH	$[LiAl_2(OH)_6](C_{10}H_9Cl_2O_3)_{0.83}(OH)_{0.17}\cdot 2.8H_2O$
Li/Al-2,4,5T LDH	$[LiAl_2(OH)_6](C_8H_4Cl_3O_3)_{0.65}(OH)_{0.35}\cdot 2.2H_2O$
Mg/Al-2,4,5T LDH	$[Mg_2Al(OH)_6](C_8H_4Cl_3O_3)_{0.77}(OH)_{0.23}\cdot 1.9H_2O$
Zn_5-2,4,5T HS	$[Zn_5(OH)_8](C_8H_4Cl_3O_3)_2\cdot 2.3H_2O$
Ca/Al-Dichlorprop LDH	$[Ca_2Al(OH)_6](C_9H_7Cl_2O_3)\cdot 1.7H_2O$
Li/Al-Dichlorprop LDH	$[LiAl_2(OH)_6](C_9H_7Cl_2O_3)_{0.6}(OH)_{0.4}\cdot 1.2H_2O$
Mg/Al-Dichlorprop LDH	$[Mg_2Al(OH)_6](C_9H_7Cl_2O_3)_{0.45}(OH)_{0.55}\cdot 2.1H_2O$

3.6.2 Anti-Inflammatory Drugs

The approximate formulae for the anti-inflammatory LMH intercalates, as determined by the methods mentioned above, are summarised in Table 3.2.

The loadings of the drug molecules within the LDHs are uniformly greater than for the herbicides. Once again, the Zn_5-HS appears to be an excellent reservoir for the uptake of the target anion, absorbing it with 100% selectivity, with complete exchange of the precursor nitrate anions. If these high loadings are combined with lengthy release times, then the HS compounds should serve as excellent hosts for the release of either of the classes of target anions intercalated here.

Table 3.2: Approximate chemical formulae of the drug-intercalated LDHs and HSs.

Compound	Approximate Formula
Ca/Al-Diclofenac LDH	$[Ca_2Al(OH)_6](C_{14}H_{10}Cl_2NO_2)_{0.99}(OH)_{0.01}\cdot 2.9H_2O$
Li/Al-Diclofenac LDH	$[LiAl_2(OH)_6](C_{14}H_{10}Cl_2NO_2)_{0.64}(OH)_{0.36}\cdot 3.2H_2O$
Mg/Al-Diclofenac LDH	$[Mg_2Al(OH)_6](C_{14}H_{10}Cl_2NO_2)_{0.6}(OH)_{0.4}\cdot 3.8H_2O$
Zn_5-Diclofenac HS	$[Zn_5(OH)_8](C_{14}H_{10}Cl_2NO_2)_2\cdot 3.1H_2O$
Ca/Al-Ibuprofen LDH	$[Ca_2Al(OH)_6](C_{13}H_{17}O_2)_{0.74}(OH)_{0.26}\cdot 2.9H_2O$
Li/Al-Ibuprofen LDH	$[LiAl_2(OH)_6](C_{13}H_{17}O_2)\cdot 3.3H_2O$
Zn_5-Ibuprofen HS	$[Zn_5(OH)_8](C_{13}H_{17}O_2)_2\cdot 5H_2O$
Ca/Al-Naproxen LDH	$[Ca_2Al(OH)_6](C_{14}H_{13}O_3)_{0.6}(OH)_{0.4}\cdot 3.1H_2O$
Li/Al-Naproxen LDH	$[LiAl_2(OH)_6](C_{14}H_{13}O_3)_{0.65}(OH)_{0.35}\cdot 3.4H_2O$
Mg/Al-Naproxen LDH	$[Mg_2Al(OH)_6](C_{14}H_{13}O_3)_{0.65}(OH)_{0.35}\cdot 3.5H_2O$

3.7 Release Experiment Procedures

In the case of the herbicide-intercalated LMHs, the release experiments were performed by the addition of 0.2g of the intercalated hybrid to the top of a column of soil. 5mL of tap water was added periodically to the top of the column (to represent rainfall), and the liquid that drained through to the bottom of the column was extracted and analysed by UV/Vis spectroscopy.

For the drug-intercalated hosts, the compounds were first immobilised in alginate beads. Sodium alginate was dissolved in water, added dropwise to a small amount of the drug hybrid which had been dispersed in deionised water, and the mixture stirred at 40°C for one hour. This mixed solution was then added dropwise at a strictly controlled dropping rate to a solution of calcium chloride, causing approximately spherical beads to form instantaneously. The beads were then recovered by filtration

and dried. To measure the release of the drugs from these beads, they were added to a pH 2.1 buffer solution at 37°C, and stirred at a slow rate (50rpm), to mimic the churning of the human stomach. After two hours, the beads were transferred to a pH 7.3 buffer solution at the same temperature, with similar stirring. This reflected the change in acidity observed in the upper small intestine. During both of these periods, aliquots were regularly extracted for analysis by UV/Vis spectroscopy. Both of these release methods are described in greater detail in Chapter 6, Section 6.3.

3.8 Release of Herbicides

3.8.1 Release Profiles

Figures 3.22, 3.23 and 3.24 show the release profiles for the 2,4DB, 2,4,5T and Dichlorprop intercalates respectively.

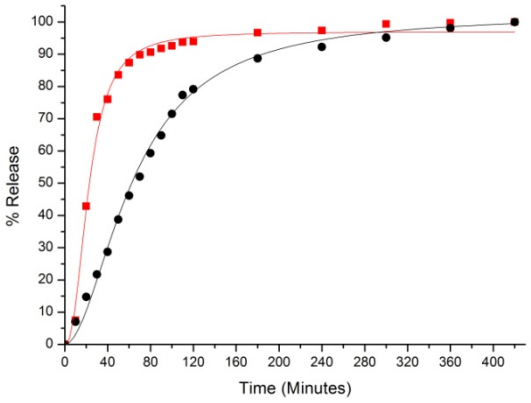

Figure 3.22: Release profiles of the Ca/Al-2,4DB LDH (■), and the Li/Al-2,4DB LDH (●), determined from their concentrations in the water draining through the soil column.

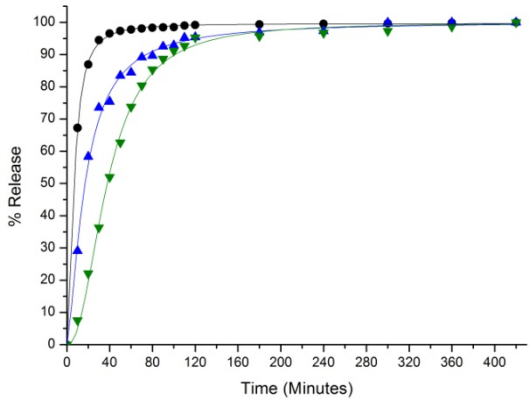

Figure 3.23: Release profiles of the Li/Al-2,4,5T LDH (●), the Mg/Al-2,4,5T LDH (▲), and the Zn_5-2,4,5T HS (▼), determined from their concentrations in the water draining through the soil column.

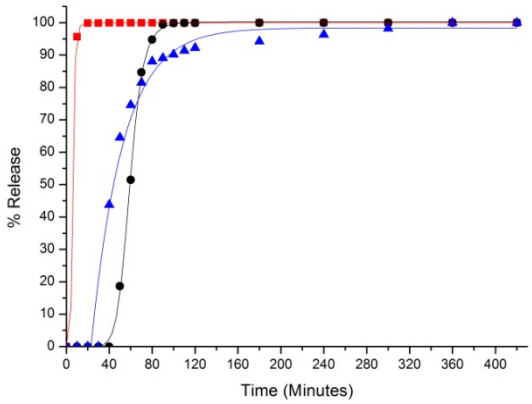

Figure 3.24: Release profiles of the Ca/Al-Dichlorprop LDH (■), the Li/Al-Dichlorprop LDH (●), and the Mg/Al-Dichlorprop LDH (▲), determined from their concentrations in the water draining through the soil column.

In almost every case, all of the intercalated herbicide anions have been released within four hours. This is too rapid for the required application, so it is probable that post-synthetic modification or immobilisation of the hydroxide carrier would be required to allow the release to take place on a timescale of days or weeks. The most gradual release from the LMHs is that from the Li/Al-LDHs (the 2,4,5T intercalate excepted), and from the Zn_5-2,4,5T HS. One unusual release behaviour that may be observed from these graphs is the significant induction period seen in the release of the guests from the Li/Al- and Mg/Al-Dichlorprop LDHs. In these two cases, no herbicide is observed in the drained-through aliquots until 30 and 40 minutes after the

first application of water, respectively; after this point, they release their guests over a short time period. It is possible that this effect is observed here, and not for similar LDHs stirred in solutions, due to the limited contact of the solids' surfaces with the surrounding water, reducing the surface area for exchange or leaching to occur.

The data above have been used to determine t_{90} values for the release of the guests; the comparative values for each LDH-Herbicide system are summarised in Table 3.3.

Table 3.3: The t_{90} values for the release of the guest anion from the listed host, in minutes. The t_{90} value is defined as the amount of time required for 90% of the anions intercalated in the host to be released into solution.

Herbicide	**Host**	**t_{90} (minutes)**
2,4DB	Ca/Al	82
	Li/Al	250
2,4,5T	Li/Al	29
	Mg/Al	81
	Zn_5	119
Dichlorprop	Ca/Al	9
	Li/Al	97
	Mg/Al	96

While the release properties of these compounds have never previously been studied, some analogous LDH-Herbicide compounds have been synthesised, and their t_{90} values determined in a pH 7 buffer solution.[1] The average t_{90} values reported for the Ca/Al-, Mg/Al- and Li/Al-LDH systems reported fell between 20 and 30 minutes. As estimates of herbicide release rates in practical situations, it is apparent that these are underestimates given the values determined above from a more realistic release method.

3.8.2 Kinetics

The five kinetic models introduced in Chapter 1, Section 1.7 were fitted to the data for analysis. Least-squares fits of all five models to the release data for Li/Al-2,4DB LDH are shown in Figure 3.25.

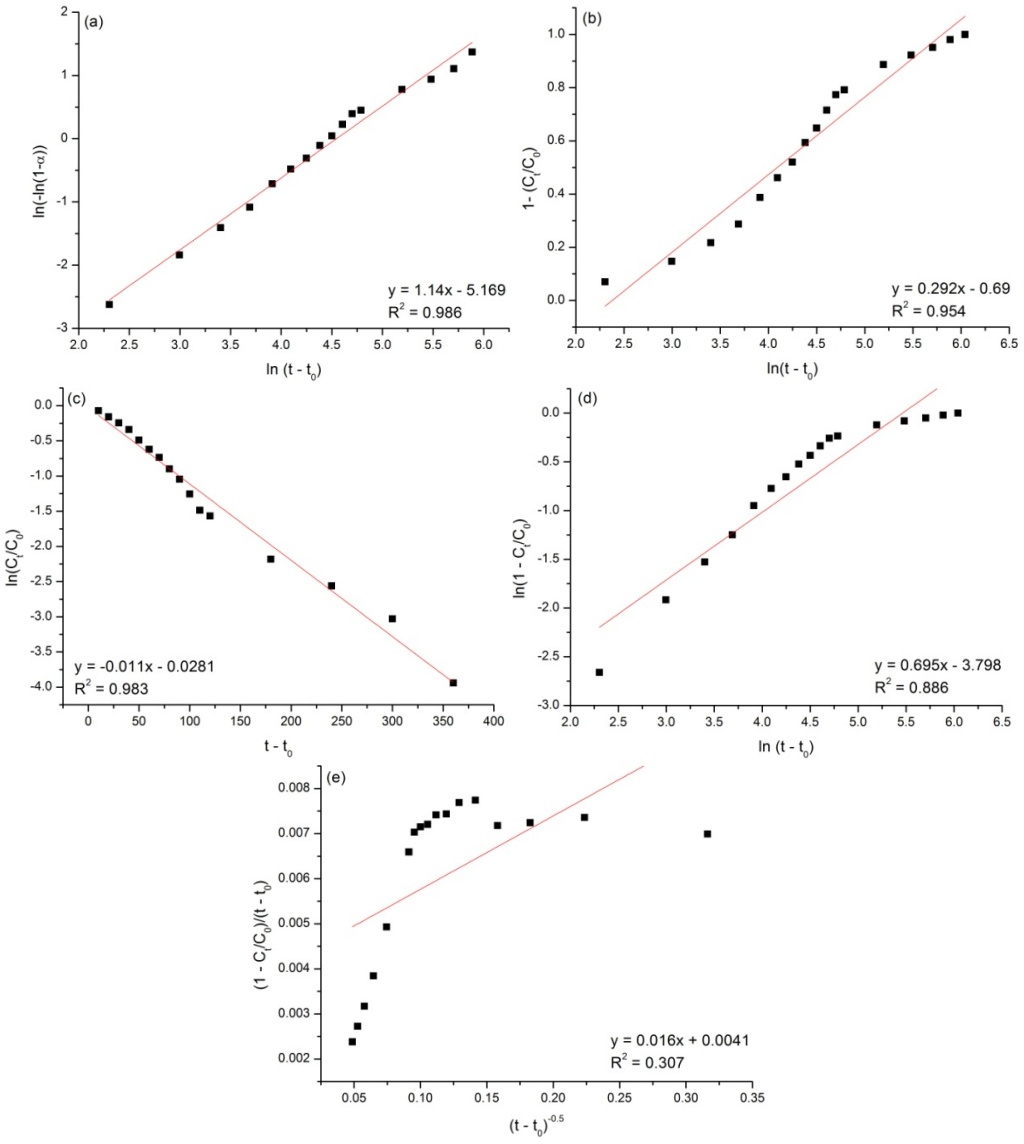

Figure 3.25: Least-squares fits of the various models to the release of 2,4DB from the Li/Al-2,4DB LDH in the soil column. Fits for (a) the Avrami-Erofe'ev model, (b) the Elovich model, (c) the First-Order model, (d) the Freundlich model, and (e) the parabolic diffusion model are shown.

It is difficult to predict which kinetic model is likely to provide the best fits to the data, as many of the common assumptions required for modelling reaction systems

are not applicable here; it is even possible that conventional release models may fail in this instance. It is apparent in much of the data that there appears to be a clear change of gradient in almost every plot, which is particularly noticeable in the Avrami-Erofe'ev and Freundlich plots (Figure 3.25(a) and (d)). This change occurs in each plot at around 110-120 minutes. Table 3.4 summarises the two values of n (the Avrami-Erofe'ev reaction exponent) extracted from the kinetic data: one using the release data up to and including 110 minutes, and the other using the data from 120 minutes onwards.

Table 3.4: Values of the Avrami-Erofe'ev reaction exponent (n) for the release of herbicides from the LMH-Herbicide intercalates, comparing the values before 110 minutes ($n_{t<110}$) with the values after ($n_{t>110}$)

Metals in LMH	**Guest Anion**	$n_{t<110}$	$n_{t>110}$
Ca/Al	2,4DB	1.32	0.70
	Dichlorprop	0.28	0.63
Li/Al	2,4DB	1.26	0.79
	2,4,5T	0.54	0.25
	Dichlorprop	4.49	0.20
Mg/Al	2,4,5T	0.83	0.78
	Dichlorprop	1.38	0.48
Zn	2,4,5T	1.47	0.28

In most cases there is a significant decrease in the value of n after 110 minutes: the only exceptions to this are Ca/Al- and Li/Al-Dichlorprop LDHs, which both release their guests over such a short timescale that the Avrami-Erofe'ev model cannot be effectively applied. When the Avrami-Erofe'ev model is applied to such systems, the values of n produced lie outside of the range from which physical meaning may be

interpreted (such as a reaction exponent of 4.49 for release from the Li/Al-Dichlorprop LDH)

3.9 Release of Anti-Inflammatory Drugs

3.9.1 Release Profiles

Figures 3.26, 3.27 and 3.28 show the release profiles for the alginate-coated diclofenac, ibuprofen and naproxen intercalates respectively.

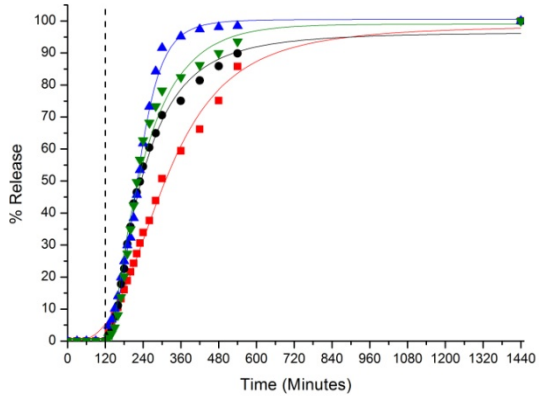

Figure 3.26: Release profiles of the Ca/Al-Diclofenac LDH (■), the Li/Al-Diclofenac LDH (●), the Mg/Al-Diclofenac LDH (▲), and the Zn_5-Diclofenac HS (▼) from alginate beads in pH 2.1 buffer solution (up to 120 minutes), and pH 7.3 buffer solution (after 120 minutes).

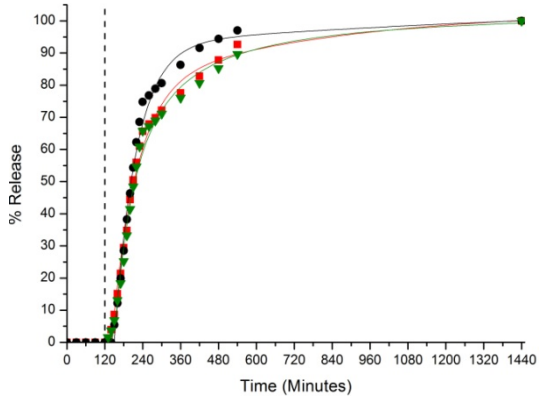

Figure 3.27: Release profiles of the Ca/Al-Ibuprofen LDH (■), the Li/Al-Ibuprofen LDH (●), and the Zn_5-Ibuprofen HS (▼) from alginate beads in pH 2.1 buffer solution (up to 120 minutes), and pH 7.3 buffer solution (after 120 minutes).

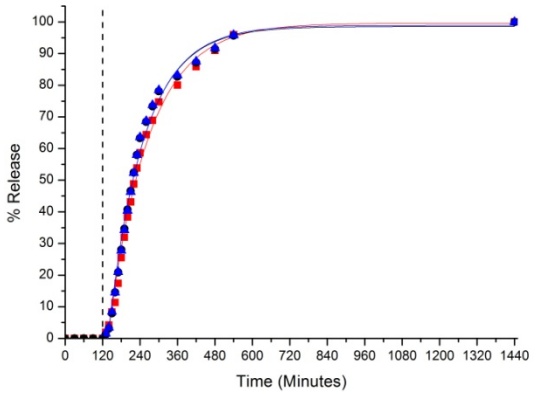

Figure 3.28: Release profiles of the Ca/Al-Naproxen LDH (■), the Li/Al-Naproxen LDH (●), and the Mg/Al-Naproxen LDH (▲) from alginate beads in pH 2.1 buffer solution (up to 120 minutes), and pH 7.3 buffer solution (after 120 minutes).

Each system shows no release of the guest during the two hours of stirring in the pH 2.1 buffer solution, as expected. After transfer to the mildly basic buffer solution, the release is much more gradual than that typically seen for LMHs. Furthermore, in many cases the release rates for different LMHs containing the same guest anion are virtually identical; the plots for the ibuprofen- and naproxen-intercalated hosts show this very clearly. This suggests that the breakdown of the alginate is the principal limiting factor controlling the release rate, although the varying rates of release in the diclofenac system suggest that the factors controlling the rate are perhaps more complex.

To demonstrate the stabilising effect of the alginate matrix on the dissolution of the hydroxide host in the acidic buffer solution, the same release reactions were performed on unprotected ibuprofen-intercalated LDHs. The t_{90} values of the protected and unprotected hosts are compared in Table 3.5.

The time for release of 90% of the drug is hugely increased by the enteric coating in all cases, even for the Zn_5-HS which, when unprotected, shows much more resistance to acidity than the LDHs. The t_{90} values for most of the compounds above are around

420-480 minutes, which is an appropriate timescale for the theoretical application of these materials.

Table 3.5: The t_{90} values (in minutes) for the release of the guest anion from the unprotected (UP) and protected (P) drug hybrids.

Metals in LMH	Guest Anion	t_{90} (UP)	t_{90} (P)	t_{90} (P) – 120
Ca/Al	Diclofenac	6	830	710
	Ibuprofen	12	550	430
	Naproxen	6	490	370
Li/Al	Diclofenac	28	680	560
	Ibuprofen	13	400	280
	Naproxen	17	440	320
Mg/Al	Diclofenac	22	460	340
	Naproxen	3	440	320
Zn	Ibuprofen	201	560	440

3.9.2 Kinetics

The five kinetic models used to investigate the herbicide release in Section 3.8.2 were applied to the data for the release of the anti-inflammatory drugs. Graphs showing the least-squares fits of all five models to the release data for the Zn_5-Ibuprofen HS are shown in Figure 3.29. The graphs below use only the data from 120 minutes onwards, after the transfer of the beads into the pH 7.3 buffer solution. The Avrami-Erofe'ev and First-Order models consistently provide the best fits to the data, with the Elovich model slightly worse but still moderately accurate. The Freundlich model is inconsistent, and the parabolic diffusion model is poor for all hosts and all guest anions. It is apparent that once again there is a noticeable change in the gradients of the both the release profiles and the kinetic model fits that occurs approximately 120 minutes after the transfer of the beads into the pH 7.3 buffer

solution (240 minutes in the release profiles). This change of gradient is absent in the release of ibuprofen from the unprotected Zn_5-Ibuprofen HS.

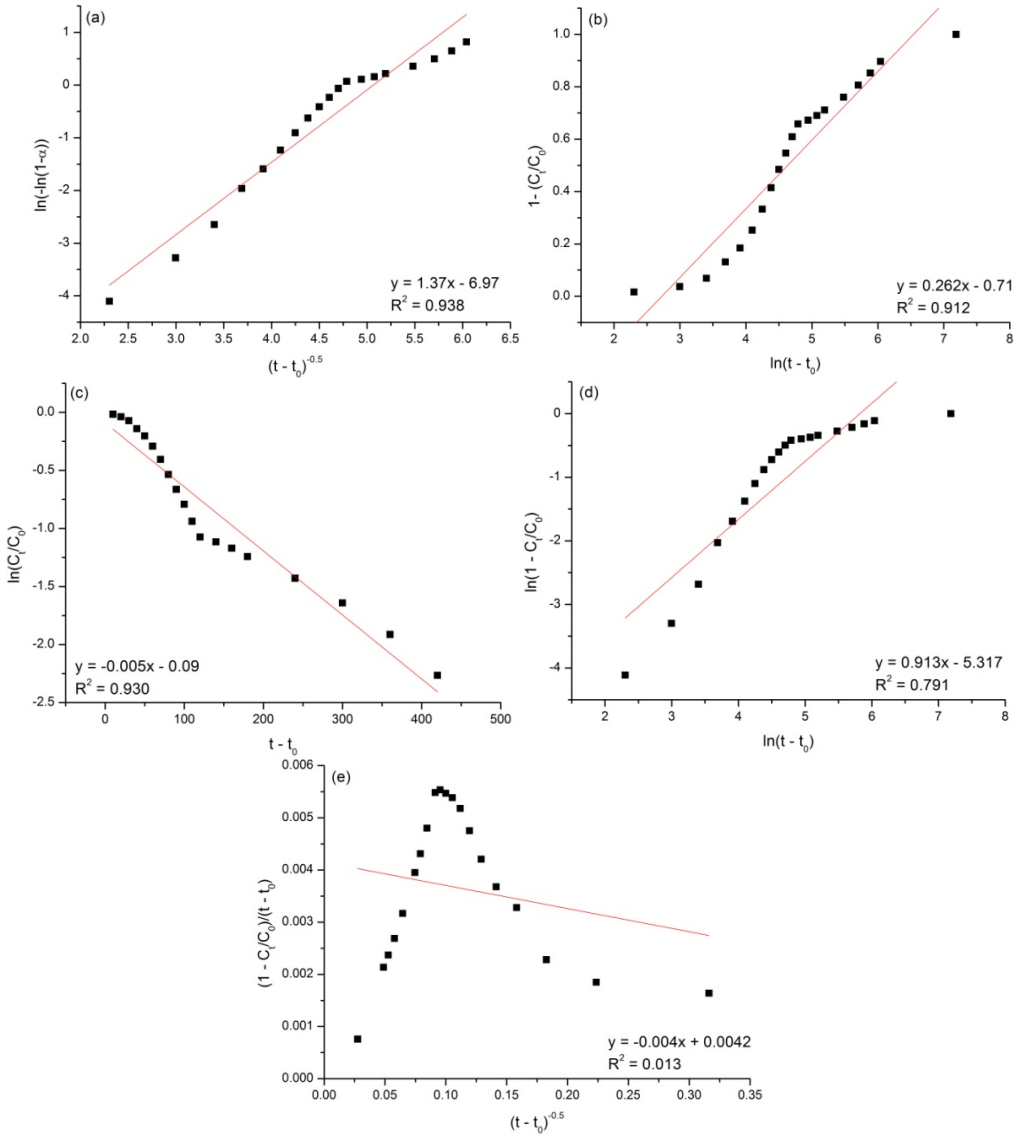

Figure 3.29: Least-squares fits of the release of Ibuprofen from Zn_5-Ibuprofen HS immobilised in alginate beads. Fits for (a) the Avrami-Erofe'ev model, (b) the Elovich model, (c) the First-Order model, (d) the Freundlich model, and (e) the parabolic diffusion model are shown.

The Avrami-Erofe'ev model was used to calculate the values of the reaction exponent (*n*) before and after the 240 minute point at which the change of gradient is observed, and the values before and after that point are summarised in Table 3.6.

Table 3.6: Values of the reaction exponent (n) for the release of anti-inflammatory drugs from the LMH-Drug intercalates, comparing the values before 240 minutes ($n_{t<240}$) with the values after ($n_{t>240}$)

Metals in LMH	Guest Anion	$n_{t<240}$	$n_{t>240}$
Ca/Al	Diclofenac	0.13	0.28
	Ibuprofen	1.85	0.68
	Naproxen	1.60	0.95
Li/Al	Diclofenac	0.22	0.19
	Ibuprofen	0.31	0.12
	Naproxen	1.84	0.84
Mg/Al	Diclofenac	0.20	0.13
	Naproxen	0.25	0.16
Zn_5	Ibuprofen	1.77	0.62

In every case but that of the Ca/Al-Diclofenac LDH (in which the release process has completed within twenty minutes of transfer into the the pH 7.3 buffer), there is a significant reduction in the reaction exponent that occurs after approximately 120 minutes of stirring in the pH 7.3. While the specific time of 120 minutes is the apparent point at which a mechanistic change occurs in both this and the rather different herbicide soil column system, it is likely that the similarity of the timescales is a coincidence, even if the mechanistic justification for the change may be somewhat similar.

3.10 Discussion of Results

The discontinuities in the gradients of the release profiles, and thus the implied changes of mechanism, observed in the seemingly disparate herbicide and drug systems above are linked by the one apparent commonality between the two: the limited degree of contact between the host and the release medium, which enforces an

external limit on the rate of release of the guest from the solid. These discontinuities are observed for all of the examined LMH hosts, as well as for each guest molecule, implying that the mechanistic change observed is independent of these factors, and it further appears to be more than an inclusion phenomenon arising from the immobilisation of the host in the alginate beads, given that it is observed in the herbicide systems with unprotected hosts as well.

A recent paper by Duan *et al.*, in which two-phase release was observed from an unmodified LDH host, suggested an explanation for the change:[35] firstly, guest molecules absorbed on the exterior surface of the host are released rapidly, followed by more gradual release of the interior, intercalated anions. It would seem unlikely that this is the justification for the change in gradient observed here: firstly, comparison of the protected Zn_5-Ibuprofen HS with its unprotected analogue indicates that while release from the former progresses in two stages, the latter shows only a single phase of release (implying that despite any differentiation between surface-bound and intercalated guests, they must be released at approximately the same rate). Furthermore, by the 110-120 minute point at which the change of mechanism is observed, typically 50-70% of the guest molecules have already been released – this is far too great a proportion to be surface-bound, given the particle sizes observed in the SEM data.

It is possible, though, to propose a similar mechanistic pathway to account for the observed change. When the LMH-Herbicide powder is dispersed on the upper surface of the soil column, a portion of the solid is directly in contact with the soil itself, while another portion is in contact with the tap water (the release medium). However, much of the solid is immediately surrounded only by other host particles in all directions. In the case of the anti-inflammatory drug intercalates, the beads are very

large compared to the size of the LMH particles they encapsulate (which are approximately 1mm in diameter). The host particles will be dispersed throughout the beads, and whilst some will inevitably be on or near the surface, many of them will be towards the centre, away from the release medium.

Therefore, the change in mechanism may possibly occur due to the particles that are in direct contact with the release medium releasing their anions first, and fairly rapidly. The second observed phase of release is from the remaining particles that are not in contact with the release medium; this process is slower (as the released guest must diffuse out of the particle, and also pass around other particles to escape the aggregate). A simplified schematic of this process is illustrated below in Figure 3.30.

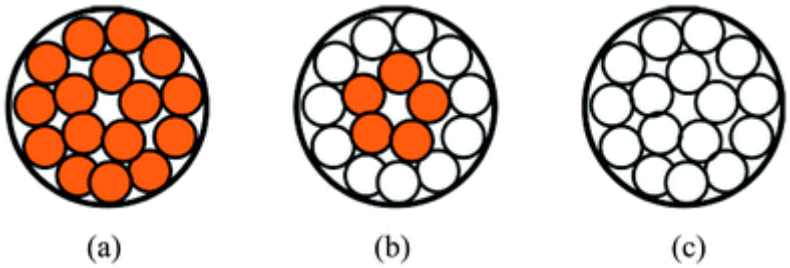

Figure 3.30: Diagram of the proposed release process from hosts with restricted contact to the release medium. (a) The intercalated particles (orange) pack within the bead/aggregate, with some in contact with the surface (and the release medium). (b) In the first step, these surface particles release their guests fairly rapidly. (c) In the second step, the remaining intercalated particles release their guests more slowly, as they must diffuse out of the bead/aggregate around the leftover expended particles.[36]

3.11 Conclusions

Layered double hydroxides and hydroxynitrate salts have been used to intercalate commonly used herbicides and non-steroidal anti-inflammatory drugs (NSAIDs), and their release has been studied in situations mimicking their real-world applications.

Eight herbicide hybrids have been synthesised and fully characterised, with the release of their guests studied by dispersal of the solid on the upper surface of a soil

column, and the concentration of the herbicide released quantified from the drained-through water by UV/Vis spectroscopy. Ten anti-inflammatory drug hybrids have also been synthesised and characterised; these were immobilised in alginate beads, to stabilise them towards acidity for potential use in oral drug delivery systems.

While the release of the guest anions from the herbicide materials was too rapid for practical use as synthesised (with more than 90% of the guest released in under four hours for every compound), further immobilisation and post-synthetic modification of the solids may lead to more useful and sustained release. The release of the anti-inflammatory drugs was much more successful, taking on average 6-7 hours to release 90% of the guest when stirred in a pH 7.3 solution designed to break down the alginate beads after no release was observed in a pH 2.1 buffer solution. The timescale for this release is, on average, 20 times longer than that observed for an unprotected LDH in the same solution.

Analysis of the kinetics of the release processes, as determined by the Avrami Erofe'ev model, provided an insight into the mechanism of release from the particles. In both the case of release in the soil column and from the alginate beads, a distinct change in release rate was observed after approximately two hours of reaction, which the Avrami-Erofe'ev kinetic model implied was the result of a change in the release mechanism. A tentative suggestion for this two-phase release process has been proposed, based on a first step of rapid release from accessible surface particles in contact with the release medium, followed by slower release from the occluded particles, as the guest anions diffuse out of the aggregate surrounding them.

3.12 References

1. A. I. Khan, A. Ragavan, B. Fong, C. Markland, M. O'Brien, T. G. Dunbar, G. R. Williams and D. O'Hare, *Industrial & Engineering Chemistry Research*, 2009, **48**, 10196-10205.

2. Z. Xu, Z. Gu, X. Cheng, F. Rasoul, A. Whittaker and G. Lu, *Journal of Nanoparticle Research*, **13**, 1253-1264.
3. V. Bugatti, G. Gorrasi, F. Montanari, M. Nocchetti, L. Tammaro and V. Vittoria, *Applied Clay Science*, 2011, **52**, 34-40.
4. M. L. Zheludkevich, S. K. Poznyak, L. M. Rodrigues, D. Raps, T. Hack, L. F. Dick, T. Nunes and M. G. S. Ferreira, *Corrosion Science*, 2009, **52**, 602-611.
5. M. Z. Bin Hussein, N. Hashim, A. Yahaya and Z. Zainal, *Journal of Nanoscience and Nanotechnology*, 2009, **9**, 2140-2147.
6. M. Ahmed Khan, C.-L. Choi, D.-H. Lee, M. Park, B.-K. Lim, J.-Y. Lee and J. Choi, *Journal of Physics and Chemistry of Solids*, 2007, **68**, 1591-1597.
7. L. P. Cardoso, R. Celis, J. Cornejo and J. o. B. Valim, *Journal of Agricultural and Food Chemistry*, 2006, **54**, 5968-5975.
8. F. Li, L. Jin, J. Han, M. Wei and C. Li, *Industrial & Engineering Chemistry Research*, 2009, **48**, 5590-5597.
9. M. del Arco, A. Fernández, C. Martín and V. Rives, *Applied Clay Science*, 2009, **42**, 538-544.
10. H. Zhang, D. Pan, K. Zou, J. He and X. Duan, *Journal of Materials Chemistry*, 2009, **19**, 3069-3077.
11. A. Akelah, *Journal of Chemical Technology & Biotechnology. Chemical Technology*, 1984, **34**, 263-286.
12. Z. Gerstl, *Behaviour of Organic Agrochemicals in Irrigated Soils*, The Royal Society of Chemistry, 1991.
13. E.-R. Kenawy, *Journal of Macromolecular Science - Reviews in Macromolecular Chemistry & Physics*, 1998, **38**, 365 - 390.
14. M. Cruz-Guzman, R. Celis, M. C. Hermosin, W. C. Koskinen and J. Cornejo, *Journal of Agricultural and Food Chemistry*, 2005, **53**, 7502-7511.
15. L. Cox, W. C. Koskinen, R. Celis, M. C. Hermosin, J. Cornejo and P. Y. Yen, *Soil Science Society of America Journal*, 1998, **62**, 911-915.
16. M. J. Carrizosa, W. C. Koskinen, M. C. Hermosin and J. Cornejo, *Applied Clay Science*, 2001, **18**, 223-231.
17. E. González-Pradas, M. Villafranca-Sánchez, M. Socías-Viciana, M. Fernández-Pérez and M. D. Ureña-Amate, *Journal of Chemical Technology & Biotechnology*, 1999, **74**, 417-422.
18. M. A. Ulibarri, I. Pavlovic, M. C. Hermosín and J. Cornejo, *Applied Clay Science*, 1995, **10**, 131-145.
19. V. Sokolova and M. Epple, *Angewandte Chemie International Edition*, 2008, **47**, 1382-1395.
20. S.-J. Choi, J.-M. Oh and J.-H. Choy, *Journal of Materials Chemistry*, 2008, **18**, 615-620.
21. S.-J. Choi, J.-M. Oh, T. Park and J.-H. Choy, *Journal of Nanoscience and Nanotechnology*, 2007, **7**, 4017-4020.
22. P. A. S. Breslin, T. N. Gingrich and B. G. Green, *Chemical Senses*, 2001, **26**, 55-65.
23. F. Liu and A. W. Basit, *Journal of Controlled Release*, 2010, **147**, 242-245.
24. Z.-Z. Piao, M.-K. Lee and B.-J. Lee, *International Journal of Pharmaceutics*, 2008, **350**, 205-211.
25. J.-P. Zhang, Q. Wang, X.-L. Xie, X. Li and A.-Q. Wang, *Journal of Biomedical Materials Research Part B: Applied Biomaterials*, 2010, **92B**, 205-214.

26. J.-M. Oh, T. T. Biswick and J.-H. Choy, *Journal of Materials Chemistry*, 2009, **19**, 2553-2563.
27. W. Feitknecht, *Helvetica Chimica Acta*, 1933, **16**, 427-454.
28. W. Stählin and H. R. Oswald, *Acta Crystallographica*, 1970, **B26**, 860-863.
29. G. G. C. Arizaga, K. G. Satyanarayana and F. Wypych, *Solid State Ionics*, 2007, **178**, 1143-1162.
30. E. Delahaye, S. Eyele-Mezui, J.-F. Bardeau, C. Leuvrey, L. Mager, P. Rabu and G. Rogez, *Journal of Materials Chemistry*, 2009, **19**, 6106-6115.
31. J. Tronto, F. Leroux, M. Dubois, C. Taviot-Gueho and J. B. Valim, *Journal of Physics and Chemistry of Solids*, 2006, **67**, 978-982.
32. S. Yamanaka, T. Sako, K. Seki and M. Hattori, *Solid State Ionics*, 1992, **53-56**, 527-533.
33. J.-H. Yang, Y.-S. Han, M. Park, T. Park, S.-J. Hwang and J.-H. Choy, *Chemistry of Materials*, 2007, **19**, 2679-2685.
34. E. Kandare and J. M. Hossenlopp, *Inorganic Chemistry*, 2006, **45**, 3766-3773.
35. X. Kong, L. Jin, M. Wei and X. Duan, *Applied Clay Science*, 2010, **49**, 324-329.
36. R. M. R. Bull, C. Markland, G. R. Williams and D. O'Hare, *Journal of Materials Chemistry*, 2011, **21**, 1822-1828.

Chapter 4

Intercalation and Release of Dyes and Colour Fixants

4.1 Introduction

Contrary to the ubiquity of research concerning the absorption and intercalation of dyes by LDHs,[1-6] almost no research has been performed regarding the deintercalation or controlled release of dye molecules from these materials.[7] Given the selectivity of common LDH hosts for intercalation of the carbonate anion preferentially over any other, it is possible that an LDH-Dye hybrid could be used to visually indicate the presence of carbonate in a solution. A particular application of this would be for rapid visual identification of the 'hardness' of water. 'Hard' water contains dissolved calcium carbonate in greater than normal concentrations, and the precipitation of this solid in household appliances (such as kettles and washing machines) can lead to considerable amounts of damage. An optimal dye-containing LDH, when added to 'soft' water containing only trace amounts of carbonate, should release no dye into solution, whilst even the modest amount of carbonate present in 'hard' water should cause an immediate visible colour change. Many 'hard' water detection systems employ titration methods, utilising chemicals with a finite shelf-life.[8] The dye molecule that is intercalated should meet a number of criteria: it should be anionic; it should absorb light strongly in the visible region of the spectrum; it should demonstrate a colour change in 'hard' water in no more than a few minutes; and it should ideally be relatively inexpensive if large-scale syntheses of the hybrid are to be required. For the sample case of exploring this functionality, the anionic dye tartrazine was selected. The structure of the tartrazine trianion is shown in Figure 4.1.

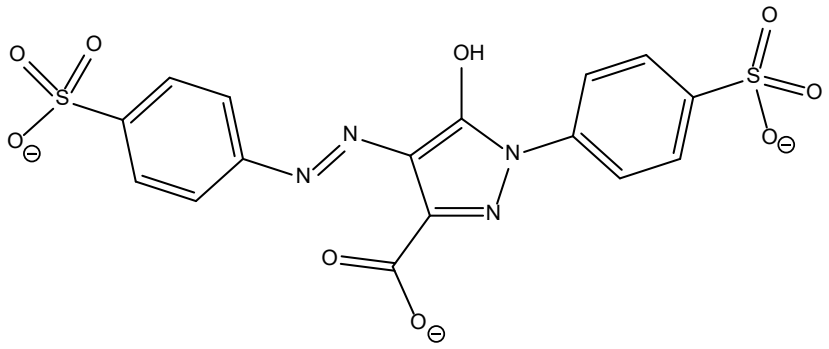

Figure 4.1: The trianionic form of tartrazine

Although well known as a strong yellow-orange colourant used particularly in soft drinks, there is scant research concerning its intercalation into layered double hydroxides,[9, 10] and none regarding its release.

In most instances where industrial dyes are used, it is important to ensure that they remain 'fixed' to the object which they are colouring. One of the most common, and chemically simple of these is the thiosulfate anion ($S_2O_3^{2-}$). It has an abundance of practical applications as a titration standard,[11] a rapid means of dechlorinating water,[12] and as an antidote to cyanide poisoning (providing a source of sulfur to promote conversion of cyanide to thiocyanate by the enzyme rhodanese).[13] Investigations of its LDH intercalation compounds mostly concern the ability of the intercalated anions to complex metal cations from solution,[14, 15] or the oxidative removal of iodide from radioactive waste streams.[16] A further common application of the thiosulfate anion is as a colour fixant in washing powders, reacting with residual hypochlorite to protect them from running in the presence of bleach.[17] For the anion to be gradually released over the course of a washing cycle (to ensure a sustained concentration of the anion) would be ideal for this application.

The syntheses of the intercalation compounds of both thiosulfate and tartrazine into the Li/Al-Cl LDH ($[LiAl_2(OH)_6]Cl{\cdot}yH_2O$), the Mg/Al-$NO_3$ LDH ($[Mg_2Al(OH)_6]NO_3{\cdot}yH_2O$), and the Mg/Fe-Cl LDH ($[Mg_2Fe(OH)_6]Cl{\cdot}yH_2O$) systems

are described below, along with the characterisation of their physical and structural properties. The kinetics of their release in functionally appropriate systems is also studied and analysed using a number of kinetic models.

4.2 Powder X-ray Diffraction Data

4.2.1 Thiosulfate

The thiosulfate anion was intercalated into the LDH systems by addition of a precursor nitrate or chloride LDH to a solution containing a four- to fivefold excess of sodium thiosulfate. The mixture was aged at 80°C for 24 hours, and the solid recovered by vacuum filtration.

The X-ray diffraction pattern of the Li/Al-, Mg/Al-, and Mg/Fe-Thiosulfate LDHs are depicted in Figures 4.2, 4.3 and 4.4, along with those of their precursor LDHs.

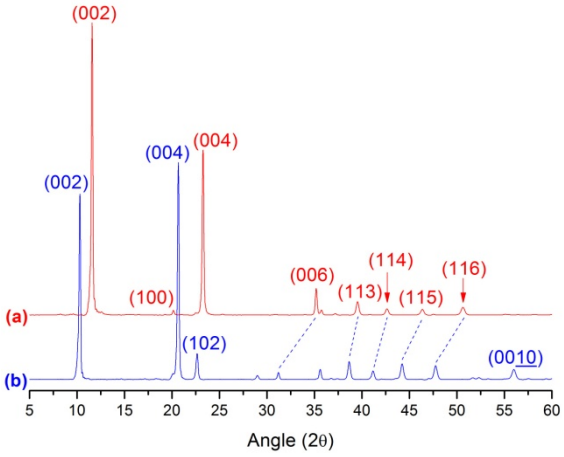

Figure 4.2: Powder XRD patterns of (a) the Li/Al-Cl LDH and (b) the Li/Al-Thiosulfate LDH. The d-spacings of the (002) reflections of the above patterns are 7.2 and 8.6Å respectively. Reflections indexed with the same Miller indices are connected by dashed lines.

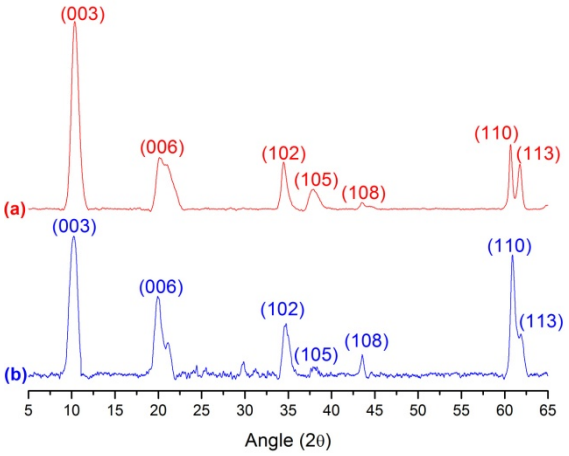

Figure 4.3: Powder XRD patterns of (a) the Mg/Al-NO_3 LDH and (b) the Mg/Al-Thiosulfate LDH. The d-spacings of the (003) reflections of the above patterns are 8.5 and 8.6Å respectively.

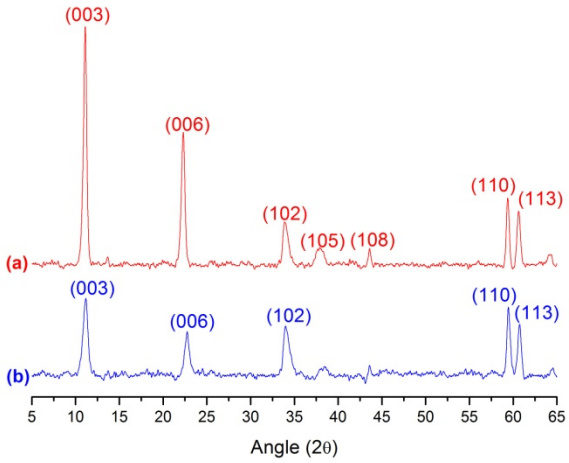

Figure 4.4: Powder XRD patterns of (a) the Mg/Fe-Cl LDH and (b) the Mg/Fe-Thiosulfate LDH. The d-spacings of the (003) reflections of the above patterns are 8.0 and 7.9Å respectively.

The data demonstrate a noticeable change in the positions of the reflections for the intercalated compound: the gallery height increases from 2.3Å to 3.8Å in the Li/Al system and from 3.7Å to 3.8Å in the Mg/Al system, corresponding well in the latter case to observed values from the literature.[18] The change in the *c* parameter in the Mg/Fe-Thiosulfate LDH suggests a very slight decrease in the gallery height from 3.2Å to 3.1Å. The elemental analyses of the compounds (in Section 4.5.1) indicate that the Mg/Fe-Thiosulfate LDH compound loses some of its cointercalated water

following ion exchange with thiosulfate, and it is possible that the contraction of the interlayer space that accompanies this may be masking the expected increase due to the intercalation of a larger anion. There is also a possibility that the thiosulfate molecule may bind directly to the layers (as has been observed in the Ca/Al-NO_3 LDH system),[19] causing a reduction in the interlayer spacing instead of an increase, but the lack of any apparent change in the FTIR spectrum upon intercalation (in Section 4.3.1) suggests that this is unlikely.

4.2.2 Tartrazine

Tartrazine was intercalated into the LDH systems in much the same way as thiosulfate: the precursor LDH was added to a fivefold excess solution of tartrazine (a trisodium salt), and stirred at 80°C for 72 hours. However, the Mg/Fe-Tartrazine LDH could only be synthesised with low loadings by direct ion-exchange methods. As a result, this compound was synthesised by the reconstruction method: a Mg/Fe-Cl LDH was synthesised by coprecipitation, and the chloride exchanged for carbonate. This carbonate LDH was then heated at 500°C for two hours to produce the Mg/Fe layered double oxide (LDO), which was then stirred in a threefold excess solution of tartrazine in a sealed Schlenk tube for 120 hours at 60°C to produce the final Mg/Fe-Tartrazine LDH product. Further details of these methods are reported in Chapter 6, Section 6.4.

The diffraction patterns of the Li/Al-, Mg/Al-, and Mg/Fe-Tartrazine LDH compounds are shown in Figures 4.5, 4.6 and 4.7, with their precursor LDHs.

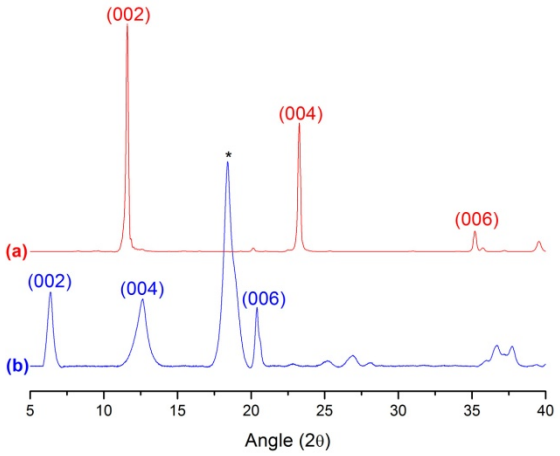

Figure 4.5: Powder XRD patterns of (a) the Li/Al-Cl LDH and (b) the Li/Al-Tartrazine LDH. The d-spacings of the (002) reflections of the above patterns are 7.2 and 13.8Å respectively. The strong reflection at *ca.* 18º, marked with a black asterisk, arises from gibbsite.

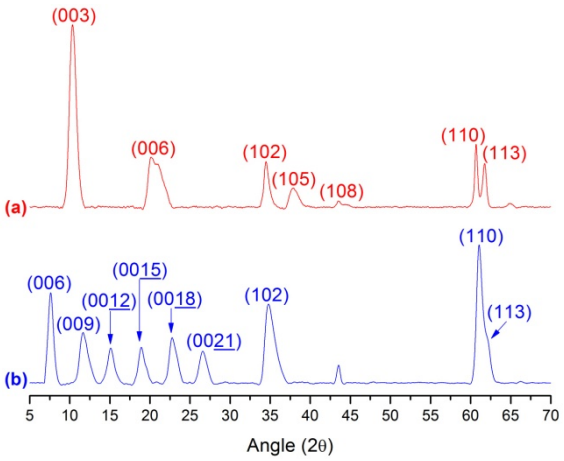

Figure 4.6: Powder XRD patterns of (a) the Mg/Al-NO_3 LDH and (b) the Mg/Al-Tartrazine LDH. The d-spacings of the (003) reflections of the above patterns are 8.5 and 8.7Å respectively.

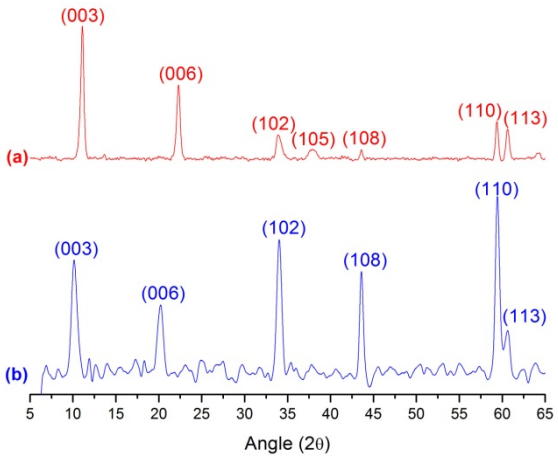

Figure 4.7: Powder XRD patterns of (a) the Mg/Fe-Cl LDH and (b) the Mg/Fe-Tartrazine LDH. The d-spacings of the (003) reflections of the above patterns are 8.0 and 8.7Å respectively.

The first Bragg reflection observed in Figure 4.6(b) is the second (00*l*) basal reflection expected to be seen in the pattern. Examination of the solid at low angles allows the first expected reflection, (003), to be observed at the predicted position (corresponding to a d-spacing of approximately 23.6Å).

The gallery heights of the LDHs increase from 2.3Å to 9.0Å for the Li/Al-LDH compound, and from 3.7Å to 18.8Å for the Mg/Al-LDH. The expansion observed in the Mg/Fe-LDH is less significant, increasing from 3.2Å to 3.9Å. The pattern of the Li/Al-Tartrazine LDH also shows an unusually intense reflection at *ca.* 18°, which can be attributed to the (002) reflection of gibbsite, indicating some degree of lithium deintercalation from the starting material (although there may be some contribution from the (006) reflection of the LDH product, expected to be present at approximately the same position in the pattern).

These greatly varying expansions suggest that tartrazine must adopt quite different arrangements within the interlayer space for each compound. Given that one molecule of tartrazine has an approximate end-to-end length of 19.3Å, and that the approximate thickness of an LDH layer is 4.8Å,[20] it is possible to suggest orientations of the

molecules in the interlayer space. By simple trigonometry, the tilt angle of the tartrazine molecules between the layers are calculated for the Li/Al-, Mg/Al- and Mg/Fe-Tartrazine LDHs to be 26.8°, 66.9° and 11.3° respectively. These angles are illustrated in Figure 4.8.

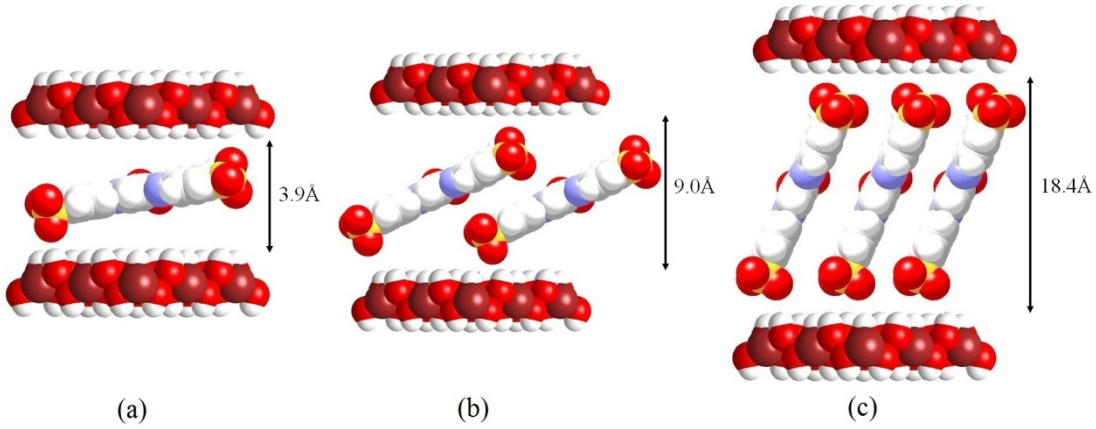

Figure 4.8: Illustration of the increasing interlayer tilting angles of tartrazine in (a) the Mg/Fe-Tartrazine LDH, (b) the Li/Al-Tartrazine LDH, and (c) the Mg/Al-Tartrazine LDH. The interlayer spacings are also shown.

Due to the length and high charge of the molecule, a single tartrazine molecule lying at 11.3° as in the Mg/Fe-Tartrazine LDH occupies a flat area equivalent to six formula units within a single layer. This would limit the maximum percentage loading of tartrazine in the compound to 16.7%, which suggests a possible explanation for the seemingly low amount of intercalated tartrazine in the Mg/Fe-LDH product, as observed by elemental analysis (in Section 4.5.2).

4.3 FTIR Data

4.3.1 Thiosulfate

FTIR spectroscopy was used to qualitatively analyse the presence of thiosulfate in the product LDHs. The IR spectra of the Li/Al- and Mg/Al-Thiosulfate LDHs are shown in Figures 4.9 and 4.10. As before, the absorptions found in each spectrum

between 2400 and 1900cm^{-1} are attributed to the diamond reflectance surface of the spectrometer.

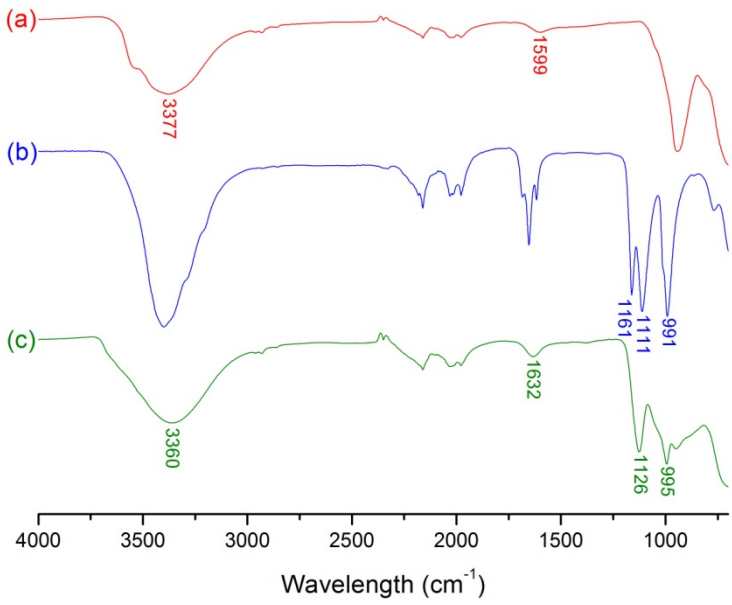

Figure 4.9: FTIR Transmittance Spectra of (a) the Li/Al-Cl LDH, (b) sodium thiosulfate and (c) the Li/Al-Thiosulfate LDH.

The broad absorption at *ca.* 3370cm^{-1} is attributed to the ν_{OH} absorptions of the cointercalated water. The other absorptions deriving solely from the LDH lattice are the peaks at *ca.* 1600cm^{-1} (the δ_{OH} mode of the hydroxide layers), and the two broad peaks below 1000cm^{-1} which arise from Al-O stretching modes. The symmetric ν_{SO} absorption of thiosulfate is found at 991cm^{-1} in the sodium salt, and 995cm^{-1} in the LDH intercalate, while the bands attributable to the asymmetric SO_3 stretch, found at 1111 and 1161cm^{-1} in the sodium salt, are found coalesced into a single absorption at 1126cm^{-1} in the LDH product.[21, 22]

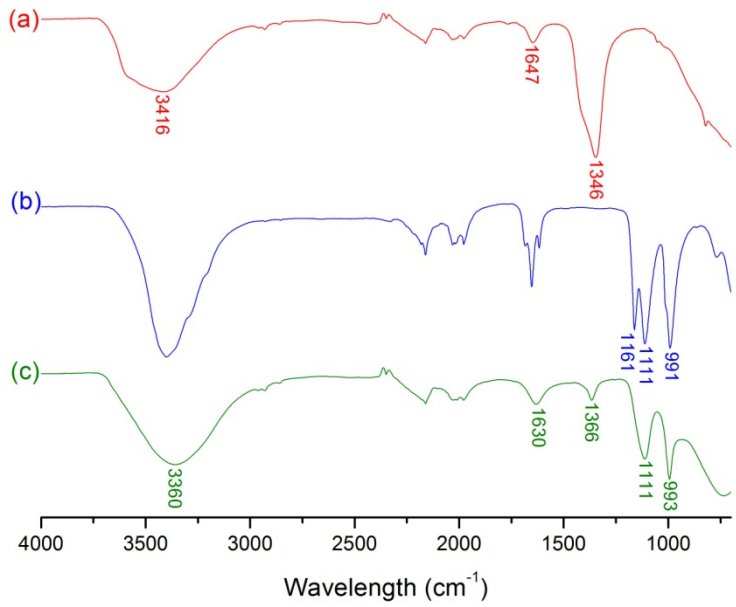

Figure 4.10: FTIR Transmittance Spectra of (a) the Mg/Al-NO_3 LDH, (b) sodium thiosulfate, and (c) the Mg/Al-Thiosulfate LDH.

The strong absorptions observed in the Mg/Al- LDHs that are not seen in the Li/Al-LDH spectra are those associated with carbonate and nitrate. The ν_{CO} and ν_{NO} absorptions of these two anions are both found in the region of 1350-1370cm^{-1} (Meng *et al.* report a separation of 14cm^{-1}),[23] and in this case the elemental analysis results are the key to their correct attributions, as the presence or absence of carbon or nitrogen in the solid compound can be used to identify the anion from which the absorptions arise. The Mg/Al-NO_3 LDH precursor contains a trace of carbonate, which is entirely masked by the intense nitrate absorption, but is visible in the thiosulfate intercalate (which contains no unexchanged nitrate, only the small of amount of carbonate which persists). The Mg/Fe-Cl LDH similarly shows a little carbonate in the starting material, and a somewhat increased amount in the product LDH.

4.3.2 Tartrazine

IR spectroscopy was also used to analyse the presence of tartrazine in the relevant intercalation products. The IR spectra of the Li/Al- and Mg/Al-Tartrazine LDH intercalates are depicted in Figures 4.11 and 4.12.

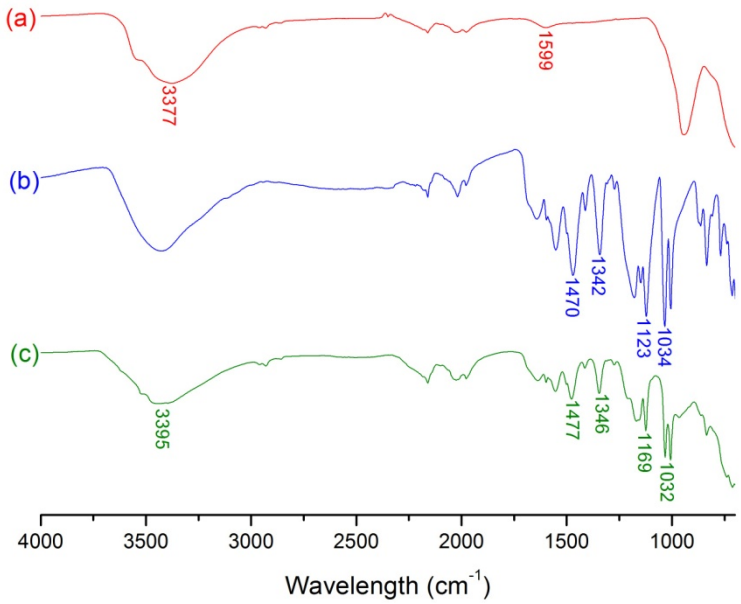

Figure 4.11: FTIR Transmittance Spectra of (a) the Li/Al-Cl LDH, (b) tartrazine, and (c) the Li/Al-Tartrazine LDH.

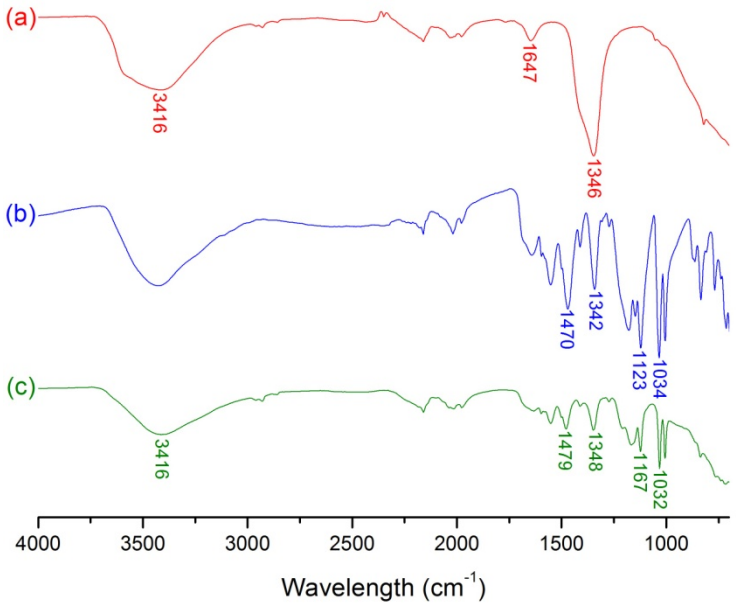

Figure 4.12: FTIR Transmittance Spectra of (a) the Mg/Al-Cl LDH, (b) tartrazine, and (c) the Mg/Al-Tartrazine LDH.

Each of the tartrazine LDH spectra shows a number of distinctive absorptions. The most prominent, marked in the spectra above, are: the C-N=N bend ($\delta_{C\text{-}N=N}$) at *ca.* 1480cm^{-1}; the symmetric $\nu_{N=N}$ absorption at *ca.* 1345cm^{-1}; the C-N stretch ($\nu_{C\text{-}N}$) at *ca.* 1170cm^{-1}; and the pair of sharp absorptions at *ca.* 1030cm^{-1}, corresponding to the asymmetric $\nu_{N=N}$ and the symmetric $\nu_{S\text{-}O}$ absorptions.[24] These absorptions are also observed in the Mg/Fe-Tartrazine LDH, although somewhat more weakly than in the Li/Al- or Mg/Al-LDH analogues.

4.4 TGA Data

4.4.1 Thiosulfate

Thermogravimetric analysis (TGA) was used to determine the amount of co-intercalated water in the thiosulfate LDHs, and the progression of their decomposition at high temperatures. An example TGA plot of the Li/Al-Thiosulfate LDH is shown below in Figure 4.13.

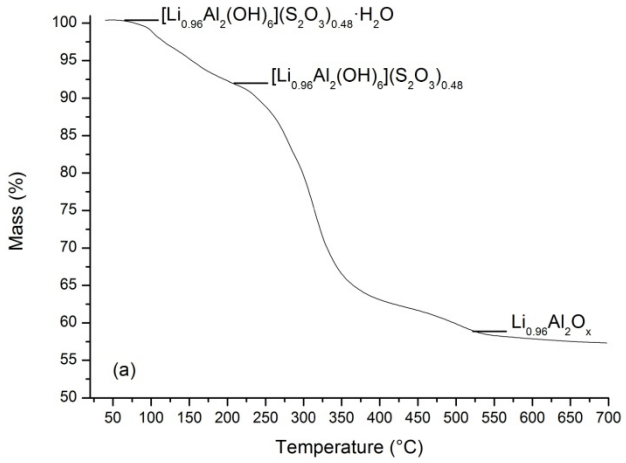

Figure 4.13: The TGA plot of the Li/Al-Thiosulfate LDH.

This TGA plot is typical for a simple LDH compound. Two distinct losses can be seen; the first corresponds to the loss of the co-intercalated water in the structure, leading to the anhydrous form of the LDH (calculated to correspond to 7.7% of the

original mass; a loss of 7.8% is observed). The second mass loss is the result of the decomposition of the thiosulfate anion to gaseous sulfur oxide products, and the loss of much of the hydroxide layers as water (calculated 32.2%; observed 33.4%). After the second major mass loss, the product that remains is an amorphous lithiated alumina (in the case of the Li/Al-Thiosulfate LDH). For the Mg/Al- and Mg/Fe-Thiosulfate LDHs, a mixture of bimetallic spinels and unary metal oxides is observed by powder diffraction as the product after heating to 700ºC.

4.4.2 Tartrazine

The LDH-Tartrazine compounds were also subjected to thermogravimetric analysis. The TGA plot of the Li/Al-Tartrazine LDH is depicted in Figure 4.14.

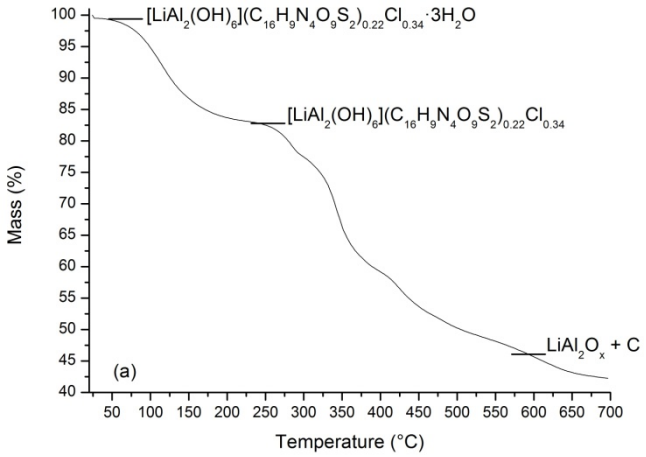

Figure 4.14: The TGA plot of the Li/Al-Tartrazine LDH.

The TGA plot of this tartrazine intercalate is similar to that of the thiosulfate equivalent, as the first major mass loss may be attributed to the loss of cointercalated water (calculated 16.3%, observed 17.0%), while the second corresponds to the decomposition of the interlayer anion, along with dehydroxylation of the LDH layers (calculated 36.3%, observed 37.0%). It is also possible to see that the decomposition of the tartrazine anion between 200 and 500°C progresses through a number of distinct steps, arising from successive decarboxylations and desulfonations; the

temperature range for this decomposition is lower than that previously noted in the literature for the sodium salt.[25] The chemical formulae of the final decomposition products are indistinct, as the metal oxide products are invariably contaminated by a significant amount of carbon soot that has not been evolved in gaseous form during the initial decomposition steps.

4.5 Elemental Analysis Data

4.5.1 Thiosulfate

The approximate formulae of the thiosulfate LDHs were determined through a combination of the TGA data and CHN/ICP elemental microanalysis. The results are summarised in Table 4.1.

Table 4.1: Approximate chemical formulae of the three thiosulfate LDHs.

Compound	Approximate Formula
Li/Al-Thiosulfate LDH	$[Li_{0.96}Al_2(OH)_6](S_2O_3)_{0.48}\cdot H_2O$
Mg/Al-Thiosulfate LDH	$[Mg_2Al(OH)_6](S_2O_3)_{0.49}(CO_3)_{0.01}\cdot 1.2H_2O$
Mg/Fe-Thiosulfate LDH	$[Mg_{2.2}Fe(OH)_6](S_2O_3)_{0.64}(CO_3)_{0.06}\cdot 2H_2O$

The traces of carbonate found in the Mg/Al- and Mg/Fe-Thiosulfate LDH products are the result of atmospheric contamination, and are also present in slightly smaller amounts in their respective precursors (these utilise highly basic solutions in their syntheses, which are prone to dissolving atmospheric carbon dioxide). A small amount of Li^+ is leached from the Li/Al-Cl LDH during thiosulfate intercalation, leading to a deviation from the optimal Li:Al ratio in the product.

4.5.2 Tartrazine

The approximate formulae for the tartrazine LDHs are shown in Table 4.2.

Table 4.2: Approximate chemical formulae of the three tartrazine LDHs.

Compound	Approximate Formula
Li/Al-Tartrazine LDH	$[LiAl_2(OH)_6](C_{16}H_9N_4O_9S_2)_{0.22}Cl_{0.34}\cdot 3H_2O$
Mg/Al-Tartrazine LDH	$[Mg_2Al(OH)_6](C_{16}H_9N_4O_9S_2)_{0.24}(NO_3)_{0.28}\cdot 3.9H_2O$
Mg/Fe-Tartrazine LDH	$[Mg_{2.2}Fe(OH)_6](C_{16}H_9N_4O_9S_2)_{0.13}(OH)_{1.01}\cdot 2.8H_2O$

As tartrazine exists as a trianion, complete occupation of all guest sites would result in an optimal formula of $[LDH](C_{16}H_9N_4O_9S_2)_{0.33}\cdot yH_2O$. This full occupation may be at least partially prevented by the geometric constraints mentioned in Section 4.2.2. In particular, the long flat-lying anions in the Mg/Fe-Tartrazine LDH may be one of the root causes of its seemingly poor loading. It should also be noted that the number of molecules of cointercalated water per formula unit is slightly greater than average for an LDH (*cf.* the thiosulfate LDHs in Section 4.5.1). The long, highly charged anion may be heavily coordinated by water molecules, which may also serve a structural purpose in preventing the collapse of the interlayer space when the separation of the layers is so great.

4.6 UV/Vis Measurements and Calibration

In both cases, the UV measurements of the concentrations of the released anions in solution suffered from the same measurement problems as for the sweetener molecules, reported in Chapter 2, Section 2.7.2. This was particularly the case for tartrazine which, as a highly conjugated azo dye, shows an intense visible absorption even at very low concentrations. An example comparison of the UV spectra of two samples of tartrazine in water is demonstrated in Figure 4.15. The two principal absorptions of tartrazine, at *ca.* 260 and 430nm, are clearly visible.[26]

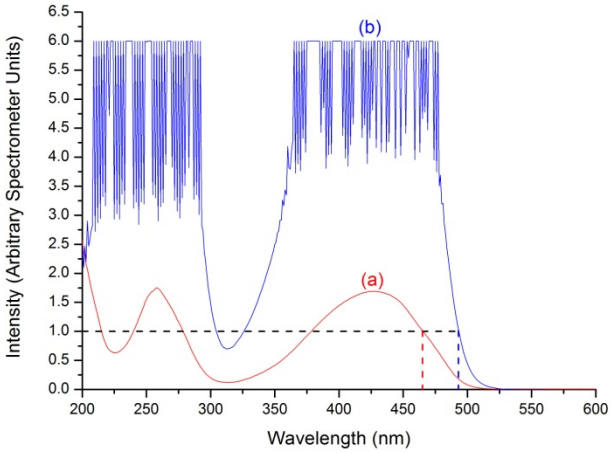

Figure 4.15: UV/Visible absorption spectra of (a) a highly diluted tartrazine solution, and (b) a tartrazine solution from a preliminary release experiment. The dotted line shows the points at which the λ_{CROSS} values were collected (here, at 465.2 and 493.3nm respectively).

The logarithmic relationships between the concentrations and λ_{CROSS} values for both thiosulfate and tartrazine were found to be of the following forms, for the crossing of an arbitrary intensity of '1':

$$\lambda_{CROSS}(\text{Thiosulfate}) = 11.095.\ln[\text{Thiosulfate}] + 324.38$$

$$\lambda_{CROSS}(\text{Tartrazine}) = 8.516.\ln[\text{Tartrazine}] + 558.76$$

An example plot of λ_{CROSS} against ln[Tartrazine] is given in Figure 4.16.

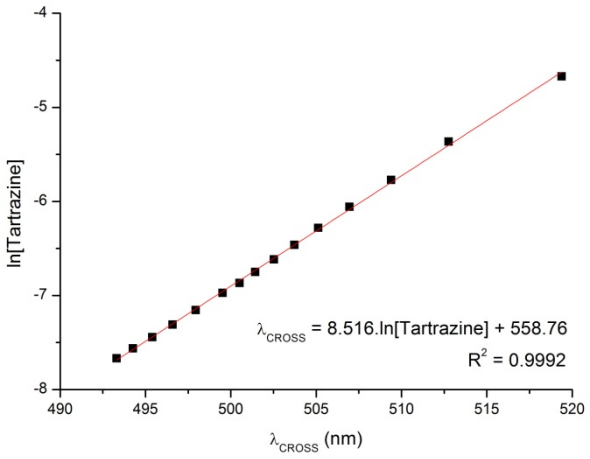

Figure 4.16: Plot of λ_{CROSS} against ln[Tartrazine], with a linear regression line.

4.7 Release of Thiosulfate

4.7.1 Release Profiles

The release reactions of thiosulfate were performed at three temperatures (20, 50 and 80°C), and, given its potential application in washing powder, both in the presence and absence of sodium dodecylsulfate ('NaDDS'), a typical anionic surfactant. Data was collected periodically from 10 minutes to 4 hours after the beginning of the reaction. The profiles of the release from the Li/Al-, Mg/Al- and Mg/Fe-Thiosulfate LDHs are depicted in Figures 4.17, 4.18 and 4.19.

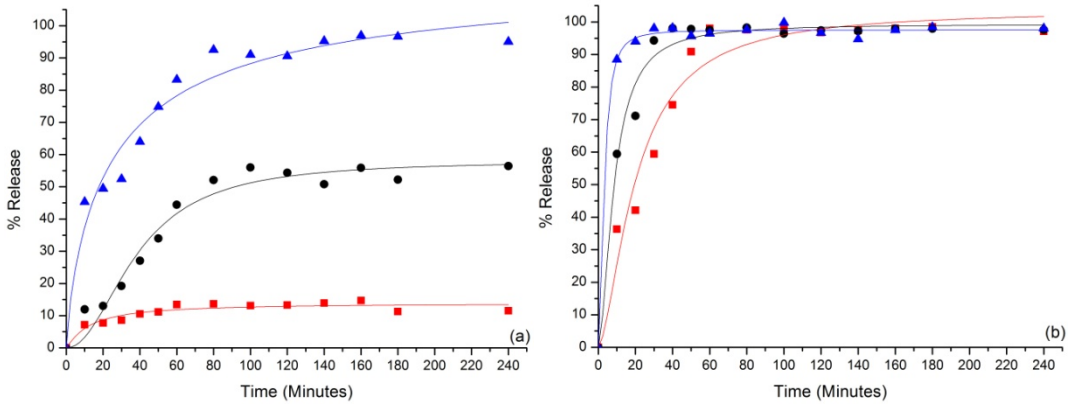

Figure 4.17: Release profiles of the Li/Al-Thiosulfate LDH at 20°C (■), 50°C (●), and 80°C (▲) in (a) deionised water and (b) a 0.007M solution of sodium dodecylsulfate. Fitted sigmoidal lines are shown to guide the eye.

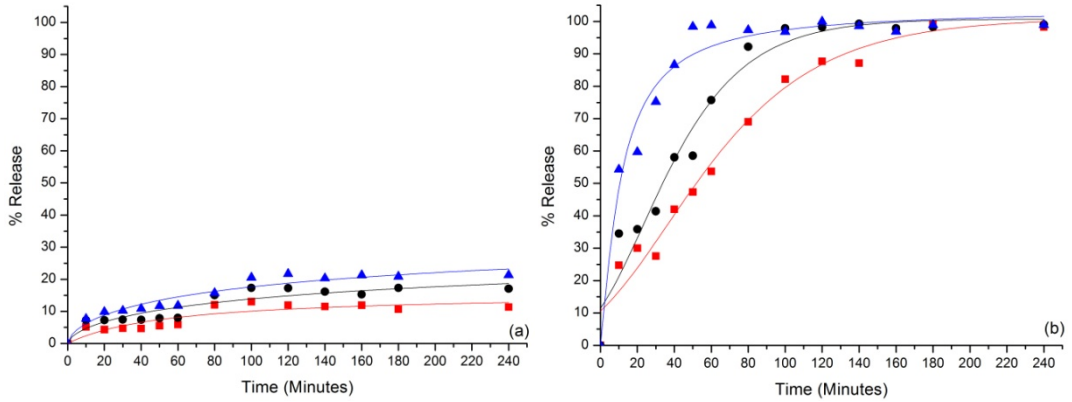

Figure 4.18: Release profiles of the Mg/Al-Thiosulfate LDH at 20°C (■), 50°C (●), and 80°C (▲) in (a) deionised water and (b) a 0.007M solution of sodium dodecylsulfate. Fitted sigmoidal lines are shown to guide the eye.

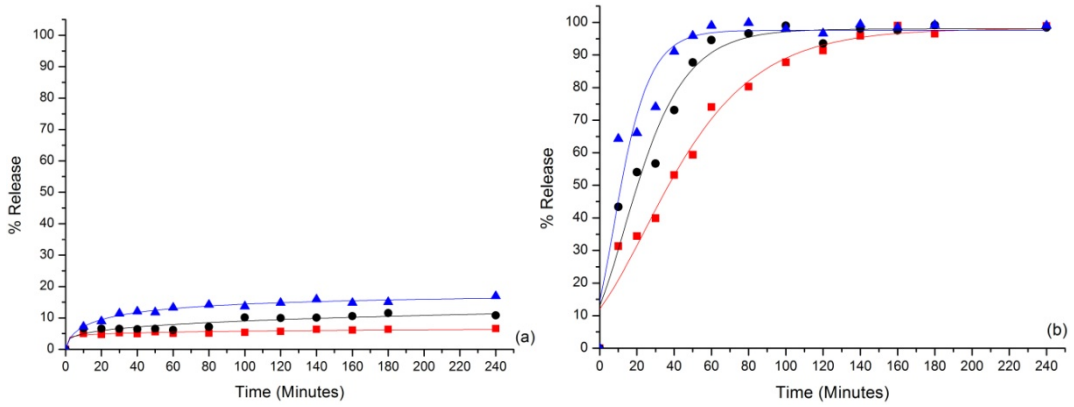

Figure 4.19: Release profiles of the Mg/Fe-Thiosulfate LDH at 20°C (■), 50°C (●), and 80°C (▲) in (a) deionised water and (b) a 0.007M solution of sodium dodecylsulfate. Fitted sigmoidal lines are shown to guide the eye.

As might have been expected, the release from each LDH is more rapid in the presence of sodium dodecylsulfate, as the anion provides an alternative route for the loss of thiosulfate from the solid (*via* ion exchange) which is considerably faster than the simple leaching of the anions into solution. Even for the Li/Al-LDH, where this leaching occurs much more rapidly due to a convenient mechanism (as described in Section 4.2.2), the possible concurrent intercalation of dodecylsulfate significantly increases the rate of thiosulfate release, suggesting that ion exchange is the kinetically dominant mechanism when a significant quanitity of a new guest anion is present.

When other factors are kept constant, the rate of thiosulfate release increases as Mg/Fe-LDH < Mg/Al-LDH < Li/Al-LDH. Whilst the more rapid release from the Li/Al-LDH compound can be justified due to the alternative leaching mechanism, it is also found that release from the Mg/Al-Thiosulfate LDH is consistently faster than from the corresponding Mg/Fe-LDH. This may be due to the greater interlayer separation found in the Mg/Al-LDH, which could allow for both freer movement of the intercalating dodecylsulfate (when it is present), and, due to reduced guest-host interactions, a smaller thermodynamic disincentive associated with the loss of thiosulfate from the structure.

4.7.2 Kinetics

The kinetics of the release from each system were analysed by the five methods outlined in Chapter 1, Section 1.7. Figure 4.20 demonstrates examples of the fitting graphs for all five kinetic models to the release of thiosulfate from the Mg/Fe-LDH system at 20ºC in 0.007M sodium dodecylsulfate solution.

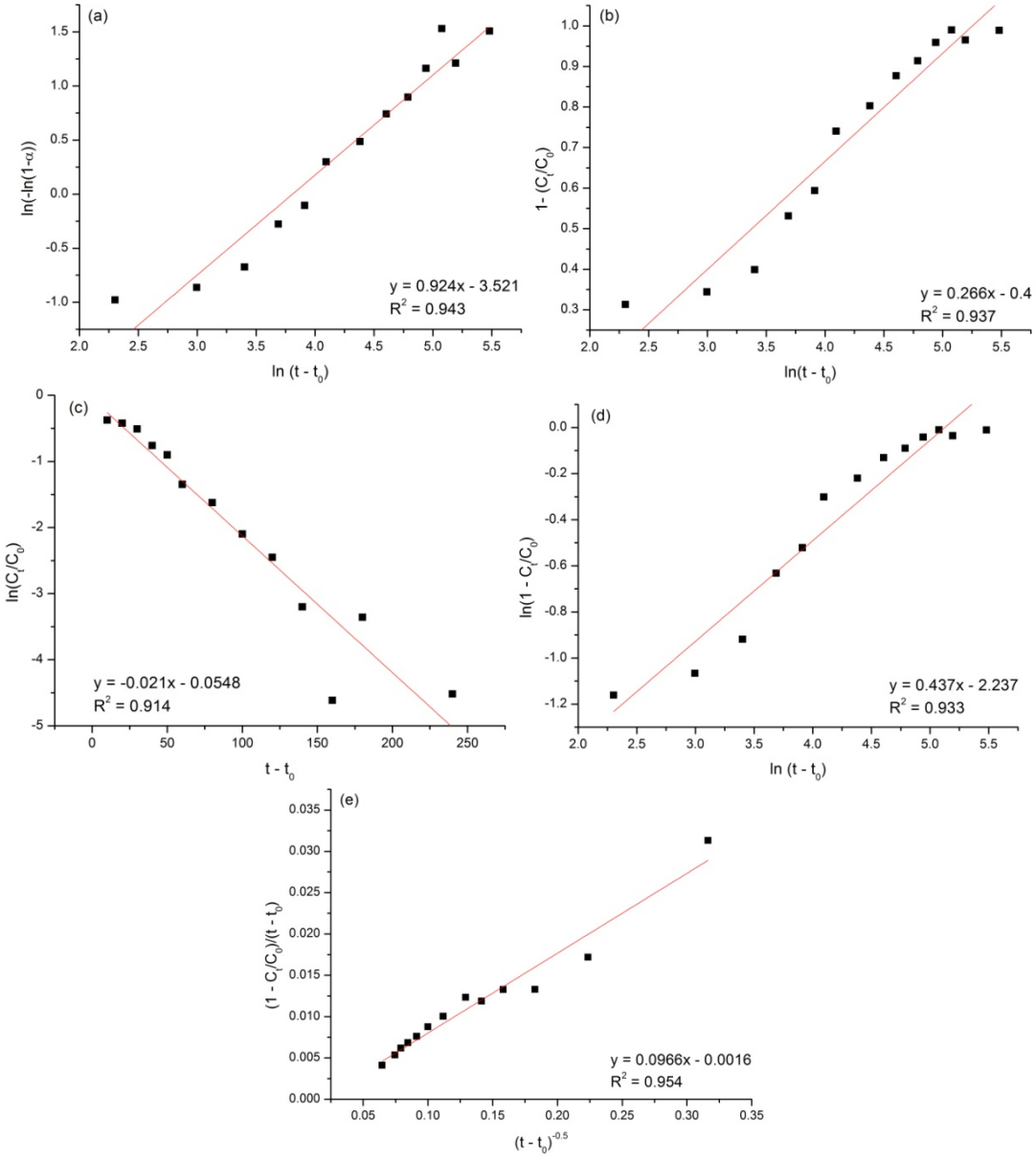

Figure 4.20: Least-squares fitting of the release of thiosulfate from Mg/Fe-Thiosulfate LDH in 0.007M sodium dodecylsulfate solution. Fits for (a) the Avrami-Erofe'ev model, (b) the Elovich model, (c) the First-Order model, (d) the Freundlich model, and (e) the parabolic diffusion model are shown.

The best fit to the data overall is found using the Avrami-Erofe'ev model; it provides a particularly accurate simulation for the Mg/Al- and Mg/Fe-LDH intercalates, although the parabolic diffusion model seems to be marginally better for covering the release from the Li/Al-Thiosulfate LDH. The First-Order model provides a poor fit to the data for all LDHs, under each set of conditions, further indicating that the thiosulfate release proceeds through a variety of processes that cannot be described using such a simple model.

From the Sharp-Hancock plot of the Avrami-Erofe'ev data above, it is possible to extract useful information about the mechanism of the reaction from the reaction exponent *n*, derived from the gradient of the plot. The values of *n* for each set of reaction conditions are summarised in Table 4.3.

Table 4.3: Values of the reaction exponent (*n*) for the release of thiosulfate from the three LDH intercalates, at three different temperatures, in deionised water ('H_2O') and a 0.007M solution of sodium dodecylsulfate ('NaDDS').

	n					
	H_2O			**NaDDS**		
Product	**20°C**	**50°C**	**80°C**	**20°C**	**50°C**	**80°C**
Li/Al-Thiosulfate LDH	0.22	0.70	0.72	0.79	0.41	0.17
Mg/Al-Thiosulfate LDH	0.42	0.40	0.41	1.01	0.98	0.67
Mg/Fe-Thiosulfate LDH	0.10	0.23	0.26	0.92	0.75	0.59

One clearly noticeable trend in the data is the change of the value of reaction exponent with temperature for release reactions in dodecylsulfate solutions. All of the LDH-Thiosulfate hybrids show a reaction exponent approximately equal to 1 at low temperatures in solutions of sodium dodecylsulfate – this corresponds to a 2D phase boundary-controlled reaction (following instantaneous nucleation). When the same release reactions are performed at increasingly higher temperatures, the value of the reaction exponent progresses towards 0.5, the value of *n* traditionally associated with

pure diffusion control (which is also observed in each of the release reactions performed in deionised water). At this point, the physical limitations of the LDH towards intercalation become irrelevant, and the rate of diffusion of the intercalating dodecylsulfate anion becomes the principal limiting factor. The significant concentrations of dodecylsulfate found intercalated in the LDH solids recovered after the release reactions, as determined by powder diffraction and elemental microanalysis, appear to suggest that ion exchange exists as a particular driving factor in this process.

A number of the reactions show reaction exponents with intermediate values not approximately equal to either 1 or 0.5. This is mostly likely the result of multiple competing release processes occurring simultaneously, or in certain cases (such as that of the Mg/Fe-Thiosulfate release in deionised water) from the release process proceeding to completion before the collection of the first release aliquot.

4.7.3 *In situ* EDXRD Results

In order to more accurately examine the process of deintercalation, the release of thiosulfate from the LDHs in water was observed using *in situ* energy-dispersive X-ray diffraction (EDXRD). The data were collected at Station 16.4 at the Synchrotron Radiation Source at Daresbury in Cheshire, which provides an X-ray beam of both high intensity and large energy bandwidth.

The release of thiosulfate from the Li/Al-Thiosulfate LDH in deionised water at 80°C was studied in detail by this method. It was determined that this system could provide accurate measurements of the kinetics of the reaction, as it could be monitored by the evolution of two visible reflections: the (002) Bragg reflection of the starting material at 8.58Å, which should diminish in intensity as the reaction proceeds, and the (002) reflection of the gibbsite polymorph of $Al(OH)_3$ that should

increase in intensity as greater amounts of Li^+ and $S_2O_3^{2-}$ leach from the starting material.

When the Li/Al-Thiosulfate LDH was suspended in water, the starting material reflection expected at 8.58Å was not observed. A strong reflection was found to be present at 10.68Å; this was later found, by *ex situ* powder XRD measurements of a damp sample of the Li/Al-Thiosulfate LDH, to be the (002) reflection: the structure had swelled significantly, absorbing further water into the interlayer space and causing an expansion of approximately 50% in the gallery height. After drying the same sample, the (002) reflection was found to return to its initial position at 8.58Å. This phenomenon has only been observed in certain LDH intercalates, such as the sulfate intercalate of a Li/Al-LDH, the most similar characterised compound to the Li/Al-Thiosulfate LDH.[27-29]

The (002) reflection of the gibbsite formed from the leaching of thiosulfate from the LDH was found to be of very low intensity, and barely distinguishable from the background. While this reflection was clear and intense when observed *ex situ* after the release product had been dried, the solid gave a much less clear pattern when suspended in water. The gibbsite formed by deintercalation and leaching from a Li/Al-LDH is typically found to be poorly crystalline.[30]

It was possible, though, to monitor the evolution of the 10.68Å reflection, and a three-dimensional plot of its development during release is illustrated in Figure 4.21.

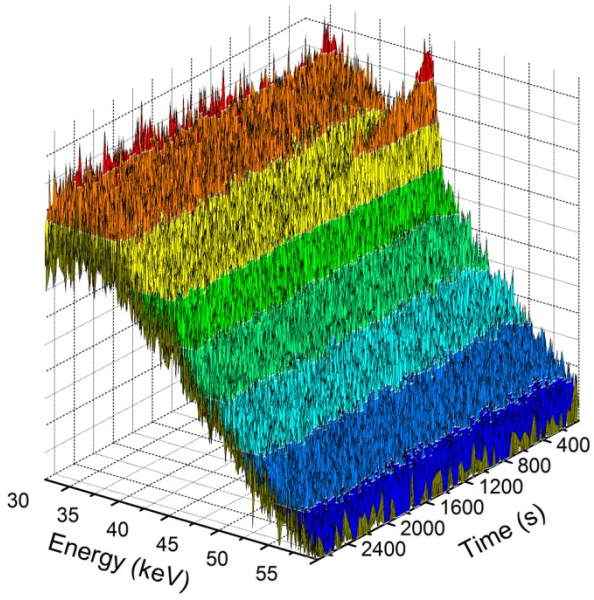

Figure 4.21: Plot of the evolution of the *in situ* EDXRD data from the Li/Al-Thiosulfate LDH in deionised water at 80°C. The (002) reflection becomes indistinguishable from the background radiation after approximately 30 minutes.

The integral of the (002) reflection was determined at each point during the reaction and analysed using the Avrami-Erofe'ev model (setting the value at the beginning of the reaction to correspond to $\alpha = 1$). The resulting data are shown in Figure 4.22.

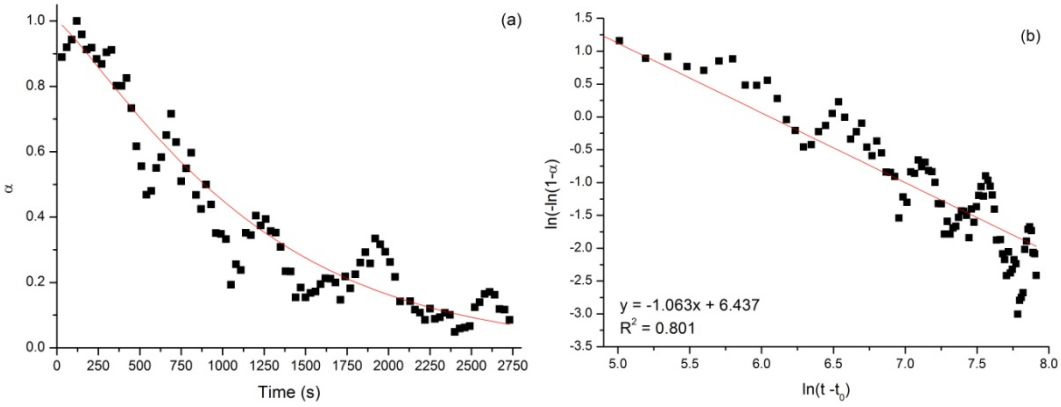

Figure 4.22: (a) Plot of the evolution of the integral of the 10.68Å reflection over time, (b) the Sharp-Hancock plot of the Avrami-Erofe'ev data derived from the peak integrals in (a).

The value of the reaction exponent (*n*) determined from analysis of the peak integral data (1.063) is in good agreement with the value determined from the UV data reported in Table 4.3.

4.8 Release of Tartrazine

4.8.1 Release Profiles

The release reactions of tartrazine were performed at room temperature in four different solutions (deionised water, tap water, and 0.1M and 0.01M solutions of sodium carbonate). These were chosen to provide a range of carbonate concentrations with which to test the rate of release, both artificially created and natural: central Oxford's tap water contains, on average, 266mg/l dissolved $CaCO_3$ equivalent and the location is thus classed as a 'hard water' area.[31] Data were collected periodically from 1 minute to 60 minutes after the beginning of the reaction. The profiles of the release from the Li/Al-, Mg/Al- and Mg/Fe-Tartrazine LDHs are shown below in Figure 4.23.

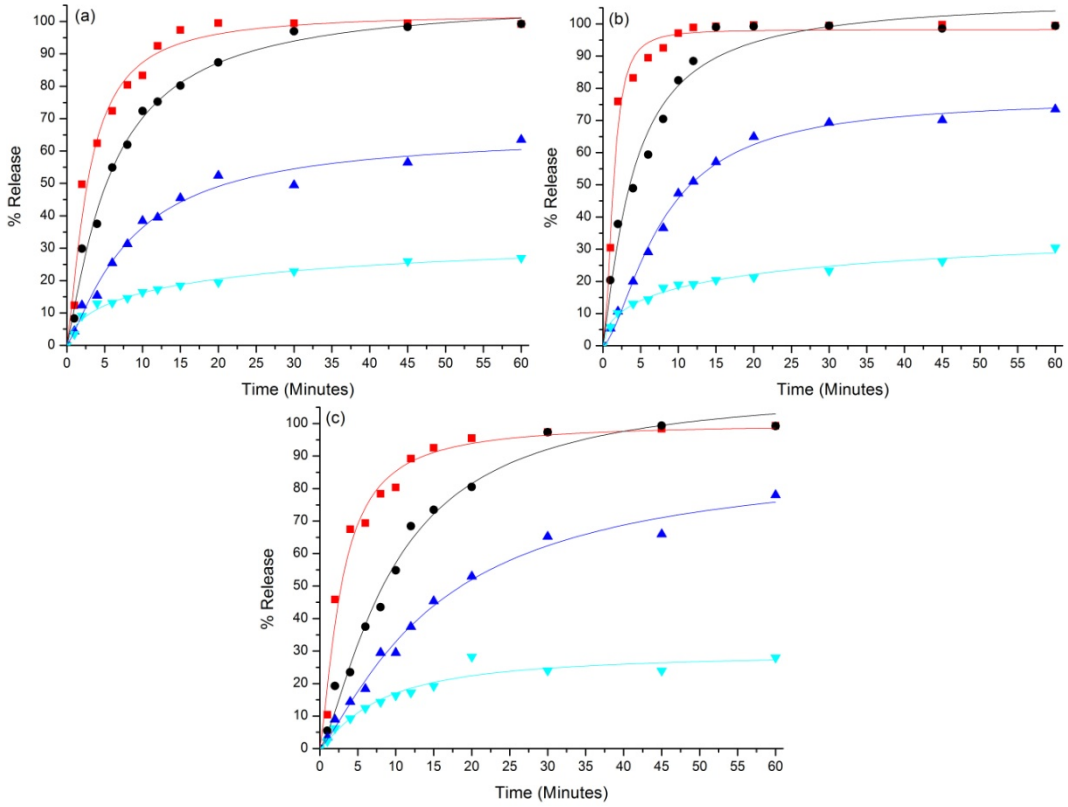

Figure 4.23: Release profiles of (a) the Li/Al-Tartrazine LDH, (b) the Mg/Al-Tartrazine LDH, and (c) the Mg/Fe-Tartrazine LDH in 0.1M Na_2CO_3 solution (■), 0.01M Na_2CO_3 solution (●), tap water (▲) and deionised water (▼). Fitted sigmoidal lines are shown to guide the eye.

As with the thiosulfate intercalates, there is a predictable progression in both the release rates and overall extents of the release increasing as deionised water < tap water < 0.01M CO_3^{2-} < 0.1M CO_3^{2-}. The previously observed rate progression that is dependent on the metallic content (Mg/Fe-LDH < Mg/Al-LDH < Li/Al-LDH) is also observed, but to a less pronounced degree than for the LDH-Thiosulfate materials. In particular, it can be seen that whilst the Mg/Fe-Tartrazine LDH compound releases noticeably more slowly in the more highly concentrated carbonate solutions, its release rates in deionised water and the very low carbonate concentration of the tap water are approximately the same as those of the Mg/Al-Tartrazine LDH.

4.8.2 Kinetics

The kinetics of release for each system and release medium were analysed by the same five methods as for thiosulfate. Figure 4.24 demonstrates examples of the least-squares fits for all five kinetic models to the release of tartrazine from the Li/Al-Tartrazine LDH in 0.01M Na_2CO_3 solution.

The goodness of fit observed in these fitting diagrams reflects the general trend found in modelling the kinetics of tartrazine release from the LDHs. The Avrami-Erofe'ev model provides a consistently close fit to the data, whilst the parabolic model is typically poor, as is the Freundlich model. The Elovich model describes the data almost as closely as the Avrami model. The First-Order model, whilst providing a good fit to the data in the plot shown in Figure 4.24(c), is very inconsistent, showing no particular trends in its reliability as a function of release medium or metallic combination in the LDH.

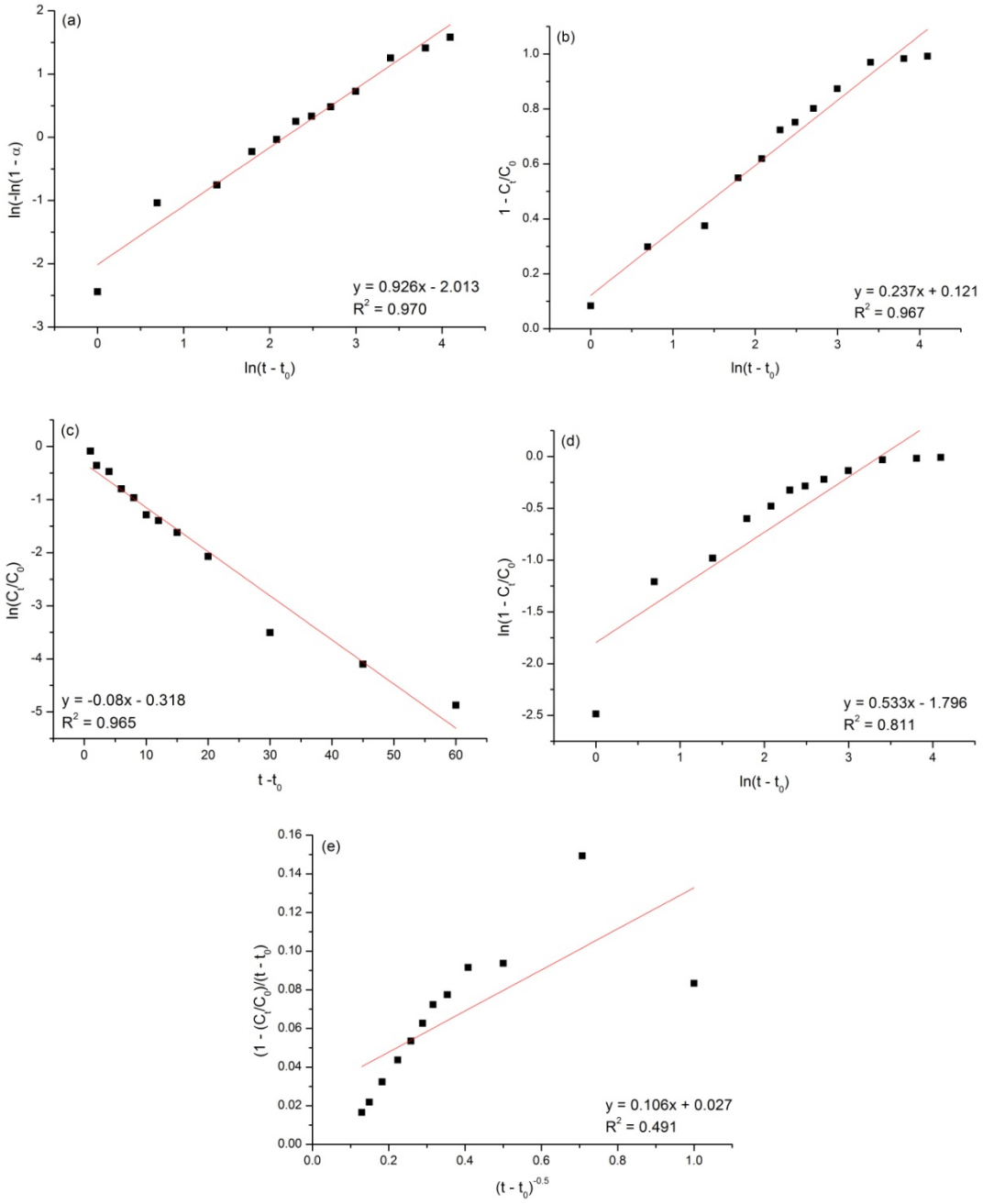

Figure 4.24: Least-squares fits of the kinetic models of release of tartrazine from the Li/Al-Tartrazine LDH in 0.01M sodium carbonate solution. Fits for (a) the Avrami-Erofe'ev model, (b) the Elovich model, (c) the First-Order model, (d) the Freundlich model, and (e) the parabolic diffusion model are shown.

Once again, the reaction exponents (n) were extracted from the gradients of the Sharp-Hancock plots of the Avrami-Erofe'ev data. The values of n for each set of reaction conditions are summarised in Table 4.4.

Table 4.4: Values of the reaction exponent (*n*) for the release of tartrazine from the three LDH intercalates in deionised water ('Deionised'), tap water ('Tap') and 0.1M and 0.01M solutions of sodium carbonate ('0.1M' and '0.01M').

	n			
Product	**0.1M**	**0.01M**	**Tap**	**Deionised**
Li/Al-Tartrazine	1.22	0.93	0.72	0.46
Mg/Al-Tartrazine	1.08	1.02	0.81	0.39
Mg/Fe-Tartrazine	0.84	1.13	0.90	0.60

The sharp change in the value of *n* in deionised water suggests an apparent change in mechanism observed in the absence of carbonate. The values of *n* for all of the reactions in deionised water are close to 0.5, while the exponents for the release reactions in carbonate-containing solutions are close to 1; the tap water values are, predictably, intermediate between the two.

4.8.3 *In situ* EDXRD Results

The Li/Al-Tartrazine LDH was the only system found to be consistently sufficiently crystalline for the development of its reflections to be studied by *in situ* X-ray diffraction. As with the LDH-Thiosulfate hybrids, no gibbsite was observed after deintercalation. Reactions with concentrated carbonate solutions were expected to display the (002) product reflections of LDH-Carbonate materials after ion exchange, but these were also not observed. Nevertheless, the (002) reflection of the starting material at 13.8Å was clearly observed to decrease in intensity as the reaction progressed. No swelling of the interlayer space was observed when the solid was suspended in water. Figure 4.25 illustrates the evolution of the (002) reflection of the Li/Al-Tartrazine LDH in 0.1M Na_2CO_3 solution at room temperature.

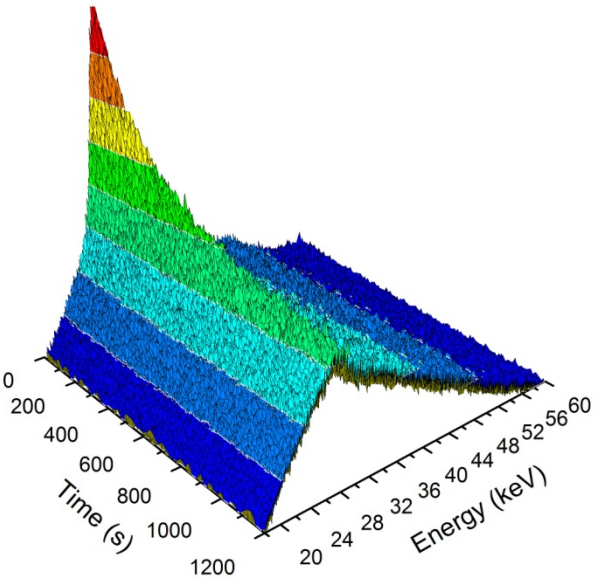

Figure 4.25: Plot of the evolution of the *in situ* EDXRD data corresponding to the (002) reflection of the Li/Al-Tartrazine LDH in a 0.1M solution of Na_2CO_3 at room temperature.

The diminishing intergral of the (002) reflection was analysed using the Avrami-Erofe'ev model (setting the value at the beginning of the reaction to correspond to α = 1). The resulting data are depicted in Figure 4.26.

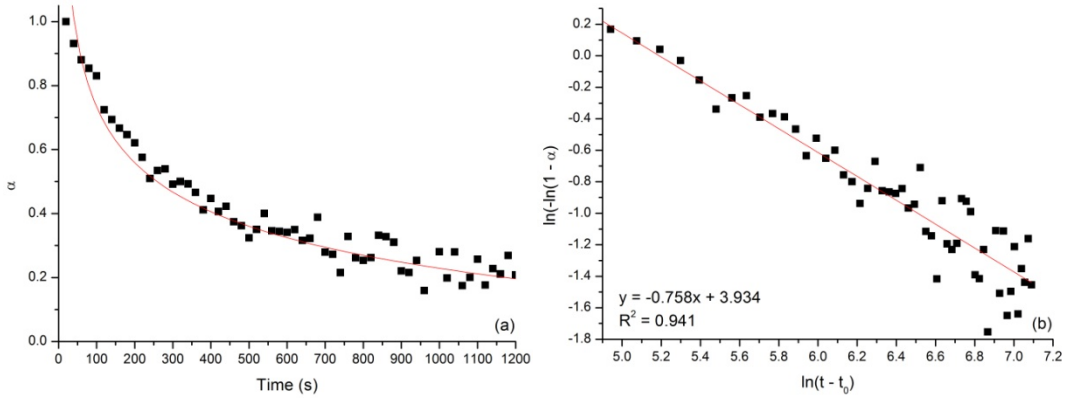

Figure 4.26: (a) Plot of the extent of reaction with respect to time, (b) the Sharp-Hancock plot of the same data.

Once again, there is decent agreement between the value of the reaction exponent determined here (0.758) and the value determined from the UV measurements, shown in Table 4.4.

4.9 Discussion of Results

With respect to the specified application of the thiosulfate release (for washing powders), it would seem from the above data that the LDH most suited to the purpose would be the Li/Al-Thiosulfate LDH system. Both with and without dodecylsulfate present, it is able to release over 98% of its interlayer anions within one hour of immersion in water at 80°C, and almost 50% at 50°C even in the absence of dodecylsulfate. Due to the comparatively low atomic masses of lithium and aluminium, the LDH also holds the greatest mass of thiosulfate per mass of solid (0.236g of thiosulfate per gram of LDH) of any of the three systems investigated. In addition, the Li/Al-Cl LDH precursor is the easiest of the three to synthesise in large quantities, and neither the precursor nor product LDHs contains any trace of carbonate contamination.

From a qualitative point of view, the use of the LDH-Tartrazine materials as a visual indicator of the hardness of water is successful; Figure 4.27 below shows a comparison between the filtrates that result from stirring the Mg/Al-Tartrazine LDH in deionised water and in a 0.1M Na_2CO_3 solution for 10 minutes.

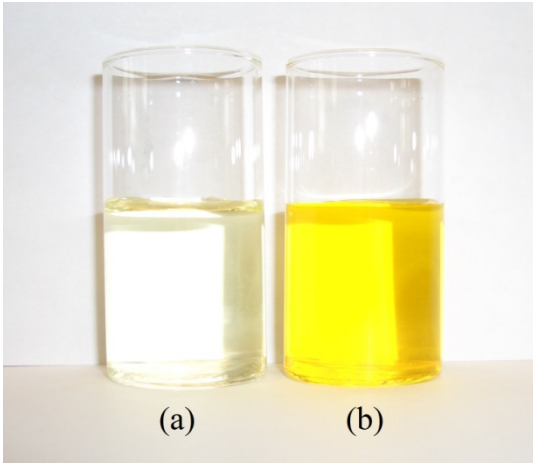

Figure 4.27: Comparison of the filtrates collected from release experiments after 10 minutes of stirring the Mg/Al-Tartrazine LDH in (a) deionised water, and (b) 0.1M Na_2CO_3 solution.[32]

When using tap water, the clarity of the colour difference is not apparent on very short timescales (1-2 minutes), and after longer timescales (>20 minutes) both solutions appear yellow, with the tap water being only marginally more intensely coloured. For an ideal quick test of water hardness, the colour difference would need to be very apparent and evident after a brief shaking of the powder in room temperature water (roughly equivalent to magnetically stirring the suspension for 1-2 minutes). Using the LDHs considered in this Chapter 'as-prepared' does not provide the necessary clarity on this short timescale. There are a number of possible synthetic modifications that could be applied to these solids, such as altering the particle size of the precursor LDH, which could allow the release rates to be modified to a more practical timescale.

4.10 Conclusions

Three thiosulfate-intercalated LDHs have been synthesised, and the rates and kinetics of anion release studied and analysed for the first time. One of these, the Li/Al-Thiosulfate LDH is a new hybrid, showing excellent crystallinity and thiosulfate loading. The release of thiosulfate from these LDHs has been studied over a range of temperatures and in solutions of sodium dodecylsulfate (a commercially-used anionic surfactant), and a great variety of release rates was observed, dependent on the temperature, the release medium, and the metallic combination present in the LDH layers. Of the thiosulfate LDHs studied, the Li/Al-Thiosulfate LDH system seems to be particularly appropriate for use in commercial systems.

Three LDHs intercalated with the azo dye tartrazine have been synthesised, with the intention of studying their application as a rapid test for the 'hardness' of tap water. Two of these, the Li/Al- and Mg/Fe-LDH hybrids, have never previously been synthesised. The three systems show a large structural dependence on the metals

present in the LDH layers, as the long tartrazine molecules arrange themselves at greatly varying angles from near-parallel to virtually perpendicular with respect to the layers. The release of tartrazine from these compounds has been studied in a variety of solutions including deionised water, 'hard' tap water and artificial carbonate solutions of differing concentrations. While these hybrids demonstrate a visible difference in solution colour when stirred in deionised water and 'hard' tap water, the timescales and colour differences are not quite suitable for detection purposes when used 'as-prepared'. However, post-synthetic modification of these compounds should allow these properties to be altered, increasing their suitability for their required purpose.

4.11 References

1. P. Tang, Y. Feng and D. Li, *Dyes and Pigments*, 2011, **90**, 253-258.
2. C. Chakraborty, K. Dana and S. Malik, *The Journal of Physical Chemistry C*, **115**, 1996-2004.
3. S. Mandal, D. Tichit, D. A. Lerner and N. Marcotte, *Langmuir*, 2009, **25**, 10980-10986.
4. I. Y. Park, K. Kuroda and C. Kato, *Journal of the Chemical Society, Dalton Transactions*, 1990, 3071-3074.
5. S. Miyata, *Clays and Clay Minerals*, 1983, **31**, 305-311.
6. J.-H. Choy, Y.-K. Kim, Y.-H. Son, Y. B. Choy, J.-M. Oh, H. Jung and S.-J. Hwang, *Journal of Physics and Chemistry of Solids*, 2008, **69**, 1547-1551.
7. A. I. Khan, A. Ragavan, B. Fong, C. Markland, M. O'Brien, T. G. Dunbar, G. R. Williams and D. O'Hare, *Industrial & Engineering Chemistry Research*, 2009, **48**, 10196-10205.
8. D. L. Smith and J. S. Fritz, *Analytica Chimica Acta*, 1988, **204**, 87-93.
9. L. Benes, K. Melanova, V. Zima and J. Svoboda, *Collection of Czechoslovak Chemical Communications*, 2005, **70**, 259-268.
10. A. R. Auxilio, P. C. Andrews, P. C. Junk and L. Spiccia, *Australian Journal of Chemistry*, 2010, **63**, 83-91.
11. R. T. Plimpton and J. C. Chorley, *Journal of the Chemical Society, Transactions*, 1895, **67**, 314-315.
12. F. J. Hallinan and W. R. Thompson, *Journal of the American Chemical Society*, 1939, **61**, 265-270.
13. R. Gracia and G. Shepherd, *Pharmacotherapy*, 2004, **24**, 1358-1365.
14. A. V. Lukashin, A. A. Eliseev, N. G. Zhuravleva, S. V. Kalinin, A. A. Vergetel and Y. D. Tret'yakov, *Doklady Chemistry*, 2002, **383**, 93-96.
15. A. V. Lukashin, A. A. Eliseev, N. G. Zhuravleva, A. A. Vergetel, Y. D. Tret'yakov, O. I. Lebedev and G. van Tendeloo, *Mendeleev Communications*, 2004, 174.
16. N. Thomas and M. Rajamathi, *Langmuir*, 2009, **25**, 2212-2216.

17. V. A. Willson, *Industrial & Engineering Chemistry Analytical Edition*, 1935, **7**, 44-45.
18. X. Yu, Z. Chang, X. Sun, X. Lei, D. G. Evans, S. Xu and F. Zhang, *Chemical Engineering Journal*, 2011, **169**, 151-156.
19. G. Renaudin and M. Francois, *Acta Crystallographica Section C*, 1999, **C55**, 835.
20. B. J. Teppen, K. Rasmussen, P. M. Bertsch, D. M. Miller and L. Schäfer, *The Journal of Physical Chemistry B*, 1997, **101**, 1579-1587.
21. R. Olar, M. Badea, O. Carp, D. Marinescu, V. Lazar, C. Balotescu and A. Dumbrava, *Journal of Thermal Analysis and Calorimetry*, 2008, **92**, 245-251.
22. J. S. Church and D. J. Evans, *Spectrochimica Acta Part A: Molecular and Biomolecular Spectroscopy*, 2008, **69**, 256-262.
23. W. Meng, F. Li, D. G. Evans and X. Duan, *Materials Research Bulletin*, 2004, **39**, 1185-1193.
24. N. Peica, I. Pavel, S. Cîntă Pînzaru, V. K. Rastogi and W. Kiefer, *Journal of Raman Spectroscopy*, 2005, **36**, 657-666.
25. T. Vlase, G. Vlase, D. Modra and N. Doca, *Journal of Thermal Analysis and Calorimetry*, 2007, **88**, 389-393.
26. N. Dossi, R. Toniolo, S. Susmel, A. Pizzariello and G. Bontempelli, *Chromatographia*, 2006, **63**, 557-562.
27. V. R. L. Constantino and T. J. Pinnavaia, *Inorganic Chemistry*, 1995, **34**, 883-892.
28. G. R. Williams and D. O'Hare, *The Journal of Physical Chemistry B*, 2006, **110**, 10619-10629.
29. A. M. Fogg, A. J. Freij and G. M. Parkinson, *Chemistry of Materials*, 2002, **14**, 232-234.
30. K. A. Tarasov, V. P. Isupov, L. E. Chupakhina and D. O'Hare, *Journal of Materials Chemistry*, 2004, **14**, 1443-1447.
31. *Water Hardness Levels in your Area*, http://www.thameswater.co.uk/cps/rde/xchg/corp/hs.xsl/899.htm.
32. M. O'Brien, Part II Thesis, University of Oxford, 2008.

Chapter 5

Novel Syntheses of Layered Metal Hydroxides by the Salt-Oxide Method

5.1 Introduction

The principal method by which layered double hydroxides are synthesised is by coprecipitation of the solid compound by the reaction of a mixed solution containing salts of the desired metals with a basic solution. Many variants of this method exist:[1] the reaction may be performed at low supersaturation (wherein the metal salt and base solutions are added simultaneously, but separately, to an aqueous solution of the intended interlayer anion maintained at constant pH),[2-4] high supersaturation (wherein the metal salt solution is added directly, but slowly, to the base solution),[5-7] or by recently pioneered methods involving separation of the nucleation and aging steps,[8, 9] or coprecipitation in water-in-oil reverse microemulsions.[10, 11] The latter two approaches yield uniform nanoscale LDH particles, often with unusual morphologies. Modifications to this simple method comprise almost the entirety of known homogeneous solution-phase syntheses of LDHs, aside from seldom-implemented sol-gel and electrochemical methods.[12-14]

A number of solid-solid syntheses are known using metal-containing precursors as starting materials. Due to the inevitable slow kinetics of solid phase reactions, but acknowledging the tendency towards decomposition of LDH materials above *ca.* 350ºC, these reactions are often performed under hydrothermal reaction conditions, or following activation of the starting materials by grinding in a ball-mill. The metal-containing precursors are often oxides and hydroxides;[15-18] the existence of

hydrotalcite-like phases arising from these conditions is well-known in the field of cement chemistry.[19]

There does exist, however, a highly effective heterogeneous synthesis method from which a number of layered double hydroxides may be prepared. The direct reaction of a metal oxide or hydroxide with the solution of a salt of a different metal provides a direct route to hydrotalcite-like compounds. This reaction may proceed by a topotactic route; the archetypical example of this is the so-called 'imbibition' of lithium salts by aluminium hydroxide (the gibbsite, bayerite or nordstrandite polytypes),[20, 21] a reaction which has been recently extended to several other metal salt solutions through activation of the solid and hydrothermal treatment, yielding LDHs with the general formulae $[MAl_4(OH)_{12}](NO_3)_2 \cdot yH_2O$. [22-25]

A much greater variety of reaction products may arise when non-topotactic reactions are considered. Reactions of gibbsite with metal (II) salt solutions may lead to the formation of hydrotalcite-like LDH compounds, with formulae of the form $[M_2Al(OH)_6]NO_3 \cdot yH_2O$; since this necessitates a significant structural change, from gibbsite-type layers to brucite-type layers, it is likely that this proceeds by a dissolution-reprecipitation-type mechanism, such as that observed by Radha *et al.* in their reactions of freshly-precipitated $Al(OH)_3$ gels with solutions of magnesium and nickel salts.[26] Even more flexibility is observed when considering the reaction of metal (II) oxides and hydroxides with metal (III) salt solutions, given the greater degree of basicity of the former and acidity of the latter. The first example of such a reaction was reported by Boehm *et al.*,[27] after investigating the poorly-interpreted observation by Morrison and Bonnelle[28] that a solution of chromium (III) nitrate suspended over a zinc oxide catalyst support for five minutes will no longer oxidise ferrocyanide. The authors assumed that a pink discoloration of the zinc oxide was

attributable to a disproportionation of the chromium ions in solution, when it was instead the result of the formation of the LDH compound $[Zn_2Cr(OH)_6]NO_3 \cdot 2H_2O$. It was later found to be possible to form LDHs by the direct reaction of a chromium (III) chloride solution with copper (II) oxide to form $[Cu_2Cr(OH)_6]Cl \cdot yH_2O$, and with cadmium (II) oxide to form $[Cd_3Cr(OH)_8]Cl \cdot yH_2O$.[29, 30] In each case, the reaction was performed by adding the solid oxide to a one-molar solution of trivalent metal chloride solution, and stirring at room temperature for 24 hours – at this point, the solid phase is extracted by filtration, and resuspended in a new one-molar solution of the trivalent metal salt. The reaction is then allowed to proceed for thirteen days before recovery and characterisation of the solid. These synthesis methods are highly effective, producing pure phases with little wastage of the metal cations and, furthermore, avoiding the chromium oxide and hydroxide by-products typically found when attempting to synthesise chromium LDHs by coprecipitation. Albiston *et al.* further showed that hydrotalcite-like products may result from the direct reaction of a magnesium oxide slurry with a solution of aluminium nitrate.[31] The most recent and significant work in this area has been performed by Chitrakar and co-workers: after outlining a solvent-free synthesis of $[Zn_2Al(OH)_6]Cl \cdot yH_2O$ by a direct hydrothermal reaction of zinc oxide with solid aluminium chloride (with the water of hydration of the salt as the only source of liquid),[32] this method was expanded to demonstrate the possibility of synthesising $[Mg_2Al(OH)_6]Cl \cdot yH_2O$, $[Mg_2Fe(OH)_6]Cl \cdot yH_2O$ and $[Zn_2Al(OH)_6]Cl \cdot yH_2O$ by stirring the relevant metal (II) oxide in a solution of the appropriate metal (III) salt for two days at 30ºC.[33] Further research indicated similar results from the reaction of $Mg(OH)_2$ with solutions of iron (III) salts in the presence of the carbonate anion.[34] This method is highlighted as superior to that of Boehm and

El Malki, which required replacement of the metal salt solution during the reaction to maintain the reactivity to proceed to the desired product.

In spite of the demonstrated flexibility of the salt-oxide synthesis method, and its advantages over conventional coprecipitation methods, only a limited number of studies as described above have been performed. Many metal (II) oxides and metal (III) salts exist which have never been systematically tested for the synthesis of hydrotalcite-like compounds using this method. Given the effectiveness of the salt-oxide method for the synthesis of chromium-containing LDHs which are difficult to prepare by coprecipitation, it is expected that such investigations may lead to the discovery of novel LDH phases.

The purpose of this chapter is to undertake a systematic investigation of reactions between metal (II) oxides and metal (III) salt solutions in order to determine if this method may provide a simpler, more direct route to conventional LDH materials, and furthermore to examine whether novel phases may result from such reactions.

5.2 Identification of Synthesis Candidates

5.2.1 Metal (II) Oxides

The known metal oxides with the formula MO are summarised in Table 5.1.

A number of these compounds may be immediately eliminated as potential reaction candidates. A great number exist only as transient species at high temperatures, as part of thin films, or in the vapour phase (such as ScO, MoO, and GeO), or are otherwise inaccessible due to the nature of their metallic content (such as PtO, PdO and PuO). Others, despite the listed formulae, are not metal (II) oxides: AgO contains an equimolar mixture of Ag^{I} and Ag^{III}, while the lanthanide oxides LaO, CeO, PrO, NdO

and SmO are electride-type oxides, containing metal (III) centres with the charge balanced by oxide anions and delocalised electrons.

Table 5.1: Summary of metal oxides with the chemical formula MO.

s-block	**d-block**[35-38]	**d-block** [39, 40]	**p-block**[41]	**f-block**[42-44]
BeO	ScO	NbO	GeO	LaO
MgO	TiO	MoO	SnO	CeO
CaO	VO	PdO	PbO	PrO
SrO	CrO	AgO		NdO
BaO	MnO	CdO		SmO
	FeO	PtO		EuO
	CoO	HgO		YbO
	NiO			PuO
	CuO			
	ZnO			

Certain listed oxides are quasi-metallic non-stoichiometric solids, or will not react with acidic solutions in water (except by undergoing oxidation or reduction), such as TiO, VO, CrO, FeO, NbO, EuO and YbO. SnO, PbO and HgO were discarded due to the strong opposition to octahedral coordination found for the metal cations required for adoption into brucite-type layers, along with BeO (as a result of its unusually small size, lack of typical ionic bonding, and coordination preferences).

The remaining metal oxides, which will be the subject of the following work, are detailed in Table 5.2. Hydrotalcite-like compounds have been synthesised containing all of the dications in these oxides, with the exception of strontium. Only a single instance has been reported of a barium-containing LDH, a Ba/Fe compound of indeterminate composition synthesised fortuitously under hyperalkaline conditions by Srankó *et al.*;[45] the powder X-ray diffraction patterns and subsequent X-ray

absorption studies of the material suggest an unusual, distorted layered structure.[46] Direct salt-oxide reactions yielding LDH structures have been reported only for MgO, CuO, ZnO and CdO.

Table 5.2: Summary of the metal oxides to be examined for reactivity in this chapter.

s-block	MgO	CaO	SrO	BaO		
d-block	MnO	CoO	NiO	CuO	ZnO	CdO

5.2.2 Metal (III) Salts

The known water-soluble ionic metal (III) salts of the form MX_3 are summarised in Table 5.3. For accessibility and solubility reasons, the salt anions considered here are nitrate and halides.

Table 5.3: Summary of metal (III) salts with the chemical formula MX_3. 'Ln' represents all lanthanides from lanthanum to lutetium.

d-block	**d-block**[47-50]	**d-block**[51, 52]	**p-block**	**f-block**
ScX_3	YX_3	HfX_3	AlX_3	LnX_3
TiX_3	ZrX_3	TaX_3	GaX_3	AcX_3
VX_3	NbX_3	WX_3	InX_3	ThX_3
CrX_3	MoX_3	ReX_3	TlX_3	UX_3
MnX_3	TcX_3	IrX_3	BiX_3	
FeX_3	RuX_3	AuX_3		
CoX_3	RhX_3			
	PdX_3			

Once again, many of these may be eliminated due to radioactivity (AcX_3, ThX_3, UX_3 and TcX_3), chemical instability in the presence of air or water (TiX_3, CoX_3, ZrX_3, NbX_3, MoX_3, PdX_3, HfX_3 and TaX_3), or excessive cost (ScX_3, RuX_3, RhX_3, WX_3, ReX_3, IrX_3 and AuX_3). The nitrates of bismuth and thallium, upon addition to neutral or basic aqueous solutions, immediately precipitate solid oxychloride species; it may be possible to synthesise LDH species by coprecipitation using these metals,

but not by the salt-oxide method (indeed, an unusual series of mixed bismuth-iodine oxides resembling hydrotalcite-like compounds have been recently reported).[53] While some work has been previously performed to produce lanthanide-containing LDH materials, it has been unsuccessful except in cases where only fractional substitution of the metal (III) ions is required.[54-56] However, there exists a number of layered monometallic rare-earth hydroxide materials containing exchangeable interlayer anions which have been well-characterised.[57-61]

Due to the failure of previous attempts to synthesise LDH phases containing only lanthanides as the tripositive cations (perhaps due to the preferences of rare-earths for coordination numbers of eight or nine), lanthanum chloride will be used to test for reactivity only in the most promising cases discovered. MnX_3 has been ruled out, as the only available such compound (MnF_3) is known to be strongly oxidising, and to hydrolyse in water to produce a solution of HF. However, Mn^{3+} in solution is accessible through the use of manganese (II) salts, which are allowed to oxidise by exposure to air – such an approach is often used to synthesise Mn^{3+}-containing LDH phases.[62, 63]

The remaining metal (III) salts to be used for syntheses are listed in Table 5.4.

Table 5.4: Summary of metal (III) salts to be examined for reactivity in this chapter.

d-block	VX_3	CrX_3	MnX_2	FeX_3	YX_3
p-block	AlX_3	GaX_3	InX_3		

Hydrotalcite-like phases are known containing each of the metal (III) cations listed in Table 5.4. Similarly to lanthanum, yttrium-containing hydrotalcite-like compounds have been reported, but only by partial substitution of Al^{3+} in a Mg/Al-LDH system.[64, 65] The metal salts listed will be those used, in their most accessible forms as chlorides or nitrates, for the standard testing of the metal (II) oxides.

In considering the likelihood of LDH formation, it is often important also to consider the relative ionic radii of the two metal cations in the layers. This data is summarised in Table 5.5.

Table 5.5: Shannon's crystal radii for the cations studied for LDH synthesis in this chapter, assuming octahedral coordination of the cations.[66]

Metal (II) Cation	Crystal Radius (pm)	Metal (III) Cation	Crystal Radius (pm)
Mg^{2+}	86	V^{3+}	78
Ca^{2+}	114	Cr^{3+}	76
Sr^{2+}	132	Mn^{3+}	79
Ba^{2+}	149	Fe^{3+}	79
Mn^{2+}	97	Y^{3+}	104
Co^{2+}	89	Al^{3+}	68
Ni^{2+}	83	Ga^{3+}	76
Cu^{2+}	87	In^{3+}	94
Zn^{2+}	88	La^{3+}	117
Cd^{2+}	109		

While initially it was often thought that a degree of similarity in size between the dipositive and tripositive cations in the LDH layers was necessary for its stability, and ensuring a regular structure of the brucite-like layers,[67, 68] more recent studies indicate otherwise – indeed, the existence of the stable LDH $[Ca_2Al(OH)_6]NO_3 \cdot yH_2O$, in which the radius of the dipositive cation is almost exactly twice that of the tripositive ion, suggests that other thermodynamic concerns may be more important in considering the potential stability of new LDH compounds.

5.3 Synthesis Method

5.3.1 Reaction Conditions

The reaction conditions used for a typical reaction in this work are similar to those used by Chitrakar *et al.*[33] 1g of the metal (II) oxide was added to 50mL of deionised water containing an appropriate amount of the metal (III) salt to give a M^{II}:M^{III} ratio of 2:1 (the most common ratio found in LDHs). The reactions were all initially performed at room temperature for five days; if the X-ray powder pattern indicated the presence of a hydrotalcite-like phase, the experiment was repeated at 80ºC for 24 hours to see if a more crystalline phase could be prepared. All reactions were performed under nitrogen, except for those of $MnCl_2$, which were performed under an air atmosphere to allow oxidation of the solution cation to Mn^{3+}. The resultant solid from each reaction was washed with deionised water and dried under vacuum at room temperature.

Where the X-ray patterns of the products suggested the possibility of an LDH phase having formed, attempts were made to demonstrate this by intercalation of a standard anion. The anion chosen was the cyclohexylsulfamate ("cyclamate") anion, an artificial sweetener (introduced in Chapter 2). This guest was chosen due to its high solubility in water, ease of anion exchange resulting in high loading percentages, and the characteristic large interlayer spacing that results from its intercalation. The intercalation was performed by a standard ion exchange process – 0.5g of the host was stirred with a threefold excess of sodium cyclamate in deionised water at 80ºC for 16 hours under nitrogen, and the product was filtered, washed and dried as detailed above.

5.3.2 Potential Competing Reactions

There are a number of possible alternative reaction pathways that could occur when a metal (II) oxide is suspended in a metal (III) salt solution. The most likely of these which would result in non-LDH products are:

i) The solid oxide undergoes no reaction, and the resulting filtered solid is merely the starting material.

ii) The metal (II) oxide hydrates upon suspension in water, and the final collected solid is the metal (II) hydroxide (or a hydrated oxide equivalent).

iii) The metal (III) salt solution may react with the metal (II) oxide purely as a base, resulting in a solid which contains only the metal (III) cation by a pathway that proceeds independently of the presence of the metal (II) species.

To ensure that none of these products were misidentified as new hydrotalcite-like phases, the identities of the products resulting from pathways ii) and iii) were determined. In the first case, this was achieved by stirring the metal oxide for 16 hours in water at 80ºC and, in the second case, by reacting the metal (III) salt solution with an equimolar solution of sodium hydroxide and aging for 16 hours at the same temperature.

When the metal (II) oxides were recovered from reaction with water, some were found to be unchanged, although with a slight loss in crystallinity in most cases: specifically, the transition metal oxides MnO, CoO, CuO, and ZnO. The remainder formed the corresponding hydroxides (or hydroxide hydrates), namely $Mg(OH)_2$, $Ca(OH)_2$, $Sr(OH)_2 \cdot 8H_2O$, $Ba(OH)_2 \cdot 8H_2O$, and $Cd(OH)_2$. None of these show reflections that may be mistaken for those from LDH-type phases.

The solids collected from the reactions of the metal (III) salts with sodium hydroxide, and their identities as determined by powder X-ray diffraction, are summarised in Table 5.6.

Table 5.6: Summary of the solid products resulting from the reactions of the metal (III) salt solutions with sodium hydroxide. The products given in parentheses are minor products.

Metal Salt	Solution Colour	Product Colour	Product Identity
VCl_3	Dark yellow/brown	Dark green/brown	V_2O_3 (VO_2)
$CrCl_3$	Dark green	Blue/Green	$Cr_2O_3 \cdot yH_2O$
$MnCl_2$	Pale pink	Orange/Brown	Mn_3O_4
$FeCl_3$	Yellow	Brown	$Fe_2O_3 \cdot yH_2O$
YCl_3	Colourless	White	$[Y_2(OH)_5]Cl \cdot yH_2O$
$AlCl_3$	Colourless	White	α-$Al(OH)_3$ (γ-$Al(OH)_3$)
$GaCl_3$	Colourless	White	α-Ga(OOH) ($Ga(OH)_3$)
$InCl_3$	Colourless	White	$In(OH)_3$
$LaCl_3$	Colourless	White	$La(OH)_3$

The majority of the above products do not show reflections that might be mistaken for hydrotalcite-like phases. The one exception to this is yttrium chloride; the addition of sodium hydroxide to a solution of this salt gives a white precipitate of yttrium hydroxychloride, as described by Fogg *et al.*[59] This compound produces X-ray reflections which appear superficially similar to those of an LDH, and furthermore displays almost identical anion exchange chemistry to LDH phases. Figure 5.1 compares the simulated X-ray powder patterns of a Mg/Fe-Cl LDH, and that of an ytterbium hydroxychloride. Although no single crystal structure has been determined for the expected yttrium hydroxychloride product $[Y_2(OH)_5]Cl \cdot yH_2O$ to allow simulation of a powder pattern, refinement of powder XRD data suggests that its most common orthorhombic form is almost isostructural to the ytterbium analogue, for which a single-crystal structure is available, and is shown below.

The simulated patterns of reference products, such as those shown in the figure below and throughout this Chapter, are simulated powder patterns derived from single-crystal structures from the Inorganic Crystal Structural Database.

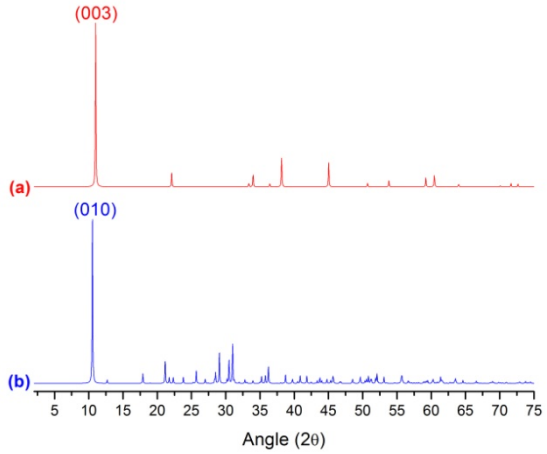

Figure 5.1: The simulated powder X-ray patterns (from the Inorganic Crystal Structure Database) of (a) $[Mg_3Fe(OH)_8]Cl{\cdot}2H_2O$,[69] and (b) the orthorhombic form of ytterbium hydroxychloride $[Yb_2(OH)_5]Cl{\cdot}yH_2O$.[59]

Given that the strong reflection shown by the yttrium hydroxychloride which appears in the same region as the first basal reflection of a chloride- or carbonate-intercalated LDH, great care must be taken to discern whether the layered species formed from reactions of the Y^{3+} cation in basic aqueous solutions may be described as a true LDH, or a M^{II}-free rare-earth hydroxyhalide species.

5.4 Reactions of Alkaline Earth Oxides

5.4.1 Reactions of Magnesium Oxide (MgO)

Magnesium oxide possesses the rock salt structure, but upon stirring in water rapidly hydrates to form magnesium hydroxide, which adopts the brucite structure analogous to a layered double hydroxide. As reactions proceed through addition of the magnesium oxide directly to a solution of the metal (III) salt, it is not clear whether the reactions will occur with the oxide or after hydration to the hydroxide. However,

the mechanism of the salt-oxide reaction as proposed by Chitrakar[32] suggests that these reactions must necessarily proceed via the metal (II) hydroxide intermediate, and so the matter is effectively rendered moot.

The solid product that is collected from the reaction of MgO with a solution of vanadium (III) chloride can be identified as poorly crystalline $Mg(OH)_2$, with a small amount of V_2O_3 also present. Upon attempting to increase the crystallinity by performing the reaction at 80ºC, the same products result with barely improved crystallinity. Furthermore, the filtrate from the 80ºC reaction is sky blue in colour, indicating the presence of the vanadyl cation (VO^{2+}) and suggesting that the elevation in temperature has increased the rate of reduction of water by V^{3+}. No hydrotalcite-like phases are apparent in any of the solid products.

Given the previously-reported successful salt-oxide reactions of chromium (III) chloride with CuO and CdO, the reaction of MgO with $CrCl_3$ was studied under both conventional and hydrothermal conditions. In the case of the conventional reactions, at both room temperature and 80ºC the grey-green solid product obtained is virtually amorphous, although it shows very faint reflections attributable to $Mg(OH)_2$. No reflections from chromium-containing or hydrotalcite-like phases were apparent. This reaction was also studied under hydrothermal conditions: 0.25g of MgO was added to 10mL of a $CrCl_3$ solution, maintaining a 2:1 ratio of Mg:Cr, and the mixture was heated at 160ºC for 12 hours. The only phase identifiable by X-ray diffraction from the grey-green solid recovered was a highly crystalline magnesium hydroxide; again, no chromium-containing or LDH phases could be seen.

The reaction of magnesium oxide with a solution of manganese (II) chloride leads to the formation of more interesting products. The solid recovered after performing the reaction at room temperature is brown, indicating that a degree of oxidation of the

manganese to Mn^{3+} has taken place. The apparent product is a mixture of the Mg/Mn-Cl LDH with a significant amount of Mn_3O_4 present. Figure 5.2 compares XRD data from the MgO/$MnCl_2$ reaction product with that of Mn_3O_4.

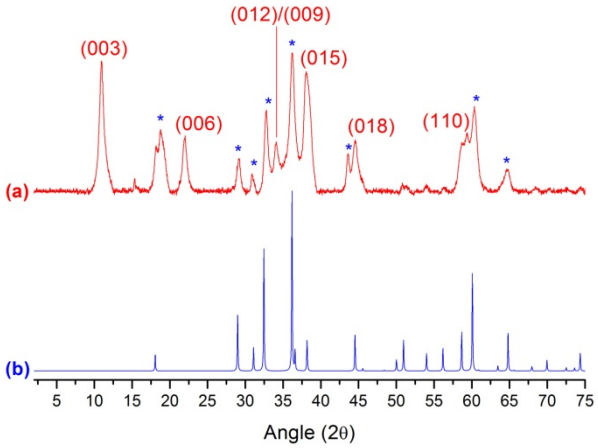

Figure 5.2: The powder X-ray patterns of (a) the solid product of the reaction of MgO with a solution of $MnCl_2$, and (b) Mn_3O_4.[70] LDH-phase reflections are identified with red Miller indices, while blue asterisks identify reflections that may readily be assigned to Mn_3O_4.

Altering the Mg:Mn ratio did not provide any significant reduction in the amount of Mn_3O_4 contaminating the product. Although this LDH has been previously reported,[62] and the salt-oxide method has not been found here to provide a clean synthesis route to the product, the existence of the LDH phase in the mixture indicates at least a degree of success; providing a more oxidising atmosphere to attempt to ensure the absence of Mn^{2+} in the solution may lead to reduced amounts of the mixed-oxidation state product.

The reaction of MgO with a solution of iron (III) chloride leads to formation of a red-brown solid. Under all conditions the solid is found to be poorly crystalline; traces of the LDH phase reported by Chitrakar[33] were only found when the reaction was performed at 80ºC. This product is illustrated in Figure 5.3, along with a simulated pattern of a Mg/Fe-Cl LDH similar to the predicted product.

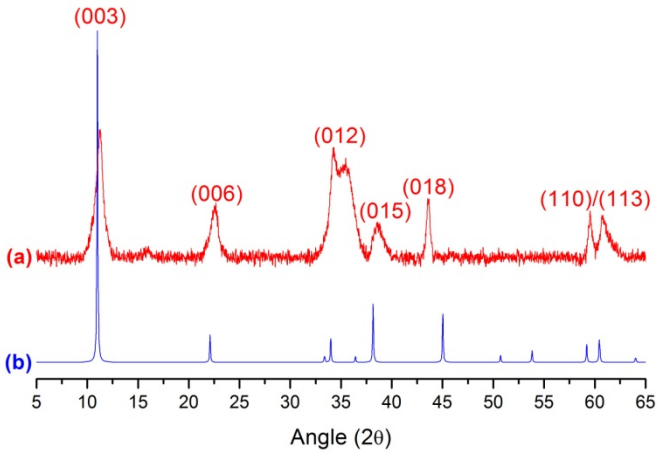

Figure 5.3: The powder X-ray patterns of (a) the solid product of the reaction of MgO with a solution of $FeCl_3$ at 80ºC, (b) $[Mg_3Fe(OH)_8]Cl{\cdot}2H_2O$.[69]

The products of the reactions of MgO and a number of other oxides with solutions of YCl_3 lead to products which showed similar structural features; these products are discussed separately in Section 5.7.1.

The product of the reaction of MgO with a solution of $AlCl_3$ gives a highly-crystalline Mg/Al-Cl LDH, as previously reported.[33] The reaction is also found to proceed cleanly with $Al(NO_3)_3$, although with a slight reduction in crystallinity. The reaction of the same oxide with gallium nitrate also leads to the formation of an LDH phase. XRD patterns of products using each of these metal solutions are given in Figure 5.4 overleaf.

While this once again leads to the formation of previously reported LDHs,[71] the Mg/Ga-LDH compound has never been reported by a salt-oxide synthesis method. The basal (00*l*) reflections in the pattern of the purported Mg/Ga-NO_3 LDH above are broad and irregularly shaped; it appears that two sets of (00*l*) reflections are present in the compounds, representing slightly different interlayer separations. This appears to be due to the same hydration-based effect which has previously been observed in two of the most similar LDHs to this systems, namely the Mg/Al-NO_3 LDH,[72] and Ca/Ga-NO_3 LDH (see Section 5.3.2 below).

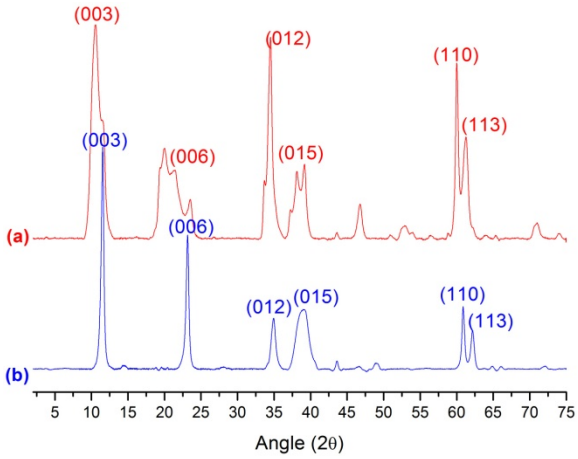

Figure 5.4: The powder X-ray patterns of (a) the solid product of the reaction of MgO with a solution of $Ga(NO_3)_3$, and (b) the solid product of the reaction of MgO with a solution of $AlCl_3$.

As with the products synthesised using YCl_3, a series of similar products were recovered from the reactions of MgO and the other metal oxides with $InCl_3$ solutions. These will also be discussed separately in Section 5.7.2.

As magnesium oxide had been found to produce LDHs upon reaction with a number of salt solutions, it was also reacted similarly with a solution of lanthanum chloride to see if a hydrotalcite-like phase would result. The white solid recovered comprised only a pure phase of $La(OH)_3$.

5.4.2 Reactions of Calcium Oxide (CaO)

The reaction of calcium oxide with vanadium trichloride progressed exactly as the reaction of the same solution with magnesium oxide. The only identifiable, poorly crystalline product was V_2O_3. Similar reactions are seen with manganese (II) chloride, iron (III) chloride and chromium (III) chloride; the only products recovered are identical to those produced by reactions of sodium hydroxide with the same solutions.

Reactions of calcium oxide with p-block metal salt solutions were more successful. The reaction of the oxide with a solution of aluminium chloride clearly yields an LDH phase, although somewhat contaminated with calcium carbonate, arising from

contamination from atmospheric carbon dioxide. The powder patterns of these three compounds are compared in Figure 5.5.

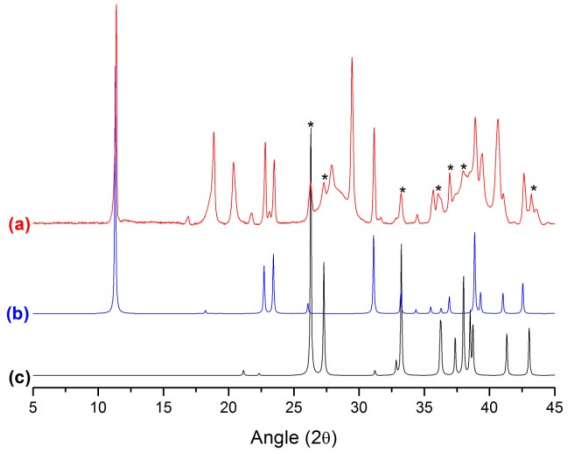

Figure 5.5: The powder X-ray patterns of (a) the solid product of the reaction of CaO with a solution of $AlCl_3$, (b) $[Ca_2Al(OH)_6]Cl{\cdot}2H_2O$,[73] and (c) the aragonite polymorph of $CaCO_3$.[74]

Once again, a significant amount of this common LDH phase is present in the product. This reaction is also found to work as effectively using aluminium nitrate as the metal (III) salt.

The product collected from the reaction of calcium oxide with gallium nitrate is an almost-pure LDH phase. The product is shown below, compared to a simulated X-ray pattern of $[Ca_2Al(OH)_6]NO_3{\cdot}yH_2O$, in Figure 5.6.

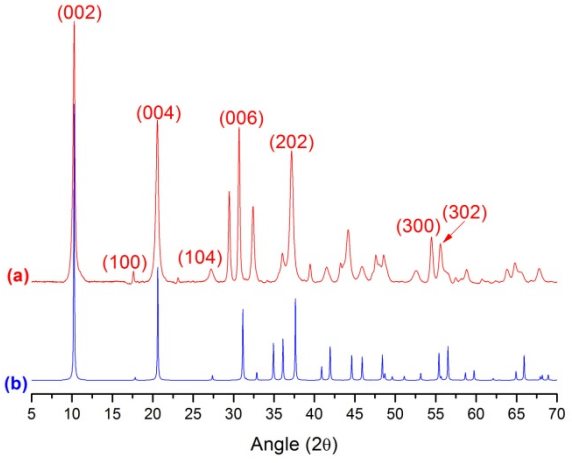

Figure 5.6: The powder X-ray patterns of (a) the solid product of the reaction of CaO with a solution of $Ga(NO_3)_3$, and (b) $[Ca_2Al(OH)_6]NO_3{\cdot}2H_2O$.[75] Indexable reflections are marked with red Miller indices.

An LDH structure containing calcium and gallium has only previously been reported by a coprecipitation method.[73] It appears to form in a nearly pure form by the salt-oxide method at room temperature, with little apparent contamination arising from the hydroxides of either the divalent or trivalent cation present.

An exploratory reaction of calcium oxide with lanthanum chloride was also performed, yielding poorly crystalline lanthanum hydroxide as the only solid product.

5.4.3 Reactions of Strontium Oxide (SrO)

Strontium oxide is prone to reacting rapidly with water to form its sparingly soluble hydroxide. The strongly basic nature of the oxide leads to the formation of identical products to the SrO/H_2O reaction when SrO is reacted with metal (III) salt solutions, except in the case of vanadium chloride.

At room temperature, the reaction of strontium oxide with a solution yields a dark green solid identifiable as V_2O_3; however, when the reaction is run at 80ºC, the reaction is found, several hours after addition of the solid, to form a dark red solid, with an unusual flaky texture. The powder X-ray pattern appeared to show the first basal reflection of an LDH phase; consequently, the solid was reacted with sodium cyclamate in an attempt to synthesise an intercalation compound. The pattern of the initial reaction product, and the same material after the attempted intercalation, are shown in Figure 5.7.

The original product appears to display some of the characteristic peaks of an LDH compound, including the first (00*l*) reflection at ca. 10º, and the two closely-spaced (110) and (113) reflections at ca. 60º. However, there are many reflections that cannot be assigned to a hydrotalcite-like phase, and the X-ray pattern of the post-intercalation product suggests no intercalation, since no Bragg reflections appear to have changed position as would be expected following a structural change in the product.

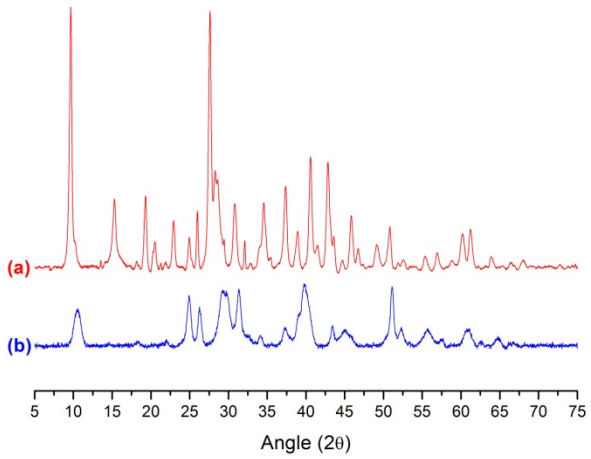

Figure 5.7: The powder X-ray patterns of (a) the solid product of the reaction of SrO with a solution of VCl_3 at 80ºC, and (b) the product of the attempted intercalation of cyclamate into this material.

Furthermore, elemental microanalysis indicates that there is less than 1% carbon content present after the reaction with cyclamate, and no trace of nitrogen, suggesting that it is highly unlikely that the first product is, in fact, an LDH phase. A possible identity for this phase, which tallies with its apparent lack of intercalation ability, is the mixed oxide phase $Sr_4V_2O_9$, which shows a similar powder pattern, and arises from the direct acid-base reaction of SrO with V_2O_3.[76]

Given the possible significance of this product, attempts were made to form the putative Sr/V-LDH compound by a coprecipitation method, by the dropwise addition of a mixed solution of NaOH and NaCl to a mixed solution of $SrCl_2$ and VCl_3 at 80ºC. Interestingly this yields a different, grey solid product which again resembles, at low 2θ values, a hydrotalcite-like product, albeit with a different first-reflection d-spacing and dissimilar reflections at higher 2θ values. Attempts were once again made to intercalate cyclamate into this solid product, and the starting material and post-intercalation products are both illustrated in Figure 5.8.

The pale yellow product of the intercalation reaction shows an identical series of high-intensity reflections, but the less intense reflections show subtle alterations: most

notably, a new, sharp Bragg reflection is found at 5.7º (corresponding to a d-spacing of 15.4Å). However, this supposed intercalation product contains only 1.5% carbon content by mass, and no traces of the nitrogen expected from the cyclamate molecule, implying once more that this does not represent a genuine intercalation reaction. A complex strontium vanadate compound is, once again, the more likely product.

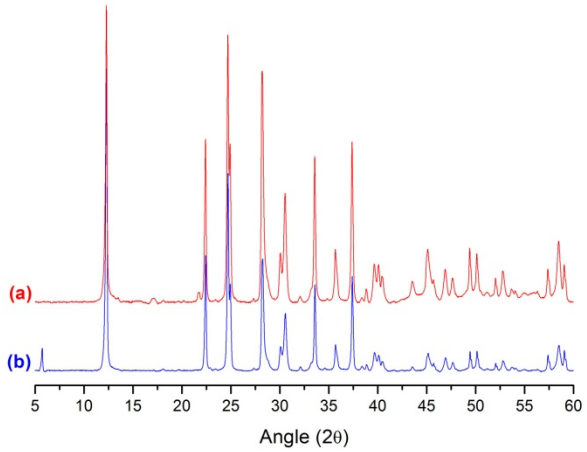

Figure 5.8: The powder X-ray patterns of (a) the solid product of a coprecipitation reaction of $SrCl_2$ and VCl_3 with a solution of NaOH and NaCl at 80ºC, and (b) the product of the attempted intercalation of cyclamate into this material.

5.4.4 Reactions of Barium Oxide (BaO)

When barium oxide is added to water, a violent exothermic reaction results in the near-immediate formation of barium hydroxide. While this compound is moderately soluble in water, the reactions of this oxide with the metal (III) salt solutions are found uniformly to result in the same products as their reactions with sodium hydroxide, with some $Ba(OH)_2$ also present. No traces of LDH phases are observed in any of the products; it is likely that the harsh basicity of the solid, and its much more favourable reaction with water, does not permit the formation of hydrotalcite-like phases by this method.

5.5 Reactions of Transition Metal Oxides

5.5.1 Reactions of Manganese Oxide (MnO)

The reaction of manganese oxide with vanadium chloride, in a very similar manner to SrO, leads to a brown solid product that appears to possess the (00*l*) reflections characteristic of an LDH phase. As above, this solid was reacted with a solution of sodium cyclamate to determine whether anionic intercalation into the solid was possible. The product of the salt-oxide reaction, and the attempted successive intercalation, are shown in Figure 5.9.

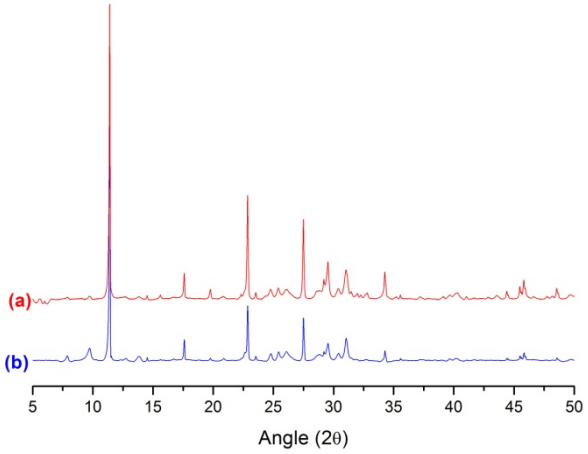

Figure 5.9: The powder X-ray patterns of (a) the solid product of the reaction of MnO with a solution of VCl_3 at 80ºC, and (b) the product of the attempted intercalation of cyclamate into this material.

There does not appear to have been any structural change between the two solids upon intercalation; furthermore, elemental analysis results suggest that there is no carbon content in the post-intercalation product, indicating that no cyclamate incorporation has taken place. The only noticeable difference in the patterns (apart from a loss of crystallinity) is the appearance of two Bragg reflections below 10º - however, further low-angle XRD analysis of the initial product shows that these two reflections are present at low intensities. It seems highly unlikely that this is, in fact, an LDH phase, as a number of characteristic reflections appear to be absent. This is

also reflected in the lack of any observable carbon content by elemental microanalysis in the attempted intercalation compound. If an intercalation reaction is attempted with sodium carbonate, or sodium terephthalate, the same unaltered product is found.

The remainder of the metal (III) salts in solution give solids that are typically a mixture of the products from their reactions with sodium hydroxide, with a large amount of Mn_3O_4, arising from partial oxidation of the manganese in the oxide. Mn_3O_4 is also the sole product resulting from the reaction of manganese oxide with a solution of $MnCl_2$.

The only other reaction product of MnO that may yield a hydrotalcite-like product, albeit a heavily-contaminated one, is that which arises from the reaction of the oxide with a solution of $AlCl_3$. The powder pattern of the resulting product, compared to that of its major contaminant Mn_3O_4, is given in Figure 5.10.

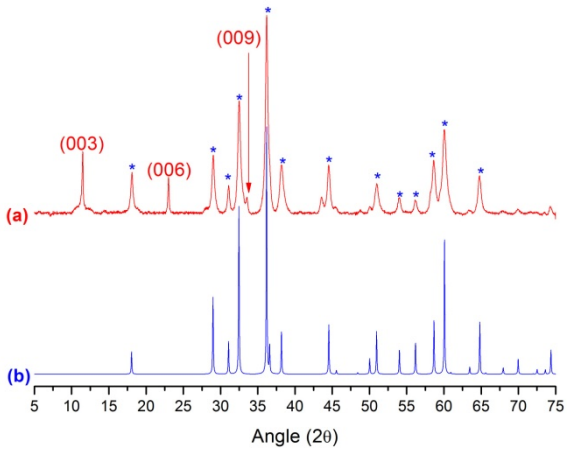

Figure 5.10: The powder X-ray patterns of (a) the solid product of the reaction of MnO with a solution of $AlCl_3$, and (b) Mn_3O_4.[70] LDH-phase reflections are identified with red Miller indices, while blue asterisks identify reflections that may readily be assigned to Mn_3O_4.

The three reflections identified as belonging to an LDH phase in the pattern above correspond in their positioning to the basal reflections of a chloride-intercalated LDH. However, there do not appear to be any other clearly attributable reflections from an LDH; the characteristic closely-spaced (110) and (113) reflections at *ca.* 60º, if present, would be entirely masked by the two similar reflections of Mn_3O_4. The

Mn/Al-Cl LDH has previously been reported,[77] but its apparent production from a salt-oxide reaction is highly interesting given that the previous reported synthesis required a continuous reducing atmosphere of hydrogen to be present during coprecipitation to prevent oxidation (an inert atmosphere alone would not suffice). In this salt-oxide reaction, it appears to have formed in significant quantities without the presence of a hydrogen atmosphere, although the reductive capability of the latter would undoubtedly limit the degree of Mn_3O_4 contamination of the LDH.

5.5.2 Reactions of Cobalt Oxide (CoO)

The reactions of cobalt oxide with solutions of vanadium, chromium, manganese and iron chloride solutions in a 2:1 ratio yield only the same products as the reactions of the metal (III) salt solutions with sodium hydroxide, with some unreacted CoO present in the product. Cobalt (II) oxide is notably less basic than many of the others used, so such contamination is likely to occur in salt-oxide products.

When cobalt oxide is stirred in a solution of aluminium chloride, the only apparent solid product is an LDH phase. While typical Co/Al LDHs synthesised by coprecipitation are rose-red in colour, similar to $Co(OH)_2$, the solid product of this reaction shows the same dark brown colour of the oxide from which it was synthesised, even though no oxide contamination of the LDH product is apparent from the X-ray powder pattern. The XRD pattern of the product is compared to a simulated pattern from a Co/Al-CO_3 LDH in Figure 5.11: this LDH has never been synthesised by a salt-oxide method according to the extant literature.

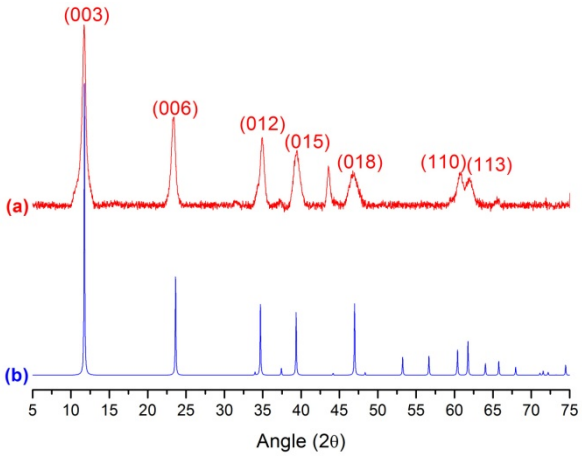

Figure 5.11: The powder X-ray patterns of (a) the solid product of the reaction of CoO with a solution of $AlCl_3$, (b) $[Co_2Al(OH)_6](CO_3)_{0.5}\cdot 1.5H_2O$.[78]

It was also found to be possible to intercalate cyclamate into this compound, expanding the interlayer spacing of the compound from 7.5Å to 19.1Å, although with a significant loss of crystallinity in the product accompanying this large separation of the layers. The X-ray patterns of the Co/Al-Cl LDH, and its cyclamate intercalation product, are shown in Figure 5.12.

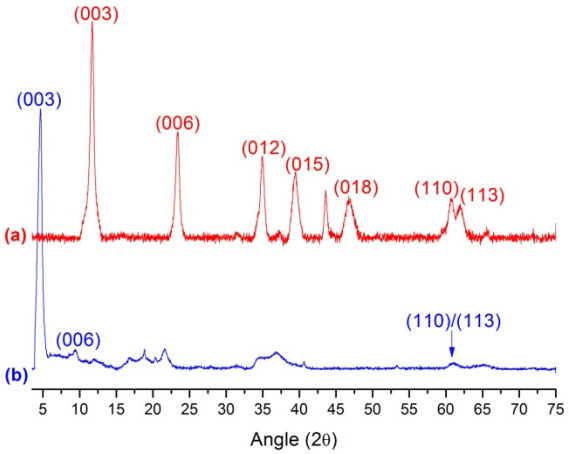

Figure 5.12: The powder X-ray patterns of (a) the solid product recovered from the reaction of CoO with a solution of $AlCl_3$, and (b) the product of the attempted intercalation of cyclamate into this material. The d-spacings of the (003) reflections of the above patterns are 7.5 and 19.1Å respectively.

The apparent chemical formula of this intercalation compound, as determined by elemental microanalysis, is $[Co_2Al(OH)_6](C_6H_{12}NO_3S)_{0.78}Cl_{0.22}\cdot 3H_2O$.

The reaction of cobalt oxide with a solution of gallium nitrate leads only to a poorly crystalline solid with no apparent hydrotalcite-like phases present.

5.5.3 Reactions of Nickel Oxide (NiO)

The reactions of vanadium, chromium, and manganese chloride solutions with nickel oxide do not yield LDH phases under any sets of reaction conditions. As with cobalt oxide, the less basic nickel oxide is found as a major contaminant in many of these products.

When nickel oxide is stirred in a solution of iron (III) chloride, the product, while poorly crystalline, may be identified as an LDH phase. The product of this reaction is shown in Figure 5.13, along with a simulated pattern of a Mg/Fe-Cl LDH which should show very similar X-ray reflections. While once again this does not provide a novel LDH,[79] this method of synthesis is previously unreported.

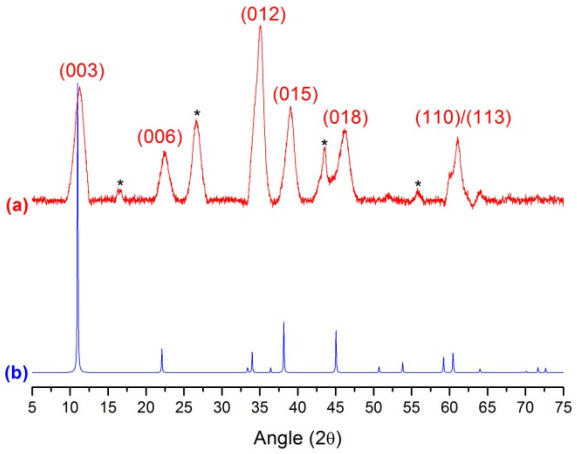

Figure 5.13: The powder X-ray patterns of (a) the solid product of the reaction of NiO with a solution of $FeCl_3$, (b) $[Mg_3Fe(OH)_8]Cl{\cdot}2H_2O$.[69] The reflections marked with black asterisks may be attributed to non-LDH phases, including NiO and goethite.

The reaction of nickel oxide with a solution of aluminium chloride at 80ºC also yields a pure LDH phase as the product, much like the reaction of the same solution with cobalt oxide. This reaction is also found to proceed effectively with aluminium

nitrate; the X-ray powder data for the nitrate product is shown in Figure 5.14, and compared to a simulated pattern of hydrotalcite.

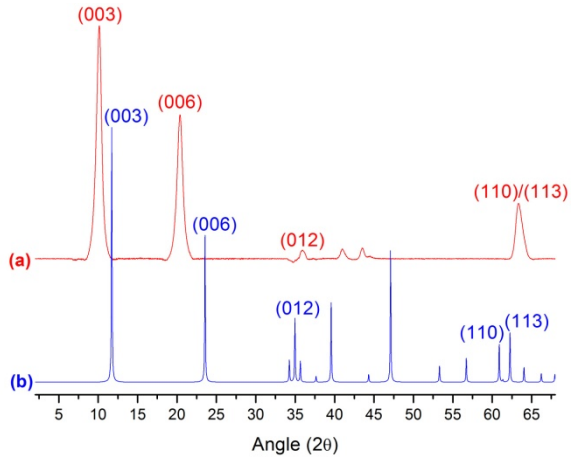

Figure 5.14: The powder X-ray patterns of (a) the solid product of the reaction of NiO with a solution of $Al(NO_3)_3$, (b) hydrotalcite ($[Mg_2Al(OH)_6](CO_3)_{0.5}\cdot 1.5H_2O$).[78]

Intercalation of cyclamate into this material was found to be successful: the product of the reaction of NiO with a solution of $Al(NO_3)_3$ is illustrated in Figure 5.15, along with its cyclamate intercalate.

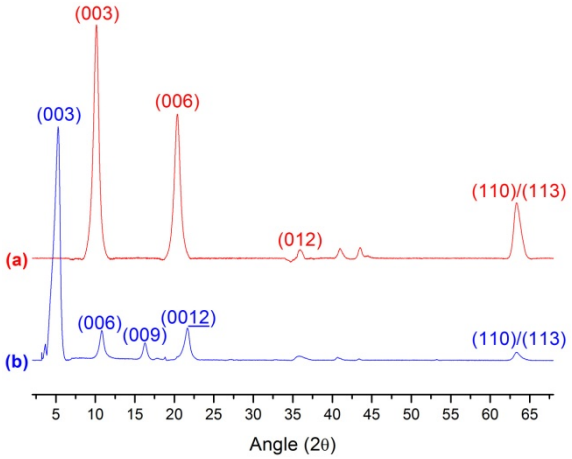

Figure 5.15: The powder X-ray patterns of (a) the solid product recovered from the reaction of NiO with a solution of $Al(NO_3)_3$, and (b) the product of the attempted intercalation of cyclamate into this material. The d-spacings of the (003) reflections of the above patterns are 8.7 and 16.8Å respectively.

Upon the intercalation of cyclamate, the interlayer spacing of the solid increases from 8.7Å to 16.8Å. The chemical formula of the cyclamate intercalate, as determined

from elemental microanalysis, may be approximately expressed as $[Ni_2Al(OH)_6](C_6H_{12}NO_3S)_{0.96}(NO_3)_{0.04}\cdot 1.2H_2O$.

The reaction of nickel oxide with gallium nitrate in solution provides only gallium oxyhydroxide and unreacted nickel oxide as the products.

5.5.4 Reactions of Copper Oxide (CuO)

The sole reaction product arising from a stirred reaction of copper oxide in a solution of vanadium (III) chloride is V_2O_3; no LDH phases are apparent in the X-ray powder pattern.

The efficacy of the synthesis of Cu/Cr-LDHs by the direct reaction of the chloride salt of chromium with copper oxide is well established, yielding a pure and relatively crystalline product.[29] The product of such a reaction is shown below in Figure 5.16, and compared to a simulated pattern of hydrotalcite ($[Mg_2Al(OH)_6](CO_3)_{0.5}\cdot 1.5H_2O$).

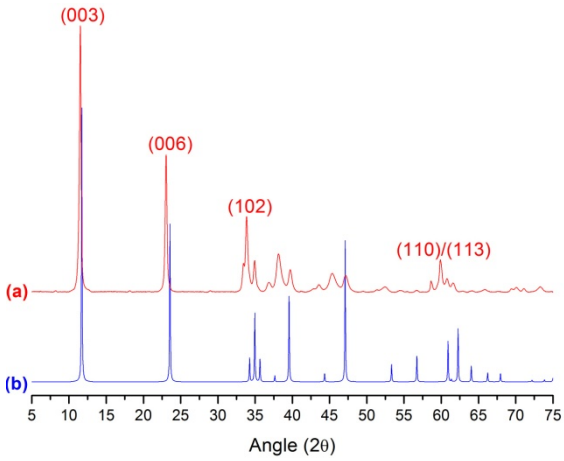

Figure 5.16: The powder X-ray patterns of (a) the solid product of the reaction of CuO with a solution of $CrCl_3$, and (b) hydrotalcite ($[Mg_2Al(OH)_6](CO_3)_{0.5}\cdot 1.5H_2O$).[78]

The reactions of copper oxide with solutions of manganese (II) chloride and iron (III) chloride yield only amorphous products analogous to those synthesised by reaction of the solutions with sodium hydroxide.

The reaction of copper oxide and a solution of aluminium chloride yields an LDH phase; this reaction also proceeds successfully with aluminium nitrate. Figure 5.17 shows the pattern of the nitrate product, compared to a pattern of hydrotalcite.

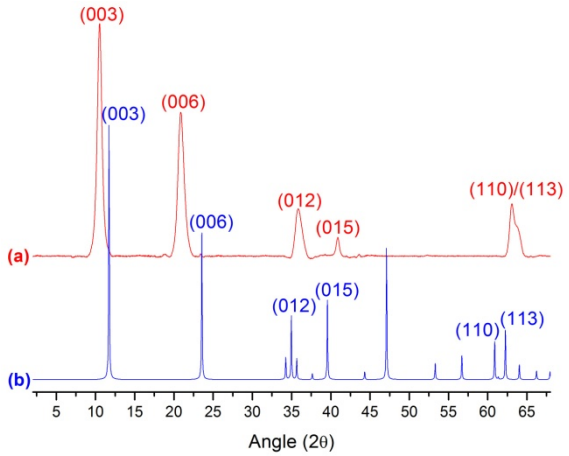

Figure 5.17: The powder X-ray patterns of (a) the solid product of the reaction of CuO with a solution of $Al(NO_3)_3$, (b) hydrotalcite ($[Mg_2Al(OH)_6](CO_3)_{0.5}\cdot 1.5H_2O$).[78]

This nitrate-containing product is capable of intercalating the cyclamate anion, and the powder patterns of the nitrate precursor and the cyclamate intercalation product are illustrated in Figure 5.18.

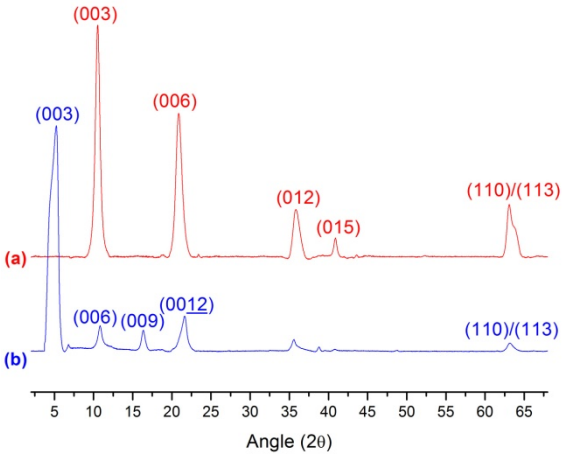

Figure 5.18: The powder X-ray patterns of (a) the solid product recovered from the reaction of CuO with a solution of $Al(NO_3)_3$, and (b) the product of the attempted intercalation of cyclamate into this material. The d-spacings of the (003) reflections of the above patterns are 8.4 and 17.0Å respectively.

The pattern of both the Cu/Al-NO_3 LDH product and the cyclamate compound formed from it are both very similar to their Ni/Al-LDH analogues. The elemental

microanalysis data for this compound suggests complete exchange of the nitrate ions, giving a solid with the approximate formula $[Cu_2Al(OH)_6](C_6H_{12}NO_3S)\cdot 1.1H_2O$. This represents a further example of a previously unknown salt-oxide synthesis of a known LDH host.

The reaction of copper oxide with gallium nitrate leads to a solid in which the sole phase identifiable by X-ray diffraction is gallium oxyhydroxide.

5.5.5 Reactions of Zinc Oxide (ZnO)

While the only product identifiable as resulting from the reaction of zinc oxide with a vanadium trichloride solution is V_2O_3, the reaction of the oxide with chromium chloride leads to a well-crystallised LDH phase, previously synthesised by this method accidentally by Morrison and Bonelle, and intentionally by Boehm.[27, 28] The powder X-ray pattern of the Zn/Cr-LDH product is given in Figure 5.19, and compared to a simulated powder pattern of hydrotalcite.

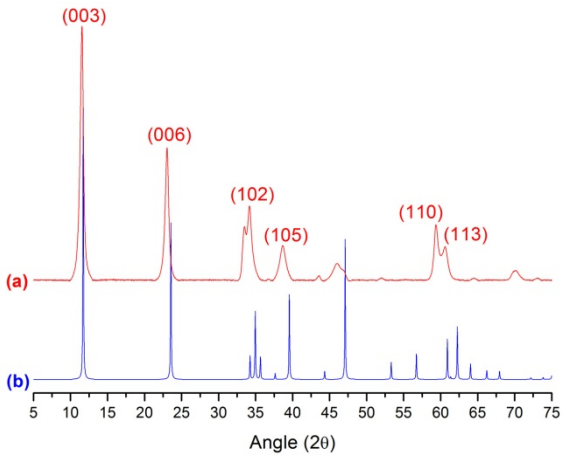

Figure 5.19: The powder X-ray patterns of (a) the solid product of the reaction of ZnO with a solution of $CrCl_3$, and (b) hydrotalcite ($[Mg_2Al(OH)_6](CO_3)_{0.5}\cdot 1.5H_2O$).[78]

Reacting zinc oxide with solutions of manganese (II) chloride or iron (III) chloride both lead to nearly amorphous products, with no identifiable LDH phase reflections in either.

As previously reported by Chitrakar *et al.*, solid zinc oxide will readily react with solutions of $AlCl_3$ to produce an LDH structure.[33] Reacting this oxide with solutions of aluminium nitrate will also yield a pure LDH phase; the powder patterns of these two products are illustrated in Figure 5.20.

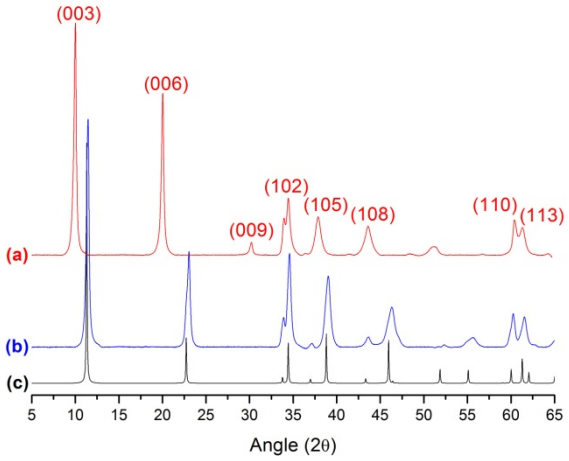

Figure 5.20: The powder X-ray patterns of the solid product from the reaction of zinc oxide with a solution of (a) aluminium nitrate, and (b) aluminium chloride. The simulated pattern of $[Zn_2Al(OH)_6]Cl{\cdot}2H_2O$ is shown as (c).[80]

The reaction of zinc oxide with a solution of gallium nitrate yields a similarly phase-pure LDH product, if a slightly more poorly-crystallised one. Figure 5.21 overleaf compares this product to its Zn/Al-LDH analogue, as synthesised by the salt-oxide method.

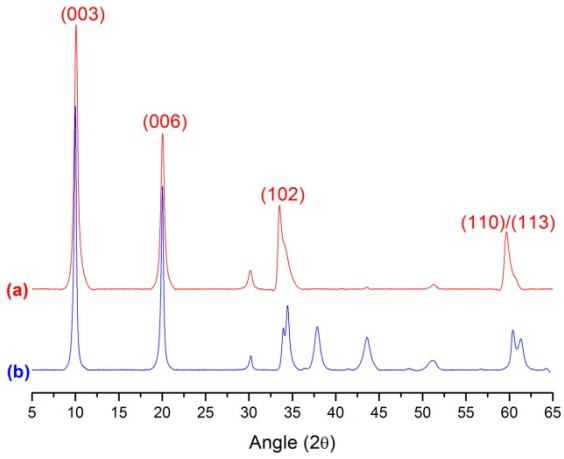

Figure 5.21: The powder X-ray patterns of the solid product from the reaction of zinc oxide with a solution of (a) gallium nitrate, and (b) aluminium nitrate.

The Zn/Ga-LDH product readily intercalates cyclamate, yielding a product which, according to elemental microanalysis, possesses the chemical formula $[Zn_2Ga(OH)_6](C_6H_{12}NO_3S)_{0.79}(NO_3)_{0.21}\cdot 2H_2O$. The powder patterns of the nitrate-containing product, and the post-intercalation cyclamate material, are illustrated in Figure 5.22.

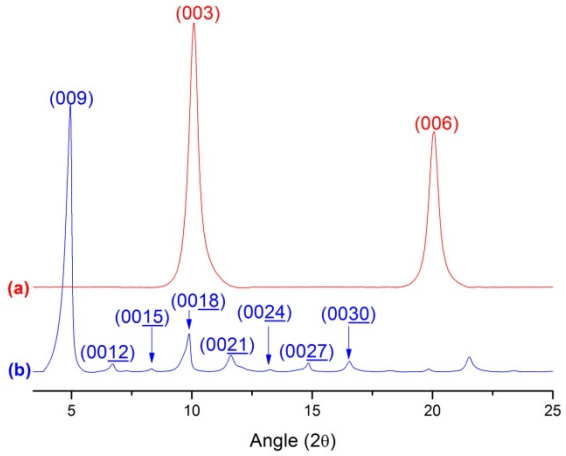

Figure 5.22: The powder X-ray patterns of (a) the solid product recovered from the reaction of ZnO with a solution of $Ga(NO_3)_3$, and (b) the product of the attempted intercalation of cyclamate into this material. The d-spacings of the (003) reflections of the above patterns are 8.8 and 53.2Å respectively.

The structure of this unusual intercalation compound is discussed at greater length in Section 5.7.4

5.5.6 Reactions of Cadmium Oxide (CdO)

The reaction of cadmium oxide with a vanadium trichloride solution yields no LDH phase; nonetheless, reports exist of reaction of the oxide with a solution of chromium (III) chloride has been reported to produce a Cd/Cr LDH.[30] However, the reactions of CdO with this solution at room temperature, 80ºC and under hydrothermal conditions were found to yield no LDH phases, only near-amorphous green solids containing only traces of cadmium (according to metals analysis). The only identifiable reflections were found to correspond to hydrated Cr_2O_3. Varying the Cd:Cr ratio was

found to give near-identical products, ultimately leading to only cadmium hydroxide at high values, and Cr_2O_3 at low values.

The products of stirring cadmium oxide in solutions of manganese (II) chloride and iron (III) chloride, under each set of reaction conditions, were found to produce only poorly crystalline Mn_3O_4 and FeO(OOH), respectively.

The reaction of cadmium oxide with a solution of aluminium chloride yields an LDH phase, although this reaction is more effective when the nitrate salt is used; the product is somewhat contaminated with cadmium hydroxide formed from the hydration of the unreacted CdO. The product from the reaction of the oxide with a solution of aluminium nitrate is illustrated in Figure 5.23, along with a simulated pattern of a Ca/Al-LDH (which contains two cations with similar ionic radii to the Cd/Al-LDH). The nitrate and carbonate forms of this LDH have been reported by Vichi and Alves, synthesised by a coprecipitation method.[81] The salt-oxide method has never been used to synthesise this host in previous literature.

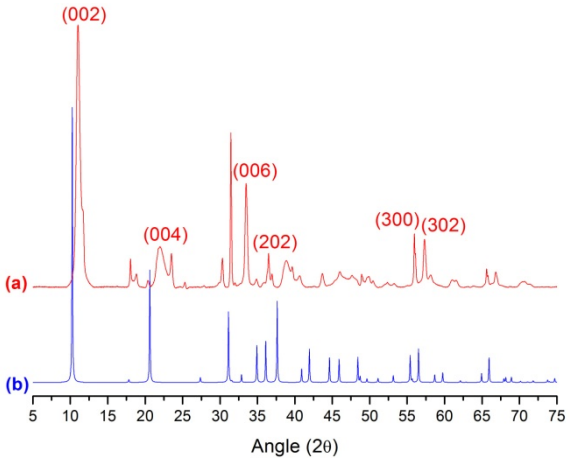

Figure 5.23: The powder X-ray patterns of (a) the solid product of the reaction of CdO with a solution of $Al(NO_3)_3$, and (b) $[Ca_2Al(OH)_6]NO_3{\cdot}2H_2O$.[75]

When cadmium oxide is stirred in a solution of gallium nitrate at room temperature, the solid recovered is once again an LDH. It is also possible to achieve the formation

of the same product by a coprecipitation method. Both of these products are shown in Figure 5.24, along with the simulated pattern of hydrotalcite.

There have been no previous literature reports of a Cd/Ga hydrotalcite-like phase. The products of this synthesis, by both the salt-oxide and coprecipitation methods, are unprecedented.

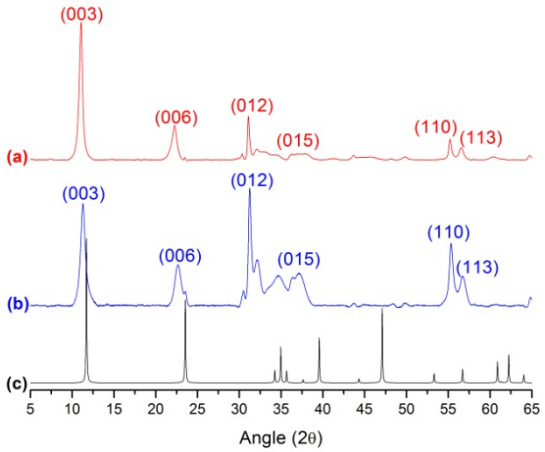

Figure 5.24: The powder X-ray patterns of (a) the solid product of the reaction of CdO with a solution of $Ga(NO_3)_3$, (b) the product of a coprecipitation reaction between $Cd(NO_3)_2$ and $Ga(NO_3)_3$, and (c) hydrotalcite ($[Mg_2Al(OH)_6](CO_3)_{0.5}\cdot 1.5H_2O$).[78]

As with many of the other new LDH phases synthesised, it was found that the Cd/Ga-LDH would readily intercalate the cyclamate anion. The product of this intercalation reaction, and its precursor as synthesised by the salt-oxide method, are given in Figure 5.25. The altered positions of the (00*l*) reflections in the cyclamate-intercalated product suggest an expansion of the gallery height from 3.6Å to 11.7Å upon exchanging nitrate for cyclamate. Due to the novelty of this phase, further investigations into the nature of these products are discussed in Section 5.7.3.

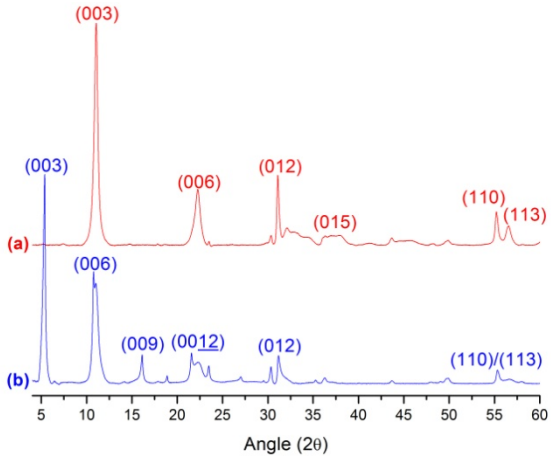

Figure 5.25: The powder X-ray patterns of (a) the solid product recovered from the reaction of CdO with a solution of $Ga(NO_3)_3$, and (b) the product of the attempted intercalation of cyclamate into this material. The d-spacings of the (003) reflections of the above patterns are 8.4 and 16.5Å respectively.

5.6 Exploration of Hydroxy Double Salt Synthesis

A number of hydroxy double salts, layered compounds similar to LDHs possessing only dipositive cations within the layers, are most commonly synthesised by the reaction of a metal (II) oxide with a solution of a metal (II) salt solution. The zinc hydroxynitrate salt $[Zn_5(OH)_8](NO_3)_2 \cdot yH_2O$, used as an intercalation host in Chapter 3, is typically synthesised by stirring zinc oxide in a solution of zinc nitrate at room temperature for several days.[82] A somewhat similar copper hydroxynitrate salt, $[Cu_2(OH)_3NO_3] \cdot yH_2O$, may be synthesised by the directly analogous reaction of copper oxide with a copper nitrate solution,[83] while mixed hydroxy double salts containing combinations of Co^{2+}, Ni^{2+}, Cu^{2+}, and Zn^{2+} may be synthesised by the interreactions between the oxide of one metal and a nitrate salt solution of the other.[84] Each of the monometallic hydroxy salts may also be synthesised by titration of the metal nitrate salts with sodium hydroxide.[85] Although observation of the relative cation sizes in known hydroxy double salts leads to the conclusion that these layer compounds display a much lesser tolerance for greatly differing cation sizes within

the layers, it is quite possible that there may be previously unknown hydroxy double salt phases that may be synthesised by salt-oxide methods. A number of possible new pairings were examined, although not as exhaustively and systematically as for the LDH syntheses above; rather, attention was focused on a number of cases that, given the observed reactivities from the LDH syntheses, were expected to lead to hydroxy double salt products.

The reactions of magnesium oxide with solutions of copper, zinc and cobalt salts were studied, given the previous success of many of the MgO reactions in forming LDH phases. The reaction of the oxide with a solution of copper chloride yielded copper hydroxide as the sole product, but an identical reaction using copper nitrate led to an apparent hydroxy salt as the solid product. Given that the structure of the hydroxy salts includes nitrate molecules bound to the layers, it has been found that the presence of nitrate is critical in many cases as both a directing and structural component for the final product to form. The powder pattern of the hydroxy salt formed is shown below, and compared to a simulated pattern of $[Cu_2(OH)_3]NO_3$.

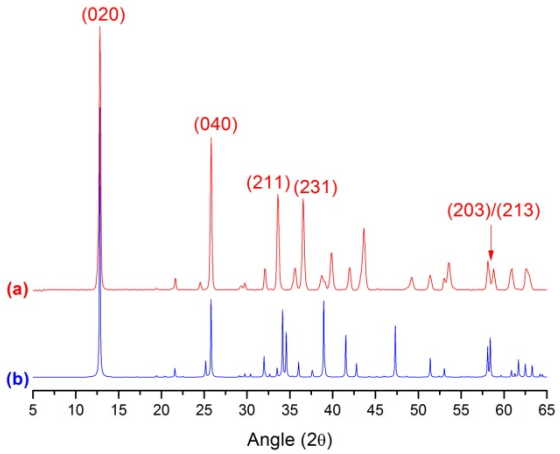

Figure 5.26: The powder X-ray patterns of (a) the solid product of the reaction of MgO with a solution of $Cu(NO_3)_2$, and (b) $[Cu_2(OH)_3]NO_3$.[86]

The product from the reaction of MgO also readily undergoes ion exchange with the cyclamate anion, to produce an intercalation compound. The powder pattern of

this compound, and its precursor, are illustrated in Figure 5.27. The approximate formula of the cyclamate intercalate, according to its carbon and nitrogen contents, is $[Cu_2(OH)_3](C_6H_{12}NO_3S)_{0.58}(NO_3)_{0.42}$.

Subsequent metals analysis of these reaction products indicated that the solids did not contain any traces of magnesium, suggesting that the initial compound formed is a monometallic copper hydroxynitrate salt. This method for synthesising copper hydroxy salts is somewhat similar to that recently reported by Giraldo *et al.*,[87] by adding a copper nitrate solution to a suspension of magnesium hydroxide; given the rapid hydration of magnesium oxide upon stirring in water, these methods may be considered to be equivalent.

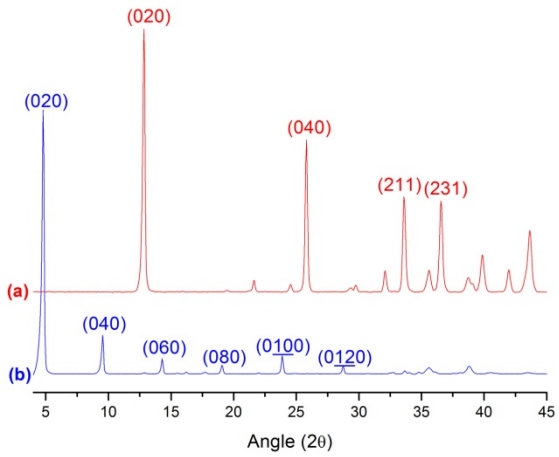

Figure 5.27: The powder X-ray patterns of (a) the solid product recovered from the reaction of MgO with a solution of $Cu(NO_3)_2$, and (b) the product of the attempted intercalation of cyclamate into this material. The d-spacings of the (020) reflections of the above patterns are 6.9 and 18.5Å respectively.

Further investigation indicates that the same copper hydroxy salt product is formed when calcium oxide is used in place of MgO.

Using a solution of cobalt (II) nitrate, two similar hydrotalcite-like compounds are formed upon reaction of the solution with either magnesium or cadmium oxides at 80ºC. The powder patterns of these two products are shown in Figure 5.28.

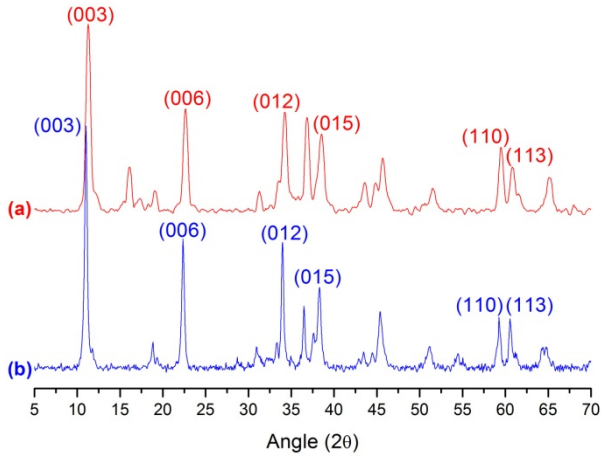

Figure 5.28: The powder X-ray patterns of the solid products recovered from a solution of cobalt (II) nitrate with (a) MgO, and (b) CdO.

These two almost identical structures do not contain either of the cations present in the original solid oxide; the only metallic cation found in the product compounds is cobalt. These powder patterns resemble those of the series with the general formula $Co(OH)_{2-x}(NO_3)_x{\cdot}yH_2O$, reported by Vishnu Kamath *et al.*[88] There does not appear to be a precedent for this salt-oxide synthesis of cobalt hydroxide nitrate compounds.

Reactions to produce layered hydroxide phases are also found to occur upon the addition of magnesium oxide or calcium oxide to a solution of zinc nitrate. By analogy to the reactions above, the most likely monometallic product of the reaction is the zinc hydroxynitrate salt $[Zn_5(OH)_8]NO_3{\cdot}yH_2O$. The powder pattern of the solid product recovered from the reaction of calcium oxide with zinc nitrate is given in Figure 5.29, along with a simulated pattern of the zinc hydroxynitrate salt.

The powder pattern apparently shows the zinc hydroxynitrate as the only solid product, and this is confirmed by metals analysis which shows no trace of alkaline earth cations in the solid. Forming this hydroxynitrate by a salt-oxide method without using zinc oxide is a novel process, although applications of this variant synthesis would appear to be somewhat limited.

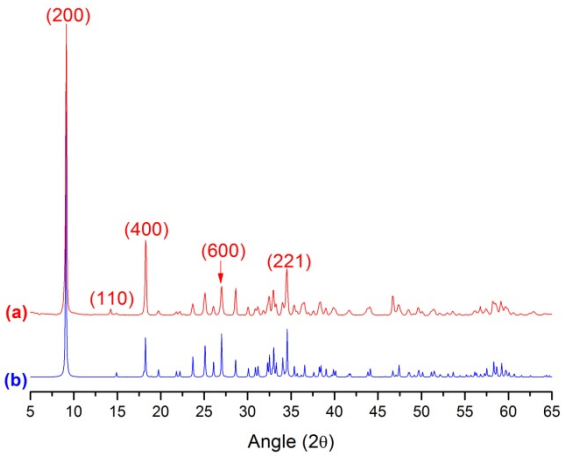

Figure 5.29: The powder X-ray patterns of (a) the solid product of the reaction of CaO with a solution of $Zn(NO_3)_2$, and (b) $[Zn_5(OH)_8]NO_3{\cdot}yH_2O$.[89]

A final unusual result from these syntheses arises from a reaction of cadmium nitrate solution with cadmium oxide. By analogy with the same reaction using the oxide and salt of zinc, one might naïvely expect the product to be the cadmium hydroxide nitrate salt $[Cd_5(OH)_8]NO_3{\cdot}yH_2O$, and this indeed appears to be the case: the product of the salt-oxide reaction, compared to a simulated pattern of the cadmium hydroxide nitrate salt, is illustrated in Figure 5.30.

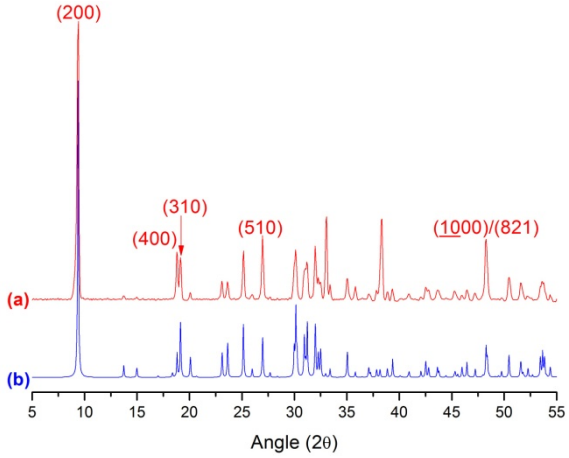

Figure 5.30: The powder X-ray patterns of (a) the solid product of the reaction of CdO with a solution of $Cd(NO_3)_2$, and (b) $[Cd_5(OH)_8]NO_3{\cdot}2H_2O$.[90]

Remarkably, despite its exact analogy to the zinc hydroxynitrate salt and the well-characterised nature of the solid, the salt-oxide synthesis of this compound appears to have never been reported. Previous syntheses, particularly those requiring single

crystals for powder analysis, are formed by diffusion of ammonia over a solution of cadmium nitrate,[91] and the similar layered cadmium hydroxynitrate salt $[Cd_3(OH)_5]NO_3 \cdot yH_2O$ has been observed to form when $Cd(OH)_2$ is suspended in nitrate-rich aqueous solutions.[92] The salt-oxide synthesis of this compound yields only a single cadmium hydroxynitrate phase, and is both simpler and more rapid to reach completion than the diffusion method previously reported.

5.7 Discussion of Results

5.7.1 Products of Reactions of Metal (II) Oxides with YCl_3

A number of structural similarities were observed for the products of the reactions of metal (II) oxides with solutions of yttrium chloride. In almost every case, the apparent reaction product is, in fact, the yttrium hydroxychloride species predicted in Section 5.3.2. In these cases, elemental microanalysis shows no metal (II) present in the solid, and, where there is, it can be matched to traces of the unreacted oxide visible in the X-ray powder pattern. There are no previous reports of rare earth hydroxychlorides being synthesised by a salt-oxide method. X-ray data for several of the reaction products of metal (II) oxides with yttrium chloride are shown in Figure 5.31, along with that of the isostructural ytterbium hydroxychloride. The exceptionally well-crystallised product from the NiO/YCl_3 reaction was used for cyclamate intercalation. The intercalation was found to be successful, with cyclamate making up 64% of the charge-balancing anions, and indicating an apparent expansion of the gallery height from 2.5Å to 30.7Å. The powder patterns of the "Ni/Y" product, and its cyclamate intercalation product, are shown in Figure 5.32.

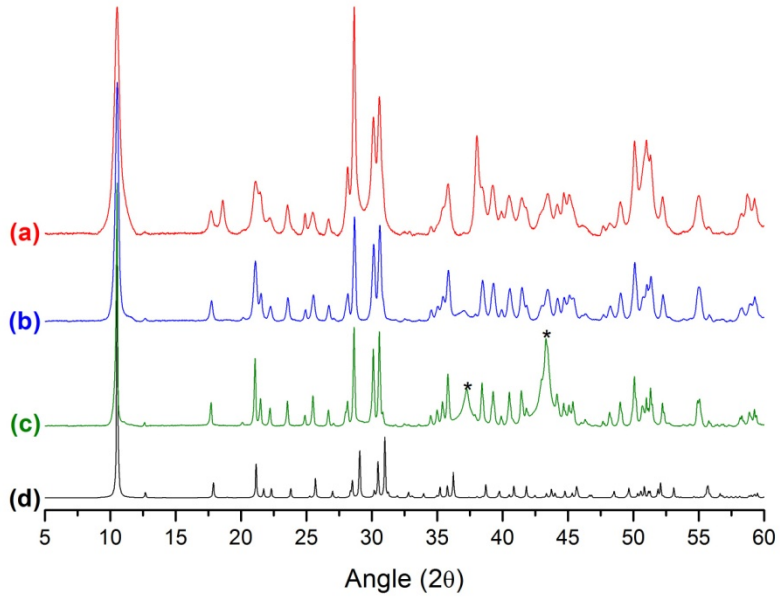

Figure 5.31: The products of the reactions of a solution of yttrium chloride with (a) MgO, (b) CoO, and (c) NiO. The orthorhombic form of ytterbium hydroxychloride $[Yb_2(OH)_5]Cl{\cdot}yH_2O$ is shown as (d). Reflections marked with black asterisks may be attributed to nickel oxide.

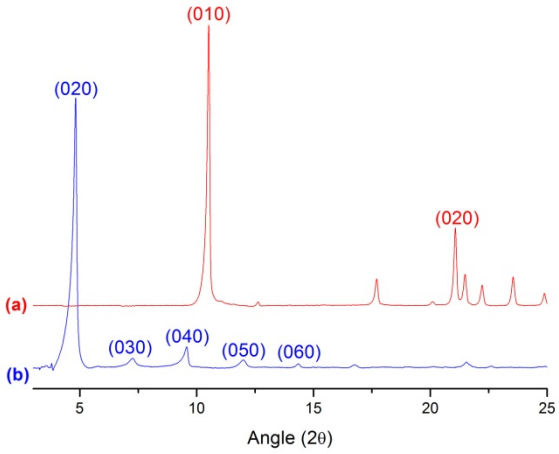

Figure 5.32: The powder X-ray patterns of (a) the solid product recovered from the reaction of NiO with a solution of YCl_3, and (b) the product of the attempted intercalation of cyclamate into this material. The d-spacings of the (010) reflections of the above patterns are 8.4 and 36.6Å respectively.

The unusual structure of this intercalation product is discussed at greater length in Section 5.7.4.

The only reaction of yttrium chloride which appears to yield a different product is that with copper oxide. The powder pattern of the reaction product is illustrated in

Figure 5.33, along with the simulated patterns of the ytterbium analogue of $[Y_2(OH)_5]Cl{\cdot}yH_2O$ and copper oxide.

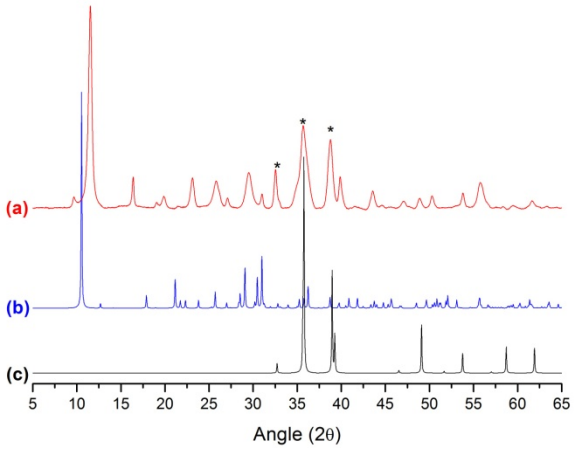

Figure 5.33: The powder X-ray patterns of (a) the solid product of the reaction of CuO with a solution of YCl_3, (b) the orthorhombic form of ytterbium hydroxychloride $[Yb_2(OH)_5]Cl{\cdot}yH_2O$,[59] and (c) copper oxide.[93] Reflections that may be readily attributed to copper oxide are marked with black asterisks.

The product powder pattern varies markedly from that of the yttrium hydroxychloride. Despite a number of intense reflections clearly arising from unreacted CuO, the pattern in many ways resembles a hydrotalcite-like compound, rather than an yttrium hydroxychloride as observed for the products of other salt-oxide reactions using YCl_3.

Metals analysis indicates a total Cu:Y ratio for this mixed product of 1.75:1, which barely lies within the range observed for LDH materials. Despite possessing no carbon content, the compound would not undergo intercalation with the sodium salts of cyclamate, terephthalate or carbonate – this suggests that the above powder pattern of the unidentifiable phase formed possesses only a superficial similarity to LDH materials, and may not in fact be a layered compound.

5.7.2 Products of Reactions of Metal (II) Oxides with $InCl_3$

The commonality found between the reaction products of the metal (II) oxides with indium chloride solutions is the abundance of indium hydroxide which forms as a by-product, and dominates the powder diffraction patterns. However, beyond the reflections attributable to this contaminant are several products which show low angle reflections that may well arise from the presence of LDH phases. A number of these are given as examples in Figure 5.34, along with the simulated pattern of $In(OH)_3$ for comparison.

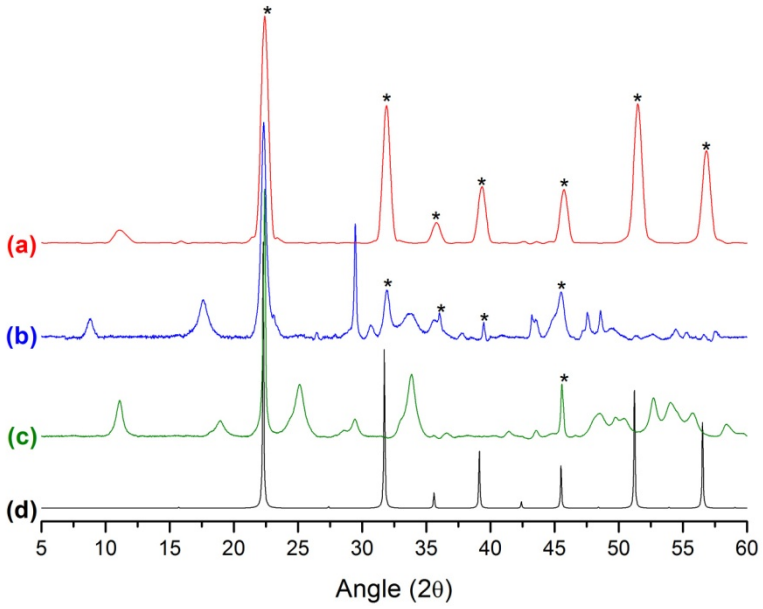

Figure 5.34: The products of the reactions of a solution of indium chloride with (a) MgO, (b) CaO, and (c) NiO. Indium hydroxide is shown for reference as (d):[94] peaks attributed to $In(OH)_3$ are marked with black asterisks.

While Mg/In-LDH materials have been previously prepared,[95] no LDH phases are known containing the other metal cations in combination with indium. If the first peaks in the three examples shown in Figure 5.34 are assumed to be the (003) peaks of LDH materials, then the apparent interlayer spacings for the magnesium, calcium and nickel compounds would be 8.0Å, 10.1Å, and 7.9Å. While this is an excellent match to typical interlayer spacing of a chloride-intercalated LDH in the magnesium

and nickel cases,[69] the calcium compound shows a much larger interlayer spacing, even though the intercalated anion is the same (and no alternative orientations of the anion are possible).

Further doubt may be cast upon the identification of these compounds as LDHs by their intercalation chemistry: although none of the as-synthesised products contain any carbon content, attempting to intercalate cyclamate, terephthalate or carbonate into these hosts yields only the starting materials, with no traces of carbon present in the products. Investigation of purer phases of these compounds may provide more useful evidence of their structures: this could perhaps be attained by a modified method in which the pH is controlled to minimise contamination by indium hydroxide.

As with the yttrium chloride reactions, there is an exception to these results: the reaction of zinc oxide with a solution of indium chloride gives rise to an apparent hydrotalcite-like phase. Its powder pattern is compared to that of indium hydroxide in Figure 5.35.

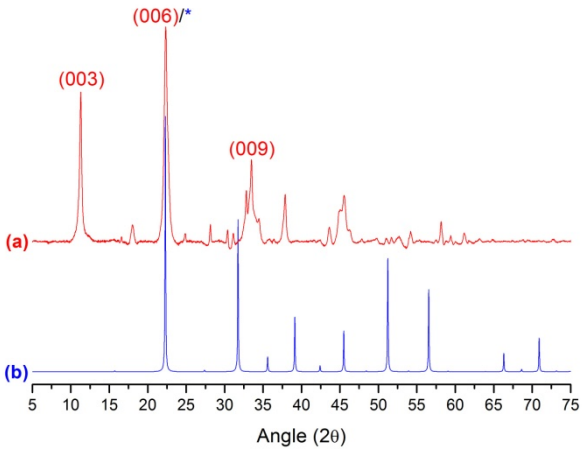

Figure 5.35: The powder X-ray patterns of (a) the solid product of the reaction of ZnO with a solution of $InCl_3$, and (b) $In(OH)_3$.[94] LDH-phase reflections are identified with red Miller indices, while blue asterisks identify reflections that may readily be assigned to $In(OH)_3$.

The pattern appears to suggest the formation of a hydrotalcite-like phase, with almost no contamination by $In(OH)_3$. An LDH host containing only zinc and indium has never been previously reported. Attempts at intercalation into this compound appear to be successful: structural information determined from the X-ray pattern suggests an increase in the interlayer spacing from 7.8Å in the chloride starting material to 20.8Å in the cyclamate-intercalated product. The powder pattern of the Zn/In-LDH product, and its cyclamate intercalate, are shown in Figure 5.36.

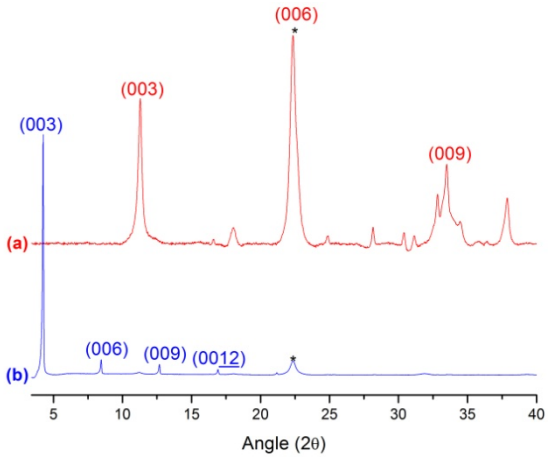

Figure 5.36: The powder X-ray patterns of (a) the solid product recovered from the reaction of ZnO with a solution of $InCl_3$, and (b) the product of the attempted intercalation of cyclamate into this material. . The d-spacings of the (003) reflections of the above patterns are 7.8 and 20.8Å respectively.

Elemental microanalysis of the carbon content of the solid implies only partial intercalation of cyclamate, replacing 10-20% of the chloride anions; a precise value of the loading could not be determined due to the significant amounts of indium hydroxide present in the product.

5.7.3 Characterisation of the Cd/Ga-LDH

The apparent product of the reaction of CdO with a solution of gallium nitrate is an LDH phase, as illustrated in Figure 5.24 (*vide supra*). The powder patterns of the Cd/Ga-NO_3 LDH products (formed by the salt-oxide method, and by coprecipitation)

differ slightly from that of hydrotalcite, especially due to the significant increase in the *a* lattice parameter (by approximately 10%) due to the much increased sizes of cadmium and gallium compared to magnesium and aluminium. As a result, the (110) and (113) reflections are found at ca. 55º in the Cd/Ga-NO_3 LDH, but closer to ca. 61º in hydrotalcite.

Elemental microanalysis gives the approximate formula of the solid produced by the salt-oxide method as $[Cd_2Ga(OH)_6]NO_3{\cdot}yH_2O$. No carbon content was found in the solid, and the absence of carbonate is confirmed by the FTIR spectrum, which only shows a strong absorption attributable to the nitrate anion. The spectrum of the Cd/Ga-NO_3 LDH product is compared to that of a Mg/Al-NO_3 LDH in Figure 5.37.

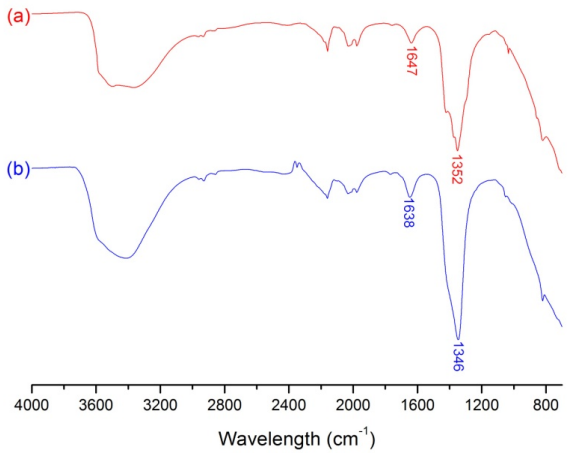

Figure 5.37: The FTIR absorption spectra of (a) $[Cd_2Ga(OH)_6]NO_3{\cdot}0.6H_2O$, and (b) $[Mg_2Al(OH)_6]NO_3{\cdot}1.2H_2O$.

The spectra are almost identical: the only diagnostic absorptions visible are the ν_{OH} absorptions from cointercalated water found at *ca.* 3400cm^{-1}, the δ_{OH} of the hydroxide layers at *ca.* 1640cm^{-1}, and the ν_{NO} absorption from nitrate at *ca.* 1350cm^{-1}. None of these are found to be significantly displaced upon exchanging the metals in the structure.

The apparent chemical formula of the Cd/Ga-Cyclamate LDH compound is $[Cd_2Ga(OH)_6](C_6H_{12}NO_3S)_{0.58}(NO_3)_{0.42}{\cdot}1.2H_2O$, as determined by elemental analysis

data. This product has also been examined by FTIR; the spectrum of this product, along with those of sodium cyclamate and the analogous Mg/Al-Cyclamate LDH, are depicted in Figure 5.38.

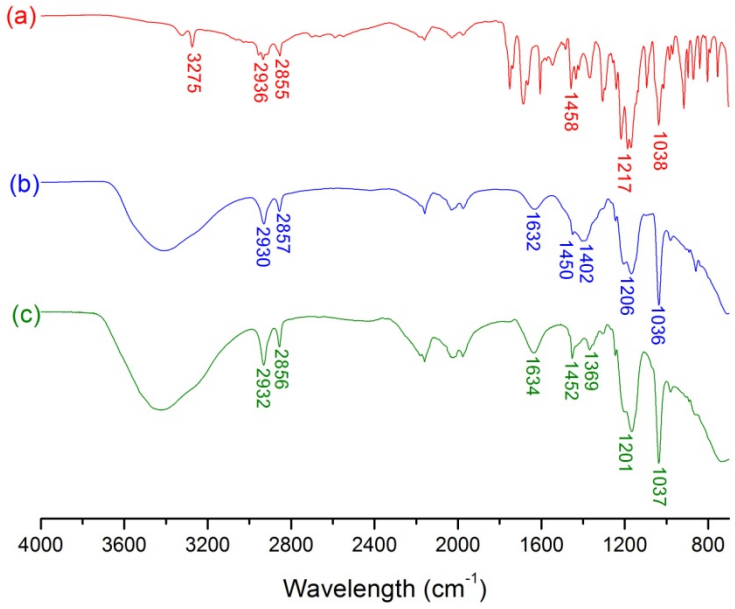

Figure 5.38: The FTIR absorption spectra of (a) sodium cyclamate, (b) the Cd/Ga-Cyclamate LDH, and (c) the Mg/Al-Cyclamate LDH.

The characteristic peaks of sodium cyclamate are the ν_{NH} absorption at 3275cm^{-1}, the various ν_{CH} bands from the aliphatic ring at 2850-2950cm^{-1}, the corresponding aliphatic δ_{CH} absorption at *ca.* 1450cm^{-1}, and the antisymmetric and symmetric $\delta_{S=O}$ absorptions at *ca.* 1210 and 1035cm^{-1} respectively.[96] These are all visible in the Cd/Ga- and Mg/Al-Cyclamate LDH products, with the exception of the ν_{NH} absorption which is swamped by the broad ν_{OH} band arising from the cointercalated water in the LDH structure. Many of the weaker absorptions observed in sodium cyclamate are not apparent, due to the partial intercalation of the anion into the solid; as a result, the ν_{NO} absorptions of the unexchanged nitrate ions are still visible at *ca.* 1360cm^{-1}. The δ_{OH} bands from the layer hydroxide groups can also be seen in both LDH products at 1632 and 1634cm^{-1}.

Thermogravimetric analysis of the new compound suggests that it demonstrates the typical thermal decomposition behaviour of an LDH, and provides the precise amount of cointercalated water. The TGA plot of the Cd/Ga-NO_3 LDH when heated up to 800ºC under argon is shown in Figure 5.39.

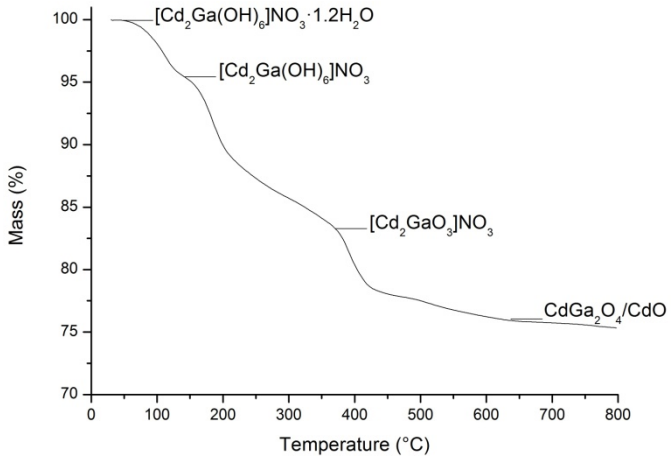

Figure 5.39: TGA plot of the Cd/Ga-NO_3 LDH.

The progression of mass loss in this compound may be broken down into three individual steps. The first corresponds to the loss of the cointercalated water molecules; given the previous knowledge of the compound from elemental microanalysis, the number of cointercalated water molecules per mole may be calculated to be 1.2 (calculated mass loss 4.5%, observed mass loss 4.5%). The second mass loss arises from the dehydroxylation of the LDH layers, resulting in a layered mixed oxide (calculated 11.2%, observed 12.2%); the final step, which follows almost immediately, is the result of the decomposition of the nitrate anions to gaseous nitrogen oxide species (calculated 10.1%, observed 8.0%).[97]

The golden yellow product remaining after this final step was identified by X-ray powder diffraction as a mixture of cadmium oxide and a mixed-metal cadmium gallium spinel oxide ($CdGa_2O_4$). The pattern of the product and the simulated patterns of its two oxide components are illustrated in Figure 5.40.

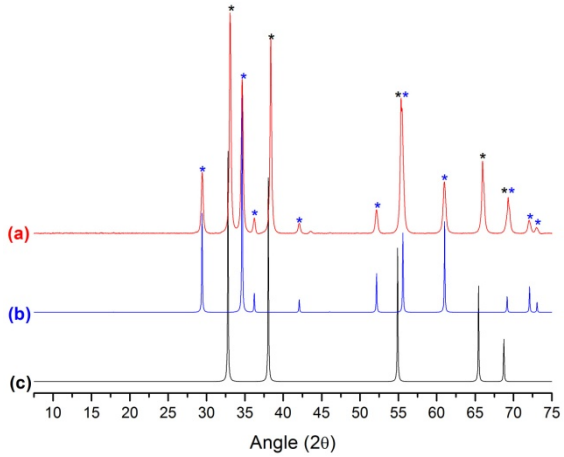

Figure 5.40: The powder X-ray patterns of (a) the product of heating the Cd/Ga-NO_3 LDH to 800ºC under argon, (b) the spinel $CdGa_2O_4$,[98] and (c) cadmium oxide.[99] Reflections that may be readily attributed to the spinel phase are marked with blue asterisks, while those that arise from cadmium oxide are marked with black asterisks.

The cadmium gallium spinel is a useful functional material; it shows unusual luminescent and gas sensing properties,[100, 101] and is a transparent conducting oxide with a wider band gap than the commonly-used indium tin oxide.[102, 103] This material is typically produced by a ceramic solid-state reaction of CdO and Ga_2O_3, but the synthesis of this compound *via* an LDH precursor affords much greater structural flexibility (as LDHs may be formed as nanoparticles, nanostructures, thin films and so on).[8, 10, 104, 105]

The Cd/Ga-NO_3 LDH was also studied by scanning electron microscopy (SEM) in order to determine information about the particle morphologies, and to determine its elemental content by energy-dispersive X-ray spectroscopy (EDX). SEM images of the Cd/Ga-LDH at two different magnifications are shown in Figure 5.41, in addition to the EDX spectrum of one of the particles.

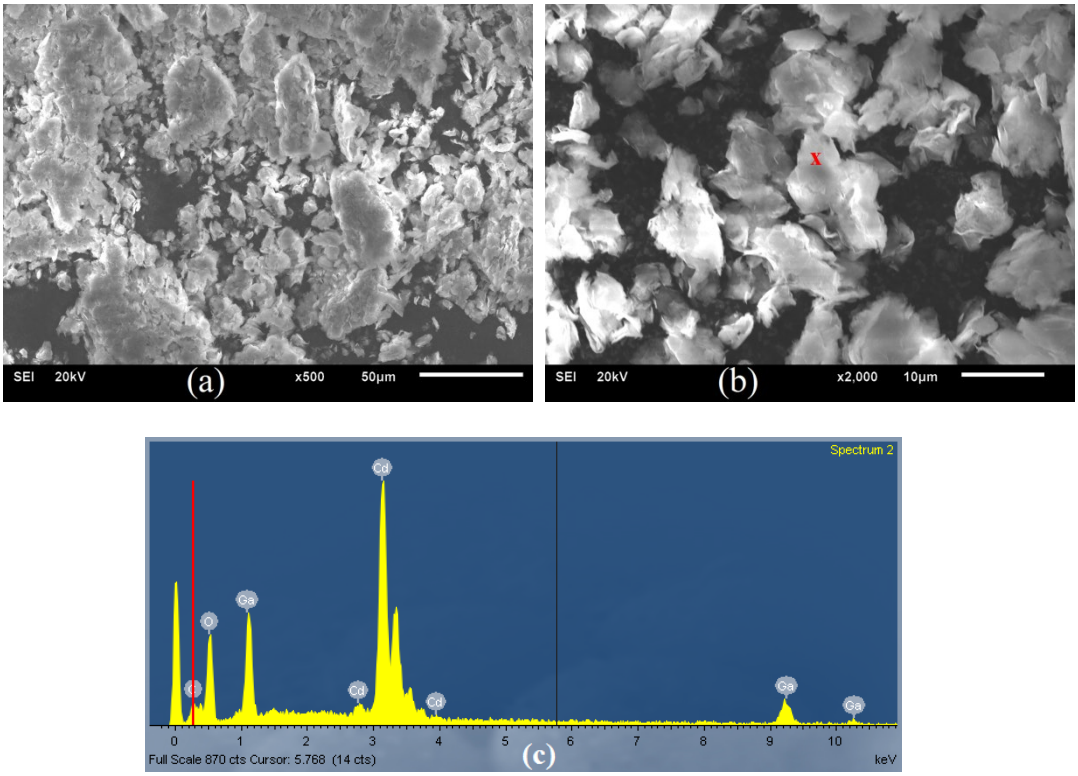

Figure 5.41: Particles of the Cd/Ga-NO_3 LDH at (a) approximately 500x magnification, (b) approximately 2000x magnification, and (c) the EDX spectrum of the particle marked with a red 'x' in image (b).

The particles are irregularly shaped, with some present as aggregate particles larger than 10µm in diameter (visible in Figure 5.41(a)), while others form as thin flakes of less than 1µm thickness (seen in Figure 5.41(b)). The EDX data, once adjusted for the relative emission intensities of the various atoms, implies a Cd:Ga ratio of 2.03:1, and this is found to be consistent for the particles examined, varying by no more than ±0.05. This suggests that the compound is an LDH material of uniform composition, with a Cd:Ga ratio that reflects the concentration of each metal in the original synthesis mixture.

5.7.4 Cyclamate Intercalation Products

Two of the cyclamate LDH products were found to show unusually large interlayer separations when recovered from the intercalation reactions, namely the Zn/Ga-Cyclamate LDH, and the "Ni/Y-Cyclamate" compound (which is, in fact, and

yttrium hydroxychloride intercalated with cyclamate, with no nickel present in the layers). It was thought that this behaviour might be connected to the swelling behaviour seen in the Li/Al-Cyclamate LDH compound in Chapter 2 (Section 2.2.1), and so each product was placed in an oven and heated at 80ºC to see if any structural changes could be observed.

The powder X-ray patterns of the Zn/Ga-Cyclamate compound as synthesised, and after oven heating at 80ºC for one hour, are illustrated in Figure 5.42.

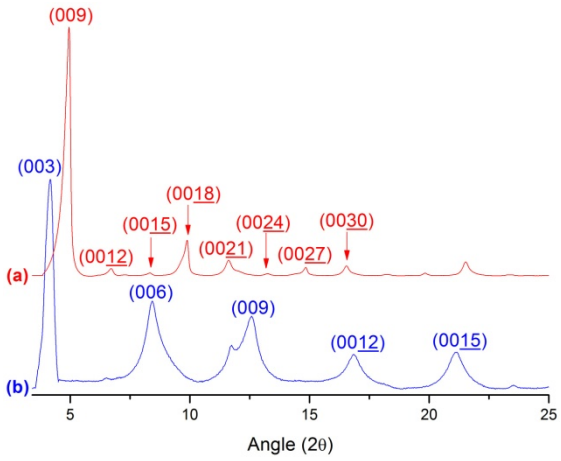

Figure 5.42: The powder X-ray patterns of (a) the solid product of the reaction of ZnO with a solution of $Ga(NO_3)_3$, after stirring in a solution of sodium cyclamate, and (b) the same compound after heating at 80ºC for one hour. The d-spacings of the (003) reflections of the above patterns are 53.2 and 21.3Å respectively.

The initially synthesised Zn/Ga-NO_3 LDH product shows a gallery height of 4.0Å, which expands to 16.5Å in the post-oven heated cyclamate product. The intermediate product, which is the first product formed after the ion exchange reaction, shows a sequence of apparent basal Bragg reflections separated by *ca.* 1.66º, implying a first (003) reflection at the same position, and thus a gallery height of 48.7Å. This equates to an interlayer separation of almost five times the maximum length of the cyclamate molecule (10.2Å). It seems highly unlikely that an ordered structure has given rise to such a separation between the layers, given the length of the intercalated molecule; justifying this as a hydration effect, as in the Li/Al-Cyclamate LDH product seems

highly unlikely, given the moderate hydration of the compound and the extreme separation. One possible explanation for this observation is that the stacking sequence of the LDH, which in an ordered Zn/Al-NO_3 LDH leads to a repeat unit in the *c* direction of three layers to the unit cell, has become so greatly disordered there is no consistent stacking order. As a result, the basal reflections in the powder pattern above should not be indexed as multiples of (003), but rather as multiples of (001). If this were the case, this would suggest a gallery height in the original product of 16.2Å, which approximately matches the gallery height of the post-oven-heating product (16.5Å); the slight difference may be due to a small alteration in the orientation of the cyclamate molecules. It quite possible, in this case, that the observed change in the X-ray pattern for the Zn/Ga-Cyclamate LDH product before and after heating can be attributed to a temperature-induced return to stacking order in the product.

The X-ray patterns of the cyclamate-intercalated yttrium hydroxy salt product, both before and after oven heating, are shown in Figure 5.43.

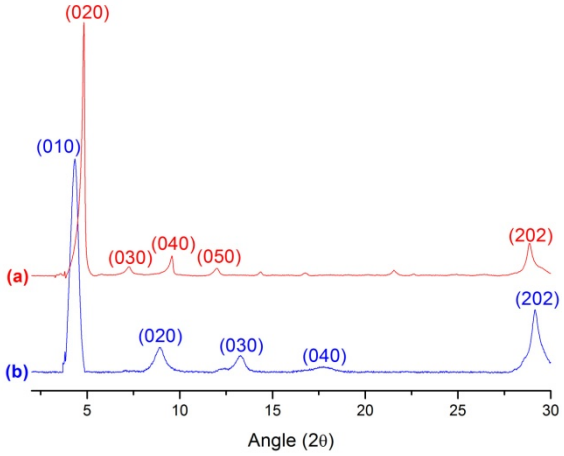

Figure 5.43: The powder X-ray patterns of (a) the solid product of the reaction of NiO with a solution of YCl_3, after stirring in a solution of sodium cyclamate, and (b) the same compound after heating at 80ºC for one hour. The d-spacings of the (010) reflections of the above patterns are 36.6 and 20.4Å respectively.

In this case, the expanded interlayer spacing, 30.7Å, corresponds to almost exactly three times the maximum possible length of the molecule. After heating in an oven at

80ºC for one hour, the interlayer spacing was found to have reduced to 14.5Å. It is likely that significant hydration of the interlayer anions is responsible for this effect, as observed in the analogous Li/Al-LDH compound.

A summary of the changes in interlayer spacings resulting from the intercalation of cyclamate is given in Table 5.7, as compared to those observed in the Ca/Al-, Li/Al-, and Mg/Al-LDHs reported in Chapter 2. The copper hydroxynitrate shows a noticeably smaller interlayer separation than the other hosts, due to the direct interaction between the nitrate anions and the layers; no significant contraction is shown in the cyclamate product after ion exchange, and FTIR spectroscopy also suggests that there is no direct bonding between the new guest and the layers.

Table 5.7: Summary of the changes in gallery heights observed upon cyclamate intercalation, and the ratio of the gallery height to the length of a cyclamate molecule. The thickness of an LDH layer is 4.8Å,[106] that of the HS is 3.7Å,[86] and that of the LHS is 5.9Å.[59]

Starting Material	**Gallery Height of Precursor (Å)**	**Gallery Height with Cyclamate (Å)**	**Gallery Height/Length of Cyclamate Molecule**
Ca/Al-NO_3	3.8	10.7	1.0
Mg/Al-NO_3	3.7	17.0	1.7
Ni/Al-NO_3	3.9	12.0	1.2
Cu/Al-NO_3	3.6	12.2	1.2
Zn/Ga-NO_3	4.0	48.7 / 16.5	4.8 / 1.6
Cd/Ga-NO_3	3.6	11.7	1.1
Cu-NO_3 HS	3.2	14.8	1.5
Li/Al-Cl	2.3	32.4 / 15.5	3.2 / 1.5
Co/Al-Cl	2.7	14.3	1.4
Zn/In-Cl	3.0	16.0	1.6
Y-Cl LHS	2.5	30.7 / 14.5	3.0 / 1.4

5.7.5 General Discussion and Summary of Results

The results of the various salt-oxide reactions performed in this chapter are visually summarised in Table 5.8.

Table 5.8: Visual summary of the phases formed from salt-oxide reaction. Reactions producing no LDH phase or an unidentifiable phase are marked in red. Those where the product is possibly an LDH, or an LDH heavily contaminated with another material, are marked in yellow. The reactions producing a pure (or near-pure) LDH phase are marked in green.

	VX_3	CrX_3	MnX_2	FeX_3	YX_3	AlX_3	GaX_3	InX_3
MgO								
CaO								
SrO								
BaO								
MnO								
CoO								
NiO								
CuO								
ZnO								
CdO								

A number of general trends can be seen; certain oxides are highly unlikely to form layered double hydroxide materials from reactions with salt solutions, such as SrO, BaO and MnO. Similarly, particular metal (III) salts are also inappropriate for LDH formation, such as vanadium (III) salts (most likely due to their redox activity), manganese (II) salts (which, when partially oxidised, preferably form Mn_3O_4), and yttrium (III) salts (which form monometallic layered yttrium hydroxy salts). In

contrast, MgO, ZnO and, to a certain extent, CaO and NiO readily form LDH phases in reactions with salt solutions, and the metal salts most likely to lead to LDH formation are those of the p-block metals, especially aluminium.

The exceptions to this generalisation are indium salts, the products from which display a tendency to be heavily contaminated with indium hydroxide; it is likely that pH control would minimise the presence of this by-product in LDH syntheses. An alternative approach to reduce the presence of the hydroxide would be to replace the metal (III) solution with a fresh solution after having allowed the reaction to proceed for a fixed amount of time. This method has been applied by a number of other practitioners of the salt-oxide method, with some success.[27, 29]

Attempting to understand the preferences of LDH formation from salt-oxide reactions by considering the relative sizes of metal cations in the layers appears to be somewhat ineffective here, as discussed in Section 5.2.2. The 'novel' LDH phases implied by a number of the reaction products are unremarkable in their cation size ratios. It may be possible to justify the apparent crystallinity and effectiveness of ion exchange found in the Zn/In-LDH as arising from the optimal size match of any pairwise combination with In^{3+}, and the same may be true for the case of the Ni/Fe LDH. However (considering the reactions of aluminium and gallium salts), the only oxides which will not form LDH phases at all from solutions of aluminium salts are strontium oxide and barium oxide; while it may be tempting to attribute this to the huge size disparity between the cations, given the violence of the reactions of these oxides with water and the alkaline earth hydroxides observed as the principal products, it appears that a thermodynamic perspective is considerably more useful for discussing these matters (especially given the aforementioned abundance and stability of the Ca/Al-LDHs, with almost the same cation size ratio). Other phases observed to

be formed by these reactions, including the Cd/Al- and novel Cd/Ga-LDH phases show similar size 'mismatches', but do not show any propensity towards decomposition during the synthesis reaction, or while attempting anion exchange.

The brief foray into salt-oxide hydroxy double salt synthesis has provided a tantalising glimpse into the expansion of this group of materials – a cursory excursion finds that these compounds are readily formed, particularly from nitrate salt solutions. The limited evidence collected for the salt-oxide LDH syntheses with regards to altering the anion of the metal (III) salt in general appears to show little difference in the chemical identity of the final product (except for the intercalated anion), rather the only consequence is typically a slight loss in crystallinity which cannot be correlated consistently with either chloride or nitrate as the anion. While some systematic investigation has been performed in this area,[84] a somewhat more exhaustive approach may indicate the existence of an expanded family of these materials.

5.8 Conclusions

By systematic application of the salt-oxide method of LDH synthesis, a number of unreported and novel layered hydroxide phases have been synthesised and characterised. Many previously known LDH systems have been synthesised by this simplified method for the first time, including systems containing Mg/Mn, Mg/Ga, Ca/Al, Ca/Ga, Co/Al, Ni/Al, Cu/Al and Zn/Ga as the cation pairings present in the hydroxide layers. Furthermore, the unreported LDH system containing cadmium and gallium, with an approximate chemical formula $[Cd_2Ga(OH)_6]NO_3 \cdot 0.6H_2O$, has been synthesised and characterised by powder X-ray diffraction. X-ray diffraction data also show tentative evidence for an expanded family of indium-based layered double hydroxide species, including compounds with calcium, cobalt, nickel and zinc as the dipositive cations.

Investigations into similar reactions with solutions of dipositive ions have shown that many layered hydroxy salts and related compounds may also be formed by the reaction of the divalent salt solutions with magnesium and calcium oxides, in addition to those previously known. A direct salt-oxide solution synthesis of the layered cadmium hydroxide nitrate $[Cd_5(OH)_8]NO_3 \cdot yH_2O$ has also been successfully demonstrated, yielding the product in greater quantities and at a faster rate than earlier vapour-diffusion based methods.

5.9 References

1. X. Duan and D. G. Evans, eds., *Layered Double Hydroxides*, Springer, 2006.
2. M. Meyn, K. Beneke and G. Lagaly, *Inorganic Chemistry*, 1990, **29**, 5201-5207.
3. S. K. Yun and T. J. Pinnavaia, *Chemistry of Materials*, 1995, **7**, 348-354.
4. K. Klemkaite, I. Prosycevas, R. Taraskevicius, A. Khinsky and A. Kareiva, *Central European Journal of Chemistry*, 2011, **9**, 275-282.
5. V. R. L. Constantino and T. J. Pinnavaia, *Inorganic Chemistry*, 1995, **34**, 883-892.
6. E. Gardner, K. M. Huntoon and T. J. Pinnavaia, *Advanced Materials*, 2001, **13**, 1263-1266.
7. W. Meng, F. Li, D. G. Evans and X. Duan, *Materials Research Bulletin*, 2004, **39**, 1185-1193.
8. Y. Zhao, F. Li, R. Zhang, D. G. Evans and X. Duan, *Chemistry of Materials*, 2002, **14**, 4286-4291.
9. Y. Wang, F. Zhang, S. Xu, X. Wang, D. G. Evans and X. Duan, *Industrial & Engineering Chemistry Research*, 2008, **47**, 5746-5750.
10. G. Hu and D. O'Hare, *Journal of the American Chemical Society*, 2005, **127**, 17808-17813.
11. C. J. Wang, Y. A. Wu, R. M. J. Jacobs, J. H. Warner, G. R. Williams and D. O'Hare, *Chemistry of Materials*, 2011, **23**, 171-180.
12. L. Legrand, M. Abdelmoula, A. Géhin, A. Chaussé and J. M. R. Génin, *Electrochimica Acta*, 2001, **46**, 1815-1822.
13. S. Paredes, G. Fetter, P. Bosch and S. Bulbulian, *Journal of Materials Science*, 2006, **41**, 3377-3382.
14. M. S. Yarger, E. M. P. Steinmiller and K.-S. Choi, *Inorganic Chemistry*, 2008, **47**, 5859-5865.
15. M. Nayak, T. R. N. Kutty, V. Jayaraman and G. Periaswamy, *Journal of Materials Chemistry*, 1997, **7**, 2131-2137.
16. S. Mitchell, T. Biswick, W. Jones, G. Williams and D. O'Hare, *Green Chemistry*, 2007, **9**, 373-378.
17. M. Ogawa and Y. Sugiyama, *Journal of the Ceramic Society of Japan*, 2009, **117**, 179-184.

18. W. N. Budhysutanto, D. van Agterveld, E. Schomaker, B. D. Rossenaar, G. M. van Rosmalen and H. J. M. Kramer, *Applied Clay Science*, 2011, **52**, 374-380.
19. G. Renaudin, M. Francois and O. Evrard, *Cement and Concrete Research*, 1999, **29**, 63-69.
20. K. R. Poeppelmeier and S. J. Hwu, *Inorganic Chemistry*, 1987, **26**, 3297-3302.
21. A. M. Fogg, A. J. Freij and G. M. Parkinson, *Chemistry of Materials*, 2002, **14**, 232-234.
22. A. M. Fogg, G. R. Williams, R. Chester and D. O'Hare, *Journal of Materials Chemistry*, 2004, **14**, 2369-2371.
23. S. Britto and P. V. Kamath, *Inorganic Chemistry*, 2010, **49**, 11370-11377.
24. R. Chitrakar, Y. Makita, A. Sonoda and T. Hirotsu, *Journal of Hazardous Materials*, 2011, **185**, 1435-1439.
25. G. R. Williams, S. J. Moorhouse, T. J. Prior, A. M. Fogg, N. H. Rees and D. O'Hare, *Dalton Transactions*, 2011, **40**, 6012-6022.
26. A. V. Radha and P. Vishnu Kamath, *Bulletin of Materials Science*, 2003, **26**, 661-666.
27. H.-P. Boehm, J. Steinle and C. Vieweger, *Angewandte Chemie International Edition in English*, 1977, **16**, 265-266.
28. S. R. Morrison and J. P. Bonnelle, *Journal of Catalysis*, 1972, **25**, 416-424.
29. K. El Malki, A. De Roy and J. P. Besse, *European Journal of Solid State Inorganic Chemistry*, 1989, **26**, 339.
30. E. Zhouri and A. El Hajbi, *Annales de Chimie Science des Matériaux*, 1999, **24**, 57-62.
31. L. Albiston, K. R. Franklin, E. Lee and J. B. A. F. Smeulders, *Journal of Materials Chemistry*, 1996, **6**, 871-877.
32. R. Chitrakar, S. Tezuka, A. Sonoda, K. Sakane, K. Ooi and T. Hirotsu, *Chemistry Letters*, 2007, **36**, 446-447.
33. R. Chitrakar, S. Tezuka, A. Sonoda, K. Sakane and T. Hirotsu, *Industrial & Engineering Chemistry Research*, 2008, **47**, 4905-4908.
34. G. V. Manohara, S. V. Prasanna and P. V. Kamath, *European Journal of Inorganic Chemistry*, 2011, **2011**, 2624-2630.
35. V. Dufek, V. Brožek and F. Petrů, *Monatshefte für Chemie / Chemical Monthly*, 1969, **100**, 1628-1630.
36. W. Dawihl and K. Schröter, *Zeitschrift für anorganische und allgemeine Chemie*, 1937, **233**, 178-183.
37. M. Frandsen, *Journal of the American Chemical Society*, 1952, **74**, 5046-5046.
38. H. Lux and E. Proeschel, *Zeitschrift für anorganische Chemie*, 1948, **257**, 73-78.
39. D. Wang, D. S. Su and R. Schlögl, *Zeitschrift für anorganische und allgemeine Chemie*, 2004, **630**, 1007-1014.
40. M. Rubel, M. Pszonicka, M. F. Ebel, A. Jablonski and W. Palczewska, *Journal of the Less Common Metals*, 1986, **125**, 7-24.
41. L. M. Dennis and R. E. Hulse, *Journal of the American Chemical Society*, 1930, **52**, 3553-3556.
42. J. M. Leger, N. Yacoubi and J. Loriers, *Journal of Solid State Chemistry*, 1981, **36**, 261-270.
43. M. W. Shafer, *Journal of Applied Physics*, 1965, **36**, 1145-1152.
44. F. Reshetnikov, *Atomic Energy*, 2007, **103**, 911-913.

45. D. Srankó, A. Pallagi, E. Kuzmann, S. E. Canton, M. Walczak, A. Sápi, Á. Kukovecz, Z. Kónya, P. Sipos and I. Pálinkó, *Applied Clay Science*, 2010, **48**, 214-217.
46. D. Srankó, M. Sipiczki, É. G. Bajnóczi, M. Darányi, Á. Kukovecz, Z. Kónya, S. E. Canton, K. Norén, P. Sipos and I. Pálinkó, *Journal of Molecular Structure*, 2011, **993**, 62-66.
47. F. Basile, E. Chassaing and G. Lorthioir, *Journal of the Less Common Metals*, 1984, **98**, 1-10.
48. C. H. Brubaker and R. C. Young, *Journal of the American Chemical Society*, 1951, **73**, 4179-4180.
49. A. K. Mallock and D. A. Edwards, in *Inorganic Syntheses*, John Wiley & Sons, Inc., Editon edn., 2007, pp. 178-181.
50. F. Poineau, E. V. Johnstone, P. F. Weck, E. Kim, P. M. Forster, B. L. Scott, A. P. Sattelberger and K. R. Czerwinski, *Journal of the American Chemical Society*, 2010, **132**, 15864-15865.
51. A. W. Struss and J. D. Corbett, *Inorganic Chemistry*, 1970, **9**, 1373-1376.
52. H. Schäfer, H. Scholz and R. Gerken, *Zeitschrift für anorganische und allgemeine Chemie*, 1964, **331**, 154-168.
53. J. L. Krumhansl and T. M. Nenoff, *Applied Geochemistry*, 2011, **26**, 57-64.
54. H. Curtius and K. Ufer, *Clays and Clay Minerals*, 2007, **55**, 354-360.
55. P. Gunawan and R. Xu, *The Journal of Physical Chemistry C*, 2009, **113**, 17206-17214.
56. X. Gao, M. Hu, L. Lei, D. O'Hare, C. Markland, Y. Sun and S. Faulkner, *Chemical Communications*, 2011, **47**, 2104-2106.
57. F. Gándara, J. Perles, N. Snejko, M. Iglesias, B. Gómez-Lor, E. Gutiérrez-Puebla and M. Á. Monge, *Angewandte Chemie International Edition*, 2006, **45**, 7998-8001.
58. L. J. McIntyre, L. K. Jackson and A. M. Fogg, *Chemistry of Materials*, 2007, **20**, 335-340.
59. L. Poudret, T. J. Prior, L. J. McIntyre and A. M. Fogg, *Chemistry of Materials*, 2008, **20**, 7447-7453.
60. H. V. Goulding, S. E. Hulse, W. Clegg, R. W. Harrington, H. Y. Playford, R. I. Walton and A. M. Fogg, *Journal of the American Chemical Society*, 2010, **132**, 13618-13620.
61. J. Liang, R. Ma, F. Geng, Y. Ebina and T. Sasaki, *Chemistry of Materials*, 2010, **22**, 6001-6007.
62. S. Tezuka, R. Chitrakar, K. Sakane, A. Sonoda, K. Ooi and T. Tomida, *Bulletin of the Chemical Society of Japan*, 2004, **77**, 2101-2107.
63. R. Chitrakar, S. Tezuka, A. Sonoda, K. Sakane, K. Ooi and T. Hirotsu, *Journal of Colloid and Interface Science*, 2005, **290**, 45-51.
64. J. M. Fernández, C. Barriga, M. A. Ulibarri, F. M. Labajos and V. Rives, *Chemistry of Materials*, 1997, **9**, 312-318.
65. J. M. García-García, M. E. Pérez-Bernal, R. J. Ruano-Casero and V. Rives, *Solid State Sciences*, 2007, **9**, 1115-1125.
66. R. Shannon, *Acta Crystallographica Section A*, 1976, **32**, 751-767.
67. W. Feitknecht, *Helvetica Chimica Acta*, 1942, **25**, 555-569.
68. A. I. Khan, A. Ragavan, B. Fong, C. Markland, M. O'Brien, T. G. Dunbar, G. R. Williams and D. O'Hare, *Industrial & Engineering Chemistry Research*, 2009, **48**, 10196-10205.

69. R. S. W. Braithwaite, P. J. Dunn, R. G. Pritchard and W. H. Paar, *Mineralogical Magazine*, 1994, **58**, 79-85.
70. G. Aminoff, *Zeitschrift für Kristallographie, Kristallgeometrie, Kristallphysik, Kristallchemie*, 1926, **64**, 475-490.
71. M. R. Weir, J. Moore and R. A. Kydd, *Chemistry of Materials*, 1997, **9**, 1686-1690.
72. M. Jobbágy and N. Iyi, *The Journal of Physical Chemistry C*, 2010, **114**, 18153-18158.
73. I. Rousselot, C. Taviot-Gueho, F. Leroux, P. Leone, P. Palvadeau and J. P. Besse, *Journal of Solid State Chemistry*, 2002, **167**, 137-144.
74. W. L. Bragg, *Proceedings of the Royal Society of London, Series A: Mathematical and Physical Sciences*, 1924, **105**, 16-39.
75. G. Renaudin and M. Francois, *Acta Crystallographica Section C*, 1999, **C55**, 835.
76. W.-S. Lee, T. Isobe and M. Senna, *Solid State Ionics*, 1999, **123**, 293-300.
77. F. Malherbe, C. Forano and J. P. Besse, *Journal of Materials Science Letters*, 1999, **18**, 1217-1219.
78. A. V. Radha, P. V. Kamath and C. Shivakumara, *Acta Crystallographica B*, 2007, **63**, 243-250.
79. F. B. D. Saiah, B.-L. Su and N. Bettahar, *Journal of Hazardous Materials*, 2009, **165**, 206-217.
80. A. Ennadi, A. Legrouri, A. de Roy and J. P. Besse, *Journal of Solid State Chemistry*, 2000, **152**, 568-572.
81. F. M. Vichi and O. L. Alves, *Journal of Materials Chemistry*, 1997, **7**, 1631-1634.
82. W. Feitknecht, *Helvetica Chimica Acta*, 1933, **16**, 427-454.
83. H. Hayashi and M. J. Hudson, *Journal of Materials Chemistry*, 1995, **5**, 781-783.
84. M. Meyn, K. Beneke and G. Lagaly, *Inorganic Chemistry*, 1993, **32**, 1209-1215.
85. S. P. Newman and W. Jones, *Journal of Solid State Chemistry*, 1999, **148**, 26-40.
86. B. Bovio and S. Locchi, *Journal of Crystallographic and Spectroscopic Research*, 1982, **12**, 507-517.
87. J. M. Aguirre, A. Gutiérrez and O. Giraldo, *Journal of the Brazilian Chemical Society*, 2011, **22**, 546-551.
88. M. Rajamathi and P. V. Kamath, *International Journal of Inorganic Materials*, 2001, **3**, 901-906.
89. W. Stählin and H. R. Oswald, *Acta Crystallographica*, 1970, **B26**, 860-863.
90. P. Benard, M. Louer and D. Louer, *Powder Diffraction*, 1991, **6**, 10-15.
91. P. Benard, M. Louër, J. P. Auffredic and D. Louër, *Journal of Solid State Chemistry*, 1991, **91**, 296-305.
92. H.-S. Shim, V. R. Shinde, J. W. Kim, T. P. Gujar, O.-S. Joo, H. J. Kim and W. B. Kim, *Chemistry of Materials*, 2009, **21**, 1875-1883.
93. G. Tunell, E. Posnjak and C. J. Ksanda, *Zeitschrift für Kristallographie, Kristallgeometrie, Kristallphysik, Kristallchemie*, 1935, **90**, 120-142.
94. D. F. Mullica, G. W. Beall, W. O. Milligan, J. D. Korp and I. Bernal, *Journal of Inorganic and Nuclear Chemistry*, 1979, **41**, 277-282.
95. M. A. Aramendía, V. Borau, C. Jiménez, J. M. Marinas, J. M. Luque, J. R. Ruiz and F. J. Urbano, *Materials Letters*, 2000, **43**, 118-121.

96. M. Cavicchioli, C. Q. F. Leite, D. N. Sato and A. C. Massabni, *Archiv der Pharmazie*, 2007, **340**, 538-542.
97. C. Nyambo, D. Chen, S. Su and C. A. Wilkie, *Polymer Degradation and Stability*, 2009, **94**, 1298-1306.
98. W. Ruedorff and B. Reuter, *Zeitschrift für anorganische und allgemeine Chemie*, 1947, **253**, 177-177.
99. P. Scherrer, *Zeitschrift für Kristallographie, Kristallgeometrie, Kristallphysik, Kristallchemie*, 1922, **57**, 186-189.
100. T.-M. Chen and Y. W. Chen, *Journal of Solid State Chemistry*, 2000, **150**, 204-208.
101. C. Xiangfeng and Z. Chenmou, *Materials Chemistry and Physics*, 2004, **88**, 110-112.
102. O. Takahisa, U. Naoyuki, H. Naoko, U. Kazushige, M. Hiroshi, H. Takuya and K. Hiroshi, *Applied Physics Letters*, 1993, **62**, 499-500.
103. H. Kawazoe and K. Ueda, *Journal of the American Ceramic Society*, 1999, **82**, 3330-3336.
104. P. Ding, B. Qu, L. Shi, C. Ge and H. Yang, *Materials Letters*, 2008, **62**, 3815-3817.
105. H. Zhu, S. Huang, Z. Yang and T. Liu, *Journal of Materials Chemistry*, 2011, **21**, 2950-2956.
106. R. Allmann, *Chimia*, 1970, **24**, 99-108.

Chapter 6

Experimental Details

6.1 Analytical Techniques

6.1.1 Powder X-ray Diffraction

Powder X-ray data were collected using a PANAnalytical X'Pert Pro diffractometer in reflection mode at 40kV and 40mA using Cu K_α radiation (α_1 = 1.54057Å, α_2 = 1.54433Å, weighted average = 1.54178Å). Patterns were recorded between 2º and 75º, with a scan speed of 0.12º min^{-1}. The samples were mounted on stainless steel sample holders whose reflections did not interfere with characterisation.

6.1.2 FTIR Spectroscopy

Infrared spectra were recorded in attenuated reflectance mode from 700cm^{-1} to 4000cm^{-1} on a Biorad FTS 6000 FTIR Spectrometer equipped with a DuraSamplIR II diamond surface accessory. Typically, 50 scans were recorded at 4cm^{-1} resolution. The strong absorptions seen in each spectrum in the range 2500-1667cm^{-1} arise from the DuraSamplIR diamond surface.

6.1.3 Thermogravimetric Analysis

Thermogravimetric analysis was carried out using a Netzsch STA 409 PC instrument. Approximately 50mg of sample was heated in a corundum crucible between 20 and 800ºC at a rate of 10ºC min^{-1} under a flowing stream of argon.

6.1.4 Elemental Microanalysis

Elemental microanalysis was performed by the Analytical Services Department of the Inorganic Chemistry Laboratory at the University of Oxford, or by Stephen Boyer at the School of Human Sciences, London Metropolitan University. C, H and N analyses were performed by a quantitative oxidative combustion technique. Metals analysis was performed by Dr. Gareth Williams at London Metropolitan University, using inductively-coupled plasma-optical emission spectroscopy on a Perkin-Elmer Optima 4300 DV instrument.

6.1.5 Ultraviolet Spectroscopy

Ultraviolet (UV) spectroscopy was performed on a PG Instruments T60U UV/Vis/NIR spectrometer using wavelength scan mode and quartz cuvettes from 170 to 350nm.

6.1.6 ^{13}C Solid-State NMR

^{13}C cross-polarisation magic angle spinning (CP/MAS) NMR spectra were recorded by Dr. Nicholas Rees on a Varian/Chemagnetics Infinity Spectrometer at 50.32MHz using 7.5mm OD rotors containing *ca.* 300mg of sample. A cross-polarisation sequence with a variable X-amplitude spin-lock pulse[1] and phase-modulated proton decoupling were applied. Typically, 4000 transients were acquired using a contact time of 3.5ms, an acquisition time of 80ms (1600 data points zero-filled to 16K), and a recycle delay of 10 seconds. All spectra were referenced to adamantane as a secondary reference (the upfield methine resonance was taken to be at δ = 29.5ppm on a scale where δ(TMS) = 0).[2]

6.1.7 Scanning Electron Microscopy and EDX

The images produced by Scanning Electron Microscopy (SEM) were collected by Dr. Gareth Williams on a JEOL JSM-840F Electron Microscope with a field emission gun at the Begbroke Science Park, or by Dr. Qiang Wang and Chengle Wang on a JEOL JSM-6610 Electron Microscope at the Harwell Science and Innovation Campus. The solid LDH samples were mounted onto discs of adhesive, electrically conductive carbon film and set into aluminium tubes before being examined.

6.1.8 *In situ* Energy-Dispersive X-ray Diffraction

In situ energy-dispersive X-ray diffraction (EDXRD) data was collected at Station 16.4 of the UK Synchrotron Radiation Source (SRS), located at Daresbury in Cheshire. The X-ray flux provided by this source is continuous over the range of 5-120keV. Further details of the design of Station 16.4 and the EDXRD technique have been published elsewhere.[3-5]

EDXRD differs considerably from conventional powder diffraction. In the latter case, a monochromatic X-ray beam sweeps through a range of angles with respect to a detector – this process may be dubbed 'Angular-Dispersive X-ray Diffraction' (ADXRD). Conversely, EDXRD uses a polychromatic beam containing the full range of wavelengths present in the synchrotron radiation beam, allowing a wide range of d-spacings to be measured. As a result, the Bragg reflections become separated by their differing energies, rather than by their special coordinate, with much shorter data collection times than those required for ADXRD.

The relationship between the detector angle, the d-spacing of the peak of interest, and the incident wavelength is found by combining Bragg's Law ($n\lambda = 2d\sin\theta$) with the Planck relationship ($E = hc/\lambda$) to give:

$$2d\sin\theta = \frac{hc}{E} \qquad \textbf{Equation 6.1}$$

In Equation 6.1, E is the energy of a photon (in keV) that has been diffracted by a crystallographic plane with a d-spacing of *d* Å.

A full spectrum on each of the three detectors used was collected every 30 seconds for one hour. The data were processed using software on the 'xrdsv1' server at the Daresbury Laboratory to convert them to an analysable format. The diffraction peaks were fitted by an automated Gaussian fitting routine and integrated. The peak integrals at different times were used to provide values representing the extent of reaction, α, using the following relationship.

$$\alpha = \frac{I_{hkl}(t)}{I_{hkl(Max)}} \qquad \textbf{Equation 6.2}$$

In Equation 6.2, $I_{hkl}(t)$ is the intensity of a given peak with Miller indices (*hkl*) at time *t*, and $I_{hkl}(Max)$ is the maximum intensity of the peak.[6]

6.2 Experimental Procedures for Chapter 2

6.2.1 Synthesis of Starting Materials

The three layered double hydroxide starting materials used in this Chapter, and those following, were $[Ca_2Al(OH)_6]NO_3{\cdot}yH_2O$ ('Ca/Al-NO_3 LDH), $[LiAl_2(OH)_6]Cl{\cdot}yH_2O$ ('Li/Al-Cl LDH'), and $[Mg_2Al(OH)_6]NO_3{\cdot}yH_2O$ ('Mg/Al-NO_3 LDH').

The Mg/Al-NO_3 LDH was synthesised by a coprecipitation method at high supersaturation.[7] Two solutions were prepared: the first, 'Solution A' contained 20.5g of $Mg(NO_3)_2{\cdot}6H_2O$ and 15g of $Al(NO_3)_3{\cdot}9H_2O$ in 100mL of deionised water; the other, 'Solution B', contained 6.7g of NaOH and 9.5g of $NaNO_3$ in 100mL of deionised water. To precipitate the LDH, Solution A was added slowly to Solution B,

which was held at 75ºC and vigorously stirred, over a period of 1-2 hours. The solid was allowed to age at this temperature for 24 hours, recovered from the solution by vacuum filtration, and washed repeatedly with deionised water in order to remove surface-adsorbed impurities. Finally, the solid product was washed with a small amount of acetone to facilitate drying, and then dried under vacuum for *ca.* 2 hours. The product formed is a white powder.

The procedure for the synthesis of the Ca/Al-NO_3 LDH was an identical coprecipitation method, differing only in the contents of Solutions A and B. In this case, Solution A contained 19.6g of $Ca(NO_3)_2 \cdot 4H_2O$ and 10.4g of $Al(NO_3)_3 \cdot 9H_2O$ in 100mL of water, while Solution B was prepared by dissolving 6.6g NaOH and 9.4g of $NaNO_3$ in the same volume of water. The white, powdery product was collected, washed and dried as described for the Mg/Al-NO_3 LDH.

The Li/Al-Cl LDH was synthesised by the intercalation of lithium into aluminium hydroxide. In a typical preparation reaction, 1g of gibbsite (γ-$Al(OH)_3$) was added to a sixfold molar excess of LiCl in deionised water at 90ºC. The suspension was vigorously stirred for 16 hours in a sealed ampoule, then recovered, washed and dried as above. The product visually resembles $Al(OH)_3$, and is a white powder.

Acesulfame K and sodium cyclamate were purchased and used without alteration; the sodium salts of saccharin, ferulic acid and theobromine were prepared in each case by dissolving the compound in a solution containing an equimolar amount of NaOH. The liquid was evaporated to produce a sodium salt subsequently used for ion exchange.

6.2.2 Intercalation Reactions

The intercalation products were prepared using an ion-exchange method. Typically, 1g of the LDH host material was added to an aqueous solution (100mL) containing a

threefold excess of the guest anion under flowing nitrogen (to prevent the formation of the carbonate intercalate). The solution was stirred vigorously at 80ºC for 16 hours, then filtered, washed and dried as in Section 6.2.1. Each intercalation product is a white powder, except for those of ferulate, which display the characteristic pale yellow colour of the acid precursor.

6.2.3 Release Reactions

Release reactions were performed either in deionised water, or an artificial saliva solution. This solution was prepared by the method described by Qiu:[8] to 500mL of deionised water at room temperature was added 22mg of NaF, 1200mg of NaCl, 700mg of KCl, 55mg of $MgCl_2$, 520mg of KH_2PO_4, and 520mg of K_2HPO_4. 150mg of $CaCl_2$ was dissolved in a further 200mL of deionised water, and this solution was slowly added to the initial 500mL solution. This mixture was then made up to 1000mL by the addition of further deionised water.

The release of the anions from their hosts was determined by UV/Vis spectroscopy. In a typical release reaction, 0.5g of the LDH-Guest composite was added to 50mL of either deionised water or the artificial saliva solution, and stirred at a moderate rate (*ca.* 200rpm) at 37ºC. After an appropriate amount of time had elapsed, the release mixture was filtered, and the concentration of released guest in the filtrate quantified by the correlation method outlined in Chapter 2, Section 2.7.2.

In order to determine the maximum degree of release possible from the solids by ion exchange, a similar release reaction was prepared for each LDH-Guest material. 0.5g of the solid was added to 50mL of a 0.1M solution of sodium carbonate solution, and stirred for 16 hours at 80ºC. The reaction was then filtered, and the concentration of guest present in the filtrate determined by UV/Vis spectroscopy, which was assumed to represent complete release of the guest, given the forcing conditions (and

the IR spectra of the post-reaction solids, which typically showed no absorptions attributable to the guest).

6.3 Experimental Procedures for Chapter 3

6.3.1 Synthesis of Starting Materials

The same three LDH starting materials were used as in Chapter 2, and were synthesised by the procedures outlined in Section 6.2.1. In addition, the hydroxynitrate salt $[Zn_5(OH)_8](NO_3)_2 \cdot yH_2O$ ('Zn_5-NO_3 HS') was also used as a host.

The Zn_5-NO_3 HS was prepared by a slightly modified version of the salt-oxide method reported by Stählin and Oswald.[9] A solution of 5.61g of $Zn(NO_3)_2 \cdot 6H_2O$ in 12mL of deionised water was prepared, and to this vigorously stirred solution was added 1g of ZnO. The reaction was allowed to age at room temperature for four days, and then collected and dried as for the host products in Section 6.2.1.

6.3.2 Intercalation Reactions

Due to the differing stabilities and solubilities of the various intercalated anions, slightly differing synthesis procedures were used for the intercalation reactions of the guests.

In order to intercalate 2,4DB and Dichlorprop, the guest solids were dissolved into a 1:1 by volume mixture of ethanol and deionised water, to which an equimolar amount of triethylamine (NEt_3) was added to form the guest anions. An amount of the LDH or HS host was added such that the guest anion was present in a threefold excess, and the reaction was allowed to stir at room temperature for 24 hours before being recovered and washed as previously described. The same method was used for the intercalation of 2,4,5T into the Li/Al and Mg/Al-LDHs. To intercalate 2,4,5T into

the Zn_5-HS, the sodium salt of 2,4,5T was first synthesised by the method described for the guest anions in Section 6.2.1. The HS host was then added to a threefold excess solution of the sodium salt of 2,4,5T in deionised water, and maintained at 60ºC for 7 days.

The intercalation of diclofenac, ibuprofen and naproxen were accomplished for the LDH hosts by adding the solid to a threefold excess solution of the sodium salt of the guest in deionised water, followed by stirring the reaction at 60ºC for 48 hours. The same reactions were used for the Zn_5-HS, although with differing temperatures and timescales: for diclofenac intercalation the reaction was stirred at 60ºC for 72 hours, while ibuprofen intercalation was achieved by stirring the reaction at 40ºC for 24 hours.

6.3.3 Release Reactions of Agrochemicals

A soil column was set up in order to test the release rates of the agrochemicals from the hosts. Soil was collected from the University Parks in Oxford, and heated in an oven overnight at 150ºC. This dried soil was used to half-fill a glass column, 2.5cm in internal diameter and 60cm in height. Deionised water was added to saturate the soil, and the excess was allowed to drain out for 16 hours.

In order to begin data collection, 0.2g of the LDH-Guest composite was added to the top of the soil in the column, in addition to 5mL of tap water (to simulate rainwater). For the first two hours, an aliquot was collected from the bottom of the column at ten-minute intervals, and a further 5mL of tap water was added to the top of the column when each aliquot was removed. After 2 hours, an aliquot was removed every hour, and 5mL of tap water added upon removal of an aliquot. After completion of the release, the aliquots were retained for analysis by UV/Vis spectroscopy, but it was not possible to salvage the solids for further analysis.

The determination of maximum release from the solids was performed as in Section 6.2.3 above, but using only 0.2g of the host material.

6.3.4 Release Reactions of Anti-Inflammatory Drugs

The LDH-Drug composites were immobilised in sodium alginate beads before the release reactions were performed. These were prepared by a modified version of the method used by Zhang *et al.*.[10] 0.2g of the LDH-Guest composite was dispersed in 7mL of deionised water, and stirred vigorously for 30 minutes. An aqueous solution of sodium alginate was prepared by stirring 0.4g of the sodium salt in 25mL of water for 30 minutes, and this was added dropwise to the LDH-Guest suspension, which was stirred at 40ºC for one hour. A further solution of 0.5g of $CaCl_2$ in 50mL of deionised water was prepared, and the LDH/Alginate mixed suspension was added to this using a hypodermic syringe pump at an addition rate of 45.5mL $hour^{-1}$ through a 1.2mm inner diameter needle. The beads formed instantly upon contact with the calcium chloride solution, and were stirred in the solution for one hour; they were then filtered over vacuum, washed with deionised water to remove the excess Ca^{2+} ions present on the beads' surfaces, then left to dry at room temperature for 48 hours. The beads showed a significant contraction in size upon drying; images of the freshly-prepared beads, and the same beads after drying, are shown in Figure 6.1.

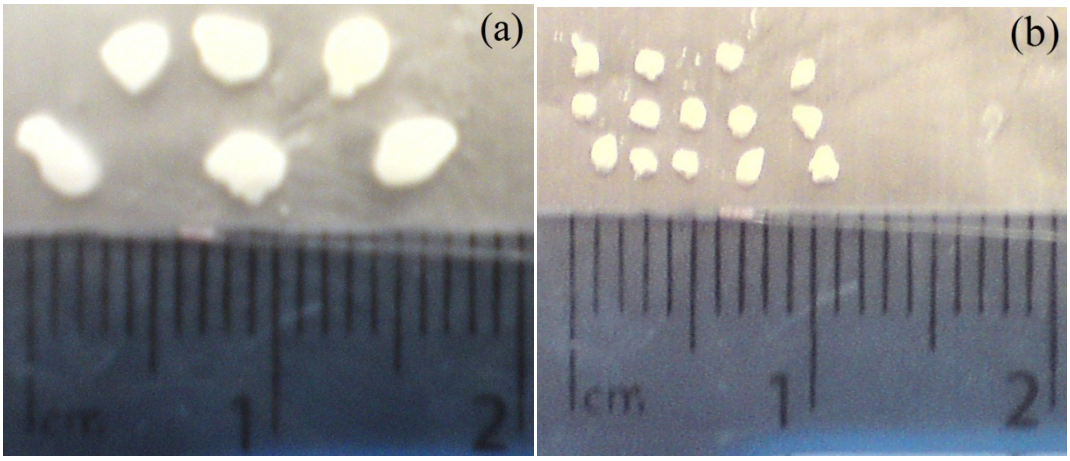

Figure 6.1: LDH/Alginate beads, as they appear (a) immediately after filtration from the calcium chloride solution, and (b) after drying at room temperature for 48 hours. The ruler at the bottom of the image shows a length of two centimetres.

The release experiments were performed in two buffer solutions. The first, a pH 2.2 buffer, was synthesised by adding 1.71mL of concentrated hydrochloric acid to a solution containing 2.25g of glycine in 150mL of deionised water. This solution was then made up to 600mL by further addition of water.[11] The other buffer, at pH 7.3, was prepared by adding a solution of 2.59g of KH_2PO_4 in 95mL of water to a second solution containing 14.11g of K_2HPO4 in 405mL of water. This was made up to 1000mL by the addition of further deionised water.[11]

To perform the release reactions themselves, 0.2g of the chosen LDH-Guest alginate beads were added to 50mL of the pH 2.2 buffer solution, and stirred slowly (at *ca.* 50rpm) for two hours. During the first hour in each buffer solution, aliquots were extracted every ten minutes, and then another aliquot was collected after the second hour. At this point, the beads were filtered, washed with deionised water, and then added to 50mL of the pH 7.3 buffer. During the next two hours, aliquots were collected every ten minutes, and then every twenty minutes during the following hour. When each aliquot was removed, 3.5mL of the solution was extracted into a glass vial, and replaced with 3.5mL of fresh buffer solution.

Total release for the alginate beads was determined by the method described in Section 6.2.3, but once again using only 0.2g of the host material. The mildly basic pH of the sodium carbonate solution was found to be sufficient to dissolve the alginate beads, while also promoting anion exchange.

6.4 Experimental Procedures for Chapter 4

6.4.1 Synthesis of Starting Materials

The Li/Al-Cl LDH and Mg/Al-NO_3 LDH hosts used in this Chapter were synthesised by the same methods as those in Chapter 2, as described in Section 6.2.1. In addition, intercalation into $[Mg_2Fe(OH)_6]Cl{\cdot}yH_2O$ ('Mg/Fe-Cl LDH') was reported.

To synthesise the Mg/Fe-Cl LDH, the same precipitation at high supersaturation method was used as for the other hosts, but with different synthesis solutions. Solution A, in this instance, contained 7.5g of $FeCl_3{\cdot}6H_2O$ and 16.7g of $MgCl_2{\cdot}6H_2O$. Solution B contained 6.69g of NaOH and 6.47g of NaCl. This product forms as a red-brown solid.

6.4.2 Intercalation Reactions

The intercalation of thiosulfate into the three hosts was accomplished by addition of the solids to a fivefold excess solution of sodium thiosulfate in deionised water at 80ºC. The mixture was allowed to age for 24 hours, and then recovered by the same method as for the products reported above. The products are white powders, except for the Mg/Fe-Thiosulfate LDH which is red-brown in colour, similar to the chloride starting material.

The intercalation of tartrazine into the Li/Al- and Mg/Al-LDHs was accomplished by a similar method, using a fivefold excess solution of tartrazine, and aging the reaction for 72 hours at 80ºC. Both products are bright orange, the same colour as the solid tartrazine salt.

For the intercalation of tartrazine into the Mg/Fe-LDH, the reconstruction method was used. The Mg/Fe-CO_3 LDH was synthesised by the addition of 1g of the Mg/Fe-Cl LDH to 50mL of a 1M solution of Na_2CO_3, which was stirred at 80ºC for 24 hours. The red-brown product of this reaction was dried over vacuum, and then placed into a ceramic crucible and placed into an oven at 500ºC for five hours in order to calcine the material. The brown Mg/Fe-LDO recovered was then added to a fivefold excess of tartrazine in deionised water under flowing nitrogen, and aged at 80ºC for 72 hours. The Mg/Al-Tartrazine LDH product is a dark orange powder.

6.4.3 Release Reactions

In a typical thiosulfate release experiment, 0.1g of a chosen LDH-Thiosulfate hybrid was added to 100mL of either deionised water, or the same volume of water containing 0.5g of dissolved sodium dodecylsulfate (NaDDS), and stirred at either 20, 50 or 80ºC for an appropriate amount of time. Aliquots were extracted every ten minutes during the first hour, and every twenty minutes thereafter until up to three hours, with a single further aliquot collected after four hours.

For tartrazine, 0.1g of the LDH-Tartrazine material was added to 100mL of the release solution (either deionised water, tap water, or a 0.1M or 0.01M solution of sodium carbonate), and stirred at room temperature. Aliquots were collected every two minutes up to twelve minutes, and then after 15, 20, 30, 45 and 60 minutes.

The concentration of guest anion corresponding to 100% release was determined by the method used in Section 6.2.3, using 0.1g of either the LDH-Thiosulfate or LDH-Tartrazine hybrid in 100mL of 0.1M sodium carbonate solution.

6.5 Experimental Methods for Chapter 5

6.5.1 Reactions of Metal (II) Oxides with Water

To test the possible hydration products of the metal (II) oxides, 1g of each oxide was added to 50mL of water, and stirred for 16 hours at 80ºC. The solids were then recovered as described in Section 6.2.1.

6.5.2 Reactions of Metal (III) Salt Solutions with Base

To test the possible reactions of the metal (III) salt solutions with base, 1.5g of the metal salt was added to 50mL of deionised water. To this was added, slowly, 25mL of an equimolar solution of sodium hydroxide. The mixture was then stirred at 80ºC for 16 hours, in order to increase the crystallinity of the product, and then recovered as described above.

6.5.3 Salt-Oxide Syntheses

The reactions of the metal (II) oxides with metal (III) salt solutions were performed by a modified version of the procedure used by Chitrakar *et al.*:[12] 1g of the metal (II) oxide was added to 50mL of a solution of the metal (III) salt, prepared such that the M^{II}:M^{III} ratio was 2:1. The reaction mixture was then allowed to age either at room temperature for five days or at 80ºC for 16 hours. In certain cases where hydrothermal synthesis was attempted, the same solid/solution mixture was prepared, but scaled down by a factor of four to allow the reaction mixture to be contained within a Teflon

autoclave liner. This liner was then sealed in an autoclave, placed in an oven and heated at 160ºC for 16 hours.

For the attempted syntheses of hydroxy double salts by the reaction of metal (II) oxides with metal (II) salt solutions an identical method was used (substituting M^{III} salts for M^{II} salts), but with the molar ratio of the two metals altered to 1:1 (the most common ratio found in HDS compounds).

In each case, the solid product was recovered, filtered and dried as in Section 6.2.1.

6.5.4 Intercalation of Cyclamate

For the attempted intercalation of cyclamate into the newly-synthesised compounds, 0.25g of the host was added to 50mL of deionised water containing a fivefold excess of sodium cyclamate. This mixture was then stirred at 80ºC for 16 hours, and the solid filtered and washed as above. In cases where this process apparently caused the decomposition of the host, the reaction would be repeated using 0.25g more of the host at room temperature for five days.

6.6 References

1. O. B. Peersen, X. L. Wu, I. Kustanovich and S. O. Smith, *Journal of Magnetic Resonance, Series A*, 1993, **104**, 334-339.
2. W. L. Earl and D. L. Vanderhart, *Journal of Magnetic Resonance*, 1982, **48**, 35-54.
3. B. C. Giessen and G. E. Gordan, *Science*, 1968, **159**, 973.
4. S. M. Clark, A. Nield, T. Rathbone, J. Flaherty, C. C. Tang, J. S. O. Evans, R. J. Francis and D. O'Hare, *Nuclear Instruments and Methods in Physics Research Section B: Beam Interactions with Materials and Atoms*, 1995, **97**, 98-101.
5. S. M. Clark, R. J. Cernik, A. Grant, S. York, P. A. Atkinson, A. Gallagher, D. G. Stokes, S. Gregory, M. C. Miller, K. Ackroyd, R. Farrow, R. J. Francis and D. O'Hare, *Materials Science Forum*, 1996, **228**, 213.
6. S. M. Clark, *Journal of Applied Crystallography*, 1995, **28**, 646.
7. X. Duan and D. G. Evans, eds., *Layered Double Hydroxides*, Springer, 2006.
8. S. Qiu, *Zhuanli Shenqing Gongkai Shuomingshu*, 1996.
9. W. Stählin and H. R. Oswald, *Acta Crystallographica*, 1970, **B26**, 860-863.

10. J.-P. Zhang, Q. Wang, X.-L. Xie, X. Li and A.-Q. Wang, *Journal of Biomedical Materials Research Part B: Applied Biomaterials*, 2010, **92B**, 205-214.
11. G. Gomori, *Methods in Enzymology*, 1955, **1**, 138-146.
12. R. Chitrakar, S. Tezuka, A. Sonoda, K. Sakane and T. Hirotsu, *Industrial & Engineering Chemistry Research*, 2008, **47**, 4905-4908.

Conclusion

A number of different aspects of the chemistry of layered double hydroxides and similar materials have been explored in this thesis. The intercalation chemistry of these compounds, in both aqueous and mixed solutions, has been explored to synthesise over forty new hybrid layered materials by ion-exchange and rehydration-reconstruction methods. The host used include both previously-reported layered hydroxide compounds, and novel host materials synthesised by the extension of heterogeneous reactions of solid oxides. The synthesis of these novel materials provides insights into the factors that control the compatibility of the metal ions that may form hydrotalcite-like structures, in addition to providing compounds that may act as the precursors of catalysts and other functional materials.

The new intercalation compounds synthesised show interlayer distances ranging from 7.1Å to 23.6Å, and demonstrate a variety of interlayer alignments as determined by powder X-ray diffraction, dependent upon both the metallic content and the degree of hydration of the host compound. The anionic contents of the interlayer regions have been further characterised through infra-red spectroscopy, elemental microanalysis, solid-state NMR and thermogravimetric analysis techniques.

The mechanism and kinetics of the release of the intercalated anions from the hosts have been studied in situations approximating their real-world applications, and the degree of release quantified by UV/Visible spectroscopy. Both the rates and mechanisms of anion release have been found to be dependent on the anion, the host, the temperature and the solution into which the anions are released; as such, the release timescales of the anions may be fined tuned through modifications of the host

materials. In addition, an explanation has been suggested for the observed change in mechanism observed in instances of release in which the host compound is in only partial contact with the release medium.

Appendix A

Lattice Parameters of Synthesised Compounds and Anion Orientation Calculations

A.1 Indexing Details

The Mg/Al- and Mg/Fe-LDHs were indexed to the hexagonal unit cells similar to those used for hydrotalcite and pyroaurite, with the *c*-direction defined as perpendicular to the layers, with three complete layers present in the unit cell.[1, 2] The Ca/Al-LDHs were also indexed to a hexagonal unit cell, but one containing only two complete LDH layers, based on the structure described by Renaudin *et al.*,[3] as were the Li/Al-LDHs.[4] Typically, the *c* lattice parameters were determined from the basal (00*l*) peaks, while the *a* and *b* parameters were identified from the (110) reflections present in all compounds.

Unidentifiable phases, or those heavily contaminated with another non-LMH solid were not structurally indexed. New host materials are fully indexed, including refinement data for characteristic observed peak positions, while the lattice parameters of new intercalation compounds are given, as refinement was often not possible due to the structural disorder observed in the solids.

A.2 Compounds from Chapter 2

A.2.1 Intercalation Compounds of Ca/Al-LDH

Guest Molecule	a = b (Å)	c (Å)
Nitrate	5.74(4)	17.23(5)

Guest Molecule	a = b (Å)	c (Å)
Cyclamate	5.74(4)	30.95(4)
Saccharin	5.73(4)	29.37(2)
Ferulate	5.75(6)	22.22(5)
Theobromine	5.74(3)	27.24(2)

A.2.2 Intercalation Compounds of Li/Al-LDH

The lattice parameters for the Li/Al-Cyclamate LDH are those for the oven-dried product; see Chapter 2, Section 2.2.1 for futher details.

Guest Molecule	a = b (Å)	c (Å)
Chloride	5.10(0)	14.29(9)
Acesulfame	5.07(8)	28.84(5)
Cyclamate	5.12(9)	40.60(3)
Saccharin	5.14(8)	30.74(9)
Ferulate	5.03(3)	34.40(9)
Theobromine	5.12(3)	35.31(1)

A.2.3 Intercalation Compounds of Mg/Al-LDH

Guest Molecule	a = b (Å)	c (Å)
Nitrate	3.05(3)	25.62(8)
Acesulfame	3.02(9)	43.01(7)
Cyclamate	3.03(2)	61.17(4)
Saccharin	3.02(6)	45.50(7)
Ferulate	3.03(9)	52.14(5)
Theobromine	3.03(7)	37.63(7)

A.3 Compounds from Chapter 3

A.3.1 Intercalation Compounds of Ca/Al-LDH

Guest Molecule	a = b (Å)	c (Å)
Nitrate	5.74(4)	17.23(5)
2,4DB	5.72(4)	37.47(2)
Dichlorprop	5.65(1)	24.21(6)
Diclofenac	5.71(2)	45.05(6)
Ibuprofen	5.74(2)	37.43(9)
Naproxen	5.70(4)	38.22(3)

A.3.2 Intercalation Compounds of Li/Al-LDH

Guest Molecule	a = b (Å)	c (Å)
Chloride	5.10(0)	14.29(9)
2,4DB	5.02(5)	43.98(4)
2,4,5T	5.03(3)	41.08(8)
Dichlorprop	5.06(8)	37.34(2)
Diclofenac	5.07(2)	44.31(5)
Ibuprofen	5.13(1)	43.64(2)
Naproxen	5.11(2)	42.14(3)

A.3.3 Intercalation Compounds of Mg/Al-LDH

Guest Molecule	a = b (Å)	c (Å)
Nitrate	3.05(3)	25.62(8)
2,4,5T	3.02(6)	55.07(0)
Dichlorprop	3.01(5)	53.70(9)

Guest Molecule	a = b (Å)	c (Å)
Diclofenac	3.03(3)	66.96(9)
Naproxen	3.04(2)	62.61(7)

A.3.4 Intercalation Compounds of Zn_5-HS

The zinc hydroxynitrate salt precursor crystallises in monoclinic unit cell, with α and $\gamma = 90^{o}$, and $\beta = 93.28^{o}$.[5] The *a*-direction is defined as perpendicular to the layers.

Guest Molecule	a (Å)	b (Å)	c (Å)
Nitrate	19.48(1)	6.23(8)	5.51(7)
2,4,5T	52.20(7)	6.22(7)	5.50(9)
Diclofenac	44.19(9)	6.21(9)	5.47(5)
Ibuprofen	53.29(4)	6.26(6)	5.51(4)

A.4 Compounds from Chapter 4

A.4.1 Intercalation Compounds of Li/Al-LDH

Guest Molecule	a = b (Å)	c (Å)
Chloride	5.10(0)	14.29(9)
Thiosulfate	5.09(2)	17.15(9)
Tartrazine	5.09(6)	27.65(9)

A.4.2 Intercalation Compounds of Mg/Al-LDH

Guest Molecule	a = b (Å)	c (Å)
Nitrate	3.05(3)	25.62(8)
Thiosulfate	3.04(1)	25.83(1)
Tartrazine	3.03(2)	70.70(5)

A.4.3 Intercalation Compounds of Mg/Fe-LDH

Guest Molecule	a = b (Å)	c (Å)
Chloride	3.11(8)	24.11(4)
Thiosulfate	3.10(5)	23.78(3)
Tartrazine	3.10(7)	26.12(3)

A.5 Compounds from Chapter 5

A.5.1 Layered Double Hydroxides formed using MgO

Note that the Mg/Co-Nitrate LDH does not contain any magnesium – it may be more accurately described as a Co^{II}/Co^{III}-NO_3 LDH; the designation 'Mg/Co-Nitrate LDH' is used to indicate that this LDH product was formed by the reaction of MgO with a solution of $Co(NO_3)_2$.

Mg/Mn-Chloride LDH: Hexagonal unit cell, space group R-3M.

a = b = 3.11(2)Å, c = 24.21(5)Å.

h	*k*	*l*	d (Calculated)	d (Observed)	Residual (Calcd.-Obsvd)
0	0	3	8.0717	8.0739	-0.0022
0	0	6	4.0358	4.0435	-0.0077
0	1	2	2.6307	2.6298	0.0009
0	1	5	2.3550	2.3593	-0.0043
0	1	8	2.0128	2.0314	-0.0186
1	1	0	1.5560	1.5561	-0.0001
1	1	3	1.5279	1.5329	-0.0050

Mg/Fe-Chloride LDH: Hexagonal unit cell, space group R-3M.

a = b = 3.10(2)Å, c = 23.56(5)Å.

h	***k***	***l***	**d (Calculated)**	**d (Observed)**	**Residual (Calcd.-Obsvd)**
0	0	3	7.8550	7.8544	0.0006
0	0	6	3.9275	3.9308	-0.0033
0	1	2	2.6192	2.6173	0.0019
0	1	5	2.3339	2.3333	0.0006
0	1	8	1.9849	2.0746	-0.0897
1	1	0	1.5510	1.5515	-0.0005
1	1	3	1.5216	1.5236	-0.0020

Mg/Co-Nitrate LDH: Hexagonal unit cell, space group R-3M.

a = b = 3.10(3)Å, c = 23.48(4)Å.

h	***k***	***l***	**d (Calculated)**	**d (Observed)**	**Residual (Calcd.-Obsvd)**
0	0	3	7.8280	7.8281	-0.0001
0	0	6	3.9140	3.9179	-0.0039
0	1	2	2.6196	2.6171	0.0025
0	1	5	2.3325	2.3334	-0.0009
0	1	8	1.9821	1.9855	-0.0034
1	1	0	1.5515	1.5517	-0.0002
1	1	3	1.5219	1.5212	0.0007

Mg/Ga-Nitrate LDH: Hexagonal unit cell, space group R-3M.

a = b = 3.08(1)Å, c = 25.16(4)Å.

h	***k***	***l***	**d (Calculated)**	**d (Observed)**	**Residual (Calcd.-Obsvd)**
0	0	3	8.3880	8.3865	0.0015

h	***k***	***l***	**d (Calculated)**	**d (Observed)**	**Residual (Calcd.-Obsvd)**
0	0	6	4.1940	4.1347	0.0593
0	1	2	2.6102	2.5983	0.0119
0	1	5	2.3574	2.3592	-0.0018
0	1	8	2.0348	2.0744	-0.0396
1	1	0	1.5405	1.5406	-0.0001
1	1	3	1.5152	1.5117	0.0035

A.5.2 Layered Double Hydroxides formed using CaO

Ca/Al-Chloride LDH: Hexagonal unit cell, space group R-3.

a = b = 5.73(7)Å, c = 15.53(4)Å.

h	***k***	***l***	**d (Calculated)**	**d (Observed)**	**Residual (Calcd.-Obsvd)**
0	0	2	7.7670	7.7673	-0.0003
0	0	4	3.8835	3.8973	-0.0138
1	1	0	2.8685	2.8687	-0.0002
1	1	2	2.6909	2.6946	-0.0037
1	1	4	2.3073	2.3126	-0.0053
3	0	0	1.6561	1.6581	-0.0020
3	0	4	1.5234	1.5249	-0.0015

Ca/Ga-Nitrate LDH: Hexagonal unit cell, space group R-3M.

a = b = 3.36(6)Å, c = 25.80(5)Å.

h	***k***	***l***	**d (Calculated)**	**d (Observed)**	**Residual (Calcd.-Obsvd)**
0	0	3	8.6017	8.6017	0.0000
0	0	6	4.3008	4.3149	-0.0141
0	1	2	2.8434	2.8346	0.0088

h	*k*	*l*	d (Calculated)	d (Observed)	Residual (Calcd.-Obsvd)
0	1	5	2.5382	2.4908	0.0474
0	1	8	2.1627	2.1750	-0.0123
1	1	0	1.6830	1.6830	0.0000
1	1	3	1.6517	1.6521	-0.0004

A.5.3 Layered Double Hydroxides formed using MnO

Mn/Al-Chloride LDH: Hexagonal unit cell, space group R-3M.

a = b = 3.14(6)Å, c = 23.09(7)Å.

h	*k*	*l*	d (Calculated)	d (Observed)	Residual (Calcd.-Obsvd)
0	0	3	7.6990	7.6971	0.0019
0	0	6	3.8495	3.8598	-0.0103
0	1	2	2.6517	2.6685	-0.0168
0	1	5	2.3467	2.3549	-0.0082
0	1	8	1.9815	1.9898	-0.0083
1	1	0	1.5730	1.5734	-0.0004
1	1	3	1.5412	1.5392	0.0020

A.5.4 Layered Double Hydroxides formed using CoO

Co/Al-Chloride LDH: Hexagonal unit cell, space group R-3M.

a = b = 3.04(7)Å, c = 22.63(5)Å.

h	*k*	*l*	d (Calculated)	d (Observed)	Residual (Calcd.-Obsvd)
0	0	3	7.5450	7.5448	0.0002
0	0	6	3.7725	3.8030	-0.0305
0	1	2	2.5699	2.5661	0.0038
0	1	5	2.2798	2.2838	-0.0004

h	*k*	*l*	d (Calculated)	d (Observed)	Residual (Calcd.-Obsvd)
0	1	8	1.9298	1.9415	-0.0117
1	1	0	1.5235	1.5236	-0.0001
1	1	3	1.4934	1.4965	-0.0031

Co/Al-Cyclamate LDH: Hexagonal unit cell, space group R-3M.

a = b = 3.03(5)Å, c = 57.26(3)Å.

A.5.5 Layered Double Hydroxides formed using NiO

Ni/Fe-Chloride LDH: Hexagonal unit cell, space group R-3M.

a = b = 3.08(3)Å, c = 23.59(2)Å.

h	*k*	*l*	d (Calculated)	d (Observed)	Residual (Calcd.-Obsvd)
0	0	3	7.8640	7.8645	-0.0005
0	0	6	3.9320	3.9536	-0.0216
0	1	2	2.6041	2.5573	0.0468
0	1	5	2.3237	2.3045	0.0192
0	1	8	1.9793	1.9625	0.0168
1	1	0	1.5415	1.5416	-0.0001
1	1	3	1.5127	1.5164	-0.0037

Ni/Al-Nitrate LDH: Hexagonal unit cell, space group R-3M.

a = b = 3.03(4)Å, c = 26.18(1)Å.

h	*k*	*l*	d (Calculated)	d (Observed)	Residual (Calcd.-Obsvd)
0	0	3	8.7270	8.7278	-0.0008
0	0	6	4.3635	4.3551	0.0084
0	1	2	2.5761	2.4989	0.0772
1	1	0	1.5170	1.5171	-0.0001

Ni/Al-Cyclamate LDH: Hexagonal unit cell, space group R-3M.

a = b = 3.02(8)Å, c = 50.32(8)Å.

A.5.6 Layered Double Hydroxides formed using CuO

Cu/Cr-Chloride LDH: Hexagonal unit cell, space group R-3M.

a = b = 3.14(6)Å, c = 23.02(4)Å.

h	***k***	***l***	**d (Calculated)**	**d (Observed)**	**Residual (Calcd.-Obsvd)**
0	0	3	7.6747	7.6745	0.0002
0	0	6	3.8373	3.8549	-0.0176
0	1	2	2.6513	2.6450	0.0063
0	1	5	2.3448	2.3572	-0.0124
0	1	8	1.9786	1.9983	-0.0197
1	1	0	1.5730	1.5731	-0.0001
1	1	3	1.5409	1.5431	-0.0022

Cu/Al-Nitrate LDH: Hexagonal unit cell, space group R-3M.

a = b = 3.04(5)Å, c = 25.19(9)Å.

h	***k***	***l***	**d (Calculated)**	**d (Observed)**	**Residual (Calcd.-Obsvd)**
0	0	3	8.3997	8.3996	0.0001
0	0	6	4.1998	4.2518	-0.0520
0	1	2	2.5811	2.5028	0.0783
0	1	5	2.3365	2.2051	0.1314
0	1	8	2.0219	2.0744	-0.0525
1	1	0	1.5225	1.4731	0.0494
1	1	3	1.4981	1.4569	0.0412

Cu/Al-Cyclamate LDH: Hexagonal unit cell, space group R-3M.

a = b = 3.01(7)Å, c = 50.89(4)Å.

A.5.7 Layered Double Hydroxides formed using ZnO

Zn/Cr-Chloride LDH: Hexagonal unit cell, space group R-3M.

a = b = 3.11(2)Å, c = 22.99(5)Å.

h	***k***	***l***	**d (Calculated)**	**d (Observed)**	**Residual (Calcd.-Obsvd)**
0	0	3	7.6650	7.6652	-0.0002
0	0	6	3.8325	3.8563	-0.0238
0	1	2	2.6239	2.6213	0.0026
0	1	5	2.3252	2.3259	-0.0007
0	1	8	1.9660	1.9712	0.0540
1	1	0	1.5560	1.5554	0.0006
1	1	3	1.5249	1.5269	-0.0020

Zn/Al-Nitrate LDH: Hexagonal unit cell, space group R-3M.

a = b = 3.06(4)Å, c = 26.49(9)Å.

h	***k***	***l***	**d (Calculated)**	**d (Observed)**	**Residual (Calcd.-Obsvd)**
0	0	3	8.8330	8.8333	-0.0003
0	0	6	4.4165	4.4286	-0.0121
0	1	2	2.6018	2.6009	0.0009
0	1	5	2.3727	2.3737	-0.0010
0	1	8	2.0709	2.0739	-0.0030
1	1	0	1.5320	1.5312	0.0008
1	1	3	1.5095	1.5107	-0.0012

Zn/Al-Chloride LDH: Hexagonal unit cell, space group R-3M.

a = b = 3.06(9)Å, c = 23.16(8)Å.

h	***k***	***l***	**d (Calculated)**	**d (Observed)**	**Residual (Calcd.-Obsvd)**
0	0	3	7.7227	7.7228	-0.0001
0	0	6	3.8613	3.8562	0.0051
0	1	2	2.5905	2.5916	-0.0011
0	1	5	2.3055	2.3068	-0.0013
0	1	8	1.9582	1.9588	-0.0006
1	1	0	1.5345	1.5349	-0.0004
1	1	3	1.5051	1.5055	-0.0004

Zn/Ga-Nitrate LDH: Hexagonal unit cell, space group R-3M.

a = b = 3.09(7)Å, c = 26.30(3)Å.

h	***k***	***l***	**d (Calculated)**	**d (Observed)**	**Residual (Calcd.-Obsvd)**
0	0	3	8.7677	8.7674	0.0003
0	0	6	4.3838	4.4239	-0.0401
0	1	2	2.6279	2.6705	-0.0426
0	1	5	2.3894	2.3543	0.0351
0	1	8	2.0783	2.0758	0.0025
1	1	0	1.5485	1.5483	0.0002
1	1	3	1.5249	1.5252	-0.0003

Zn/Ga-Cyclamate LDH: Hexagonal unit cell, space group R-3M.

a = b = 3.09(9)Å, c = 63.91(1)Å.

Zn/In-Chloride LDH: Hexagonal unit cell, space group R-3M.

a = b = 3.16(8)Å, c = 23.51(1)Å.

h	***k***	***l***	**d (Calculated)**	**d (Observed)**	**Residual (Calcd.-Obsvd)**
0	0	3	7.8370	7.8371	-0.0001
0	0	6	3.9185	3.9754	-0.0569
0	1	2	2.6718	2.6736	-0.0018
0	1	5	2.3697	2.3737	-0.0040
0	1	8	2.0055	2.0125	-0.0070
1	1	0	1.5840	1.5851	-0.0011
1	1	3	1.5526	1.5543	0.0096

Zn/In-Cyclamate LDH: Hexagonal unit cell, space group R-3M.

a = b = 3.16(7)Å, c = 62.25(4)Å.

A.5.8 Layered Double Hydroxides formed using CdO

The ‘Cd/Co-Nitrate LDH’ product contains no cadmium, and is a Co^{II}/Co^{III}-NO_3 LDH. The ‘Cd/Co’ designation represents the metal (II) oxide and metal (III) salt used in the synthesis of the solid. See the similar ‘Mg/Co’ compound in Section A.5.1.

The Cd/Al-Nitrate LDH has been indexed to a hexagonal unit cell containing only two layers, as its powder pattern resembles that of the Ca/Al-Nitrate LDH which shows a similar size discrepancy between the metal cations.

Cd/Co-Nitrate LDH: Hexagonal unit cell, space group R-3M.

a = b = 3.11(5)Å, c = 24.07(5)Å.

h	***k***	***l***	**d (Calculated)**	**d (Observed)**	**Residual (Calcd.-Obsvd)**
0	0	3	8.0250	8.0250	0.0000
0	0	6	4.0125	3.9729	0.0396
0	1	2	2.6324	2.6364	-0.0004
0	1	5	2.3535	2.3491	0.0044
0	1	8	2.0087	1.9974	0.0113
1	1	0	1.5575	1.5576	-0.0001
1	1	3	1.5289	1.5277	0.0012

Cd/Al-Nitrate LDH: Hexagonal unit cell, space group P-3c1.

a = b = 5.68(4)Å, c = 16.02(9)Å.

h	***k***	***l***	**d (Calculated)**	**d (Observed)**	**Residual (Calcd.-Obsvd)**
0	0	2	8.0133	8.0146	-0.0013
0	0	4	4.0067	4.0488	-0.0421
0	1	4	3.4395	3.5159	-0.0764
0	1	6	2.5649	2.5698	-0.0049
1	1	0	2.8420	2.8408	0.0012
1	1	2	2.6785	2.6734	0.0051

Cd/Ga-Nitrate LDH: Hexagonal unit cell, space group R-3M.

a = b = 3.35(4)Å, c = 25.09(9)Å.

h	***k***	***l***	**d (Calculated)**	**d (Observed)**	**Residual (Calcd.-Obsvd)**
0	0	3	8.3663	8.3664	-0.0001
0	0	6	4.1832	4.0769	0.1063

h	*k*	*l*	d (Calculated)	d (Observed)	Residual (Calcd.-Obsvd)
0	1	2	2.8298	2.8411	-0.0113
0	1	5	2.5141	2.5223	-0.0082
0	1	8	2.1314	2.1071	0.0243
1	1	0	1.6770	1.6775	-0.0005
1	1	3	1.6443	1.6398	0.0045

Cd/Ga-Cyclamate LDH: Hexagonal unit cell, space group R-3M.

a = b = 3.31(7)Å, c = 49.38(4)Å.

A.5.9 Copper Hydroxy Salts

The Mg/Cu-Nitrate HDS and Ca/Cu-Nitrate HDS products contain neither magnesium nor calcium, and their presence in the compound names below merely indicates the metal oxide used in the synthesis. In both cases, the product is a monometallic copper hydroxynitrate salt, with the approximate formula $[Cu_2(OH)_3]NO_3$. This compound crystallises in an orthorhombic unit cell, with the *b*-direction defined as perpendicular to the layers.[6]

Mg/Cu-Nitrate HDS: Orthorhombic unit cell, space group $P2_12_12_1$.

a = 6.08(3)Å, b = 13.77(6)Å, c = 5.57(2)Å

h	*k*	*l*	d (Calculated)	d (Observed)	Residual (Calcd.-Obsvd)
0	2	0	6.8880	6.8879	0.0001
1	0	1	4.1088	4.1059	0.0029
1	2	1	3.5287	3.6235	-0.0948
0	4	0	3.4440	3.4484	-0.0044
2	0	0	3.0415	3.0413	0.0002
0	0	2	2.7860	2.7861	-0.0001

h	***k***	***l***	**d (Calculated)**	**d (Observed)**	**Residual (Calcd.-Obsvd)**
1	4	1	2.6394	2.6641	-0.0247
0	0	4	1.3930	1.3902	0.0028

Mg/Cu-Cyclamate HDS: Orthorhombic unit cell, space group $P2_12_12_1$.

a = 6.20(1)Å, b = 36.95(4)Å, c = 5.64(6)Å.

Ca/Cu-Nitrate HDS: Orthorhombic unit cell, space group $P2_12_12_1$.

a = 6.08(5)Å, b = 13.78(9)Å, c = 5.57(8)Å.

h	***k***	***l***	**d (Calculated)**	**d (Observed)**	**Residual (Calcd.-Obsvd)**
0	2	0	6.8945	6.8934	0.0011
1	0	1	4.1118	4.1071	0.0047
1	2	1	3.5315	3.6228	-0.0913
0	4	0	3.4472	3.4521	-0.0049
2	0	0	3.0425	3.0426	-0.0001
0	0	2	2.7890	2.7891	-0.0001
1	4	1	2.6417	2.6647	-0.0230
0	0	4	1.3945	1.3909	0.0036

A.5.10 Zinc and Cadmium Hydroxynitrate Salts

The two products in this table are the hydroxynitrate salts with the general formulae $[M^{II}_5(OH)_8](NO_3)_2 \cdot yH_2O$, where M^{II} = Zn and Cd respectively. No calcium was found in the first product, and its presence in the compound name below indicates the use of its oxide in the synthesis of the hydroxynitrate salt. Cadmium oxide was correspondingly used to synthesise the second product. These compounds crystallise

in monoclinic unit cells, with α and γ = 90º, and β = 93.28º and 94.85º in the Zn and Cd compounds respectively.[5, 7]

Ca/Zn-Nitrate HDS: Monoclinic unit cell, space group C2/m.

a = 19.36(2)Å, b = 6.23(2)Å, c = 5.51(4)Å; α = 90º, β = 93.28º, γ = 90º

h	***k***	***l***	**d (Calculated)**	**d (Observed)**	**Residual (Calcd.-Obsvd)**
2	0	0	9.6651	9.6812	-0.0161
4	0	0	4.8326	4.8499	-0.0173
3	1	0	4.4796	4.4927	-0.0131
4	0	1	3.5329	3.5468	-0.0139
0	2	0	3.1160	3.1163	-0.0003
0	0	2	2.7525	2.7569	-0.0044
2	2	1	2.5920	2.5966	-0.0046
10	0	0	1.9330	1.9430	-0.0100

Cd/Cd-Nitrate HDS: Monoclinic unit cell, space group C2/m.

a = 18.86(1)Å, b = 6.85(6)Å, c = 5.93(1)Å; α = 90º, β = 94.85º, γ = 90º

h	***k***	***l***	**d (Calculated)**	**d (Observed)**	**Residual (Calcd.-Obsvd)**
2	0	0	9.3967	9.4306	-0.0339
4	0	0	4.6984	4.7127	-0.0143
3	1	0	4.6247	4.6313	-0.0066
3	1	1	3.5365	3.5384	-0.0019
0	2	0	3.4280	3.4282	-0.0002
0	0	2	2.9549	2.9653	-0.0104
8	0	0	2.3492	2.3470	0.0022
2	2	3	1.6592	1.6587	-0.0005

A.5.11 Yttrium Layered Hydroxy Salts

The yttrium hydroxy salt $[Y_2(OH)_5]Cl{\cdot}yH_2O$ was formed by the reaction of a number of different metal (II) oxides with a solution of YCl_3. The metal (II) oxide used is represented by the first metal in the compound name. This compound crystallises in an orthorhombic unit cell, with the *b*-direction defined as perpendicular to the layers.[8]

The lattice parameters for the Ni/Y-Cyclamate LHS are those for the oven-dried product; see Chapter 5, Section 5.7.4 for futher details.

Mg/Y-Chloride LHS: Orthorhombic unit cell, space group $Pca2_1$.

a = 12.63(7)Å, b = 8.34(2)Å, c = 7.11(8)Å.

h	***k***	***l***	**d (Calculated)**	**d (Observed)**	**Residual (Calcd.-Obsvd)**
0	1	0	8.3420	8.3415	0.0005
1	1	1	4.9771	4.9787	-0.0016
0	2	0	4.1710	4.1964	-0.0254
3	1	0	3.7601	3.7604	-0.0003
0	0	2	3.5590	3.5595	-0.0005
3	1	1	3.3248	3.3276	-0.0028
4	0	0	3.1593	3.1589	0.0004
2	0	2	3.1009	3.1025	-0.0016
2	1	2	2.9066	2.9115	-0.0049

Co/Y-Chloride LHS: Orthorhombic unit cell, space group $Pca2_1$.

a = 12.66(4)Å, b = 8.39(7)Å, c = 7.13(7)Å.

h	***k***	***l***	**d (Calculated)**	**d (Observed)**	**Residual (Calcd.-Obsvd)**
0	1	0	8.3970	8.3971	-0.0001

h	***k***	***l***	**d (Calculated)**	**d (Observed)**	**Residual (Calcd.-Obsvd)**
1	1	1	4.9969	4.9943	0.0026
0	2	0	4.1985	4.2071	-0.0086
3	1	0	3.7716	3.7696	0.0020
0	0	2	3.5685	3.5687	-0.0002
3	1	1	3.3346	3.3344	0.0002
4	0	0	3.1660	3.1659	0.0001
2	0	2	3.1088	3.1097	-0.0009

Ni/Y-Chloride LHS: Orthorhombic unit cell, space group $Pca2_1$.

a = 12.67(1)Å, b = 8.40(6)Å, c = 7.14(9)Å.

h	***k***	***l***	**d (Calculated)**	**d (Observed)**	**Residual (Calcd.-Obsvd)**
0	1	0	8.4060	8.4058	0.0002
1	1	1	5.0033	5.0046	-0.0013
0	2	0	4.2030	4.2121	-0.0091
3	1	0	3.7740	3.7750	-0.0010
0	0	2	3.5745	3.5747	-0.0002
3	1	1	3.3375	3.3390	-0.0015
4	0	0	3.1677	3.1675	0.0002
2	0	2	3.1132	3.1139	-0.0007

Ni/Y-Cyclamate LHS: Orthorhombic unit cell, space group $Pca2_1$.

a = 12.75(1)Å, b = 20.35(2)Å, c = 7.19(2)Å.

A.6 Molecular Sizes for Orientation Calculations

A.6.1 General Method

The length of the guest anion was determined in each case by measuring the through-space separation of the charge-bearing atom (highlighted in red) and the most distant atom in the molecule (highlighted in blue) plus the van der Waals radii of each atom. The van der Waals radii used were taken from the CRC Handbook of Chemistry and Physics (58th Edition),[9] and the interatomic distances were calculated from crystal structures of the molecules from the Cambridge Structural Database, using the program Diamond 3.0a (Crystal Impact Gbr.)

A.6.2 Intercalated Molecules from Chapter 2

Acesulfame K:

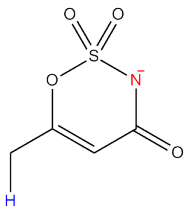

	Length (Å)
Distance between atom centres	4.802
van der Waals Radius (N)	1.5
van der Waals Radius (H)	1.2
Sum	7.502

Cyclamate:

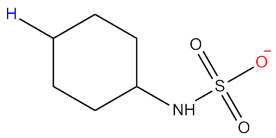

	Length (Å)
Distance between atom centres	7.634
van der Waals Radius (O)	1.4
van der Waals Radius (H)	1.2
Sum	10.234

Saccharin:

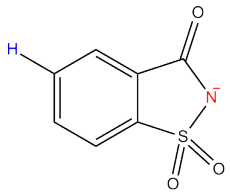

	Length (Å)
Distance between atom centres	5.887
van der Waals Radius (N)	1.5
van der Waals Radius (H)	1.2
Sum	8.587

Ferulate:

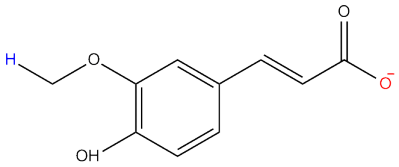

	Length (Å)
Distance between atom centres	9.315
van der Waals Radius (O)	1.4
van der Waals Radius (H)	1.2
Sum	11.915

Theobromine:

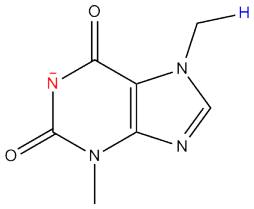

	Length (Å)
Distance between atom centres	7.299
van der Waals Radius (N)	1.5
van der Waals Radius (H)	1.2
Sum	9.999

A.6.3 Intercalated Molecules from Chapter 3

2,4DB:

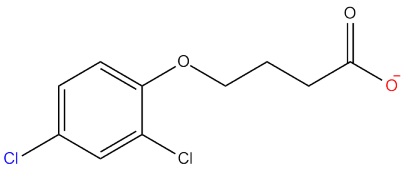

	Length (Å)
Distance between atom centres	11.853
van der Waals Radius (O)	1.4
van der Waals Radius (Cl)	1.8
Sum	15.053

2,4,5T:

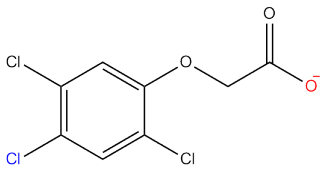

	Length (Å)
Distance between atom centres	9.059
van der Waals Radius (O)	1.4
van der Waals Radius (Cl)	1.8
Sum	12.259

Dichlorprop:

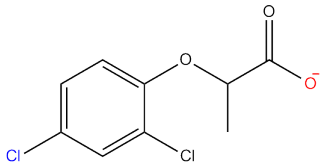

	Length (Å)
Distance between atom centres	8.649
van der Waals Radius (O)	1.4
van der Waals Radius (Cl)	1.8
Sum	11.849

Diclofenac:

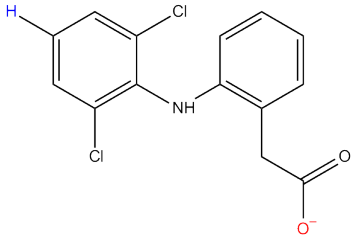

	Length (Å)
Distance between atom centres	8.575
van der Waals Radius (O)	1.4
van der Waals Radius (H)	1.2
Sum	11.175

Ibuprofen:

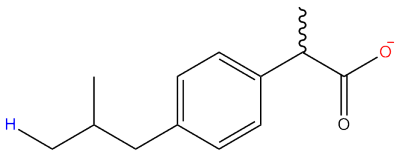

	Length (Å)
Distance between atom centres	10.030
van der Waals Radius (O)	1.4
van der Waals Radius (H)	1.2
Sum	12.630

Naproxen:

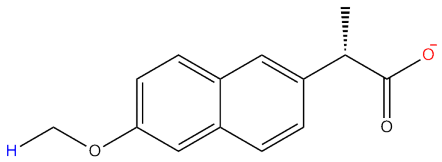

	Length (Å)
Distance between atom centres	10.79
van der Waals Radius (O)	1.4
van der Waals Radius (H)	1.2
Sum	13.39

A.6.4 Intercalated Molecules from Chapter 4

Tartrazine:

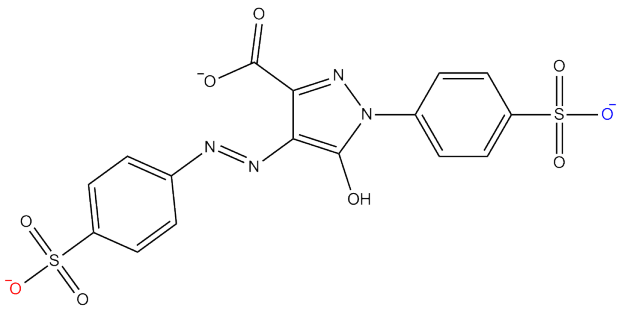

	Length (Å)
Distance between atom centres	16.52
van der Waals Radius (O)	1.4
van der Waals Radius (O)	1.4
Sum	19.32

A.7 References

1. A. V. Radha, P. V. Kamath and C. Shivakumara, *Acta Crystallographica B*, 2007, **63**, 243-250.
2. R. S. W. Braithwaite, P. J. Dunn, R. G. Pritchard and W. H. Paar, *Mineralogical Magazine*, 1994, **58**, 79-85.
3. G. Renaudin and M. Francois, *Acta Crystallographica Section C*, 1999, **C55**, 835.
4. A. V. Besserguenev, A. M. Fogg, R. J. Francis, S. J. Price, D. O'Hare, V. P. Isupov and B. P. Tolochko, *Chemistry of Materials*, 1997, **9**, 241-247.
5. W. Stählin and H. R. Oswald, *Acta Crystallographica*, 1970, **B26**, 860-863.

6. B. Bovio and S. Locchi, *Journal of Crystallographic and Spectroscopic Research*, 1982, **12**, 507-517.
7. P. Benard, M. Louer and D. Louer, *Powder Diffraction*, 1991, **6**, 10-15.
8. L. Poudret, T. J. Prior, L. J. McIntyre and A. M. Fogg, *Chemistry of Materials*, 2008, **20**, 7447-7453.
9. R. C. Weast, *Handbook of Chemistry and Physics*, 58th edn., CRC Press, 1977.

Appendix B

Elemental Analysis Data for Synthesised Compounds

B.1 Elemental Analysis Details

The elemental microanalysis data presented here was performed by the Analytical Services Department of the Inorganic Chemistry Laboratory at the University of Oxford, or by Stephen Boyer at the School of Human Sciences, London Metropolitan University, using a quantitative oxidative combustion technique.

B.2 Compounds from Chapter 2

B.2.1 Intercalation Compounds of Acesulfame

Host Metals	Chemical Formula	Predicted %	Observed %
Li/Al	$[LiAl_2(OH)_6](C_4H_4NO_4S)_{0.73}Cl_{0.27}\cdot 1.5H_2O$	C – 11.03 H – 3.78 N – 3.22	C – 10.98 H – 3.77 N – 3.12
Mg/Al	$[Mg_2Al(OH)_6](C_4H_4NO_4S)_{0.99}(NO_3)_{0.01}\cdot H_2O$	C – 13.33 H – 3.38 N – 3.93	C – 13.35 H – 3.45 N – 3.92

B.2.2 Intercalation Compounds of Cyclamate

Host Metals	Chemical Formula	Predicted %	Observed %
Ca/Al	$[Ca_2Al(OH)_6](C_6H_{12}NO_3S)_{0.76}(CO_3)_{0.12}\cdot 2.4H_2O$	C - 14.23 H – 5.08 N – 2.69	C – 14.20 H – 5.07 N – 2.62

Host Metals	Chemical Formula	Predicted %	Observed %
Li/Al	$[LiAl_2(OH)_6](C_6H_{12}NO_3S)\cdot 2.2H_2O$	C – 18.91 H – 5.93 N – 3.68	C – 18.93 H – 5.90 N – 3.71
Mg/Al	$[Mg_2Al(OH)_6](C_6H_{12}NO_3S)_{0.7}(NO_3)_{0.3}\cdot 1.4H_2O$	C – 14.65 H – 4.98 N – 4.07	C – 14.67 H – 4.93 N – 3.97

B.2.3 Intercalation Compounds of Saccharin

Host Metals	Chemical Formula	Predicted %	Observed %
Ca/Al	$[Ca_2Al(OH)_6](C_7H_4NO_3S)_{0.76}(NO_3)_{0.24}\cdot 2H_2O$	C – 16.03 H – 3.30 N – 3.51	C – 15.99 H – 3.21 N – 3.41
Li/Al	$[LiAl_2(OH)_6](C_7H_4NO_3S)\cdot 1.2H_2O$	C – 22.92 H – 3.41 N – 3.82	C – 23.01 H – 3.41 N – 3.76
Mg/Al	$[Mg_2Al(OH)_6](C_7H_4NO_3S)_{0.78}(CO_3)_{0.11}\cdot 0.9H_2O$	C – 19.53 H – 3.21 N – 3.19	C – 19.58 H – 3.04 N – 3.14

B.2.4 Intercalation Compounds of Ferulate

Host Metals	Chemical Formula	Predicted %	Observed %
Ca/Al	$[Ca_2Al(OH)_6](C_{10}H_9O_4)\cdot 1.2H_2O$	C – 28.33 H – 4.14 N – 0	C – 28.44 H – 4.05 N – 0

Host Metals	Chemical Formula	Predicted %	Observed %
Li/Al	$[LiAl_2(OH)_6](C_{10}H_9O_4)_{0.65}Cl_{0.35}\cdot 0.6H_2O$	C – 25.04 H – 4.22 N – 0	C – 25.01 H – 4.26 N – 0
Mg/Al	$[Mg_2Al(OH)_6](C_{10}H_9O_4)_{0.85}(OH)_{0.15}\cdot H_2O$	C – 28.21 H – 4.40 N – 0	C – 28.20 H – 4.09 N – 0

B.2.5 Intercalation Compounds of Theobromine

Host Metals	Chemical Formula	Predicted %	Observed %
Ca/Al	$[Ca_2Al(OH)_6](C_7H_7N_4O_2)_{0.21}(OH)_{0.79}\cdot H_2O$	C – 6.35 H – 3.72 N – 4.23	C – 6.28 H – 3.91 N – 4.22
Li/Al	$[LiAl_2(OH)_6](C_7H_7N_4O_2)_{0.61}(OH)_{0.39}\cdot H_2O$	C – 17.26 H – 4.30 N – 11.51	C – 17.20 H – 4.25 N – 11.48
Mg/Al	$[Mg_2Al(OH)_6](C_7H_7N_4O_2)_{0.69}(OH)_{0.31}\cdot H_2O$	C – 17.90 H – 4.09 N – 11.94	C – 17.91 H – 3.83 N – 11.96

B.3 Compounds from Chapter 3

B.3.1 Intercalation Compounds of 2,4DB

Host Metals	Chemical Formula	Predicted %	Observed %
Ca/Al	$[Ca_2Al(OH)_6](C_{10}H_9Cl_2O_3)_{0.34}(OH)_{0.66}\cdot 2.4H_2O$	C – 11.75 H – 4.21 N – 0	C – 11.74 H – 4.25 N – 0
Li/Al	$[LiAl_2(OH)_6](C_{10}H_9Cl_2O_3)_{0.83}(OH)_{0.17}\cdot 2.8H_2O$	C – 23.64 H – 4.60 N – 0	C – 23.71 H – 4.58 N – 0

B.3.2 Intercalation Compounds of 2,4,5T

Host Metals	Chemical Formula	Predicted %	Observed %
Li/Al	$[LiAl_2(OH)_6](C_8H_4Cl_3O_3)_{0.65}(OH)_{0.35}\cdot 2.2H_2O$	C – 16.73 H – 3.61 N – 0	C – 16.61 H – 3.60 N – 0
Mg/Al	$[Mg_2Al(OH)_6](C_8H_4Cl_3O_3)_{0.77}(OH)_{0.23}\cdot 1.9H_2O$	C – 18.04 H – 3.22 N – 0	C – 18.03 H – 3.30 N – 0
Zn	$[Zn_5(OH)_8](C_8H_4Cl_3O_3)_{1.9}(CO_3)_{0.05}\cdot 2H_2O$	C – 18.58 H – 2.00 N – 0	C – 18.34 H – 1.55 N – 0

B.3.3 Intercalation Compounds of Dichlorprop

Host Metals	Chemical Formula	Predicted %	Observed %
Ca/Al	$[Ca_2Al(OH)_6](C_9H_7Cl_2O_3)\cdot 1.7H_2O$	C – 22.86 H – 3.50 N – 0	C – 22.87 H – 3.40 N – 0
Li/Al	$[LiAl_2(OH)_6](C_9H_7Cl_2O_3)_{0.6}(OH)_{0.4}\cdot 1.2H_2O$	C – 19.57 H – 3.96 N – 0	C – 19.60 H – 3.96 N – 0
Mg/Al	$[Mg_2Al(OH)_6](C_9H_7Cl_2O_3)_{0.45}(OH)_{0.55}\cdot 2.1H_2O$	C – 14.77 H – 4.26 N – 0	C – 14.80 H – 4.27 N – 0

B.3.4 Intercalation Compounds of Diclofenac

Host Metals	Chemical Formula	Predicted %	Observed %
Ca/Al	$[Ca_2Al(OH)_6](C_{14}H_{10}Cl_2NO_2)_{0.99}(OH)_{0.01}\cdot 2.9H_2O$	C – 30.11 H – 3.96 N – 2.51	C – 30.09 H – 3.90 N – 2.40
Li/Al	$[LiAl_2(OH)_6](C_{14}H_{10}Cl_2NO_2)_{0.64}(OH)_{0.36}\cdot 3.2H_2O$	C – 19.57 H – 3.96 N – 0	C – 19.60 H – 3.96 N – 0
Mg/Al	$[Mg_2Al(OH)_6](C_{14}H_{10}Cl_2NO_2)_{0.6}(OH)_{0.4}\cdot 3.8H_2O$	C – 23.52 H – 4.70 N – 1.96	C – 23.45 H – 4.65 N – 1.92

Host Metals	Chemical Formula	Predicted %	Observed %
Zn	$[Zn_5(OH)_8](C_{14}H_{10}Cl_2NO_2)_2 \cdot 3.1H_2O$	C – 30.56 H – 3.13 N – 2.55	C – 30.50 H – 3.14 N – 2.56

B.3.5 Intercalation Compounds of Ibuprofen

Host Metals	Chemical Formula	Predicted %	Observed %
Ca/Al	$[Ca_2Al(OH)_6](C_{13}H_{17}O_2)_{0.74}(OH)_{0.26} \cdot 2.9H_2O$	C – 27.66 H – 5.95 N – 0	C – 27.55 H – 5.98 N – 0
Li/Al	$[LiAl_2(OH)_6](C_{13}H_{17}O_2) \cdot 3.3H_2O$	C – 36.49 H – 6.98 N – 0	C – 36.45 H – 6.95 N – 0
Zn	$[Zn_5(OH)_8](C_{13}H_{17}O_2)_2 \cdot 5H_2O$	C – 32.64 H – 5.48 N – 0	C – 32.61 H – 5.31 N – 0

B.3.6 Intercalation Compounds of Naproxen

Host Metals	Chemical Formula	Predicted %	Observed %
Ca/Al	$[Ca_2Al(OH)_6](C_{14}H_{13}O_3)_{0.6}(OH)_{0.4} \cdot 3.1H_2O$	C – 24.64 H – 5.03 N – 0	C – 24.70 H – 4.97 N – 0

Host Metals	Chemical Formula	Predicted %	Observed %
Li/Al	$[LiAl_2(OH)_6](C_{14}H_{13}O_3)_{0.65}(OH)_{0.35}\cdot 3.4H_2O$	C – 28.81 H – 5.74 N – 0	C – 28.79 H – 5.61 N – 0
Mg/Al	$[Mg_2Al(OH)_6](C_{14}H_{13}O_3)_{0.65}(OH)_{0.35}\cdot 3.5H_2O$	C – 27.66 H – 5.56 N – 0	C – 27.66 H – 5.54 N – 0

B.4 Compounds from Chapter 4

B.4.1 Intercalation Compounds of Thiosulfate

Host Metals	Chemical Formula	Predicted %	Observed %
Li/Al	$[Li_{0.96}Al_2(OH)_6](S_2O_3)_{0.48}\cdot H_2O$	C – 0 H – 3.50 N – 0 S – 12.77 Li - 2.80 Al – 22.45	C – 0 H – 3.40 N – 0 S – 12.83 Li – 2.77 Al – 22.41
Mg/Al	$[Mg_2Al(OH)_6](S_2O_3)_{0.49}(CO_3)_{0.01}\cdot 1.2H_2O$	C – 0.04 H – 3.33 N – 0 S – 12.33 Mg – 18.88 Al – 10.62	C – 0.10 H – 3.45 N – 0 S – 12.40 Mg – 18.90 Al – 10.65

Host Metals	Chemical Formula	Predicted %	Observed %
Mg/Fe	$[Mg_{2.2}Fe(OH)_6](S_2O_3)_{0.64}(CO_3)_{0.06}\cdot 2H_2O$	C – 0.22 H – 3.13 N – 0 S – 12.71 Mg – 16.39 Fe – 17.37	C – 0.21 H – 3.20 N – 0 S – 12.75 Mg – 16.42 Fe – 17.37

B.4.2 Intercalation Compounds of Tartrazine

Host Metals	Chemical Formula	Predicted %	Observed %
Li/Al	$[LiAl_2(OH)_6](C_{16}H_9N_4O_9S_2)_{0.22}Cl_{0.34}\cdot 3H_2O$	C – 12.75 H – 4.25 N – 3.72 S – 4.25 Li - 2.12 Al – 16.29	C – 12.71 H – 4.52 N – 3.70 S – 4.25 Li – 2.11 Al – 16.35
Mg/Al	$[Mg_2Al(OH)_6](C_{16}H_9N_4O_9S_2)_{0.24}(NO_3)_{0.28}\cdot 3.9H_2O$	C – 12.25 H – 4.28 N – 4.62 S – 4.08 Mg – 12.75 Al – 7.17	C – 12.35 H – 4.30 N – 4.51 S – 4.07 Mg – 12.77 Al – 7.17

Host Metals	Chemical Formula	Predicted %	Observed %
Mg/Fe	$[Mg_{2.2}Fe(OH)_6](C_{16}H_9N_4O_9S_2)_{0.13}(OH)_{1.01}\cdot 2.8H_2O$	C – 7.37 H – 4.10 N – 2.15 S – 2.45 Mg – 15.58 Fe – 16.51	C – 7.35 H – 4.50 N – 2.17 S – 2.46 Mg – 15.61 Fe – 16.55

B.5 Compounds from Chapter 5

B.5.1 Intercalation Compounds of Nitrate

Host Metals	Chemical Formula	Predicted %	Observed %
Cd/Ga	$[Cd_2Ga(OH)_6]NO_3\cdot 0.6H_2O$	C – 0 H – 1.54 N – 2.97	C – 0 H – 1.55 N – 2.95

B.5.2 Intercalation Compounds of Cyclamate

Host Metals	Chemical Formula	Predicted %	Observed %
Co/Al	$[Co_2Al(OH)_6](C_6H_{12}NO_3S)_{0.78}Cl_{0.22}\cdot 3H_2O$	C – 12.55 H – 4.81 N – 2.44	C – 12.54 H – 5.74 N – 2.09
Ni/Al	$[Ni_2Al(OH)_6](C_6H_{12}NO_3S)_{0.96}(NO_3)_{0.04}\cdot 1.2H_2O$	C – 15.71 H – 4.56 N – 3.18	C – 15.81 H – 5.37 N – 2.79

Host Metals	Chemical Formula	Predicted %	Observed %
Cu/Al	$[Cu_2Al(OH)_6](C_6H_{12}NO_3S)\cdot 1.1H_2O$	C – 15.90 H – 4.50 N – 3.09	C – 15.92 H – 4.59 N – 2.83
Zn/Ga	$[Zn_2Ga(OH)_6](C_6H_{12}NO_3S)_{0.79}(NO_3)_{0.21}\cdot 2H_2O$	C – 11.64 H – 4.02 N – 2.87	C – 12.07 H – 4.17 N – 2.94
Zn/In	$[Zn_2In(OH)_6](C_6H_{12}NO_3S)_{0.22}Cl_{0.78}\cdot H_2O$	C – 3.69 H – 2.50 N – 0.72	C – 3.70 H – 2.63 N – 0.58
Cd/Ga	$[Cd_2Ga(OH)_6](C_6H_{12}NO_3S)_{0.58}(NO_3)_{0.42}\cdot 1.2H_2O$	C – 7.60 H – 2.82 N – 2.55	C – 7.67 H – 2.28 N – 2.23
Y	$[Y_2(OH)_5](C_6H_{12}NO_3S)_{0.64}Cl_{0.36}$	C – 11.83 H – 3.28 N – 2.30	C – 11.34 H – 3.25 N – 1.75
Cu	$[Cu_2(OH)_3](C_6H_{12}NO_3S)_{0.58}(NO_3)_{0.42}$	C – 13.64 H – 3.28 N – 4.57	C – 13.58 H – 3.24 N – 4.44